Advanced Estimation of Credit Valuation Adjustment

Feng, Qian

DOI
10.4233/uuid:4bc92859-1268-489a-b919-84ba827e65f6

Publication date
2017

Document Version
Final published version

Citation (APA)
Feng, Q. (2017). *Advanced Estimation of Credit Valuation Adjustment*. [Dissertation (TU Delft), Delft University of Technology]. https://doi.org/10.4233/uuid:4bc92859-1268-489a-b919-84ba827e65f6

ADVANCED ESTIMATION OF CREDIT VALUATION ADJUSTMENT

Proefschrift

ter verkrijging van de graad van doctor
aan de Technische Universiteit Delft,
op gezag van de Rector Magnificus prof. ir. K. C. A. M. Luyben,
voorzitter van het College voor Promoties,
in het openbaar te verdedigen op dinsdag 4 april 2017 om 15:00 uur

door

Qian FENG

Master of Science in Applied Mathematics
Technische Universiteit Delft, Netherlands
geboren te Qiqihar, China.

This dissertation has been approved by the

promotor: Prof. dr. ir. C. W. Oosterlee

Composition of the doctoral committee:

Rector Magnificus,	chairman
Prof. dr. ir. C. W. Oosterlee	promotor
Prof. dr. B. D. Kandhai	Universiteit van Amsterdam

Independent members:

Prof. dr. R. Feng	University of Illinois at Urbana-Champaign, USA
Prof. dr.rer.nat. M. Ehrhardt	Bergische Universität Wuppertal, Germany
Prof. dr. D. Crommelin	Universiteit van Amsterdam
Prof. dr. ir. P. H. A. J. M. van Gelder	Techniek, Bestuur en Management, TU Delft
Prof. dr. ir. G. Jongbloed	Elektrotechniek, Wiskunde en Informatica, TU Delft

Keywords: Credit valuation adjustment (CVA), expected exposure (EE), potential future exposure (PFE), Bermudan option, wrong way risk (WWR), Monte Carlo simulation, least-squares method, bundling.

Printed by: IPSKAMP printing

Front & Back: Beauty in simplicity

ISBN 978-94-028-0589-5

An electronic version of this dissertation is available at
http://repository.tudelft.nl/.

Acknowledgments

This dissertation concludes my Ph.D research work in the project *Advanced Estimation of Credit Valuation Adjustment*, financially supported by the Dutch Technology Foundation STW. My work was carried out between December 2012 to December 2016 within the Scientific Computing group at Centrum Wiskunde & Informatia (CWI).

Above all, my most sincere gratitude goes to my supervisor and promotor prof. Kees Oosterlee. Throughout the past four years, I've learned greatly from Kees' patient guidance, encouragement and advice. Kees guided me to see the insight in problems, responded to my questions promptly and offered me valuable advice.

I would like to thank all my colleges in CWI for spending a great time together. I will miss the discussions at the fancy library coffee machine. I would like to thank Nada Mitrovic for all kinds of help and Duda Tepsic for her IT support. I also would like to thank my colleges in the Scientific Computing group: Álvaro Leitao, Anton van der Stoep, Zaza van der Have, Ki Wai Chau, Francisco Gaspar, Prashant Kumar, Laurent van den Bos, Svetlana Dubinkina, Sirshendu Misra, Benjamin Sanderse, Sangeetika Ruchi, Anne Eggels, Krzysztof Bisewski, Debarati Bhaumik, Bart de Leeuw, Nick Verheul, Barry Koren, Daan Crommelin and Jason Frank.

I also want to express my gratitude to Kees' former PhD students, Shashi Jain, Patrik Karlsson, Marjon Ruijter and Lech Grzelak. They offered me lots of help to understand the algorithms employed and developed in my research work. Marjon and Lech shared their MATLAB codes for the COS method. Shashi, as the initial developer of the Stochastic Grid Bundling Method, helped me to learn about the algorithm and his codes and provided insightful advice for my further research. Besides, Shashi and Patrik cooperated with me during my internship in ING. My research work couldn't be done without the knowledge shared by Kees' former students.

I would like to thank Kees de Graaf and Drona Kandhai. As the two PhD students under the same research project, Kees and me spent lots of nice time together for studying and cooperating. It is very lucky for me to have a company on the way of pushing our limits. Drona, in addition to his academy career, is also an experienced practitioner in the ING bank. Drona offers Kees and me the opportunity to talk to the quantitative analysts in the ING bank. We learned a lot via the meetings and discussions with these quants who know the market and the Basel regulations.

In addition, I want to thank the whole CVA team in the ING bank for the regular meetings, discussions and suggestions to my research work. I did a three-month internship in this team and it is a precious experience for me.

Finally, I want to thank my parents, my brother and my boyfriend. They always cheer me up and offer unconditional support whenever I need them.

Qian Feng
Amsterdam, November 2016

Summary

The financial crisis of 2007-2008 is considered as one of the worst economic disasters since the Great Depression of the 1930ties. Triggered by the US housing bubble, the crisis became global and threatened large well-known financial institutions. National governments needed to bail out some institutions to prevent their collapse.

This crisis has changed the financial modeling and risk management significantly. In particular, the requirements of understanding and managing so-called counterparty credit risk, has been emphasized by the banking regulators.

Regarding financial transactions, we distinguish exchange-traded and so-called over-the-counter (OTC) transactions. Exchange-traded deals are regulated and as such secured by, for example, a clearing house (which may compensate losses when a counterparty of a transaction would default). This is not the case for OTC transactions, that take place directly between two parties. When in this situation the counterparty of a transaction defaults, losses are not compensated and can be huge.

Counterparty credit risk (CCR) is the risk that a party, in an OTC financial derivatives contract, may fail to respect its obligations, causing significant losses to the other party. A bank is required by the financial regulator to set a certain amount of capital aside to buffer for the default risk of all counterparties in its portfolio. The framework on how banks must calculate the required capital is established by the Basel Accords-Basel I, Basel II and Basel III-issued by the Basel Committee on Banking Supervision (BCBS).

In the Basel II framework, financial institutions are required to hold capital against the variability in the market value of their portfolio. Credit exposure to a counterparty at a future time is the positive mark-to-market value of the portfolio of derivatives with this counterparty. The amount of exposure is uncertain due to the volatility in the market. There are several measures of CCR, such as the potential future exposure (PFE), expected exposure (EE), and so on. A key step of calculating these statistics is to build the future distributions of exposure based on a simulation of the market variables under the historical probability measure. The exposure on the scenarios, instead, has to be computed under the risk-neutral probability measure as it is related to the market price of financial derivatives. The computational complexity arises due to the change of probability measure. Since the calculation may require sub simulations, the number of real-world scenarios generated, limited by the computational capability, can be unreasonably low. Efficient algorithms for computing the exposure profiles are really needed in practice.

In response to the revealed deficiencies in banking regulations during the financial crisis, BCBS published Basel III to work alongside with Basel II. In Basel III, a new risk capital charge against the variability in credit valuation adjustment (CVA) , namely the CVA risk capital charge, is introduced.

CVA is an adjustment to the risk-free value of OTC deals to take into account the risk of counterparty default. CVA is commonly regarded as the market value of CCR. It was found that the majority of the losses related to CCR during the financial crisis came from the fair value adjustments on derivatives. The Basel III CVA risk capital charge is

set against the mark-to-market losses associated to the CVA volatility.

CVA can be quite complex and difficult for valuation. Modeling CVA requires at least three components: the exposure profile, the default probability of the counterparty and the loss given default. Thus, compared to the risk statistics of exposure in Basel II, CVA does not only depend on the exposure but also on the credit quality of the counterparty. The dependence between exposure and the counterparty's default probability can also make a significant contribution to CVA. So-called wrong-way risk (WWR) occurs when the exposure profile and the credit quality of the counterparty are adversely correlated.

From the perspective of risk management, the measurements of CVA risk in Basel III are CVA Value-at-Risk (VaR) and CVA Expected Shortfall (ES). CVA VaR and CVA ES may require even sub-sub-simulations, which makes the calculation of the CVA measures even more complicated.

This thesis deals with these computational problems in the pricing and measurement aspects of CCR. We employ and develop further the *Stochastic Grid Bundling Method* (SGBM), which is based on simulation, bundling and regression, to avoid the sub-simulation in the calculation of exposure profiles. We also attempt to build models for WWR to study the impact of dependence between the counterparty default and exposure to a counterparty on CVA. To provide a benchmark, we develop further the COS method, based on Fourier-cosine expansions and Fast-Fourier transformation (FFT), for the calculation of the exposure profiles. The financial derivatives we consider are option contracts, the underlyings of which are equities or also interest rate swaps. We pay special attention to options with early-exercise features, like in particular, the Bermudan-style option. The default likelihood is modeled by an intensity model, which is also called the reduced-form model. We will set the intensity as constant in the first few chapters and later model it as a stochastic variable to incorporate WWR.

As the introductory chapter, Chapter 1 presents an overview of the risk measures for CCR and CVA in mathematical formulation, and explains the risk-neutral valuation problem on simulated scenarios in detail. We describe the basic technique of the Stochastic Grid Bundling Method (SGBM). Using a simple numerical example, we demonstrate the convergence and error analysis for SGBM. The results show that SGBM converges as the number of bundles goes to infinity and the number of paths within each bundle goes to infinity too. The SGBM approach will be developed towards an efficient algorithm for computing exposure profiles avoiding sub-simulation in the chapters to follow.

Chapter 1 also describes the connection between the discounted characteristic function and the associated discounted density function, and between the discounted characteristic function and the corresponding moments. Using the former property, we can employ the Fourier-transform technique to obtain the discounted density. Using the latter relations, we are able to find analytic formulas for the corresponding moments needed in the Stochastic Grid Bundling Method.

Chapter 2 demonstrates three numerical approaches, SGBM, the COS method and the Finite Difference method, for computing the future exposure distributions of a Bermudan option contract under the risk-neutral probability measure for CVA under the Heston's stochastic volatility model. We study the impact of the stochastic volatility on the right-tail of the risk-neutral exposure distributions.

In Chapter 3, the SGBM algorithm is further developed for computing the risk-neutral

exposure of Bermudan options with stochastic interest rate and stochastic volatility under so-called hybrid asset models. SGBM's bundling techniques in case of two- or three-dimensional variables are discussed in detail. The sensitivities of expected exposure can be computed in SGBM as a by-product. The tail behavior of the exposure distributions under different hybrid models are compared.

In the following Chapter 4, models for WWR are proposed. The intensity model representing the credit quality of a counterparty is modeled as a stochastic process under the risk-neutral probability measure. We provide an alternative way of computing CVA of an option contract in the case of WWR by taking the difference between the default-free and the default-adjusted values of the contract. By varying the occurring correlation coefficients between the asset price and the firm's default probability, we study the impact of WWR on CVA. An additional contribution in this chapter is the study of the impact of CCR and WWR on the optimal early-exercise boundary of Bermudan options.

In Chapter 5, we consider the practical issue of computing the risk statistics of future exposure distributions. In back-testing and stress testing, the historical probability measure induced by the calibrated asset model may be not equivalent to the risk-neutral probability measure dynamics. The exposure distribution at some future time has to be valued on asset paths under the induced historical probability measure, whereas the valuation of exposure values should be performed under the risk-neutral probability measure. SGBM enables the risk-neutral valuation of exposure values at the real-world simulations, based on only one set of risk-neutral scenarios without any sub-simulation, and hence can significantly enhance the efficiency.

This thesis demonstrates that SGBM is a robust, accurate and efficient method for computing exposure distributions under the real-world probability measure for risk measurement of CCR and under the risk-neutral probability measure for pricing CCR (CVA). It is highly adaptive to hybrid models and efficient with the basic techniques of bundling and local regression. We show its accuracy by comparing to the COS method via numerical examples.

Samenvatting

De financiële crisis in 2007-2008 wordt gezien als één van de grootste economische rampen sinds de crisis van de jaren dertig. De kredietcrisis ontstond in de Verenigde Staten door het knappen van de huizenbubbel, waarna het een wereldwijde crisis werd die het voortbestaan van grote bekende financiële instellingen bedreigde. Nationale overheden moesten financiële steun verlenen aan een aantal van deze instellingen om ze overeind te houden.

Deze crisis heeft de financiële modellen en het risicobeheer aanzienlijk veranderd. In het bijzonder wordt er door de toezichthouders nadruk gelegd op het beoordelen en het beheren van het kredietrisico ten aanzien van de tegenpartij.
Financiële transacties kunnen op de beurs en onderhands plaats vinden. Deze laatste groep transacties wordt over-the-counter (OTC) transacties genoemd. De beurstransacties worden gereguleerd en daarmee ook verzekerd door bijvoorbeeld een centrale tegenpartij. Deze partij compenseert wanneer er sprake is van wanbetaling. OTC-transacties vinden direct plaats tussen twee partijen, waardoor er geen centrale partij is die garant staat. Doordat eventuele wanbetaling niet gecompenseerd wordt, is er risico op grote verliezen.

Counterparty credit risk (CCR) is het risico dat een partij in een OTC-transactie zijn verplichtingen niet nakomt, waardoor de andere partij mogelijk veel geld verliest. Vanwege dit risico stelt de toezichthouder een bank verplicht om voor elke tegenpartij in zijn portfolio een bepaald bedrag te reserveren. In de Baselze Akkoorden-Basel I, Basel II en Basel III-uitgegeven door het Basel-Comité is vastgelegd hoe banken de grootte van deze verplichte buffer moeten berekenen.

In Basel II is vastgelegd dat financiële instellingen kapitaal moeten vasthouden om de variabiliteit van de marktwaarde van hun portfolio op te vangen. Toekomstige blootstelling aan kredietrisico van een tegenpartij is de positieve mark-to-market waarde van het portfolio van derivaten met deze tegenpartij. De grootte van de blootstelling is onzeker door de volatiliteit van de markt. Er zijn verschillende maten om de CCR te meten, zoals bijvoorbeeld de potential future exposure (PFE) en de expected eposure (EE). Een belangrijke stap in het berekenen van deze statistische waarden is het bepalen de kansverdeling van de toekomstige risico's met behulp van simulaties van marktvariabelen onder de historische kansmaat. De risicoblootstelling in de simulaties moet daarentegen onder de risico-neutrale maat bepaald worden, omdat het samenhangt met de marktwaarde van financiële derivaten. Deze verschillende kansmaten maakt de berekeningen complex. Omdat er mogelijk sub-simulatie nodig is in de berekeningen, kunnen er relatief weinig realistische simulaties uitgevoerd worden. Om de benodigde rekencapaciteit laag te houden zijn er voor praktische doeleinden efficiënte methoden nodig.

Tijdens de kredietcrisis zijn verscheidene tekortkomingen in de toezichthouding op banken waargenomen. Hierop is naast Basel II, ook Basel III uitgegeven. Hierin is opgenomen dat de financiële instellingen ook het risico in de variabiliteit in credit valuation adjustment (CVA) moeten indekken.

CVA is een aanpassing aan de risico-neutrale waarde van OTC-transacties waarbij rekening wordt gehouden met het risico op wanbetaling van de tegenpartij. CVA wordt ook wel gezien als de marktwaarde van CCR. Tijdens de crisis werd de meerderheid van de verliezen met betrekking tot CCR veroorzaakt door deze aanpassing aan de waarde van derivaten. De CVA buffer moet de mark-to-market verliezen die voortkomen uit de volatiliteit van de CVA opvangen.

CVA is complex en kan het waarderen bemoeilijken. Het modelleren van CVA bestaat uit minstens drie componenten: de risicoblootstelling, de kans op wanbetaling door de tegenpartij en het verlies bij wanbetaling. Vergeleken met Basel II wordt er dus niet alleen naar risicoblootstelling, maar ook naar de kredietwaardigheid van de tegenpartij gekeken. De afhankelijkheid tussen de risicoblootstelling en de kans op wanbetaling draagt ook zeker bij aan CVA. Wrong-way risk (WWR) treedt op als de risicoblootstelling en de kredietwaardigheid van de tegenpartij negatief gecorreleerd zijn.

In risicobeheer wordt het CVA-risico in Basel III gegeven door de Value-at-Risk (VaR) en Expected Shortfall (ES) van CVA. Het waarderen van deze maten vereist sub-sub-simulatie, wat het berekenen van CVA nog moeilijker maakt.

Dit proefschrift behandelt deze berekeningsproblemen in het prijzen en meten van aspecten van de CCR. We (door)ontwikkelen de *Stochastic Grid Bundling Method* (SGBM). Deze methode voorkomt sub-simulatie door in de simulaties gebruik te maken van bundel- en regressietechnieken in de berekening van de risicoblootstelling. We proberen ook WWR-modellen te construeren, om zo de gevolgen van de afhankelijkheid tussen wanbetaling van en de risicoblootselling aan een tegenpartij op CVA te bepalen. Om referentiewaarden te vinden gebruiken we de COS methode. Deze methode gebruikt Fourier cosinustransformaties en Fast Fouriertransformaties. De financiële derivaten die we beschouwen zijn optiecontracten, maar ook rente-swaps, en als onderliggende gebruiken we aandelen. In het bijzonder letten we op opties met vervroegde uitoefeningsmogelijkheden, zoals Bermuda-achtige opties. De waarschijnlijkheid op wanbetaling wordt gemodelleerd met een intensiteitsmodel. De intensiteit wordt in de eerste hoofdstukken constant genomen en later als een stochastische variabele beschouwd om zo ook WWR mee te nemen.

De inleidende hoofdstuk, Hoofdstuk 1, geeft een wiskundig overzicht van risicomaten voor CCR en CVA. Ook wordt in dit hoofdstuk in detail uitgelegd wat de uitdagingen zijn bij risico-neutrale waardebepalingen van gesimuleerde scenario's. We beschrijven de basistechnieken van de SGBM. Met behulp van een eenvoudig voorbeeld demonstreren we de convergentie en foutenanalyse voor SGBM. De resultaten tonen aan dat SGBM convergeert als zowel het aantal bundels als het aantal paden per bundel naar oneindig gaat. In de verdere hoofdstukken wordt deze methode verder ontwikkeld naar een efficiënt algoritme dat zonder sub-simulatie de risicoblootstelling berekend.

Ook beschrijft Hoofdstuk 1 de relatie tussen de verdisconteerde karakteristieke functie, de bijbehorende verdisconteerde dichtheidsfunctie en de daarbij horende momenten. Hieruit volgt dat we Fouriertransformaties kunnen toepassen om de verdisconteerde kansdichtheid te bepalen. Dankzij deze relaties zijn we ook in staat om analytische formules te bepalen voor de momenten die we nodig hebben in de SGBM.

In Hoofdstuk 2 worden er drie numerieke methoden gedemonstreerd, namelijk de SGBM, de COS methode en de eindige-differentiemethode. In deze demonstratie be-

rekenen we de kansdichtheid van de toekomstige risicoblootstelling van een Bermuda optie onder de risico-neutrale maat voor CVA onder de stochastische volatiliteitsmodel van Heston. We bestuderen het effect van de stochastische volatiliteit op de rechter staart van de risico-neutrale risicoblootstellingsverdeling.

De SGBM wordt verder ontwikkeld in Hoofdstuk 3 om de risico-neutrale risicoblootstelling te berekenen van Bermuda opties met stochastische rente en stochastische volatiliteit onder hybride aandeelmodellen. De bundeltechnieken van de SGBM in het geval van twee- of driedimensionale variabelen worden bediscussieerd. Daarnaast kan met de SGBM ook een gevoeligheidsanalyse op de verwachte blootstelling aan kredietrisico uitgevoerd worden. De eigenschappen in de staart van de blootstellingsverdeling onder verschillende hybride modellen worden vergeleken.

Verschillende modellen voor WWR worden voorgelegd in Hoofdstuk 4. Het intensiteits model modelleert de kredietkwaliteit van een tegenpartij als een stochastisch proces onder de risico-neutrale maat. We verstrekken een alternatieve manier om de CVA van een optie in het geval van WWR te berekenen. Hierbij nemen we het verschil tussen de waarde waarbij geen rekening wordt gehouden met wanbetaling en de waarde waarbij de kans op wanbetaling wel is meegenomen. Door te variëren in de voorkomende correlatiecoëfficiënt tussen de aandeelprijs en de kans op wanbetaling door de tegenpartij, kunnen we de gevolgen van WWR op CVA bestuderen. Daarnaast bestuderen we in dit hoofdstuk ook het effect van CCR en WWR op de optimale uitoefeningsgrens van Bermuda opties.

In Hoofdstuk 5 beschouwen we het praktische probleem van het berekenen van de risicostatistieken van toekomstige risicoblootstellingverdelingen. Door achteraf te testen en met stresstesten kan het zijn dat de historische kansmaat gevonden met het gekalibreerde aandeelmodel niet gelijk is aan de risico-neutrale kansmaat. De blootsellingsverdeling op een toekomstig moment moet gewaardeerd worden op aandeelpaden onder de gevonden historische kansmaat, terwijl de waardering van de risicoblootstelling onder de risico-neutrale maat moet worden bepaald. Met SGBM is het mogelijk om de risico-neutrale waarde van risicoblootstellingen in realistische simulaties te bepalen, waarbij we slechts één verzameling risico-neutrale scenario's en géén sub-simulatie gebruiken. Hierdoor kan een hoge efficiëntie bereikt worden.

Dit proefschrift toont aan dat SGBM een robuuste, nauwkeurige en efficiënte methode is voor het berekenen van risicoblootstellingsverdelingen onder de marktmaat voor risicobeheer van CCR en onder de risico-neutrale maat voor het waarderen van CCR (CVA). De methode is goed aan te passen voor hybride modellen en efficiënt dankzij de bundel- en lokale regressietechnieken. In numerieke voorbeelden wordt de nauwkeurigheid van SGBM aangetoond door de resultaten te vergelijken met die van de COS methode.

Contents

CHAPTER 1

Introduction

Counterparty credit risk (CCR) is the risk arising from the possibility that a counterparty may default prior to the expiration of a financial contract and fails to fulfill the obligations. Following the CCR capital requirements in the Basel II and Basel III regulatory accords, banks have to hold a certain regulatory amount of capital to buffer the future losses due to CCR. These capital requirements are set to ensure that banks are able to cover the risk of counterparty default by setting capital aside. Pricing and measuring CCR is computationally intensive, since Monte Carlo simulation is typically used to build a large number of scenarios, and valuation on each scenario at each simulated path is needed.

We are going to deal with this computational challenge by developing an algorithm for efficient calculation of exposure profiles based on the so-called *Stochastic Grid Bundling Method* (SGBM). SGBM is based on simulation, bundling and regression techniques [50]. In this introductory chapter, we will introduce SGBM via simple examples, and present its characteristics regarding convergence and error analysis.

In this thesis, we will focus on the CCR arising from OTC (over-the-counter) derivatives. A *derivative* is a contract that derives its value from the performance of an underlying asset [47]. The most common underlying assets are stocks, bonds, currency exchange rates and market indexes. Some derivatives are traded on an exchange, and some are traded OTC. Exchange traded deals are regulated and as such secured by, for example, a clearing house (which may compensate losses when a counterparty of a transaction would default). This is not the case for OTC transactions, that take place directly between two parties. When in this situation the counterparty of a transaction defaults, losses are not compensated and can be huge.

A significant amount of derivatives are traded OTC. The future value of an OTC derivatives contract varies with the level of the underlying(s) and possibly also with decisions made by the parties in the contract.

We will start with an overview of valuation of CCR in mathematical formulation, and present the general framework of SGBM, which will be further developed under various models for different financial contracts in subsequent chapters.

1.1. Quantifying CCR

Credit *exposure* (simply known as exposure) defines the potential loss in the event of a counterparty default. For many financial instruments, notably derivatives, the creditor is not at risk for the full principle amount of the trade but only for the *replacement costs* [38]. Consequently, the exposure to the counterparty is equal to the maximum of the contract value and zero.

1

Exposure is uncertain since the mark-to-market value of a contract varies with the movement of the market. We can use some statistics of the exposure distribution, such as the mean or a high quantile, as the measures of CCR for capital requirements. The exposure distribution is built on a Monte Carlo path simulation that can reflect the evolution of the market variables, i.e. the simulation must be done under the so-called real-world probability measure. The key point in determining these risk statistics for CCR is to perform the risk-neutral valuation of the portfolio on the real-world scenarios.

Credit valuation adjustment (CVA) measures the CCR from a pricing point of view. CVA is the difference between the risk-free portfolio value and the true value that takes CCR into account. In short, CVA is the market value of CCR [7]. CVA is determined by the value of the underlying contract, the default probabilty of counterparty, as well as the loss given default (LGD) given as a percentage [38]. We will study the so-called unilateral CVA in this thesis. 'Unilateral' means that a party considers only the CCR of the other party in the contract, and not its own risk of default. The complexity in computing CVA arises from the computation of the exposure profiles, modeling of the default probability, and the correlation between these two components.

We will build the mathematical framework of quantifying counterparty credit risk and give the mathematical formulation of the exposure measures in this section .

1.1.1. EE AND PFE

Given a complete probability space $(\Omega, \mathscr{F}, \mathbb{P})$ on a finite time horizon $[0,T]$, where Ω is the sample space, $\mathscr{F}$ is the sigma algebra of all events at time T, and $\mathbb{P}: \mathscr{F} \to [0,1]$ is a probability measure. Define a stochastic process $\{\mathbf{X}_t : t \in [0,T]\}$ on the probability space $(\Omega, \mathscr{F}, \mathbb{P})$, where for each $t \in [0,T]$, $\mathbf{X}_t : \Omega \to \mathbb{R}^n$ is a random variable on Ω. Let $\{\mathscr{F}_t, t \in [0,T]\}$ denote the filtration generated by $\{\mathbf{X}_t, t \in [0,T]\}$, i.e. $\mathscr{F}_t = \sigma(\mathbf{X}_s, s \in [0,t])$ [68].

In an arbitrage-free economy, there exists an equivalent *risk-neutral* measure denoted by $\mathbb{Q}: \mathscr{F} \to [0,1]$, such that a price associated to any attainable claim is computed as the expectation of a discounted value under this probability measure. We choose the risk-neutral measure $\mathbb{Q}$ with numéraire $B_t = \exp\left(\int_0^t r_s ds\right)$, where $\{r_s, s \in [0,t]\}$ is the *risk-neutral short rate*. The numéraire B_t represents the bank savings account with $B_0 = 1$. When the short rate $r_t = r$ is a constant, the associated bank account becomes a deterministic function w.r.t. time and we will denote it by $B(t) = \exp(rt)$ [68].

Assume that $\{\mathbf{X}_t, t \in [0,T]\}$ is a *Markov* process hence we have $\mathbb{E}^{\mathbb{Q}}[\cdot|\mathscr{F}_t] = \mathbb{E}^{\mathbb{Q}}[\cdot|\mathbf{X}_t]$. Let T be the maturity time for a position, and the associated discounted and added random cash flows at time $t \le T$ be denoted by $\Pi(t,T)$. The exposure at time t for this position is given by

$$E_t := \left(\mathbb{E}^{\mathbb{Q}}\left[\Pi(t,T)\middle|\mathbf{X}_t\right]\right)^+, \tag{1.1}$$

which $E_t : \Omega \to \mathbb{R}^+ \cup \{0\}$ is a random variable on the sample space Ω and the operator $(\cdot)^+$ returns the greater value of zero and the value inside the brackets.

The Basel II accords give specific definitions for the exposure measures regarding the future credit risk [4], including potential future exposure (PFE), expected exposure (EE).

PFE measures the exposure estimated to occur at a future date at a high confidence level, like 97% or 99% [4]. It is defined as a high quantile of the exposure distribution

under the real-world probability measure $\mathbb{P}$. At a fixed time $t \in [0, T]$, the value of PFE is defined by

$$\text{PFE}_\alpha(t) = \inf\left\{ y \middle| \mathbb{P}\left(\{w : E_t(w) < y\}\right) \geq \alpha \right\}, \tag{1.2}$$

where $E_t(w) = \left(\mathbb{E}^{\mathbb{Q}}\left[\Pi(t,T)\middle|\mathbf{X}_t(w)\right]\right)^+$ with $w \in \Omega$ and α is the confidence level.

The maximum PFE (MPFE) is used to measure the peak value of the PFE over the time horizon $[0, T]$ [4], given by

$$\text{MPFE}_\alpha = \max_{t\in[0,T]} \text{PFE}_\alpha(t). \tag{1.3}$$

EE is the probability-weighted average exposure at a future date. At a fixed time $t \in [0, T]$, $\text{EE}(t)$ is given by

$$\text{EE}(t) = \mathbb{E}^{\mathbb{P}}\left[E_t\right] = \mathbb{E}^{\mathbb{P}}\left[\left(\mathbb{E}^{\mathbb{Q}}\left[\Pi(t,T)\middle|\mathbf{X}_t\right]\right)^+\right] = \int_\Omega E_t(w)d\mathbb{P}(w), \tag{1.4}$$

with $w \in \Omega$.

Expected positive exposure (EPE) is the time-weighted average of EE estimated on a given forecasting horizon (e.g. one year) [4]. Over a future horizon $[t_1, t_2]$, the value of EPE is given by:

$$\text{EPE}(t_1, t_2) = \frac{1}{t_2 - t_1}\int_{t_1}^{t_2} \text{EE}(s)ds. \tag{1.5}$$

1.1.2. MODELING THE DEFAULT PROBABILITY

A key component in quantifying the counterparty risk is to estimate the default probabilities for counterparties that a bank is exposed to. The default probability of a counterparty is associated with its survival probability. The survival probability $\text{PS}(t)$ gives the probability of no default prior to a certain time t, and the value $\text{PD}(t)$ represents the cumulative default probability prior to a certain time t. There are multiple ways of estimating the default probabilities and here we present a brief review.

The historical default probabilities are obtained via historical data of default events. A firm's credit rating reflects the evaluation of the credit risk of this firm. Agencies such as Moody's Investors Service and Standard & Poor's Corporation publish cumulative default probabilities by rating grades (Triple A, Double A, Single A, Triple B and so on) based on years of data. The historical default probability measures the likeliness of default under the real-world probability measure [38].

The so-called *equity-based approach*, also called the *firm's value approach* or the *structural approach*, estimates the default probability based on stock market information. This approach of assessing credit risk involves the Merton's model [67]. It is assumed that the value of a firm (asset value) is stochastic and that default is related to the firm's asset development. The original Merton model assumes that a firm has issued zero-coupon bonds and default occurs when the firm value is less than this liability when the issued zero-coupon bond matures. Merton's model does not allow for a premature default, in the sense that the default may only occur at the maturity of the claim. Black and Cox [9] assume a barrier representing safety covenants for the firm and default is triggered by the firm value hitting this barrier from above.

1

The market-implied default probabilities are obtained via the credit default swap (CDS) market or via its risky bonds, modeled by an *intensity model*, or known as the *reduced-form model*. In this approach, the default probability is defined by means of the *intensity* (or the *hazard rate*) of a default. The intensity model was used for pricing credit risky securities (or corporate bonds), see work done by Jarrow and Turnbull [52], by Madan and Unal [66], and by Lando [59]. Duffie and Singleton [27] present an approach to modeling the term structure of credit risky bonds and other claims. Bielecki and Rutkowski [8] give a detailed discussion of the filtration in the intensity modeling.

We choose to use the intensity model for describing the default probability in this thesis because of its properties. First of all, modeling the credit quality by the intensity allows for dependence between market risk factors and credit factors. For instance, Brigo et al. [12] present a framework with a correlation between the default probability and the interest rate. Second, it is known that the CDS premium contains information about the term structure with tenors, and Duffie and Singleton [27] present a way of modeling it using intensity. Third, the intensity can be retrieved from the market price of risky bonds or CDS contracts, so we can estimate the relevant parameters under the risk-neutral probability measure. This will be of a great help when pricing CCR.

The intensity may be deterministic or stochastic, and the latter case may capture the uncertainty in the credit quality of the associated counterparty. Here, we consider the case that the intensity is *constant* over time. The relation between a constant intensity ($\bar{h}$) and the survival probability is given by

$$\mathrm{PS}(t) = \exp\left(-\bar{h}t\right), \quad \mathrm{PD}(t) := 1 - \mathrm{PS}(t). \tag{1.6}$$

where these probabilities are measured under the risk-neutral probability measure $\mathbb{Q}$ as they are obtained via risk-neutral pricing formulas.

When assuming the intensity constant and the CDS curve is flat, there is an approximate relation between the default probability between zero to time T and the CDS premium for maturity T [38]:

$$\mathrm{PD}(T) = 1 - \exp\left(-\frac{X_T^{CDS}}{\mathrm{LGD}}T\right), \tag{1.7}$$

where X_T^{CDS} is the CDS premium with the maturity T, and LGD is the loss given default.

1.1.3. LOSS GIVEN DEFAULT

Loss given default (LGD) is usually defined as the percentage of exposure the bank might loose if a counterparty defaults [38]. When the counterparty defaults, the bank will usually be able to recover some percentage of the outstanding amount. The recovered percentage is termed the *recovery rate*. The two quantities are related via

$$\mathrm{LGD} = 1 - \text{recovery rate}. \tag{1.8}$$

which tells that a low recovery rate implies a high LGD.

Recovery values tend to show significant variation over time and recoveries also tend to be negatively correlated with the default likeliness [38], which means that a high default rate may often give rise to lower recovery rate.

In this thesis, we assume that the LGD is constant and focus on the computation of exposure and the modeling of default probabilities instead.

1.1.4. CVA, WRONG-WAY RISK, CVA VaR AND CVA ES

CVA is an adjustment to the fair value of a derivatives contract to account for CCR. In short, CVA is the price of CCR [7]. The complexity of computing CVA arises from the movements in the counterparty credit spreads as well as in the market factors of the underlying asset. The BCBS (Basel Committee on Banking Supervision) introduced the CVA variability charge in Basel III, to capitalize the risk of future changes in CVA [7].

Since it is the market price of counterparty default risk, CVA must be computed under the risk-neutral measure. Denoting the time of a counterparty default by τ, unilateral CVA is the risk-neutral expectation of the discounted loss, written as [87]:

$$\text{CVA}(0) = \text{LGD} \cdot \mathbb{E}^{\mathbb{Q}} \left[\mathbb{1}(\tau < T) \frac{E_\tau}{B_\tau} \right] = \text{LGD} \int_0^T \mathbb{E}^{\mathbb{Q}} \left[\frac{E_t}{B_t} \middle| \tau = t \right] d\text{PD}(t), \tag{1.9}$$

where the loss given default (LGD) is the fraction of the asset that is lost when the counterparty defaults, and $\text{PD}(t)$ is the risk-neutral probability of counterparty default between time zero and time t.

The expectation behind the second equality sign in (1.9) is conditional on the fact the counterparty default occurs at time $\tau = t$ [87]. This conditioning will give a non-negligible contribution to the computed CVA value when there exists dependence between the exposure and the counterparty credit quality. The dependence is known as the *right/wrong-way risk*.

The so-called *wrong-way risk* (WWR) occurs when the exposure is adversely correlated with the credit quality, i.e. the exposure tends to increase when the counterparty credit quality becomes worse. Basel III classifies two types of WWR: general and specific WWR [5]. The former appears due to positive correlations of exposure and market factors, whereas the latter is due to a wrong structure of an investment when a connection exists between the counterparty and the underlying.

Equation (1.9) is greatly simplified by assuming independence between exposure and counterparty's credit quality. We define a quantity called the risk-neutral discounted expected exposure (EE^*) by:

$$\text{EE}^*(t) := \mathbb{E}^{\mathbb{Q}} \left[\frac{E_t}{B_t} \right] = \int_\Omega \frac{E_t(w)}{B_t(w)} d\mathbb{Q}(w), \tag{1.10}$$

which is independent of the counterparty default.

Assuming independence between exposure and counterparty's credit quality, equation (1.9) simplifies to:

$$\text{CVA}(0) = \text{LGD} \int_0^T \text{EE}^*(t) d\text{PD}(t) \approx \text{LGD} \sum_{j=0}^{M-1} \text{EE}^*(t_j) \big(\text{PD}(t_{j+1}) - \text{PD}(t_j) \big), \tag{1.11}$$

where $\{0 = t_0 < t_1 < \ldots < t_M = T\}$ is a fixed monitoring time grid, and a commonly used

way of approximating the default probability in the time interval $[t_j, t_{j+1}]$ is:

$$\mathrm{PD}(t_{j+1}) - \mathrm{PD}(t_j) = \exp\left(-\frac{X^{\mathrm{CDS}}_{t_j}}{\mathrm{LGD}}\, t_j\right) - \exp\left(-\frac{X^{\mathrm{CDS}}_{t_{j+1}}}{\mathrm{LGD}}\, t_{j+1}\right). \tag{1.12}$$

CVA VaR (Value-at-Risk) is defined in the same way as the VaR measure. It is the percentile of the loss due to the change in CVA given a confidence level. CVA ES (Expected Shortfall) is the average value beyond a certain percentile of the loss in CVA. Notice that these two measures are obtained via simulations under the real-world measure, while the market value of CCR (i.e. CVA) is computed under the risk-neutral probability measure. We will present details of these two quantities in Chapter 4.

1.1.5. MONTE CARLO SIMULATION AND COMPUTATIONAL COMPLEXITY

Computation of the exposure measures in section 1.1.1 requires the future real-world exposure distribution, and computing CVA in section 1.1.4 needs the risk-neutral exposure distribution. The exposure profiles are typically computed by Monte Carlo simulation, as follows [87]:

- Generate scenarios: these scenarios are generated under the real-world probability measure for risk statistics (EE, PFE and so on). For the purpose of calculating CVA, this simulation should be done under the risk-neutral probability measure;
- Perform valuation of exposure at each monitoring date for each scenario;
- Compute the required exposure measures.

For some financial contracts, a risk-neutral simulation may be required for risk-neutral valuation of the contract. In this case, in order to have the exposure profile, sub-simulation needs to be performed, initiated at each monitoring date on each scenario. Figure 1.1 illustrates sub-simulations on five real-world scenarios at a single future time. The number of scenarios may become unreasonably low, limited by the computational capability.

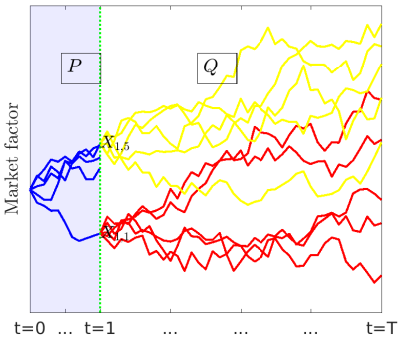

Figure 1.1: Sub-simulations.

This issue becomes more serious when dealing with the measures of the CVA risk. In order to compute the CVA VaR or CVA ES, one has to value the CVA on a set of paths that reflect the real-world market evolution. Sub-sub simulations may even be required for some financial contracts.

Another issue regarding CVA computation is how to take WWR into account. The Basel regulations have made it clear that banks must monitor, test and manage WWR in their portfolios. Different from the exposure risk statistics, CVA includes the default probability in the price of CCR. When WWR is present, the combined effects of uncertainties in the correlated exposure profiles and default probability may make significant contribution to CVA. The contribution of WWR is highly model-dependent.

We are concerned with these two problems in this thesis.

1.2. RISK NEUTRAL VALUATION OF OPTION CONTRACTS

An option is an agreement between two parties about trading an underlying asset at a certain future time. The *writer* of the option sells the option contract, and the party which purchases the option is the *holder*. The option holder has the right that the option contract grants until *maturity time* T. At the maturity time T, the option contract expires and the option becomes worthless for time later than T [76].

There are two basic types of options: The *call* option in which the holder has the right to *buy* the underlying for the *strike* K; The *put* option gives the holder the right to *sell* the underlying for the strike K.

The holder of the option can choose to *exercise* the option by buying or selling the underlying when $t \leq T$, or can choose to let the option expire when $t \geq T$ [76]. For *European options*, exercise is only permitted at expiry date T. *American options* can be exercised at any time until the expiration date. *Bermudan options* can be exercised at a set of dates up to expiration.

The price of a derivative is equal to the discounted risk-neutral expectation of future payoff in a complete market [47]. In this section, we present the pricing formulas of European and Bermudan options with an underlying stock from two perspectives.

1.2.1. FEYNMAN-KAC FORMULA

The *Feynman-Kac Formula* [68] implies that the expectation can be computed by partial differential equations (PDEs). In other words, the solution of an option pricing PDE can be represented as a risk-neutral discounted expectation of the final condition (the payoff).

Let stochastic process $\{\mathbf{X}_t, t \in [0,T]\}$ defined on probability space $(\Omega, \mathscr{F}, \mathbb{Q})$ be an Itô diffusion governed by a stochastic differential equation of the following form

$$d\mathbf{X}_t = \tilde{\mu}(\mathbf{X}_t)\,dt + \tilde{\sigma}(\mathbf{X}_t)\,d\mathbf{W}_t^{\mathbb{Q}}, \tag{1.13}$$

where $\mathbf{W}_t$ is a standard Brownian motion in $\mathbb{R}^n$ under the risk-neutral probability measure $\mathbb{Q}$; $\tilde{\mu} : \mathbb{R}^n \to \mathbb{R}^n$ and $\tilde{\sigma} : \mathbb{R}^n \to \mathbb{R}^{n\times n}$ satisfy the usual Lipschitz continuity conditions [68].

Let $g \in C_0^2(\mathbb{R}^n)$ and $q \in C(\mathbb{R}^n)$. Assume that q is bounded. A function $V : [0,T] \times \mathbb{R}^n \to$

$\mathbb{R}$ is defined as [68]

$$V(t,\mathbf{x}) = \mathbb{E}^{\mathbb{Q}}\left[\exp\left(-\int_t^T q(\mathbf{X}_s)\,ds\right) g(\mathbf{X}_T)\middle|\mathbf{X}_t = \mathbf{x}\right], \tag{1.14}$$

where $\mathbf{x} = [x_1, x_2, \ldots, x_n]^T \in \mathbb{R}^n$. Then the Feynman-Kack formula tells that V satisfies the following PDE,

$$\begin{aligned} \tfrac{\partial V}{\partial t} + \mathscr{A}V - qV = 0; \qquad & t \in [0,T], \mathbf{x} \in \mathbb{R}^n, \\ V(T,\mathbf{x}) = g(\mathbf{x}); \qquad & \mathbf{x} \in \mathbb{R}^n, \end{aligned} \tag{1.15}$$

where $\mathscr{A}$ is the generator of an Itô diffusion $\mathbf{X}_t$ given by

$$\mathscr{A}V = \sum_{j=1}^{n} \tilde{\mu}_j(\mathbf{x}) \frac{\partial V}{\partial x_j} + \frac{1}{2}\sum_{k=1}^{n}\sum_{j=1}^{n} \left(\tilde{\sigma}\tilde{\sigma}^T\right)_{k,j}(\mathbf{x}) \frac{\partial V^2}{\partial x_k \partial x_j}, \tag{1.16}$$

with $\tilde{\sigma}^T$ denotes the transpose matrix of $\tilde{\sigma}$ and $\left(\tilde{\sigma}\tilde{\sigma}^T\right)_{k,j}$ is the (k,j)-th element of the matrix.

The Feynman-Kac Formula thus implies that a function in the space $C^{1,2}(\mathbb{R}\times\mathbb{R}^n)$ which solves (1.15) must be the function defined by (1.14).

1.2.2. EUROPEAN OPTION

We use the notation S_t to represent the asset price at time t and $X_t = \log(S_t)$ (the log-asset price) is one of the elements in the vector $\mathbf{X}_t$. The value of a European option at time t which expires at maturity T is given by [47]

$$V(t,\mathbf{x}) = \mathbb{E}^{\mathbb{Q}}\left[\frac{B_t}{B_T} g(\mathbf{X}_T)\middle|\mathbf{X}_t = \mathbf{x}\right], \tag{1.17}$$

where $B_t = \exp\left(\int_0^t r_s ds\right)$ represents the bank savings account with the risk-free short rate r_s, $s \in [0,t]$; $g : \mathbb{R}^n \to \mathbb{R}^+ \cup \{0\}$ is the *payoff function* given by

$$g(\mathbf{X}_T) = \begin{cases} \max(S_T - K, 0), & \text{for a call,} \\ \max(K - S_T, 0), & \text{for a put.} \end{cases} \tag{1.18}$$

By the Feynman-Kac formula,the PDE describing the value of the European option is given by

$$\begin{aligned} &\frac{\partial V}{\partial t} + \mathscr{A}V - r_t V = 0; \quad t \in [0,T) \\ &V(T,\mathbf{x}) = g(\mathbf{x}). \end{aligned} \tag{1.19}$$

where r_t is the risk-free short rate at time t and the generator $\mathscr{A}$ is given by (1.16).

1.2.3. BERMUDAN OPTION

The holder of a Bermudan option has the right to exercise the option on any of the dates $\mathcal{T}_B = \{0 < T_1 < T_2 < \ldots < T_N = T\}$. For completeness we define $T_0 = 0$. When exercised at

time T_j, the immediate payoff of the option is given by $g\left(\mathbf{X}_{T_j}\right)$. A Bermudan option contract is an option to choose the exercise date T_j from different $j = 1,\ldots,N$ to maximize the option value.

Suppose that at any early-exercise date, the payoff function is given by $g(\mathbf{x}) \geq 0$. Find a stopping time ξ^* for the stochastic process $\{\mathbf{X}_t, t \in [0,T]\}$, with $\mathbf{X}_0 = \mathbf{x}$, such that the corresponding optimal expected payoff is given by [68]

$$V(0,\mathbf{x}) = \mathbb{E}^{\mathbb{Q}}\left[\frac{g\left(\mathbf{X}_{\xi^*}\right)}{B_{\xi^*}}\middle|\mathbf{X}_0 = \mathbf{x}\right] = \sup_{\xi\in\mathcal{T}_B}\mathbb{E}^{\mathbb{Q}}\left[\frac{g\left(\mathbf{X}_{\xi}\right)}{B_{\xi}}\middle|\mathbf{X}_0 = \mathbf{x}\right], \tag{1.20}$$

where the optimal early-exercise time is path-dependent, i.e. $\xi^* = \xi^*(w)$.

The Bermudan option pricing formula reads

$$V(T_j,\mathbf{X}_{T_j}) = \begin{cases} g(\mathbf{X}_{T_j}), & j = N, \\ \max\left(c(T_j,\mathbf{X}_{T_j}), g(\mathbf{X}_{T_j})\right), & j = N-1,\ldots,1, \\ c(0,\mathbf{X}_0), & j = 0. \end{cases} \tag{1.21}$$

with the *continuation function* defined by

$$c(T_j,\mathbf{x}) = \mathbb{E}^{\mathbb{Q}}\left[\frac{B_{T_j}}{B_{T_{j+1}}}V(T_{j+1},\mathbf{X}_{T_{j+1}})\middle|\mathbf{X}_{T_j} = \mathbf{x}\right], \quad j = 0,\ldots,N-1. \tag{1.22}$$

Using the Feynman-Kac formula, the PDE of the price of the Bermudan option is given by

$$\begin{aligned} &\frac{\partial V}{\partial t} + \mathscr{A}V - r_t V = 0, \quad t \in [T_j, T_{j+1}), \\ &V(T_j,\mathbf{x}) = \max\left(V(T_j^+,\mathbf{x}), g(\mathbf{x})\right), \quad j = 1,2,\ldots,N-1, \\ &V(T_N,\mathbf{x}) = g(\mathbf{x}), \quad T_N = T, \end{aligned} \tag{1.23}$$

where T_j^+ is the time point just before the early-exercise decision.

1.3. PROPERTIES OF DISCOUNTED CHARACTERISTIC FUNCTION

For option valuation, as well as for exposure computation, we deal with probability density function, that are often not known in closed form. Instead, we may reply on the characteristic function, which is the Fourier transform of the density function (often available in closed form).

In this section, we present two important properties of so-called *discounted characteristic functions*. The first property is the basis form for employing the Fourier-transformation technique to obtain the discounted density function, and the second property is useful within the Stochastic Grid Bundling method. Using the *discounted* characteristic function, we are able to perform the pricing directly under the risk-neutral probability measure without shifting to a forward-measure when dealing with a stochastic interest rate.

1

1.3.1. CHARACTERISTIC FUNCTION AND DENSITY FUNCTION

Given a Markov process $\{X_t \in \mathbb{R}^n, t \in [0,T]\}$ and consider a random variable $\mathbf{X}_{t_2}$ with $\mathbf{X}_{t_1} = \mathbf{x}$, $0 \le t_1 < t_2 \le T$. We define the *discounted characteristic function* (ChF), *discounted* at rate q, defined as:

$$\varphi(\mathbf{u}; t_1, t_2, \mathbf{x}) = \mathbb{E}^{\mathbb{Q}}\left[\exp\left(-\int_{t_1}^{t_2} q(\mathbf{X}_s)ds\right)\exp\left(i\mathbf{u}^T\mathbf{X}_{t_2}\right)\Big|\mathbf{X}_{t_1} = \mathbf{x}\right], \quad 0 \le t_1 < t_2 \le T, \tag{1.24}$$

where the vectors $\mathbf{u} = [u_1, u_2, \ldots, u_n]^T \in \mathbb{R}^n$ and $\mathbf{x} = [x_1, x_2, \ldots, x_n]^T \in \mathbb{R}^n$, i is the imaginary unit and the discount rate $q : \mathbb{R}^n \to \mathbb{R}$ is a function.

When the short rate is a stochastic process, the discount factor is a random variable which should therefore be placed under the expectation operator when computing the expectation of a discounted cash flow. In order to compute the discounted expectation of future option values, we will work with the *discounted density function*.

Define a random variable $z = \int_{t_1}^{t_2} q(\mathbf{X}_s)ds$, $0 \le t_1 < t_2 \le T$. Let $f_{\mathbf{X}_{t_2}, z|\mathbf{X}_{t_1}}(\mathbf{y}, z; \mathbf{x})$ be the *joint density* of $\mathbf{X}_{t_2}$ and z given $\mathbf{X}_{t_1} = \mathbf{x}$, and the associated *discounted density* is defined as its marginal probability function derived by integrating the joint density over $z \in \mathbb{R}$,

$$\widehat{f}_{\mathbf{X}_{t_2}|\mathbf{X}_{t_1}}(\mathbf{y}; \mathbf{x}) := \int_{\mathbb{R}} e^{-z} f_{\mathbf{X}_{t_2}, z|\mathbf{X}_{t_1}}(\mathbf{y}, z; \mathbf{x})dz. \tag{1.25}$$

Using (1.24) and (1.25), we have

$$\begin{aligned}
\varphi(\mathbf{u}; t_1, t_2, \mathbf{x}) &= \mathbb{E}^{\mathbb{Q}}\left[\exp\left(-\int_{t_1}^{t_2} q(\mathbf{X}_s)ds\right)\exp\left(i\mathbf{u}^T\mathbf{X}_{t_2}\right)\Big|\mathbf{X}_{t_1} = \mathbf{x}\right] \\
&= \int_{\mathbb{R}^n} \exp\left(i\mathbf{u}^T\mathbf{y}\right)\int_{\mathbb{R}} e^{-z} f_{\mathbf{X}_{t_2}, z|\mathbf{X}_{t_1}}(\mathbf{y}, z; \mathbf{x})dzd\mathbf{y} \\
&= \int_{\mathbb{R}^n} \exp\left(i\mathbf{u}^T\mathbf{y}\right)\widehat{f}_{\mathbf{X}_{t_2}|\mathbf{X}_{t_1}}(\mathbf{y}; \mathbf{x})d\mathbf{y}.
\end{aligned} \tag{1.26}$$

So, the discounted ChF is the Fourier transform of the discounted density function. We can use Fourier transformation techniques to recover the discounted density function from the corresponding discounted ChF.

1.3.2. CHARACTERISTIC FUNCTION AND MOMENTS

We use the multi-index notation $k = (k_1, k_2, \ldots, k_n)$ to represent the index when $\mathbf{X}_t = \left[X_t^{(1)}, X_t^{(2)}, \ldots, X_t^{(n)}\right]^T$, where k_1, k_2, ..., k_n are non-negative integers. Let the sum of the components be denoted by $|k| := k_1 + k_2 + \ldots + k_n$.

The power of $(\mathbf{X}_t)^k$ is thus defined by

$$(\mathbf{X}_t)^k := \left(X_t^{(1)}\right)^{k_1}\left(X_t^{(2)}\right)^{k_2}\cdots\left(X_t^{(n)}\right)^{k_n}, \tag{1.27}$$

with $k_1, k_2, \ldots k_n \in \mathbb{N}$.

The expression in (1.27) is a monomial with polynomial order $|k|$. It is easy to see that the total number of monomials with polynomial order $|k| \le d$ for $\mathbf{X}_t \in \mathbb{R}^n$ is $\frac{(d+n-1)!}{(n-1)!d!}$.

Over a time period $[t_1, t_2]$, $t_1 < t_2$, we define the k-th *discounted moment* by the expectation of random variable $(\mathbf{X}_{t_2})^k$ given information $\mathbf{X}_{t_1} = \mathbf{x}$, as:

$$\psi_k(\mathbf{x}, t_1, t_2) := \mathbb{E}^{\mathbb{Q}}\left[\exp\left(-\int_{t_1}^{t_2} q(\mathbf{X}_s)\,ds\right)(\mathbf{X}_{t_2})^k \,\middle|\, \mathbf{X}_{t_1} = \mathbf{x}\right], \tag{1.28}$$

which can be derived by the associated discounted ChF by the following equation

$$\psi_k(\mathbf{x}, t_1, t_2) = \frac{1}{(i)^{|k|}} \frac{\partial^{k_1}\varphi}{\partial u_1^{k_1}} \frac{\partial^{k_2}\varphi}{\partial u_2^{k_2}} \cdots \frac{\partial^{k_n}\varphi}{\partial u_n^{k_n}}(\mathbf{u}; t_1, t_2, \mathbf{x})\bigg|_{\mathbf{u}=0}, \tag{1.29}$$

where i represents again the imaginary unit and $\mathbf{u} \in \mathbb{R}^n$.

This relation is of great help when we employ the SGBM for deriving analytic formulas of discounted moments, in the regression phase.

1.3.3. ChF of Affine-diffusion processes

For the SDE given in (1.13), the affinity condition is satisfied when the coefficients in (1.13) are defined by:

$$\begin{aligned} \widetilde{\mu}(\mathbf{X}_t) &= K_0 + K_1\mathbf{X}_t, \quad K_0 \in \mathbb{R}^n, K_1 \in \mathbb{R}^{n\times n}, \\ (\widetilde{\sigma}(\mathbf{X}_t)\widetilde{\sigma}^T(\mathbf{X}_t))_{k,j} &= (H_0)_{k,j} + (H_1)_{k,j}\mathbf{X}_t, \quad H_0 \in \mathbb{R}^{n\times n}, H_1 \in \mathbb{R}^{n\times n\times n}, \\ q(\mathbf{X}_t) &= q_0 + q_1\mathbf{X}_t, \quad q_0 \in \mathbb{R}, q_1 \in \mathbb{R}^n, \end{aligned} \tag{1.30}$$

where $(\cdot)_{k,j}$ represents the (k, j) element in the corresponding matrix.

Duffie and Singleton [26] show that the ChF defined in (1.24) can thus be expressed as

$$\varphi(\mathbf{u}; t_1, t_2, \mathbf{x}) = \exp\left(\widetilde{A}(t_2 - t_1) + \mathbf{x}^T\widetilde{\mathbf{B}}(t_2 - t_1)\right), \tag{1.31}$$

where $\mathbf{X}_t = \mathbf{x}$ and the coefficients satisfy the following ODEs:

$$\begin{aligned} \frac{d\widetilde{\mathbf{B}}}{ds}(s) &= -q_1 + K_1^T\widetilde{\mathbf{B}}(s) + \frac{1}{2}\widetilde{\mathbf{B}}^T(s)H_1\widetilde{\mathbf{B}}(s), \\ \frac{d\widetilde{A}}{ds}(s) &= -q_0 + K_0^T\widetilde{\mathbf{B}}(s) + \frac{1}{2}\widetilde{\mathbf{B}}^T(s)H_0\widetilde{\mathbf{B}}(s), \end{aligned} \tag{1.32}$$

with initial conditions $\widetilde{\mathbf{B}}(0) = i\mathbf{u}$ and $\widetilde{A}(0) = 0$.

In Chapter 4, we will present the expression of the discounted ChF for the class of the affine-jump-diffusion models.

1.4. Introduction to Stochastic Grid Bundling Method

The Stochastic Grid Bundling Method (SGBM) is a Monte Carlo method based on *simulation*, *regression*, and *bundling*. It is originally developed by Jain and Oosterlee for pricing Bermudan options and their greeks [49, 50]. SGBM is also employed for real option valuation of modular nuclear power plants in finite time decision horizon [51]. Based on SGBM, Cong and Oosterlee proposed an algorithm for solving constrained dynamic mean-variance portfolio management problems [21]. A GPU acceleration of SGBM is

also presented in [63] for high-dimensional problems. Shen, Anderluh, and Van der Weide demonstrated the application of the SGBM algorithm for efficient computation of exposure profiles of multi-asset options under Lévy processes [78]. We generalize it to an efficient algorithm for computing exposure profiles [24, 30, 32].

In this section, we will present the components of SGBM, as well as a literature review of simulation-based methods, to understand the characteristic features of SGBM.

1.4.1. AN EXAMPLE OF SGBM

As an example, here we present SGBM for computing the price of a Bermudan option [50]. Consider a Bermudan option as in (1.20) in Section 1.2.3, which expires at time T and can be exercised at dates $\mathcal{T}_B = \{0 < T_1 < T_2 < \ldots < T_N = T\}$. Given a set of risk-neutral scenarios, we wish to find the optimal exercise time at each path. This can be performed by the backward pricing dynamics (1.21). The key is to estimate the continuation function defined in (1.22), for which SGBM makes use of bundles and moments. We summarize the procedure of the SGBM algorithm as follows:

- Generate H risk-neutral paths $\{\hat{x}_{1,h}, \hat{x}_{2,h}, \ldots, \hat{x}_{N,h}\}_{h=1}^{H}$, for all dates $\mathcal{T}_B$.
- Initialization: Set the option values $\hat{v}_{N,h} = g(\hat{x}_{N,h})$ at the terminal time $T_N = T$, $h = 1, \ldots, H$.
- Backward induction: At T_m, $m = N-1$, $N-2$, …, 1, compute the continuation values (1.22) at each path as follows:
  - Step I: Given $\{\hat{x}_{m,h}\}_{h=1}^{H}$, divide all paths at t_m into J *bundles*, and denote the collection of paths in the j-th bundle by $\mathscr{B}_{m,j}$, $j = 1, \ldots, J$.
  - Step II: Within each bundle at t_m, given $\{(\hat{v}_{m+1,h}, \hat{x}_{m+1,h}), h \in \mathscr{B}_{m,j}\}$, approximate the option values at T_{m+1} as

$$V(T_{m+1}, \mathbf{X}_{T_{m+1}}) \approx \sum_{|k|=0}^{d} \hat{\beta}_k^{m,j} \left(\mathbf{X}_{T_{m+1}}\right)^k, \tag{1.33}$$

    where $\left(\mathbf{X}_{T_{m+1}}\right)^k$ is the k-th monomial defined in (1.27); the coefficient $\hat{\beta}_k^{m,j}$ is for the k-th monomials at time T_m within the j-th bundle, obtained by regression, as follows

$$\left\{\hat{\beta}_k^{m,j}, |k| = 0, \ldots, d\right\} = \underset{b_k \in \mathbb{R}}{\arg\min} \sum_{h \in \mathscr{B}_{m,j}} \left(\hat{v}_{m+1,h} - \sum_{|k|=0}^{d} b_k \left(\hat{x}_{m+1,h}\right)^k \right)^2, \tag{1.34}$$

    where $\hat{v}_{m+1,h}$ represents the option value at time T_{m+1} at the h-th path, $h = 1, \ldots H$.
  - Step III: Approximate the continuation values in (1.22) on each path within the same bundle $\mathscr{B}_{m,j}$ by the linear combination of discounted moments,

where the associated linear coefficients are the same set of coefficients obtained in Step II, i.e.

$$\begin{aligned}\hat{c}_{m,h} = c(T_m, \hat{x}_{m,h}) &\approx \sum_{|k|=0}^{d} \hat{\beta}_k^{m,j} \mathbb{E}^{\mathbb{Q}} \left[\frac{B_{T_m}}{B_{T_{m+1}}} \left(\mathbf{X}_{T_{m+1}}\right)^k \middle| \mathbf{X}_{T_m} = \hat{x}_{m,h} \right] \\ &= \sum_{|k|=0}^{d} \hat{\beta}_k^{m,j} \psi_k(\hat{x}_{m,h}, T_m, T_{m+1}), \end{aligned} \tag{1.35}$$

where the path $h \in \mathscr{B}_{m,j}$, and analytic formulas of the discounted moments ψ_k, $|k| = 0, \ldots, d$, can be derived by (1.29).

- Step IV: Determine the exercise time on each path by comparing the immediate payoff value $g(\hat{x}_{m,h})$ and the computed continuation value $\hat{c}_{m,h}$, and consequently determine the option value by $\hat{v}_{m,h} = \max\left(\hat{c}_{m,h}, g(\hat{x}_{m,h})\right)$ at time T_m.
- Proceed to T_{m-1} and perform the procedure in Steps I, II, III, IV.

- At time $T_0 = 0$, compute the option value at time $T_=0$ by regression in the same way as in Steps II and III given $\{\hat{x}_{1,h}\}_{h=1}^{H}$.

1.4.2. LITERATURE REVIEW AND FEATURES OF SGBM

The technique of using simulation and regression for pricing American options has been previously used by Carriere [18], Tsitsiklis and Van Roy [84], and Longstaff and Schwartz (LSM) [64]. In these three methods, the required conditional expectations are approximated by a linear combination of polynomial basis functions using the least-squares method. The method of Longstaff and Schwartz [64] is different from the other two because LSM uses only 'in-the-money' paths for regression. Another feature is that the approximated conditional expectations are only used for determining the optimal early-exercise time in LSM. In addition, the value of the option is computed by taking the average of the discounted payoffs.

LSM [64] gained most popularity among practitioners. Stentoft [82] compares LSM to the algorithm of Tsitsiklis and Van Roy [84] in a realistic numerical setting for American options. Clément et al. [19] proved the almost sure convergence of the algorithm of Longstaff and Schwartz, and determined the convergence rate in the Monte-Carlo procedure to show its normalized error is asymptotically Gaussian. Glasserman and Yu [36] analyzed the convergence of LSM when the number of basis functions and the number of simulated paths increase, and got explicit results about the growth of the number of paths with the number of basis functions to ensure convergence, when the basis functions are polynomials and the underlying process is a Brownian or geometric Brownian motion. The paper by Broadie and Cao [15] proposed to use a local simulation to improve the early-exercise policy and introduced variance reduction techniques.

Another method of pricing American options in literature is the so-called *weighted Monte Carlo* method, see the work done by Broadie and Glasserman [16], and Broadie, Glasserman and Ha [17]. The weighted Monte Carlo method is different from regression-simulation methods, because in it the conditional expectations at a time step are com-

puted by weighted average option values at the later time step. Ways of determining the weights can be found in the book by Glasserman [34].

Connected to the work of the weighted Monte Carlo method, Glasserman and Yu [35] investigated the problem: which basis functions to use, in other words, *regression now* or *regression later*. LSM is a 'regression now' method, because the regression is performed based on information at the same time step as the conditional expectation to be approximated. Glasserman and Yu showed that the weighted Monte Carlo method has a regression interpretation, and is a 'regression later' method [35]. They concluded that in a single-period problem, the 'regression later' yields a better fit with smaller variance in the coefficients than the 'regression now' approach [35].

From the examples we demonstrate in Section 1.4.1, we can see that SGBM distinguishes itself from these methods by the following properties.

First, other simulation-regression methods are often 'regression-now' approaches, whereas SGBM is 'regression-later'. This can significantly enhance the accuracy in approximating the conditional expectations: In the multi-period estimation, the 'regression-now' procedure in LSM needs the discounted cash flows instead of the 'now' option values for regression, whereas the 'regression-later' procedure in SGBM can directly use the 'later' option values for regression.

Important components of SGBM are the techniques of bundling and local regression. In this way, SGBM can use information over all paths, whereas in LSM only 'in-the-money' paths are used to regression.

The approximated conditional expectations in LSM are only used for determining the optimal early-exercise time, and the option value is computed by average discounted payoffs. In SGBM, the approximated conditional expectations are directly used for computing option values. The resulting option value obtained via regression in SGBM is called the *direct estimator*. A *path estimator* can be generated in SGBM by taking the average of the discounted cash flows. It can help us determining the convergence of the algorithm.

Compared to the other 'regression later' method, i.e. the weighted Monte Carlo method, SGBM employs essentially different techniques. The paper [35] also presents a regression interpretation of the weighted Monte Carlo method. In this 'regression-later' method, there are imposed conditions, just like the basis functions are martingales. In SGBM, the basis functions are just monomials of the underlying market variables.

In the following sections, we will present the mathematical theoretical basis for SGBM based on the least-squares theory, demonstrate its convergence and convergence rate for a model test case, and present an error analysis when the underlying process is a Brownian motion.

1.5. CONVERGENCE ANALYSIS OVER A SINGLE PERIOD

In this section, we will analyze the convergence of SGBM over a single period by the theory of least-squares estimation. Instead of computing conditional expectations at a set of future dates, we will compute the expectation of the payoff at time T given information at a single time point t. We will analyze the approximation of the expectation from a theoretical perspective and from a Monte-Carlo based perspective, respectively.

We consider the most simple case, where $\{X_t \in \mathbb{R}, t \in [0,T)\}$ is a one-dimensional

Markov process. We use the notation $F_{X_T|X_t}(y;x)$ to represent the conditional distribution of the random variable X_T given $X_t = x \in \mathbb{R}$, and the notation $f_{X_T|X_t}(y;x)$ as the associated conditional density function, the simplified notation for the corresponding expectation is $\mathbb{E}_t^x := \mathbb{E}^{\mathbb{Q}}[\cdot|X_t = x]$.

From Lemma 2.1.2 in [68][pp 9], given a Borel measurable function $V : \mathbb{R}^n \to \mathbb{R}$, the value $V(X_T)$ is an $\mathscr{F}_T$- random variable. We define the L^2-norm induced by the conditional density $f_{X_T|X_t}(y;x)$, given by [58]:

$$\|V(X_T)\|_{L^2_{t,x}} := \left(\mathbb{E}_t^x\left[|V(X_T)|^2\right]\right)^{\frac{1}{2}} = \left(\int_{\mathbb{R}} |V(y)|^2 f_{X_T|X_t}(y;x)\,dy\right)^{\frac{1}{2}} < \infty. \tag{1.36}$$

With this norm the corresponding space is a *Hilbert* space, with inner product [68]

$$< V_1(X_T), V_2(X_T) >_{L^2_{t,x}} := \mathbb{E}_t^x[V_1(X_T)V_2(X_T)], \tag{1.37}$$

where $\|V_1(X_T)\|_{L^2_{t,x}} < \infty$ and $\|V_2(X_T)\|_{L^2_{t,x}} < \infty$.

The purpose is to find out the best approximation of $c(t,x) := \mathbb{E}_t^x[V(X_T)]$ via a least-squares method.

1.5.1. THEORETICAL LEAST-SQUARES ESTIMATOR

We define monomials up to order d by

$$\phi_0 := 1, \quad \phi_k := (X_T)^k, \quad k = 1,\dots,d. \tag{1.38}$$

For convenience, we define the vector $\boldsymbol{\phi} = [\phi_0, \phi_1, \dots, \phi_d]^T$.

The span of these monomials can be defined as the set of all linear combinations of these polynomial terms. The linear span is the space of polynomials, denoted by:

$$\mathscr{P}_d = \left\{ \sum_{k=0}^{d} b_k \phi_k, b_k \in \mathbb{R} \right\}, \tag{1.39}$$

which is a subset of the L^2-space.

Define the matrix

$$\boldsymbol{Q}_{XX} := \mathbb{E}_t^x\left[\boldsymbol{\phi}\boldsymbol{\phi}^T\right] = \begin{bmatrix} 1 & \mathbb{E}_t^x[\phi_0\phi_1] & \dots & \mathbb{E}_t^x[\phi_0\phi_d] \\ \mathbb{E}_t^x[\phi_1\phi_0] & \mathbb{E}_t^x[\phi_1\phi_1] & \dots & \mathbb{E}_t^x[\phi_1\phi_d] \\ \vdots & \vdots & \vdots & \vdots \\ \mathbb{E}_t^x[\phi_d\phi_0] & \mathbb{E}_t^x[\phi_d\phi_1] & \dots & \mathbb{E}_t^x[\phi_d\phi_d] \end{bmatrix}, \tag{1.40}$$

and the vector

$$\boldsymbol{Q}_{VX} = \mathbb{E}_t^x\left[V(X_T)\boldsymbol{\phi}\right] = \begin{bmatrix} \mathbb{E}_t^x\left[V(X_T)\phi_0\right] \\ \mathbb{E}_t^x\left[V(X_T)\phi_1\right] \\ \vdots \\ \mathbb{E}_t^x\left[V(X_T)\phi_d\right] \end{bmatrix}. \tag{1.41}$$

For derivation, we require the following condition [42][Section 2.18]:

1

Assumption 1.5.1. *We assume*

1. $\|V(X_T)\|^2_{L^2_{t,x}} < \infty$.
2. $\mathbb{E}^x_t\left[\sum_{k=0}^{d} \phi_k^2\right] < \infty$.
3. $\boldsymbol{Q}_{XX}$ *is positive definite, or equivalently,* $\boldsymbol{Q}_{XX}$ *is invertible.*

With these assumptions, the expectations $\mathbb{E}^x_t\left[V(X_T)\boldsymbol{\phi}\right]$ exist and are finite. We look for the solution $\boldsymbol{\beta} = [\beta_0, \beta_1, \ldots, \beta_d]^T$, which satisfies

$$\boldsymbol{\beta} = \underset{\boldsymbol{b}\in\mathbb{R}^{d+1}}{\arg\min} \left\| V(X_T) - \boldsymbol{\phi}^T\boldsymbol{b}\right\|^2_{L^2_{t,x}} = \underset{\{b_k\in\mathbb{R}, k=0,\ldots,d\}}{\arg\min} \mathbb{E}^x_t\left[\left(V(X_T) - \sum_{k=0}^{d} b_k\phi_k\right)^2\right]. \tag{1.42}$$

This problem is equivalent to finding the orthogonal projection of $V(X_T)$ onto the polynomial space $\mathscr{P}_d$ [42, 61, 65]. The expectation of the squared error is the square of the distance from $V(X_T)$ to $\sum_{k=0}^{d} b_k\phi_k$ in the space $\mathscr{P}_d$ measured by the norm $L^2_{t,x}$. Hence the solution is given by the coefficients in the orthogonal projection of $V(X_T)$ onto the space $\mathscr{P}_d$ with form $\sum_{k=0}^{d}\beta_k\phi_k$. The projection error $V(X_T) - \sum_{k=0}^{d}\beta_k\phi_k$ is orthogonal to any vector in $\mathscr{P}_d$, i.e.

$$< V(X_T) - \sum_{k=0}^{d}\beta_k\phi_k, \phi_j >_{L^2_{t,x}} = 0, \quad j = 0, 1, \ldots, d, \tag{1.43}$$

or equivalently,

$$< \sum_{k=0}^{d}\beta_k\phi_k, \phi_j >_{L^2_{t,x}} = < V(X_T), \phi_j >_{L^2_{t,x}}, \quad j = 0, 1, \ldots, d, \tag{1.44}$$

With these $(d+1)$ equations in (1.44), we find

$$\boldsymbol{Q}_{XX}\cdot\boldsymbol{\beta} = \boldsymbol{Q}_{VX}. \tag{1.45}$$

When the function V is explicitly known, and all expectations in $\boldsymbol{Q}_{XX}$ and $\boldsymbol{Q}_{VX}$ can be computed, we obtain an analytic solution for $\boldsymbol{\beta}$. With Assumption 1.5.1, $\boldsymbol{Q}_{XX}$ is invertible, the unique solution of the least-squares estimator is given by:

$$\boldsymbol{\beta} = \boldsymbol{Q}^{-1}_{XX}\cdot\boldsymbol{Q}_{VX}. \tag{1.46}$$

In addition, because we have included the constant $\phi_0 = 1$, we have

$$c(t,x) = \mathbb{E}^x_t[V(X_T)] = \mathbb{E}^x_t\left[\sum_{k=0}^{d}\beta_k\phi_k\right] = \sum_{k=0}^{d}\beta_k\mathbb{E}^x_t\left[\phi_k\right] = \sum_{k=0}^{d}\beta_k\psi_k(x,t,T), \tag{1.47}$$

where $\psi_k(x,t,T) := \mathbb{E}^x_t\left[\phi_k\right]$ is the k-th moment conditional on $X_t = x$.

We can simplify the notations using matrix representation, so the *best* linear approximation of the expectation can be expressed by

$$c(t,x) = \boldsymbol{\psi}^T\boldsymbol{\beta} = \boldsymbol{\psi}^T(\boldsymbol{Q}_{XX})^{-1}\cdot\boldsymbol{Q}_{VX}, \tag{1.48}$$

where the vector $\boldsymbol{\psi} := [\psi_0, \psi_1, \ldots, \psi_d]^T$.

When we choose the monomial basis, the constant term must be included to have (1.48).

We present some properties of the projection. The *projection error* is given by

$$\epsilon = V(X_T) - \boldsymbol{\phi}^T \boldsymbol{\beta} = V(X_T) - \sum_{k=0}^{d} \beta_k \phi_k, \tag{1.49}$$

which has the properties:

$$\begin{aligned} \|\epsilon\|^2_{L^2_{t,x}} &= \mathbb{E}_t^x\left[\epsilon^2\right] = \|V(X_T)\|^2_{L^2_{t,x}} - \left\| \sum_{k=0}^{d} \beta_k \phi_k \right\|^2_{L^2_{t,x}}, \\ <\epsilon, \phi_l> &= \mathbb{E}_t^x\left[\epsilon\phi_l\right] = 0, \quad \mathbb{E}_t^x\left[\epsilon\phi_l\right] = \mathbb{E}_t^x\left[\epsilon\right] \cdot \mathbb{E}_t^x\left[\phi_l\right] = 0, \quad l = 0, 1, \ldots, d. \end{aligned} \tag{1.50}$$

from which we see that ϵ and ϕ_l are uncorrelated for $l = 0, \ldots, d$.

We write the projection used in SGBM as follows

$$V(X_T) = \sum_{k=0}^{d} \beta_k (X_T)^k + \epsilon, \tag{1.51}$$

where the projection error satisfies (1.50).

Comments: We may have the problem of 'over-fitting' if the order of the monomial basis is chosen to be higher than the 'order' of function V. For instance, if we wish to approximate the expectation of X_T^2, then the coefficients for monomials higher than 2 will be zero.

1.5.2. MONTE CARLO LEAST-SQUARES ESTIMATOR

Suppose that we do not know the explicit expression for the function V, and we will approximate the best linear coefficients $\boldsymbol{\beta}$ in the setting of random sampling by Monte Carlo method, denoted by $\hat{\boldsymbol{\beta}}$. In this section we will show the consistency and asymptotic normality of the Monte Carlo least-squares estimator $\hat{\boldsymbol{\beta}}$ using the asymptotic theory of least-squares estimation [42].

Samples $\{\hat{x}_j\}_{j=1}^H$ are drawn from the conditional distribution function $F_{X_T|X_t}$ and we know the associated values of function $\hat{v}_j = V(\hat{x}_j)$. We will perform least-squares estimation based on H samples $(\hat{x}_j, \hat{v}_j)$, $j = 1, \ldots, H$. The j-th sample of the monomial basis vector $\boldsymbol{\phi_k}$ is $[1, \hat{x}_j, \hat{x}_j^2, \ldots, \hat{x}_j^d]^T$, $j = 1, \ldots, H$.

To derive the results in this section, the following condition must hold [42][Section 6.1]

Assumption 1.5.2. *We assume*

1. *The observations* (x_j, v_j), $j = 1, \ldots, H$, *are i.i.d;*
2. $\|V(X_T)\|^2_{L^2_{t,x}} < \infty$;
3. $\mathbb{E}_t^x\left[\sum_{k=0}^{d} \phi_k^2\right] < \infty$;

1

4. $\boldsymbol{Q}_{XX}$ *is positive definite, or equivalently,* $\boldsymbol{Q}_{XX}$ *is invertible;*

5. *For some results, we also need bounded fourth moments, i.e.* $\mathbb{E}_t^x\left[(V(X_T))^4\right] < \infty$ *and* $\mathbb{E}_t^x\left[\sum_{k=0}^d \phi_k^4\right] < \infty$.

Define the sample matrix and vector

$$\hat{X} := \begin{bmatrix} 1 & \hat{x}_1 & \hat{x}_1^2 & \dots & \hat{x}_1^d \\ 1 & \hat{x}_2 & \hat{x}_2^2 & \dots & \hat{x}_2^d \\ \vdots & \vdots & \vdots & \vdots & \vdots \\ 1 & \hat{x}_H & \hat{x}_H^2 & \dots & \hat{x}_H^d \end{bmatrix}_{H\times(d+1)}, \hat{V} := \begin{bmatrix} \hat{v}_1 \\ \hat{v}_2 \\ \vdots \\ \hat{v}_H \end{bmatrix}_{H\times(d+1)}, \tag{1.52}$$

where $H > d$ and the rank of $\hat{X}$ equals $(1+d)$.

By the models in (1.51), we have the matrix expression of the H observations

$$\hat{V} = \hat{X}\boldsymbol{\beta} + \boldsymbol{\epsilon}, \tag{1.53}$$

where $\boldsymbol{\epsilon} = [\epsilon_1, \epsilon_2, \dots, \epsilon_H]^T$.

CONSISTENCY OF THE MONTE CARLO ESTIMATOR

The Monte Carlo estimator of the coefficient $\boldsymbol{\beta}$ based on the H samples, is given by

$$\hat{\boldsymbol{\beta}} = \left(\hat{X}^T\hat{X}\right)^{-1}\hat{X}^T\hat{V}. \tag{1.54}$$

If we replace matrix $\hat{V}$ in (1.54) by the expression (1.53), the Monte Carlo least-squares estimator $\hat{\beta}$ can be expressed by

$$\hat{\beta} = \beta + \left(\hat{X}^T\hat{X}\right)^{-1}\hat{X}^T\boldsymbol{\epsilon}. \tag{1.55}$$

The error of the Monte Carlo estimator can thus be written as

$$\hat{\beta} - \beta = \left(\frac{1}{H}\hat{X}^T\hat{X}\right)^{-1}\left(\frac{1}{H}\hat{X}^T\boldsymbol{\epsilon}\right). \tag{1.56}$$

By the law of large numbers [58], we can establish

$$\frac{1}{H}\hat{X}^T\hat{X} = \begin{bmatrix} 1 & \frac{1}{H}\sum_{j=1}^{H}\hat{x}_j & \frac{1}{H}\sum_{j=1}^{H}\hat{x}_j^2 & \cdots & \frac{1}{H}\sum_{j=1}^{H}\hat{x}_j^d \\ \frac{1}{H}\sum_{j=1}^{H}\hat{x}_j & \frac{1}{H}\sum_{j=1}^{H}\hat{x}_j^2 & \frac{1}{H}\sum_{j=1}^{H}\hat{x}_j^3 & \cdots & \frac{1}{H}\sum_{j=1}^{H}\hat{x}_j^{d+1} \\ \vdots & \vdots & \cdots & \vdots & \\ \frac{1}{H}\sum_{j=1}^{H}\hat{x}_j^d & \frac{1}{H}\sum_{j=1}^{H}\hat{x}_j^{d+1} & \frac{1}{H}\sum_{j=1}^{H}\hat{x}_j^{d+2} & \cdots & \frac{1}{H}\sum_{j=1}^{H}\hat{x}_j^{d+d} \end{bmatrix}_{(d+1)\times(d+1)}$$

$$\xrightarrow[p]{} \begin{bmatrix} \mathbb{E}_t^x[\phi_0\phi_0] & \mathbb{E}_t^x[\phi_0\phi_1] & \mathbb{E}_t^x[\phi_0\phi_2] & \cdots & \mathbb{E}_t^x[\phi_0\phi_d] \\ \mathbb{E}_t^x[\phi_1\phi_0] & \mathbb{E}_t^x[\phi_1\phi_1] & \mathbb{E}_t^x[\phi_1\phi_2] & \cdots & \mathbb{E}_t^x[\phi_1\phi_d] \\ \vdots & \vdots & \cdots & \vdots & \\ \mathbb{E}_t^x[\phi_d\phi_0] & \mathbb{E}_t^x[\phi_d\phi_1] & \mathbb{E}_t^x[\phi_d\phi_2] & \cdots & \mathbb{E}_t^x[\phi_d\phi_d] \end{bmatrix} = \boldsymbol{Q}_{XX},$$

$$\frac{1}{H}\hat{X}^T\boldsymbol{\epsilon} = \begin{bmatrix} \frac{1}{H}\sum_{j=1}^{H}\epsilon_j \\ \frac{1}{H}\sum_{j=1}^{H}\epsilon_j\hat{x}_j \\ \vdots \\ \frac{1}{H}\sum_{j=1}^{H}\epsilon_j\hat{x}_j^d \end{bmatrix}_{(d+1)\times 1} \xrightarrow[p]{} \begin{bmatrix} \mathbb{E}_t^x[\epsilon\phi_0] \\ \mathbb{E}_t^x[\epsilon\phi_1] \\ \vdots \\ \mathbb{E}_t^x[\epsilon\phi_d] \end{bmatrix} = \mathbf{0}_{(d+1)\times 1}, \tag{1.57}$$

where $\xrightarrow[p]{}$ denotes the convergence with probability 1.

In short, matrix $\frac{1}{H}\hat{X}^T\hat{X}$ will converge to $\boldsymbol{Q}_{XX}$ with probability 1 as H goes to infinity. By Slutsky's theorem [37] and the continuous mapping theorem [71], we get

$$\hat{\boldsymbol{\beta}} - \boldsymbol{\beta} = \left(\frac{1}{H}\hat{X}^T\hat{X}\right)^{-1}\left(\frac{1}{H}\hat{X}^T\epsilon\right) \xrightarrow[p]{} \boldsymbol{Q}_{XX}^{-1}\cdot\mathbf{0}_{d\times 1} = 0. \tag{1.58}$$

So the Monte Carlo estimator $\hat{\boldsymbol{\beta}}$ converges in probability to the true solution $\boldsymbol{\beta}$ as H increases.

ASYMPTOTIC NORMALITY OF THE MONTE CARLO ESTIMATOR

The Monte Carlo estimator $\hat{\boldsymbol{\beta}}$ converges in probability to the true solution $\boldsymbol{\beta}$. Next we will show the asymptotic normal distribution of the estimator.

Writing

$$\sqrt{H}\left(\hat{\beta} - \beta\right) = \left(\frac{1}{H}\hat{X}^T\hat{X}\right)^{-1}\left(\frac{1}{\sqrt{H}}\hat{X}^T\boldsymbol{\epsilon}\right), \tag{1.59}$$

the inverse of the sample moment matrix $\frac{1}{H}\hat{X}^T\hat{X}$ converges to $\boldsymbol{Q}_{XX}^{-1}$, and the term $\left(\frac{1}{\sqrt{H}}\hat{X}^T\boldsymbol{\epsilon}\right)$

1

has mean zero. Because $\{\hat{x}_j\}_{j=1}^H$ are i.i.d., we have

$$\left(\frac{1}{\sqrt{H}}\hat{X}^T\boldsymbol{\epsilon}\right)\left(\frac{1}{\sqrt{H}}\hat{X}^T\boldsymbol{\epsilon}\right)^T = \frac{1}{H}\begin{bmatrix} \sum_{j=1}^H \epsilon_j^2 & \sum_{j=1}^H \epsilon_j^2 x_j & \sum_{j=1}^H \epsilon_j^2 x_j^2,\ldots & \sum_{j=1}^H \epsilon_j^2 x_j^d \\ \sum_{j=1}^H \epsilon_j^2 x_j & \sum_{j=1}^H \epsilon_j^2 x_j^2 & \sum_{j=1}^H \epsilon_j^2 x_j^d,\ldots, & \sum_{j=1}^H \epsilon_j^2 x_j^{d+1} \\ \vdots & \vdots & \vdots & \vdots \\ \sum_{j=1}^H \epsilon_j^2 x_j^d & \sum_{j=1}^H \epsilon_j^2 x_j^{d+1} & \sum_{j=1}^H \epsilon_j^2 x_j^{d+2}\ldots & \sum_{j=1}^H \epsilon_j^2 x_j^{d+d} \end{bmatrix}$$

$$\xrightarrow[p]{} \quad \boldsymbol{Q}_{X\epsilon} = \begin{bmatrix} \mathbb{E}_t^x[\epsilon^2\phi_0\phi_0] & \mathbb{E}_t^x[\epsilon^2\phi_0\phi_1] & \mathbb{E}_t^x[\epsilon^2\phi_0\phi_2] & \ldots & \mathbb{E}_t^x[\epsilon^2\phi_0\phi_d] \\ \mathbb{E}_t^x[\epsilon^2\phi_1\phi_0] & \mathbb{E}_t^x[\epsilon^2\phi_1\phi_1] & \mathbb{E}_t^x[\epsilon^2\phi_1\phi_2] & \ldots & \mathbb{E}_t^x[\epsilon^2\phi_1\phi_d] \\ \vdots & \vdots & \vdots & \vdots & \vdots \\ \mathbb{E}_t^x[\epsilon^2\phi_d\phi_0] & \mathbb{E}_t^x[\epsilon^2\phi_d\phi_1] & \mathbb{E}_t^x[\epsilon^2\phi_d\phi_2] & \ldots & \mathbb{E}_t^x[\epsilon^2\phi_d\phi_d] \end{bmatrix}_{(d+1)\times(d+1)} \tag{1.60}$$

The elements in the matrix $\boldsymbol{Q}_{X\epsilon}$ are finite by Assumptions 1.5.2. By Jensen's inequality and the Cauchy-Schwartz inequality, we find that any (k,l)-th element in $\boldsymbol{Q}_{X\epsilon}$ is finite [42][Section 6.3], given by

$$\begin{aligned} \left|\mathbb{E}_t^x[\epsilon^2\phi_k\phi_l]\right| &\leq \mathbb{E}_t^x\left[\left|\epsilon^2\phi_k\phi_l\right|\right] = \mathbb{E}_t^x\left[\epsilon^2|\phi_k||\phi_l|\right] \\ &\leq \left(\mathbb{E}_t^x\left[\epsilon^4\right]\right)^{\frac{1}{2}}\left(\mathbb{E}_t^x\left[\phi_k^2\phi_l^2\right]\right)^{\frac{1}{2}} \\ &\leq \left(\mathbb{E}_t^x\left[\epsilon^4\right]\right)^{\frac{1}{2}}\left(\mathbb{E}_t^x\left[\phi_k^4\right]\right)^{\frac{1}{4}}\left(\mathbb{E}_t^x\left[\phi_l^4\right]\right)^{\frac{1}{4}} < \infty, \end{aligned} \tag{1.61}$$

where $k,l = 1,\ldots,d$.

With a finite covariance matrix, we can apply the central limit theorem. The central limit theorem [34, 58] asserts that as the number of replications H increases, the standardized estimator $\hat{X}\boldsymbol{\epsilon}/(\sqrt{HQ_{X\epsilon}})$ converges in distribution to the standard normal, i.e.

$$\frac{\hat{X}\boldsymbol{\epsilon}}{\sqrt{H\boldsymbol{Q}_{X\epsilon}}} \xrightarrow[p]{} \mathcal{N}(0,1), \tag{1.62}$$

or equivalently,

$$\frac{1}{\sqrt{H}}\hat{X}\boldsymbol{\epsilon} \xrightarrow[p]{} \mathcal{N}(0,\boldsymbol{Q}_{X\epsilon}). \tag{1.63}$$

Applying Slutsky's theorem, we have

$$\sqrt{H}(\hat{\beta}-\beta) \xrightarrow[p]{} \mathcal{N}\left(0,\boldsymbol{Q}_{XX}^{-1}\boldsymbol{Q}_{X\epsilon}\boldsymbol{Q}_{XX}^{-1}\right), \tag{1.64}$$

so that $\sqrt{H}(\hat{\beta}-\beta)$ is asymptotically normal with an asymptotic variance $\boldsymbol{Q}_{XX}^{-1}\boldsymbol{Q}_{X\epsilon}\boldsymbol{Q}_{XX}^{-1}$.

We write the expectation approximated by the Monte Carlo least-squares estimator as

$$\hat{c}(t,x) := \sum_{k=0}^{d}\hat{\beta}_k\psi_k(x,t,T) = \boldsymbol{\psi}^T\hat{\boldsymbol{\beta}}. \tag{1.65}$$

Hence

$$\sqrt{H}\left(\hat{c}(t,x)-c(t,x)\right)=\sqrt{H}\left(\boldsymbol{\psi}^T\left(\hat{\beta}-\beta\right)\right)\underset{p}{\longrightarrow}\mathcal{N}\left(0,\boldsymbol{\psi}^T\boldsymbol{Q}_{XX}^{-1}\boldsymbol{Q}_{X\epsilon}\boldsymbol{Q}_{XX}^{-1}\boldsymbol{\psi}\right), \tag{1.66}$$

as H goes to infinity.

So, given the number of replications H, the error in $\hat{c}(t,x)$ will be approximately normally distributed with mean zero and variance $O(1/H)$.

THE VARIANCE TERM IN MONTE CARLO APPROXIMATION

The variance of $\hat{c}$ converges to $\boldsymbol{\psi}^T\boldsymbol{Q}_{XX}^{-1}\boldsymbol{Q}_{X\epsilon}\boldsymbol{Q}_{XX}^{-1}\boldsymbol{\psi}/H$ as H goes to infinity with probability 1. In this section, we will analyze the constant term $\boldsymbol{\psi}^T\boldsymbol{Q}_{XX}^{-1}\boldsymbol{Q}_{X\epsilon}\boldsymbol{Q}_{XX}^{-1}\boldsymbol{\psi}$.

Using the Gram–Schmidt process, we can orthonormalize the polynomial basis set $\{\phi_0,\ldots,\phi_d\}$, and generate a normalized orthogonal set $\{\tilde{\phi}_0,\ldots,\tilde{\phi}_d\}$, such that

$$\tilde{\boldsymbol{\phi}}=\tilde{L}\boldsymbol{\phi},\text{such that }<\tilde{\boldsymbol{\phi}},\tilde{\boldsymbol{\phi}}>_{L_{t,x}}=\mathbb{E}_t^x\left[\tilde{\boldsymbol{\phi}}\tilde{\boldsymbol{\phi}}^T\right]=I, \tag{1.67}$$

where $\tilde{\boldsymbol{\phi}}=[\tilde{\phi}_0,\ldots,\tilde{\phi}_d]^T$, I is an identity matrix and the lower triangular matrix $\tilde{L}$ with strictly positive diagonal entries is invertible.

It is easy to show that

$$\boldsymbol{Q}_{XX}^{-1}=\tilde{L}^T\tilde{L},\quad \boldsymbol{Q}_{X\epsilon}=\tilde{L}^{-1}\mathbb{E}_t^x\left[\epsilon^2\tilde{\boldsymbol{\phi}}\tilde{\boldsymbol{\phi}}^T\right]\left(\tilde{L}^{-1}\right)^T,\quad \boldsymbol{\psi}=\tilde{L}^{-1}\mathbb{E}_t^x\left[\tilde{\boldsymbol{\phi}}\right]. \tag{1.68}$$

Hence we have

$$\begin{aligned}\boldsymbol{\psi}^T\boldsymbol{Q}_{XX}^{-1}\boldsymbol{Q}_{X\epsilon}\boldsymbol{Q}_{XX}^{-1}\boldsymbol{\psi} &= \left(\mathbb{E}_t^x\left[\tilde{\boldsymbol{\phi}}\right]\right)^T\mathbb{E}_t^x\left[\epsilon^2\tilde{\boldsymbol{\phi}}\tilde{\boldsymbol{\phi}}^T\right]\mathbb{E}_t^x\left[\tilde{\boldsymbol{\phi}}\right]\\ &= \sum_{k=0}^{d}\sum_{l=0}^{d}\mathbb{E}_t^x\left[\tilde{\phi}_k\right]\mathbb{E}_t^x\left[\tilde{\phi}_l\right]\mathbb{E}_t^x\left[\epsilon^2\tilde{\phi}_k\tilde{\phi}_l\right]\\ &\le \sum_{k=0}^{d}\sum_{l=0}^{d}\mathbb{E}_t^x\left[|\tilde{\phi}_k|\right]\mathbb{E}_t^x\left[|\tilde{\phi}_l|\right]\mathbb{E}_t^x\left[\epsilon^2|\tilde{\phi}_k||\tilde{\phi}_l|\right].\end{aligned} \tag{1.69}$$

Now, we use the properties of the normalized orthogonal basis

$$\mathbb{E}_t^x\left[\tilde{\phi}_k\right]\le\mathbb{E}_t^x\left[|\tilde{\phi}_k|\right]\le\left(\mathbb{E}_t^x\left[(\tilde{\phi}_k)^2\right]\right)^{\frac{1}{2}}=1,\quad k=0,\ldots,d. \tag{1.70}$$

So,

$$\begin{aligned}\sum_{k=0}^{d}\sum_{l=0}^{d}\mathbb{E}_t^x\left[\epsilon^2|\tilde{\phi}_k||\tilde{\phi}_l|\right] &\le \sum_{k=0}^{d}\sum_{l=0}^{d}\left(\mathbb{E}_t^x\left[\epsilon^4\right]\right)^{\frac{1}{2}}\left(\mathbb{E}_t^x\left[\tilde{\phi}_k^4\right]\right)^{\frac{1}{4}}\left(\mathbb{E}_t^x\left[\tilde{\phi}_l^4\right]\right)^{\frac{1}{4}}\\ &= \left(\mathbb{E}_t^x\left[\epsilon^4\right]\right)^{\frac{1}{2}}\left(\sum_{k=0}^{d}\left(\mathbb{E}_t^x\left[\tilde{\phi}_k^4\right]\right)^{\frac{1}{4}}\right)^2,\end{aligned} \tag{1.71}$$

where the inequality is from the result in (1.61).

Here we can see that the variance is bounded by the fourth moment of the projection error. The projection error is determined by function V, the chosen monomial order d

and the norm $L^2_{t,x}$. Typically, we expect that the variance in approximation of the conditional expectation gets smaller when we increase the polynomial order d except for the 'over-fitting' case.

Further, we can see that, no matter what kind of polynomial basis functions are chosen for regression, the variance in the Monte Carlo approximation stays the same, determined by the projection error and the normalized orthogonal basis. We can simply choose monomials as the basis functions for regression.

1.5.3. TEST OF CONVERGENCE RATE

The purpose of this section is to test the conclusion presented by (1.66). We choose a function V and a dynamic for X_t, such that the analytic solution for the expectation $c(t,x) = \mathbb{E}_t^x[V(X_T)]$ is available. Perform independent Monte Carlo simulations and for each simulation employ SGBM to obtain the associate value for the Monte Carlo estimator $\hat{c}(t,x)$, then we can see if $\hat{c}$ converges to c and how fast it converges w.r.t. the number of paths.

The root-mean-square error (RMSE) is chosen to be the measure of difference between c and $\hat{c}$. If the result in (1.66) is true that $\hat{c}$ is unbiased estimator of c , RMSE should approaches zero as the number of paths goes to infinity, and also RMSE can represent the sample standard deviation of $\hat{c}$. Hence we expect the RMSE goes to zero with rate $1/\sqrt{H}$.

An example is as follows. Assume that the underlying variable follows the dynamics, given by,

$$dX_t = -\frac{1}{2}\sigma^2 dt + \sigma dW_t^{\mathbb{Q}}, \tag{1.72}$$

where volatility σ is a constant.

We choose a function $V(X_T) = \exp(X_T)$, and wish to compute $c(0,x) = \mathbb{E}_0^x\left[\exp(X_T)\right]$. Because $\exp(X_T)$ follows a log-normal distribution, it is easy to get that $\mathbb{E}_0^x\left[\exp(X_T)\right] = \exp(x)$.

In addition, the analytic solution for $\{\beta_k\}_{k=0}^d$ can also be obtained, because one can derive analytic formulas of any expectation as required in (1.45), since

$$\begin{aligned}
\mathbb{E}_t^x\left[X_T^k \exp(X_T)\right] &= \frac{1}{i^k}\frac{\partial}{\partial u^k}\mathbb{E}_t^x\left[\exp(iuX_T)\right]\Big|_{u=-i}, \\
\mathbb{E}_t^x\left[X_T^k\right] &= \frac{1}{i^k}\frac{\partial}{\partial u^k}\mathbb{E}_t^x\left[\exp(iuX_T)\right]\Big|_{u=0},
\end{aligned} \tag{1.73}$$

where $k = 0, 1, \ldots, d$, with the characteristic function

$$\mathbb{E}_t^x\left[\exp(iuX_T)\right] = \exp\left(-\frac{i}{2}\sigma^2 u(T-t) - \frac{1}{2}\sigma^2 u^2 (T-t) + iux\right). \tag{1.74}$$

So we can build the $(1+d)$ equations defined in (1.45), and get the analyic solution of the least-squares estimator $\{\beta_k\}_{k=0}^d$ using (1.46).

We choose two sets of parameters. **Test 1**: $X_0 = 0$, $\sigma = 0.2$, $T = 0.5$. **Test 2**: $X_0 = 0$, $\sigma = 1$, $T = 1$. The parameters in Test 2 are chosen to give X_T a large variance. So the value to be computed is $c(0,0) = \mathbb{E}_0^{x=0}\left[\exp(X_T)\right]$.

Implement SGBM to have the Monte Carlo estimator. Generate H independent samples of X_T, and $H = 10^n$ is increased by $n = 1,\ldots,6$. The order of the polynomial basis is chosen as $d = 1,2,3,4$. We perform 10 independent tests for a fixed H and a fixed d to compute the absolute error of the Monte Carlo approximated expectation and compare the analytic solution.

Figure 1.2 presents the convergence rate of the root-mean-square error (RMSE) of the Monte Carlo approximation against the number of samples for this test. It shows that the convergence rate of RMSE is $O(1/\sqrt{H})$ as expected. In addition, we can see that increasing the order d can significantly reduce the scale of the variance.

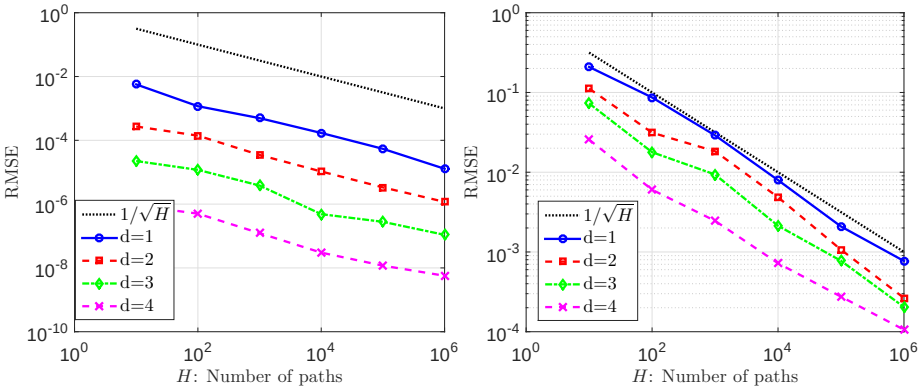

(a) Test 1 (b) Test 2

Figure 1.2: The root-mean-square error (RMSE) of approximating the conditional expectation, i.e. $\sqrt{\mathbb{E}\left[(c-\hat{c})^2\right]}$. The results are based on 10 independent tests.

We present the mean and standard deviation (Std) of Monte Carlo estimators of coefficients (β_0, β_1) against the number of samples in Table 1.1 with $d = 1$. We can observe the relation between the number of samples and the standard deviation of the Monte Carlo estimators. Compared to the analytic solution presented in the caption of Table 1.1, the results also show that the Monte Carlo estimators converge to the correct values.

If we use this way of estimating the future expectations directly, simulation has to been performed for any $X_t = x$, and thus sub-simulation cannot be avoided for computing conditional expectations at future time on each path. So, in section 1.7, we will show a way and give the error of approximation.

1.6. SENSITIVITY WITH RESPECT TO THE INITIAL VALUE

In this section, we will show that the sensitivities of the expectation with respect to the initial value can be approximated directly using the linear coefficients obtained via Monte Carlo simulation, when the underlying variable follows a normal distribution.

	Test 1		Test 2	
H	$\hat{\beta}_0$ (s.d.)	$\hat{\beta}_1$ (s.d.)	$\hat{\beta}_0$ (s.d.)	$\hat{\beta}_1$ (s.d.)
10	1.0070(0.0037)	1.0115(0.0796)	1.4548(0.5848)	1.1001(0.9030)
10^2	1.0091(0.0017)	1.0018(0.0264)	1.5089(0.1959)	0.9916(0.2130)
10^3	1.0101(0.0004)	1.0020(0.0064)	1.4932(0.0542)	0.9957(0.0585)
10^4	1.0100(0.0001)	1.0000(0.0018)	1.5019(0.0165)	1.0020(0.0215)
10^5	1.0100(0.0000)	1.0000(0.0004)	1.4992(0.0049)	0.9989(0.0057)
10^6	1.0100(0.0000)	1.0000(0.0002)	1.5011(0.0025)	1.0009(0.0031)

Table 1.1: The Monte Carlo estimator $\{\hat{\beta}_0, \hat{\beta}_1\}$ of the coefficient $\{\beta_0, \beta_1\}$ when the polynomial basis is $\{1, X_T\}$. The solution in Test 1: $\beta_0 = 1.0100$, $\beta_1 = 1.0000$; the solution in Test 2: $\beta_0 = 1.5000$, $\beta_1 = 1.0000$;

1.6.1. SENSITIVITY WITH RESPECT TO THE INITIAL VALUE

We derive the j-th derivative of a normal density $f_{\mathcal{N}}(y;\mu_y,\sigma_y^2)$ with respect to its mean μ_y and variance σ_y^2, respectively. It is easier to work with the log value of the function, given by

$$\log f_{\mathcal{N}}(y;\mu_y,\sigma_y^2) = -\frac{1}{2}\log(2\pi) - \frac{1}{2}\log(\sigma_y^2) - \frac{1}{2\sigma_y^2}(y-\mu_y)^2, \tag{1.75}$$

from which we have

$$\frac{\partial f_{\mathcal{N}}}{\partial \mu_y} = f_{\mathcal{N}} \cdot \frac{\partial \log f_{\mathcal{N}}}{\partial \mu_y}. \tag{1.76}$$

By iteration, we find the j-th derivative w.r.t. the mean

$$\frac{\partial^j f_{\mathcal{N}}}{\partial \mu_y^j} = f_{\mathcal{N}} \cdot \left(\left(\frac{\partial \log f_{\mathcal{N}}}{\partial \mu_y} \right)^j + \frac{\partial^j \log f_{\mathcal{N}}}{\partial \mu_y^j} \right), \tag{1.77}$$

with

$$\frac{\partial \log f_{\mathcal{N}}}{\partial \mu_y} = -\frac{\mu_y - y}{\sigma_y^2}, \quad \frac{\partial^2 \log f_{\mathcal{N}}}{\partial \mu_y^2} = -\frac{1}{\sigma_y^2}, \quad \frac{\partial^j \log f_{\mathcal{N}}}{\partial \mu_y^j} = 0, \quad j \geq 3. \tag{1.78}$$

Hence we have

$$\frac{\partial^j f_{\mathcal{N}}}{\partial \mu_y^j}(y;\mu_y,\sigma_y^2) = f_{\mathcal{N}}(y;\mu_y,\sigma_y^2) \cdot p_j(y), \tag{1.79}$$

where $p_j(y)$ represents a polynomial function w.r.t. y with polynomial degree j. One can derive the analytic formula for this polynomial function using (1.77) and (1.78), but here only the polynomial order of the function matters.

When the stochastic process X_t follows a Brownian Motion with drift process given in (1.72), the mean of the random variable X_T given $X_t = x$ is given by

$$\mu_{X_T} = x - \frac{1}{2}\sigma^2(T-t), \quad \frac{\partial \mu_{X_T}}{\partial x} = 1. \tag{1.80}$$

Using (1.79), the j-th derivative of the conditional density w.r.t. initial value x is given by

$$\frac{\partial^j f_{X_T|X_t}}{\partial x^j}(y;x) = f_{X_T|X_t}(y;x)\cdot p_j(y). \tag{1.81}$$

By the property given in (1.43), as long as $j \le d$, we have

$$< V(X_T), p_j(X_T) >_{L_{t,x}} = < \sum_{k=0}^{d} \beta_k \phi_k, p_j(X_T) >_{L_{t,x}} . \tag{1.82}$$

Consequently, with the least-squares estimator β obtained by monomials up to order $d \ge j$, we exchange the order of integration and differentiation and have

$$\begin{aligned}
\frac{\partial^j c}{\partial x^j}(t,x) &= \int_{\mathbb{R}} V(y)\frac{\partial^j f_{X_T|X_t}}{\partial x^j}(y;x)dy = \int_{\mathbb{R}} V(y)p_j(y)f_{X_T|X_t}(y;x)dy \\
&= < V(X_T), p_j(X_T) >_{L_{t,x}} = < \sum_{k=0}^{d} \beta_k \phi_k, p_j(X_T) >_{L_{t,x}} \\
&= \sum_{k=0}^{d} \beta_k \int_{\mathbb{R}} y^k p_j(y) f_{X_T|X_t}(y;x)dy \\
&= \sum_{k=0}^{d} \beta_k \int_{\mathbb{R}} y^k \frac{\partial^j f_{X_T|X_t}}{\partial x^j}(y;x)dy \\
&= \sum_{k=0}^{d} \beta_k \frac{\partial^j}{\partial x^j}\int_{\mathbb{R}} y^k f_{X_T|X_t}(y;x)dy = \sum_{k=0}^{d} \beta_k \frac{\partial^j \psi_k}{\partial x^j}(x,t,T).
\end{aligned} \tag{1.83}$$

Notice that when $d = 1$ we cannot compute the second derivative $\frac{\partial^2 c}{\partial x^2}$, since the equation in (1.82) is up to order $d = 1$. In order to compute the second derivative, we must have $d \ge 2$. Using a monomial basis up to order d and the associated coefficients, one can directly compute the 1-th to the d-th derivatives of function $c(t,x)$ w.r.t. x.

This result is also true when the random variables follows a log-normal distribution.

1.6.2. TAYLOR EXPANSION OF THE DENSITY W.R.T. THE PARAMETERS

In this section, we will develop some useful results, that will be used for the error analysis in Section 1.7.

TAYLOR SERIES OF $f_{X_T|X_t}$ AT x

The normal distribution function is infinitely differentiable at $X_t = x$. We use Taylor's theorem to write the Taylor series of function $f_{X_T|X_t}$ at $X_t = x$ as follows [69]

$$\begin{aligned}
f_{X_T|X_t}(y;x^*) &= \sum_{j=0}^{d} \frac{1}{j!}\frac{\partial^j f_{X_T|X_t}}{\partial x^j}(y;x)\cdot(\Delta x)^j + R_d, \\
\text{with} \quad R_d &= \frac{1}{(d+1)!}\frac{\partial^{d+1} f_{X_T|X_t}}{\partial x^{d+1}}(y;x_c)(\Delta x)^{d+1}, \quad x < x_c < x^*.
\end{aligned} \tag{1.84}$$

Using the result in (1.81) to replace the derivatives of $f_{X_T|X_t}$ in (1.84), we have

$$f_{X_T|X_t}(y;x^*) = f_{X_T|X_t}(y;x)\sum_{j=0}^{d}\frac{1}{j!}p_j(y)\cdot(\Delta x)^j + R_d,$$
$$\text{with}\quad R_d = \frac{1}{(d+1)!}f_{X_T|X_t}(y;x_c)p_{d+1}(y)(\Delta x)^{d+1},\quad x < x_c < x^*. \tag{1.85}$$

TAYLOR SERIES $f_{X_T|X_t}$ AT t

Function $f_{X_T|X_t}$ is also a function w.r.t. time t, and in this section we will present its Taylor series at time t. For this purpose, we start by deriving the Taylor series of a normal density function with its variance σ_y^2.

Similar to (1.77), by iteration, we can derive the j-th derivative of the normal density function $f_{\mathcal{N}}(y;\mu_y,\sigma_y^2)$ w.r.t. the variance (σ_y^2) as follows

$$\frac{\partial^j f_{\mathcal{N}}}{\partial(\sigma_y^2)^j} = f_{\mathcal{N}}\cdot\left(\left(\frac{\partial\log f_{\mathcal{N}}}{\partial(\sigma_y^2)}\right)^j + \frac{\partial^j\log f_{\mathcal{N}}}{\partial(\sigma_y^2)^j}\right), \tag{1.86}$$

with

$$\frac{\partial\log f_{\mathcal{N}}}{\partial(\sigma_y^2)} = -\frac{1}{2\sigma_y^2}+\frac{1}{2\sigma_y^4}(y-\mu_y)^2,\quad \frac{\partial^2\log f_{\mathcal{N}}}{\partial(\sigma_y^2)^2} = \frac{1}{\sigma_y^3}-\frac{2}{\sigma_y^5}(y-\mu_y)^2. \tag{1.87}$$

The j-th derivative w.r.t. the variance of the normal density $f_{\mathcal{N}}(y;\mu_y,\sigma_y)$ can be expressed as

$$\frac{\partial^j f_{\mathcal{N}}}{\partial(\sigma_y^2)^j}(y;\mu_y,\sigma_y^2) = f_{\mathcal{N}}(y;\mu_y,\sigma_y^2)p_{2j}(y), \tag{1.88}$$

where $p_{2j}(y)$ is a polynomial function of y with polynomial degree $2j$.

We wish to write the Taylor series of the density in a way such that the order of the appearing Taylor polynomial $2j \le d$, i.e. $j \le d/2$. For this purpose, we define the operator $\lfloor\cdot\rfloor$, which returns the nearest integer less than or equal to the value inside the symbol.

We will also replace the derivatives by (1.88) in the Taylor series. Then the Taylor series of the density $f_{\mathcal{N}}(y;\mu_y,\sigma_y^2)$ at σ_y^2 can be expressed as follows [69]:

$$f_{\mathcal{N}}(y;\mu_y,\sigma_y^2+\Delta\sigma_y^2) = f_{\mathcal{N}}(y;\mu_y,\sigma_y^2)\sum_{k=0}^{\lfloor d/2\rfloor}\frac{1}{j!}p_{2j}(y)(\Delta\sigma_y^2)^j + R_{\lfloor d/2\rfloor},$$
$$\text{with } R_{\lfloor d/2\rfloor} = \frac{1}{(\lfloor d/2\rfloor+1)!}f_{\mathcal{N}}(y;\mu_y,\sigma_c^2)p_{d+1}(y)(\Delta\sigma_y^2)^{\lfloor d/2\rfloor+1}(\Delta\sigma_y^2)^{\lfloor d/2\rfloor+1}, \tag{1.89}$$

with $\sigma_y^2 < \sigma_c^2 < \sigma_y^2+\Delta\sigma_y^2$.

Function $f_{X_T|X_t}(y;x)$ is a normal density function with mean $\mu_y = x-\frac{1}{2}\sigma^2(T-t)$ and variance $\sigma_y^2 = \sigma^2(T-t)$. It is easy to see that $\Delta\mu_y = \Delta x+\frac{1}{2}\sigma^2\Delta t$ and $\Delta\sigma_y^2 = -\sigma^2\Delta t$. We choose $\Delta x = -\frac{1}{2}\sigma^2\Delta t$ such that $\Delta\mu_y = 0$, and thus the Taylor series of $f_{X_T|X_t}$ at time t are

written by

$$f_{X_T|X_{t^*}}(y;x-\frac{1}{2}\sigma^2\Delta t) = f_{X_T|X_t}(y;x-\frac{1}{2}\sigma^2\Delta t)\sum_{k=0}^{\lfloor d/2\rfloor}\frac{1}{j!}p_{2j}(y)(\Delta t)^j + R_{\lfloor d/2\rfloor},$$
$$\text{with } R_{\lfloor d/2\rfloor} = \frac{1}{(\lfloor d/2\rfloor+1)!}f_{X_T|X_{t_c}}(y;x-\frac{1}{2}\sigma^2\Delta t)p_{2\lfloor d/2\rfloor+2}(y)(\Delta t)^{\lfloor d/2\rfloor+1}, \quad (1.90)$$

where $t < t_c < t^*$.

1.7. ERROR ANALYSIS FOR SGBM WITHOUT BUNDLES

Varying the initial value X_0 from -0.5 to 0.5 in Test 1 of Section 1.5.3, we can plot the theoretical coefficients β_0 and β_1 against the corresponding values for X_0 in Figure 1.3. Both coefficients are continuous functions w.r.t. X_0, which implies that, up to some tolerance, within a small interval $[-\Delta x + x, \Delta x + x]$, the difference in the coefficients can be ignored. This implies in turn that we may use the coefficients obtained at $X_0 = x$ to approximate the expectations conditional on values in this interval.

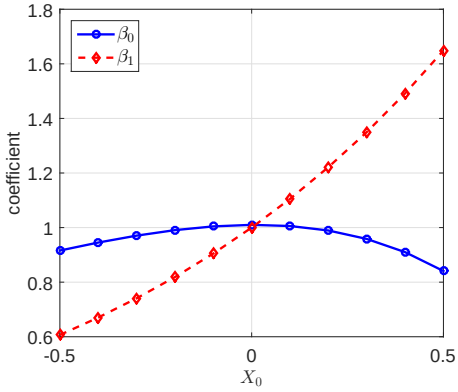

Figure 1.3: β_0 and β_1 w.r.t. X_0 in Test 1 of Section 1.5.3.

In SGBM without bundles, at a future time t_m, samples $\{\hat{x}_{m+1,h}\}_{h=1}^H$ are drawn from $F_{X_{t_{m+1}}|X_{t_0}}$, and we use these samples to approximate the conditional expectation defined by the distribution $F_{X_{t_{m+1}}|X_{t_m=\hat{x}_{m,h}}}$, $h = 1,\ldots,H$. The error will directly arise from the difference among these two functions. In this section, we will approximate the error of this approximation.

1.7.1. THEORETICAL APPROXIMATION ERROR

We adapt our notation using $\{\beta_k^{t,x}, k = 0,\ldots,d\}$ to represent the least-squares estimator of the coefficients given $X_t = x$. So,

$$c(t,x) = \mathbb{E}_t^x[V(X_T)] = \mathbb{E}_t^x\left[\sum_{k=0}^d \beta_k^{t,x}\phi_k\right] = \sum_{k=0}^d \beta_k^{t,x}\psi_k(x,t,T). \quad (1.91)$$

We approximate the conditional expectation given $X_{t^*} = x^*$ as follows

$$c(t^*, x^*) = \mathbb{E}_{t^*}^{x^*}[V(X_T)] \approx \sum_{k=0}^{d} \beta_k^{t,x} \psi(x^*, t^*, T) := c_1(t^*, x^*), \tag{1.92}$$

with $\Delta x = x^* - x$ and $\Delta t = t^* - t$.

The error in c_1 is given by

$$\begin{aligned} c(t^*, x^*) - c_1(t^*, x^*) &= \mathbb{E}^{\mathbb{Q}}\left[V(X_T)\middle| X_{t^*} = x^*\right] - \mathbb{E}^{\mathbb{Q}}\left[\sum_{k=0}^{d} \beta_k^{t,x} \phi_k \middle| X_{t^*} = x^*\right] \\ &= \int_{\mathbb{R}} \left(V(y) - \sum_{k=0}^{d} \beta_k^{t,x} y^k\right) f_{X_T|X_{t^*}}(y; x^*) dy. \end{aligned} \tag{1.93}$$

By the inner product of the projection presented in (1.82), we have

$$\int_{\mathbb{R}} \left(V(y) - \sum_{k=0}^{d} \beta_k^{t,x} y^k\right) p_j(y) f_{X_T|X_t}(y; x) dy = 0, \quad j = 0, 1, \ldots, d. \tag{1.94}$$

Use the Taylor series given in (1.85) and (1.90) to replace $f_{X_T|X_{t^*}}(y; x^*)$ respectively in (1.93) and use the result in (1.94), we have

- When $\Delta t = 0$:

$$c(t^*, x^*) - c_1(t^*, x^*) = \int_{\mathbb{R}} \left(V(y) - \sum_{k=0}^{d} \beta_k^{t,x} y^k\right) R_d dy \sim O(\Delta x^{d+1}), \tag{1.95}$$

  with $\Delta x = x^* - x$.

- When $\Delta x + \frac{1}{2}\sigma^2 \Delta t = 0$:

$$c(t^*, x^*) - c_1(t^*, x^*) = \int_{\mathbb{R}} \left(V(y) - \sum_{k=0}^{d} \beta_k^{t,x} y^k\right) R_{\lfloor d/2 \rfloor} dy \sim O(\Delta t^{\lfloor d/2 \rfloor + 1}), \tag{1.96}$$

  with $\Delta t = t^* - t$.

1.7.2. MONTE CARLO APPROXIMATION ERROR

By H samples drawn from the distribution function $F_{X_T|X_t=x}$, we get the Monte Carlo least-squares estimator $\{\hat{\beta}_k^{t,x}, k = 0, \ldots, d\}$. The approximation for the expectation conditional on $X_{t^*} = x^*$ can be expressed by the Monte Carlo least-squares linear coefficients, given by

$$c_2(t^*, x^*) := \sum_{k=0}^{d} \hat{\beta}_k^{t,x} \psi_k(x^*, t^*, T) \approx c(t^*, x^*), \tag{1.97}$$

where c_2 is the Monte Carlo estimator of c_1. When the number of samples H goes to infinity, the Monte Carlo approximation converges, i.e. $\mathbb{E}[c_1 - c_2] \xrightarrow[p]{} 0$.

The mean squared error of approximating c by c_2 can be subdivided into two parts as

$$\begin{aligned}\mathbb{E}\left[(c-c_2)^2\right] &= \mathbb{E}\left[(c-c_1+c_1-c_2)^2\right] \\ &= (c-c_1)^2+2(c-c_1)\mathbb{E}\left[(c_1-c_2)\right]+\mathbb{E}\left[(c_1-c_2)^2\right] \\ &= \text{Bias}\,(c,c_1)+\text{Var}\,(c_2)\,, \end{aligned} \tag{1.98}$$

where the bias can estimated as in (1.95) and (1.96) and the variance decays at rate $\frac{1}{H}$.

Comment: The mean squared error of SGBM without using bundles can be interpreted as the sum of a bias term and a variance term. In SGBM without bundles, using the coefficients obtained via samples with initial values $X_0 = x$, we approximate the expectation conditional on $X_t = x^*$, and thus the bias term is related to $\Delta t = t - t_0 = t$ and $\Delta x = x^* - x$. The variance arises from the Monte Carlo simulation, and decays at the rate $\frac{1}{H}$. Both the bias and the variance can be be reduced by increasing the polynomial order.

1.7.3. TEST OF THE BIAS TERM

We have tested the convergence rate in Section 1.5.3, and in this section we will focus on checking whether the bias term decays as expected in (1.95) and (1.96) for a basic test case.

Assume the stochastic process $\{X_t, t \in [0,T]\}$ evolves with SDE (1.72) in Section 1.5.3. The parameters we choose are $T = 0.2$, $\sigma = 0.6$, and $X_0 = x = 0$. Generate H independent paths $\{\hat{x}_{m,1}, \hat{x}_{m,2}, \ldots, \hat{x}_{m,H}\}_{m=1}^{10}$ on a collection of dates $\mathcal{T} = \{t_m = 0.02m, m = 0, \ldots 10\}$. The samples $\{\hat{x}_{m,h}\}_{h=1}^{H}$ can be viewed as drawn from $F_{X_{t_m}|X_0=0}$. In order to access the bias term, we choose a large sample size $H = 10^6$ to reduce the error arising from the variance.

In the first test, we wish to compute $c(t_m, x^*) = \mathbb{E}_{t_m}^{x^*}\left[\exp\left(X_{t_{m+1}}\right)\right]$, where $x^* = -\frac{1}{2}\sigma^2 t_m$. The approximation is performed by using the linear coefficients obtained via samples $\{\hat{x}_{m+1,h}\}_{h=1}^{H}$, and thus the setting is $\Delta x + \frac{1}{2}\sigma^2 t_m = 0$ and $\Delta t = t_m - t_0$. The rate of bias w.r.t. Δt is given in (1.90).

Figure 1.4 (a) presents the RMSE of approximating $c(t_m, x^*)$ against $\Delta t = t_m - t_0$. As expected in (1.96), the error goes to zero at rate $O(\Delta t)$ in the case of $d = 1$. In the case of $d = 2$ and $d = 3$, the error decays at the same rate $O(\Delta t^2)$, since $\lfloor 2/2 \rfloor + 1 = \lfloor 3/2 \rfloor + 1 = 2$. When $d = 4$, the error curve follows the rate $O(\Delta t^3)$.

In the second test, we wish to compute $c(0, x^*) = \mathbb{E}_0^{x^*}\left[\exp\left(X_{0.1}\right)\right]$, with $x^* = 1/2^j$, $j = 1, 2, \ldots, 5$. The conditional expectations are approximated using linear coefficients based on samples $\{\hat{x}_{10,h}\}_{h=1}^{H}$. So, the setting is $\Delta x = x^* - x = 1/2^j$. Figure 1.4 (b) illustrates the RMSE of the approximation w.r.t. the size of Δx. It goes as expected at the rate $O(\Delta x^{(d+1)})$ in (1.95).

We are also interested in the error of approximation over all paths. At a fixed time t, Δt is equal for all paths, and we can focus on the impact of Δx. Figure 1.5 gives the scatter plots of the approximated conditional expectations against Δx on cross-section samples at time $t_m = 0.1$. It shows that, with a fixed Δt, when $d = 1$ the error is a quadratic function of Δx, and when $d = 2$, the error is a cubic polynomial function of Δx, and so on. Most important, at the two tails of the distribution, the errors are the largest, and using a higher order d can significantly reduce the error.

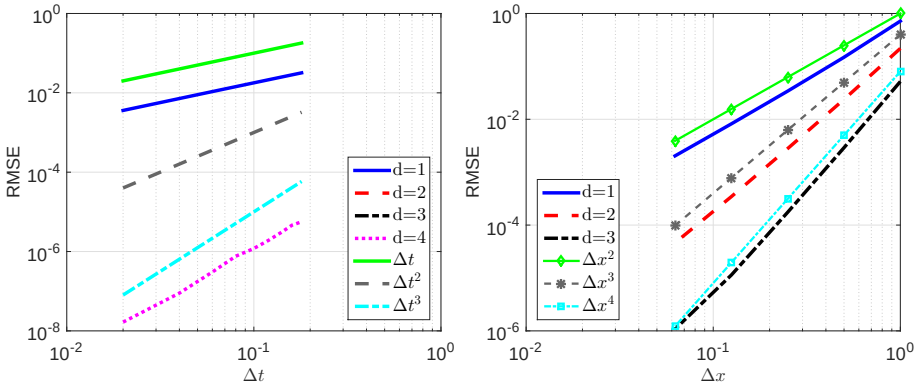

(a) Error w.r.t. Δt when $\Delta x + \frac{1}{2}\sigma^2 t = 0$

(b) Error w.r.t. $\Delta x = 0$ when $\Delta t = 0$

Figure 1.4: (a) The root mean-square error (RMSE) of approximating the expectation $\mathbb{E}\left[X_{t_{m+1}}|X_{t_m}\right]$ conditional on $X_{t_m} = 0 - \frac{1}{2}\sigma^2 t_m$, in which the linear coefficients are obtained based on simulations generated with $X_0 = 0$; (b) The root mean-square error (RMSE) of approximating the expectation $\mathbb{E}\left[X_{0.1}|X_0 = \frac{1}{2^j}\right]$ with $j = 1, 2, \ldots, 5$. The linear coefficients for approximation is obtained based on simulations generated with $X_0 = 0$. Results are based on 5 independent tests.

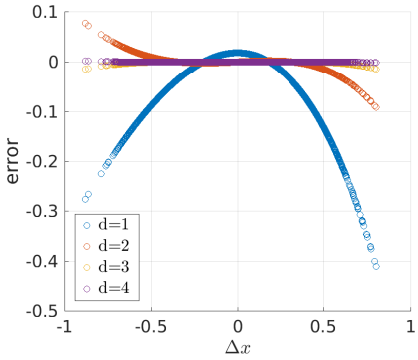

Figure 1.5: Scatter plots of error $(c - c_3)$ against $\Delta x = \hat{x}_{5,h} - x$, $h = 1, \ldots, H$ at $t = 0.1$, where $\{\hat{x}_{5,h}\}_{h=1}^{H}$ are the cross-section samples at time $t = 0.1$.

1.8. ERROR ANALYSIS FOR SGBM USING BUNDLES

We have presented using bundles and local regression in SGBM in Section 1.4.1. In this section, we will present the benefits of using bundles of SGBM.

1.8.1. THEORETICAL APPROXIMATION ERROR: THE BIAS TERM

We generate H independent paths $\{\hat{x}_{1,h}, \hat{x}_{2,h}, \ldots, \hat{x}_{M,h}\}_{h=1}^{H}$ at a fixed time grid $\{0 < t_1 < t_2 < \ldots < t_M = T\}$. At each t_m, given $\{\hat{x}_{m,h}\}_{h=1}^{H}$, we employ some bundling technique to divide all paths into J bundles $\mathscr{B}_{m,j}$, such that the realized values of the underlying

factor within each bundle form some disjoint domains. We denote these domains by

$$\mathscr{D}_{m,1} = \Big[\min_{h\in\mathscr{B}_1}(\hat{x}_{m,h}), \max_{h\in\mathscr{B}_1}(\hat{x}_{m,h})\Big), \mathscr{D}_{m,j} = \Big[\max_{h\in\mathscr{B}_{j-1}}(\hat{x}_{m,h}), \max_{h\in\mathscr{B}_j}(\hat{x}_{m,h})\Big), j = 2,3,\ldots,J. \quad (1.99)$$

We use the notations $X_m := X_{t_m}$ and $X_{m+1} := X_{t_{m+1}}$ for simplification. The conditional probability of X_{m+1} given $X_m \in \mathscr{D}_j$ at time t_m reads [70]

$$F_{\mathscr{D}_{m,j}}(y) = \mathbb{Q}\Big(X_{m+1} \le y \Big| X_m \in \mathscr{D}_{m,j}\Big) = \frac{\mathbb{Q}\left(X_{m+1} \le y, X_m \in \mathscr{D}_{m,j}\right)}{\mathbb{Q}\left(X_m \in \mathscr{D}_{m,j}\right)}. \quad (1.100)$$

Next, based on the definition of the conditional probability density function, we define a function as follows

$$\begin{aligned} f_{\mathscr{D}_{m,j}}(y) &= \frac{dF_{\mathscr{D}_{m,j}}}{dy}(y) = \frac{\int_{\mathscr{D}_{m,j}} f_{X_{m+1},X_m}(x,y)dx}{\int_{\mathscr{D}_{m,j}} f_{X_m}(x)dx} \\ &= \frac{\int_{\mathscr{D}_{m,j}} f_{X_{m+1}|X_m}(y;x) f_{X_m}(x)dx}{\int_{\mathscr{D}_{m,j}} f_{X_m}(x)dx}, \end{aligned} \quad (1.101)$$

where f_{X_{m+1},X_m} is the joint density function of (X_{m+1}, X_m) and $\int_{\mathscr{D}_{m,j}} f_{X_m}(x)dx > 0$.

The function $f_{\mathscr{D}_{m,j}}$ satisfies that $\int_{-\infty}^{\infty} f_{\mathscr{D}_{m,j}}(y)dy = 1$ and $f_{\mathscr{D}_{m,j}}(y) \ge 0$ for any $y \in \mathbb{R}$. It can be viewed as a weight function. We define a new norm with this weight function in the same way as we defined the norm with the density function:

$$\|V(X_{m+1})\|_{L^2_{\mathscr{D}_{m,j}}} = \left(\int_{\mathbb{R}} \big(V(y)\big)^2 f_{\mathscr{D}_{m,j}}(y)dy\right)^{\frac{1}{2}} < \infty \quad (1.102)$$

With this norm, we get the linear coefficients of the projection of $V(X_T)$ on the subspace $\mathscr{P}_d$, denoted by $\beta_k^{m,j}$, $k = 0,\ldots,d$, that are obtained as follows

$$\begin{aligned} \{\beta_k^{m,j}, k = 0,\ldots,d\} &= \underset{\{b_k\in\mathbb{R}, k=0,\ldots,d\}}{\operatorname{argmin}} \left\| V(X_{m+1}) - \sum_{k=0}^{d} b_k (X_{m+1})^k \right\|^2_{L^2_{\mathscr{D}_{m,j}}} \\ &= \underset{\{b_k\in\mathbb{R}, k=0,\ldots,d\}}{\operatorname{argmin}} \int_{\mathbb{R}} \left(V(y) - \sum_{k=0}^{d} b_k y^k \right)^2 f_{\mathscr{D}_{m,j}}(y)dy. \end{aligned} \quad (1.103)$$

For $x \in \mathscr{D}_{m,j}$, we approximate the conditional expectation given $X_{t_m} = x^*$ by

$$c_3(t_m, x^*) = \sum_{k=0}^{d} \beta_k^{m,j} \psi_k(x^*, t_m, t_{m+1}) \approx \mathbb{E}^{x^*}_{t_m}[V(X_{m+1})] := c(t_m, x^*). \quad (1.104)$$

The error in the approximation, i.e. $(c_3 - c)$ is determined by the difference between the function $f_{D_j}(y)$ and the function $f_{X_{m+1}|X_m}(y;x^*)$. Hence, the size of the domain $\mathscr{D}_j$ and the distribution of X_m on the domain $\mathscr{D}_j$ both have some impact on the value of the error.

If the domain $\mathscr{D}_{m,j}$ can be expressed by $(x^* - \Delta x, x^* + \Delta x)$, the error in approximating the conditional expectation approaches zero as Δx goes to zero. The size of the domain $\mathscr{D}_{m,j}$ becomes zero as it shrinks into a single point set. Typically, the size of the sub-domains can be reduced by increasing the number of bundles. Hence the bias arising in approximation can be significantly reduced by using bundles. It also implies that, when making bundles, we should ensure that the size of any of these disjoint domains gets smaller when more bundles are used.

The bias can be also reduced by increasing the order of the monomial basis, which we will demonstrate with numerical results.

1.8.2. MONTE CARLO APPROXIMATION ERROR

We employ the least-squares method based on the Monte Carlo paths. The realized values at the paths at time t_m and t_{m+1}, i.e. $\{(\hat{x}_{m,h}, \hat{x}_{m+1,h})\}$, can be regarded as i.i.d. samples drawn from the joint distribution F_{X_{m+1},X_m}. Then, for each bundle $\mathscr{B}_{m,j}$, samples can be viewed as drawn from the conditional probability $F_{\mathscr{D}_{m,j}}$, $j = 1, \ldots, J$. Denote the number of samples of the j-th bundle by H_j.

The Monte Carlo least-squares estimator of the coefficients $\left\{\beta_k^{m,j}, k = 0, \ldots, d\right\}$ can be obtained using least-squares based on the H_j samples, i.e.

$$\{\hat{\beta}_k^{m,j}, k = 0, \ldots, d\} = \underset{\{b_k \in \mathbb{R}, k=0,\ldots,d\}}{\operatorname{argmin}} \sum_{h \in \mathscr{B}_{m,j}} \left(V(\hat{x}_{m+1,h}) - \sum_{k=0}^{d} b_k (\hat{x}_{m+1})^k \right)^2. \quad (1.105)$$

Let the SGBM approximation be denoted by

$$c_4(t_m, x^*) = \sum_{k=0}^{d} \hat{\beta}_k^{m,j} \psi_k(x^*, t_m, t_{m+1}) \approx \mathbb{E}_{t_m}^{x^*}[V(X_{m+1})] := c(t_m, x^*). \quad (1.106)$$

As we have presented, the mean squared error can be expressed as the sum of the bias and variance terms, i.e.

$$\mathbb{E}\left[(c - c_4)^2\right] = \text{Bias}(c_3, c_4) + \text{Var}(c_4), \quad (1.107)$$

where the bias term approaches zero as the number of bundles goes to infinity and the variance term decays at rate $1/H_j$.

Comments:

- We can see that the result of SGBM converges as the number of bundles goes to infinity and the number of paths within each bundle goes to infinity.
- As presented, increasing the polynomial order d may help with the reduction of the bias and the variance terms when the number of paths and the number of bundles are fixed.
- A benefit of using bundles is to reduce the bias term significantly. Though the bias can also be reduced by a higher d, we prefer to use a lower polynomial monomial basis because of the curse of dimensionality.

- When the total number of paths is fixed, increasing the number of paths will cause fewer paths in each bundle, and causes a higher variance. One needs to strike a balance between the bias and the variance terms.

1.8.3. TEST OF BUNDLES

Next, we present some numerical results to see the benefits of bundles.

Using the same numerical test as in Section 1.7.3, we wish to compute the conditional expectation $\mathbb{E}\left[\exp(X_{0.2})|X_{0.1}\right]$. We will divide all paths into J bundles based on the realized values of $X_{0.1}$, such that the number of paths within each bundle is equal, i.e. $H_j = H/J$, $j = 1,\ldots,J$.

Figure 1.6 demonstrates the benefits of using bundles with a low polynomial order $d = 1$. We see in Figure 1.6 (a) that the errors get smaller as the number of bundles is increased, in particular at the left and right parts of the interval. Figure 1.6 (b) compares the analytic solution to the obtained scatter plots for the expectation. When the number of bundles is just 1, i.e. bundling technique is not used, the approximated expectation is a straight line w.r.t. the value of $X_{0.1}$. When the number of bundles is increased, the approximated expectation gradually 'bends' to the analytic solution.

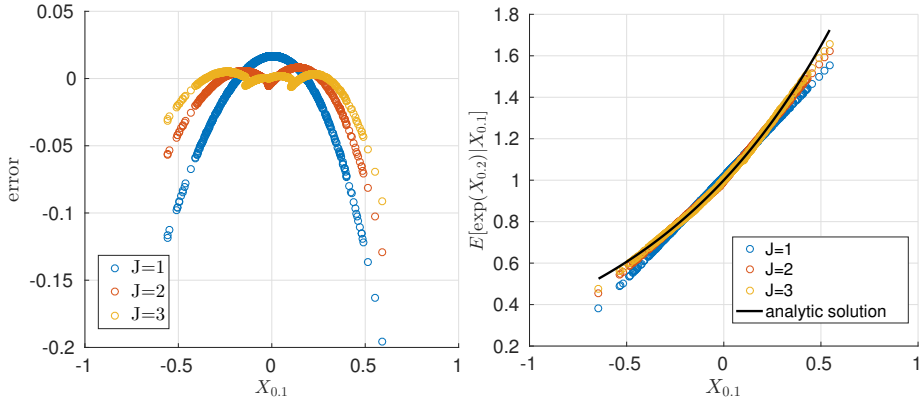

(a) SGBM error (b) SGBM approximation

Figure 1.6: (a): Scatter plots of errors $(c - c_4)$ in approximating the expectations of $\mathbb{E}[\exp(X_{0.2})|X_{0.1}]$ against the realized values of $X_{0.1}$; (b) Scatter plots of the SGBM approximation and the analytic solution of $\mathbb{E}[\exp(X_{0.2})|X_{0.1}]$ against the realized values of $X_{0.1}$. The polynomial order in SGBM is chosen to be $d = 1$. $H = 10^6$.

Figure 1.7 illustrates the impact of the number of paths on the accuracy of SGBM. In order to estimate the error over all paths, we use the L^2 norm of the errors over all paths to measure the average error at a single time point t_m, i.e.

$$\sqrt{\frac{1}{H}\sum_{h=1}^{H}\left(V(\hat{x}_{m,h}) - V_{\text{SGBM}}(\hat{x}_{m,h})\right)^2}.$$

A convergence test for SGBM is to increase the number of bundles for a fixed sample number H, and compute the corresponding error (measured by L^2 norm).We choose the

number of paths $H = 10^6$ in Figure 1.7 (a) and a smaller one $H = 10^3$ in Figure 1.7 (b). As expected, the error can be reduced by increasing the number of bundles, but when H is small, i.e. $H = 10^3$, the convergence stops at $J = 8$. This is because when the number of paths is relatively small, increasing the number of bundles will significantly reduce the number of paths within each bundle, and then the error is limited by the variance term. So, with a fixed total number of paths, the error over all paths can be improved only to some extent.

Figure 1.7 also demonstrates that using higher order monomials basis can further improve the accuracy with a fixed number of paths and a fixed number of bundles.

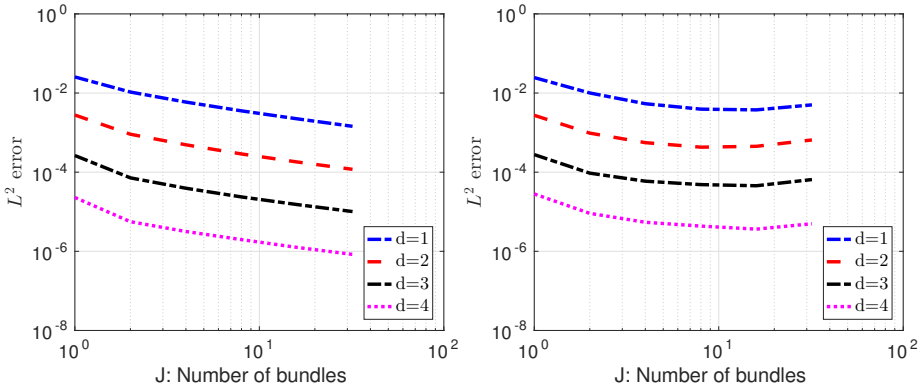

(a) $H = 10^6$ (b) $H = 10^3$

Figure 1.7: L^2 norm of errors over all paths against the number of bundles when $d = 1,2,3,4$. (a) $H = 10^6$; (b): $H = 10^3$. The value we wish to compute is $\mathbb{E}\left[\exp\left(X_{0.2}\right)|X_{0.1}\right]$.

1.9. THESIS ORGANIZATION

In this chapter, we have introduced the concepts of EE, PFE ad CVA, and the computational and modeling issues in this field of risk management. Using a simple example, we presented a discussion about the convergence and error analysis for the SGBM algorithm. One purpose of this thesis is to further develop the SGBM algorithm for the computational issues in quantifying CCR under hybrid stochastic asset models. Another goal is to develop models for WWR in a CVA calculation.

The structure of the thesis is outlined as follows.

Chapter 2 and Chapter 3 are concerned with the computation of the exposure profiles under the risk-neutral probability measure needed for CVA calculation. Chapter 2 provides a general framework for computing exposure profiles based on Monte Carlo paths. We present three numerical schemes, the Finite Difference method, the COS method and the SGBM approach for the valuation of contract values on the generated paths under the Heston stochastic volatility model. We show the exposure distributions for the Bermudan option along the risk horizon. The benchmark is the COS method, which is based on Fourier-cosine expansions and FFT, developed by Fang and Oosterlee [29]. This chapter basically contains the contents of paper [24].

Chapter 3 studies the impact of stochastic volatility and stochastic interest rate on the exposure profiles. The SGBM scheme is further developed for the two- to three-dimensional hybrid models, such as the Heston model and Heston Hull-White model. We present the sensitivities of EE w.r.t. the initial values on the risk horizon. Besides Bermudan options, we also study the exposure profile of barrier options. The benchmark for the two-dimensional model is based on the 2D COS method developed by Ruijter and Oosterlee [72], and for the three-dimensional model is based on the 3D COS method developed by Lech and Oosterlee [39]. The contents of this chapter can be found in the paper [32].

Chapter 4 studies the WWR. The default probability is modeled by an intensity model. In this chapter, the intensity is considered as a random variable, and we propose three models to describe the dependency structure between intensity and other market factors. Different from the previous chapters, in this chapter we compute CVA as the difference between the default-free and default-adjusted values of the option contracts. In this setting and along with the SGBM algorithm, we present the computation of CVA VaR and CVA ES without sub-simulations. We show the impact of WWR to the value of CVA for a European option contract by varying the correlation coefficients. Besides, for Bermudan options, we study the impact of CCR and WWR on the early-exercise regions assuming that option holders will have different exercise decisions. This chapter essentially contains the contents of paper [31].

The EE and PFE reflecting the real-world risk are studied in Chapter 5. In this chapter, we clarify the importance of using real-world simulations for computing risk-statistics measures of CCR, and show how to make SGBM into an efficient algorithm for computing the real-world exposure profiles without any sub-simulation. In this chapter, the SGBM is developed for pricing Bermudan swaptions under the Hull-White and the G2++ models. The COS method is also further developed to pricing Bermudan swaptions to provide a benchmark. The contents of this paper are based on the paper [30].

Chapter 6 presents conclusions and an outlook for future research.

CHAPTER 2

Efficient computation of exposure profiles for counterparty credit risk

This chapter presents three computational techniques for approximation of exposure under the risk-neutral probability measure for pricing CCR of a financial contract. The three techniques all involve a Monte Carlo path discretization and simulation of the underlying entities. Along the generated paths, the corresponding values and distributions are computed during the entire lifetime of the option. Option values are computed by either the finite difference method for the corresponding partial differential equations, or the simulation based Stochastic Grid Bundling Method (SGBM), or by the COS method, based on Fourier-cosine expansions. In this research, the studied financial contracts are option contracts with early-exercise opportunities. The underlying asset dynamics are given by either the Black-Scholes or the Heston stochastic volatility model. We study the impact of the stochastic volatility on the exposure distributions.

2.1. INTRODUCTION

We investigate the future exposure distributions of Bermudan options during the life of the option contracts with stochastic volatility under the Heston's model. We present three numerical methods for computation of exposure values. All methods presented contain essentially two elements, a forward sweep for generating future scenarios and a backward sweep to calculate exposures along the generated asset paths. The forward Monte Carlo method generates the asset paths from initial time up to maturity. Along the paths, option values are determined at each exercise time.

Because of the complexity of this problem, efficient computation of the option prices is required. The COS Fourier option pricing method may seem a suitable candidate because of its speed and accuracy particularly for Lévy processes, see [29]. Also the finite difference method, approximating solutions to partial differential equations, may be suitable as it typically results in approximate option prices for a grid of underlying values. This feature may be exploited in the EE context, as all grid points can then be used to generate option densities. The recent development of the Stochastic Grid Bundling Method (SGBM), which is a Monte Carlo based method particularly suitable for high-dimensional early-exercise options, in [50], is another candidate because it also rapidly converges and is accurate.

The set-up of this chapter is as follows. In Section 2.2 brief descriptions of the Heston

This chapter is based on the article 'Efficient computation of exposure profiles for counterparty credit risk', published in *International Journal of Theoretical and Applied Finance*, 17(04):1450024, 2014 [24], and it also appeared in CSL de Graaf's PhD thesis [23].

model and the exposure of Bermudan options are presented. The underlying asset dynamics and the Monte Carlo discretization technique applied are also discussed. In Section 2.3 we describe the computation of the exposure measures by the finite difference method, SGBM and the COS method, respectively. In Section 2.4 the methods are validated and compared and we present an assessment of the impact of stochastic volatility on the exposures. Finally, conclusions are presented in Section 2.5.

2.2. EXPOSURE OF BERMUDAN OPTIONS UNDER HESTON'S MODEL

We will present methods for the computation of the exposure of Bermudan options under the Heston stochastic volatility asset dynamics, given by

$$\begin{aligned} dS_t &= rS_t dt + \sqrt{v_t} S_t \left(\sqrt{1-\rho^2}\, dW_t^1 + \rho dW_t^2 \right), \\ dv_t &= \kappa(\bar{v} - v_t) dt + \gamma \sqrt{v_t} dW_t^2, \end{aligned} \tag{2.1}$$

where W_t^1 and W_t^2 are independent Wiener processes under the risk-neutral measure $\mathbb{Q}$, κ is the speed of mean reversion parameter in the CIR process for the variance, $\bar{v}$ represents the level of mean reversion, and γ is the so-called volatility of volatility parameter; r is the constant risk-free interest rate.

The market factors evolve as in (2.1) over the risky horizon $[0, T]$. We will monitor the exposure at future time at a set of equally-spaced monitoring dates, denoted by

$$\mathcal{T} = \{t_1, t_2, \ldots, t_M\}, \tag{2.2}$$

where M denotes the number of monitoring dates, and the time step size is Δt.

2.2.1. BERMUDAN OPTIONS

A Bermudan option is defined as an option where the buyer has the right to exercise at a set of (discretely spaced) time points. We assume that *the early-exercise dates coincides with the monitoring dates*, i.e. the collection of early-exercise dates is the same as the collection of exposure monitoring dates $\mathcal{T}$.

The state of the process at time t_m is denoted by the pair (S_m, v_m) with S_m the price of the underlying and v_m the variance at time t_m. At the initial time t_0 exercise is not common. At each exercise time in $\mathcal{T}$, the exercise value, given by the payoff function, and the continuation value of the option are compared.

The immediate payoff of exercising the option at time t_m is given by,

$$g(S_m) = \begin{cases} (S_m - K)^+, & \text{for a call,} \\ (K - S_m)^+, & \text{for a put,} \end{cases} \tag{2.3}$$

where we refer to the function g as the exercise function.

It is assumed that the holder of the option will exercise when the payoff value is higher than, or equal to, the continuation value, and then the contract terminates. At maturity t_M, the option value is equal to the payoff value. The following recursive scheme

can be set-up to price a Bermudan option:

$$V(t_m, S_m, v_m) = \begin{cases} g(S_M), & \text{for } m = M, \\ \max\big(c(t_m, S_m, v_m), g(S_m)\big), & \text{for } m = M-1, \ldots, 2, 1, \\ c(t_0, S_0, v_0), & \text{for } m = 0, \end{cases} \tag{2.4}$$

where the continuation function c at time t_m is defined by

$$c(t_m, S_m, v_m) = e^{-r\Delta t}\mathbb{E}^{\mathbb{Q}}\left[V(t_{m+1}, S_{m+1}, v_{m+1})\middle|(S_m, v_m)\right], \tag{2.5}$$

with $V(t_{m+1}, S_{m+1}, v_{m+1})$ the option value at time t_{m+1}.

2.2.2. EXPOSURE AND CVA

By definition the exposure of an option equals zero once the option is exercised; otherwise, the exposure is equal to the continuation value of the option. The Bermudan option exposure at a future time t_m can thus be formulated as:

$$E_m = \begin{cases} 0, & \text{if exercised,} \\ c(t_m, S_m, v_m), & \text{if not exercised,} \end{cases} \qquad m = 1, 2, \cdots, M-1. \tag{2.6}$$

In addition, $\mathrm{E}_0 = c(t_0, S_0, v_0)$ and $\mathrm{E}_M = 0$.

The exposure value needs to be calculated via backward induction. The Bermudan option is computed via (2.4) from time t_M to time t_0. As we update the optimal early exercise time, the exposure values are being updated. Loosely speaking, the exposure values are zero in the early-exercise region and the optimal early-exercise boundary, and in the continuation region the exposure values are equal to the continuation values. Using the dynamics of the market factors (S_m, v_m) in (2.6), we can obtain the distribution of the exposure at each monitoring time t_m under the risk-neutral measure $\mathbb{Q}$.

The key point of computing CVA is to calculate the exposure distribution under the risk-neutral measure. Assuming independence between exposure and the counterparty's default probability, we can formulate the expression for credit valuation adjustment (CVA) as follows [38]:

$$\mathrm{CVA} \approx \mathrm{LGD}\sum_{m=0}^{M-1}\frac{\mathrm{EE}^{\mathbb{Q}}(t_m)}{B(t_m)}\left(\mathrm{PD}(t_{m+1}) - \mathrm{PD}(t_m)\right), \tag{2.7}$$

where $B(t_m) = \exp(r\,t_m)$ and the default probability given by $\mathrm{PD}(t) = 1 - \exp\left(-\bar{h}\,t\right)$ with here a constant intensity $\bar{h}$, and EE at time t is given by

$$\mathrm{EE}^{\mathbb{Q}}(t_m) := \mathbb{E}^{\mathbb{Q}}\left[\mathrm{E}_m\right]. \tag{2.8}$$

In this setting, the expression $\mathrm{EE}^{\mathbb{Q}}$ in (2.8) represents the average of future risk-neutral exposure. In order to capture the tail behavior of the exposure distribution at future times, we also look into the 97.5% percentile of the risk-neutral exposure, defined in the following way

$$\mathrm{PFE}_{\alpha}^{\mathbb{Q}}(t_m) = \inf\left\{x : \mathbb{Q}(E_m \le x) \ge \alpha\right\}, \tag{2.9}$$

where $\alpha = 97.5\%$.

Here we use 'EE' and 'PFE' defined in (2.8) and (2.9) to show the statistical properties of the risk-neutral exposure. These two statistics of exposure distribution are not used to determine the reserved capital under the Basel regulations. Instead, we employ these two statistics to study the impact of the stochastic volatility on the risk-neutral exposure distribution.

2.3. NUMERICAL METHODS TO COMPUTE EXPOSURE PROFILES

In this section, three methods are presented to compute the expected exposure for Bermudan options under the Heston dynamics. All three methods can also be used to simply calculate the value of a Bermudan option at time t_0. In combination with Monte Carlo forward path simulation, and based on the same common technique, they can be extended to value the exposure of Bermudan options.

2.3.1. GENERAL PRICING APPROACH

The market state depends on two random variables, (S_m, v_m), at time point t_m and therefore the exposure E_m is also a stochastic variable. An option value distribution at future time points can be computed by generating risk-neutral scenarios, and for that purpose a Monte Carlo simulation is employed.

For the Monte Carlo simulation the highly accurate Quadratic Exponential (QE) scheme [2] is used to generate the Heston stochastic volatility asset paths. Starting from simulated underlying values and variances, the exposures can be calculated by a backward valuation procedure. At each path, for each exercise time, the continuation value is calculated and compared to the exercise value on the path. When the exercise value is higher than, or equal to, the continuation value, the option is exercised at this path and the exposure for later time points is set to zero. At every time point the resulting exposure values for all paths generate a distribution.

The essential technique of modeling the exposure of Bermudan options can be presented as follows:

- Generate scenarios by Monte Carlo simulation under the risk-neutral probability measure;
- Calculate continuation/option values and the exercise values to decide whether to exercise or not;
- Set the exposure at each path as the continuation value if the option is not exercised; otherwise the exposure equals 0;
- Compute the empirical distribution of the exposure at each monitoring time;
- Calculate the mean and the 97.5% quantile of the obtained empirical exposure distribution.

In the remainder of this section, we will describe three methods to calculate the required continuation/option values at the simulated paths.

2.3.2. THE FINITE DIFFERENCE MONTE CARLO METHOD

An often used option pricing technique is the finite difference method [83]. The method calculates option prices based on the option pricing partial differential equation, for an entire grid of underlying values and can therefore also easily be used to compute the sensitivities (for example, the derivatives of the option prices w.r.t. the asset prices). In the scope of this research, the resulting grid of option values facilitates to determine distributions of option values at different time points. The method developed by C. S. L. de Graaf is called the *Finite Difference Monte Carlo* (FDMC) method. Solving the Heston PDE to price European or American options is extensively studied, see, for example, [33],[40] and [41].

In the case of the Heston's model, a generalized Black-Scholes operator is defined by

$$\mathscr{L}V = \frac{\partial V}{\partial t} - \frac{1}{2}\gamma^2 v\frac{\partial^2 V}{\partial v^2} - \rho\gamma v S\frac{\partial^2 V}{\partial S\partial v} - \frac{1}{2}vS^2\frac{\partial^2 V}{\partial S^2} - \kappa(\bar{v}-v)\frac{\partial V}{\partial v} - rS\frac{\partial V}{\partial S} + rV. \quad (2.10)$$

The linear complementarity problem for the price of the American put option can be derived as follows

$$\mathscr{L}V \geq 0, \quad (2.11a)$$
$$V \geq g, \quad (2.11b)$$
$$(V-g)(\mathscr{L}V) = 0, \quad (2.11c)$$

in the domain $\{(S,v,t)|S \geq 0, v \geq 0, t \in [0,T]\}$ with the initial condition $V(T,S,v) = g(S)$. The boundary conditions are stated in Table 2.1.

Table 2.1: Heston model boundary conditions for a put option.

Boundary	Value
$S \to \infty$	$V = 0$
$S = 0$	$V = K$
$v \to \infty$	$\frac{\partial^2 V}{\partial v^2} = 0$
$v = 0$	$\frac{\partial V}{\partial t} - rS\frac{\partial V}{\partial S} - \kappa\bar{v}\frac{\partial V}{\partial v} + rV = 0$

Note that in (2.11) the option can be exercised for each $t \in [0,T]$. A discrete version easily results in the pricing of a Bermudan-style option. In this research the Brennan-Schwartz [11] algorithm is used, which is a well-known technique from literature. At each exercise time, this method first solves $\mathscr{L}V = 0$, after which the option value is taken to be the maximum of this value and the exercise value. The schemes used for discretizing (2.10) in asset and variance directions are second-order accurate central schemes or one-sided second-order schemes where needed at boundaries.

The option price is computed backwards in time, from maturity T back to time t_0. The equations that need to be solved as a result of the finite difference discretization are linear systems of equations. Such a system of equations can be represented as a matrix-vector problem where the operators are represented by matrices and the (intermediate) solutions by vectors. For the time integration scheme a particular Alternating

Direction Implicit (ADI) scheme, namely the Hundsdorfer-Verwer scheme is employed, which exhibits second-order convergence in time. Next to that, due to the splitting of matrices, it involves the inversion of tridiagonal matrices while in general for (fully) implicit schemes, the matrices are not tridiagonal and may have several non-zero diagonals. For more details we refer to [33].

To ensure that all forward paths are contained in the computational domain of the finite difference technique, the boundaries $S_{\max}$ and $v_{\max}$ are prescribed such that all Monte Carlo path values at all time points are contained.

The paths attain values that are, most likely, not grid points of the finite difference grid. From this grid, specific option values are then determined by interpolation. Because this interpolation introduces errors at every point, second-order accurate *spline* interpolation is used.

In general, only a small part of the discretized grid is a region of interest, therefore one can concentrate grid points in that region. This is done by stretching the grid so that a non-uniform grid results, applied in the variance as well as in the asset dimension [40]. As here we need option values at each exercise time for many combinations of spot and variance values, non-uniformity is even more important when we compute exposure.

Because tests show that the impact of the spot dimension on the error is highest, the non-uniform grid in [40] is slightly adjusted. The grid employed is a combination of a uniform and a non-uniform grid. An interval $[S_{\text{left}}, S_{\text{right}}]$ containing K is introduced in which the mesh is uniform. We choose:

$$S_{\text{left}} = \lambda K \text{ and } S_{\text{right}} = K, \tag{2.12}$$

where $\lambda \in [0.3, 0.7]$ can be chosen depending on the quantity that needs to be computed (PFE or EE). An accurate computation of EE requires accurate pricing around the mean, which implies a high value of λ, whereas for accurate computation of quantiles, also an accurate computation of extreme values is needed for which a smaller value of λ should be chosen. So, when we compute the PFE, the dense region is shifted towards the outer regions of the domain.

Outside the interval $[S_{\text{left}}, S_{\text{right}}]$ the grid follows a hyperbolic sine function with:

$$\xi_{\min} = \sinh^{-1}\left(\frac{-S_{\text{left}}}{d_1}\right), \quad \xi_{\text{int}} = \frac{S_{\text{right}} - S_{\text{left}}}{d_1}, \quad \xi_{\max} = \xi_{\text{int}} + \sinh^{-1}\left(\frac{S_{\max} - S_{\text{right}}}{d_1}\right),$$

where d_1 is a scaling parameter, $S_{\max}$ is the chosen maximum value of the S grid (the interval $[S_{\text{left}}, S_{\text{right}}] \subset [0, S_{\max}]$), and $\xi_{\min} < 0 < \xi_{\text{int}} < \xi_{\max}$. A *uniform* grid of $m_1 + 1$ points between $\xi_{\min}$ and $\xi_{\max}$ can be built by: $\xi_0 = \xi_{\min}$, $\xi_j = \xi_0 + j\Delta\xi$, $\Delta\xi = \frac{\xi_{\max} - \xi_{\min}}{m_1}$, $j = 1, \ldots, m_1$.

Now, a *non-uniform* grid for S, $0 = s_0 < s_1 < \ldots < s_{m_1} = S_{\max}$, can be constructed via the uniform grid $\xi_0 < \xi_1 < \ldots < \xi_{m_1}$ as follows

$$s_j = \begin{cases} S_{\text{left}} + d_1 \sinh(\xi_j), & \text{if } \xi_{\min} \le \xi_j < 0, \\ S_{\text{left}} + d_1 \xi_j, & \text{if } 0 \le \xi_j \le \xi_{\text{int}}, \\ S_{\text{right}} + d_1 \sinh(\xi_j - \xi_{\text{int}}), & \text{if } \xi_{\text{int}} < \xi_j \le \xi_{\max}. \end{cases}$$

Smaller values of d_1 result in a smaller number of grid points in $[S_{\text{left}}, S_{\text{right}}]$, whereas higher values of d_1 will result in a higher density of grid points in this interval.

For the v direction many points at the boundary $v = 0$ are desired and for larger values of v the mesh can be less dense. Let m_2 be the number of points to be considered and d_2 another scaling parameter. Now the grid, $0 = v_0 < v_1 < \ldots < v_{m_2} = v_{\max}$, is defined by: $v_j = d_2 \sinh\left(\frac{j}{m_2}\sinh^{-1}(v_{\max}/d_2)\right)$, $j = 0,\ldots,m_2$.

These grids are smooth in the sense that there are real-valued constants C_0, C_1 and C_2 such that:

$$C_0\Delta\xi \le \Delta s_j \le C_1\Delta\xi \text{ and } |\Delta s_{j+1} - \Delta s_j| \le C_2(\Delta\xi)^2.$$

When the finite difference method is used to price a single option, only a single grid point at initial time is used. The FDMC method however uses a large portion of the grid points for option pricing at all exercise times which makes this method computationally attractive.

2.3.3. THE STOCHASTIC GRID BUNDLING METHOD

Here, we extend the SGBM method from [50] towards the Heston model, and exposure distributions along the time horizon are naturally obtained. The SGBM method generates a direct estimator, a lower bound for the option value, as well as an optimal early-exercise policy.

We will use one-dimensional monomials as the basis functions and provide a bundling method for this two-dimensional model. We choose the monomials of the log-stock variable up to order d to be the basis functions for the regression of the option values at time t_{m+1}, denoted by

$$\phi_k = \left(\log(S_{m+1})\right)^k, k = 0,1,\ldots,d, \tag{2.13}$$

where when $k = 0$, the basis function is the constant.

We choose only the monomials of the log-stock variable $\log(S_{m+1})$ for this 2D model, because the variance is just a factor in the evolution of the stock process. The variable S_{m+1} also contains information about the evolution of the variance factor. The risk-neutral expectations of the basis functions in (2.13) are functions w.r.t. (S_m, v_m), defined by

$$\psi_k(S_m, v_m, \Delta t) = \mathbb{E}^{\mathbb{Q}}\left[\left(\log(S_{m+1})\right)^k \middle| (S_m, v_m)\right], \tag{2.14}$$

with $k = 0,1,\ldots,d$.

These moments can be derived from the ChF of the Heston model with respect to the variable $\log(S_m)$, defined by

$$\begin{aligned}\varphi(u; t_m, t_{m+1}, \log(S_m), v_m) &= \mathbb{E}^{\mathbb{Q}}\left[\exp\left(iu\log(S_{m+1})\right) \middle| (X_m, v_m)\right] \\ &= \exp\left(\widetilde{A}(\Delta t) + \widetilde{B}_1(\Delta t)\log(S_m) + \widetilde{B}_2(\Delta t)v_m\right),\end{aligned} \tag{2.15}$$

where the coefficients

$$\begin{aligned}\widetilde{B}_1(\Delta t) &= iu, \quad \widetilde{B}_2(\Delta t) = \frac{1}{\gamma^2}\left(\kappa - iu\gamma\rho + D_1\right) - \frac{2D_1}{\gamma^2\left(1 - D_2\exp\left(-D_1\Delta t\right)\right)}, \\ \widetilde{A}(\Delta t) &= \frac{\kappa\bar{v}}{\gamma^2}\left[\left(\kappa - iu\gamma\rho - D_1\right)\Delta t - 2\log\left(\frac{1 - D_2\exp\left(-D_1\Delta t\right)}{1 - D_2}\right)\right] \\ &\quad + r(iu_1 - 1)\Delta t,\end{aligned} \tag{2.16}$$

with

$$D_2 = \frac{\kappa - iu\gamma\rho - D_1}{\kappa - iu\gamma\rho + D_1}, \quad D_1 = \sqrt{(\kappa - iu\gamma\rho)^2 + \gamma^2 u(u+i)}. \tag{2.17}$$

The moments can be derived by the relations (1.28). As an example, we present the analytic formula of the first moment

$$\psi_1(S_m, v_m, t_m, t_{m+1}) = \log(S_m) + \left(\gamma - \frac{1}{2}\bar{v}\right)\Delta t + \frac{1}{2\kappa}\left(1 - \exp\left(-\kappa\Delta t\right)\right)(\bar{v} - v_0). \tag{2.18}$$

In this chapter, we propose a bundling technique based on the recursive bifurcation bundling method introduced in [50]. In the Heston model, the asset variable and the variance variable are correlated. If we directly apply the recursive bifurcation bundling method in the case of a correlation, we may find that there are few paths within some bundles, and this problem can be hardly improved by increasing the total number of paths. As an improvement, we propose that we first perform a 'rotation' procedure on the cross-section data (S_m, v_m), such that

$$\widetilde{S}_m = \cos(\theta)S_m + \sin(\theta)v_m, \quad \widetilde{v}_m = -\sin(\theta)S_m + \cos(\theta)v_m, \tag{2.19}$$

where

$$\cos(\theta) = \sqrt{\frac{1}{1+l^2}}\,\mathrm{sign}(l), \quad \sin(\theta) = \sqrt{\frac{l^2}{1+l^2}}, \quad l = \mathrm{Cov}(S_m, v_m)\sqrt{\frac{\mathrm{Var}(S_m)}{\mathrm{Var}(v_m)}}. \tag{2.20}$$

Then we employ the recursive bifurcation bundling method on the rotated data $(\widetilde{S}_m, \widetilde{v}_m)$ to determine the bundles. Figure 2.1 demonstrates the bundles obtained without rotation (a) and with rotation (b) based on the recursive bifurcation method. In Figure 2.1, each colored block represents the realized values within one bundle. After rotation, the paths can be subdivided into bundles in a more 'average' sense w.r.t. the number of paths.

Suppose we deal with a Bermudan option with tenor T and M exercise dates. First a stochastic grid is generated, i.e. we generate H paths of the underlying under the Heston model. It is easy to see that the option value at time $t_M = T$ is equal to the corresponding payoff value, which gives us the initial setting for the SGBM method at each path, expressed by

$$V(t_M, S_M, v_M) = g(S_M). \tag{2.21}$$

At times t_m, $m = M-1, \ldots, 1$, these paths are clustered into J bundles, based on their stock and variance values. The bundle set at time t_m is denoted by $\{\mathscr{B}_{m,j}\}_{j=1}^{J}$. Paths within the same bundle are assumed to share some common realized values of the market factor.

The essential idea in SGBM is that, for paths in the j-th bundle $\mathscr{B}_{m,j}$ at time t_m, the option value at time t_{m+1} can be approximated by

$$V(t_{m+1}, S_{m+1}, v_{m+1}) \approx \sum_{k=0}^{d} \beta_k^{m,j} \left(\log(S_{m+1})\right)^k, \tag{2.22}$$

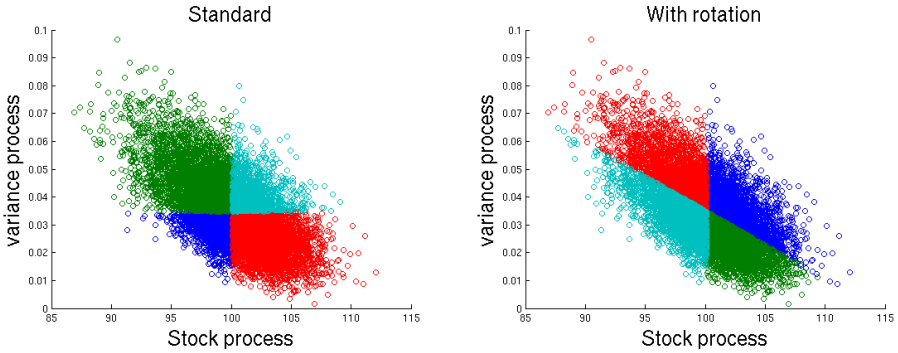

Figure 2.1: Comparison of the bundles obtained via the recursive bifurcation method without rotation (a) and with rotation(b).

where the coefficients $\left\{\beta_k^{m,j}\right\}_{k=0}^{d}$ are obtained by minimizing the sum of residuals based on the paths in the bundle $\mathcal{B}_{m,j}$.

When the option values $V(t_{m+1}, S_{m+1}, v_{m+1})$ at the stochastic paths are determined, the coefficient set $\left\{\beta_k^{m,j}\right\}_{k=0}^{d}$ can be obtained by regression. Equation (2.22) can be substituted into (2.5) which gives us:

$$\begin{aligned} c(t_m, S_m, v_m) &= e^{-r\Delta t}\mathbb{E}^{\mathbb{Q}}\left[V(t_{m+1}, S_{m+1}, v_{m+1})\middle|(S_m, v_m)\right] \\ &\approx e^{-r\Delta t}\mathbb{E}^{\mathbb{Q}}\left[\sum_{k=0}^{d}\beta_k^{m,j}(X_{m+1})^k\middle|(S_m, v_m)\right] \\ &= e^{-r\Delta t}\sum_{k=0}^{d}\beta_k^{m,j}\psi_k(S_m, v_m, t_m, t_{m+1}). \end{aligned} \tag{2.23}$$

Since we know the explicit formula of the moments $\{\psi_k\}_{k=0}^{d}$, the continuation values at time t_m can be computed, and, subsequently, the option values at time t_m can be obtained with the scheme in (2.4).

At time t_0, we deal with one bundle, as all paths originate from (S_0, v_0), and the option value at time t_0 is equal to the continuation value $c(t_0, S_0, v_0)$. In this way, option values are calculated backward in time from t_M to t_0. By (2.6), the exposure at each path along the time horizon is calculated as a by-product. We are thus able to determine the empirical exposure distribution at each time point for the calculation of EE and PFE.

We call the approximation obtained by regression the *direct estimator*. An alternative way of computing the average of the exposure, is to calculate EE as the average of the discounted cash flow over all paths, as in the Least-Squares method (LSM) for Bermudan options in [64]. In short, the optimal exercise strategy is determined by comparing the immediate exercise value and the approximated continuation value, and then the exercise decision is made when the immediate exercise value is highest. We update the strategy and save the corresponding realized cash flows at each path during the backward procedure. Once the option at a path is determined to be exercised at time t_m, the

exposure on this path at t_m and later than t_m is updated to zero. The EE and option values at time 0 approximated by the average of discounted cash flows represent the *path estimator*.

For pricing Bermudan options, the direct estimator is considered as the upper bound of the true value while the path estimator is often the lower bound [50]. Hence we can analyzed the converge of SGBM by comparing these two estimators.

2.3.4. THE COS MONTE CARLO METHOD

In the third computational method, we combine the generated stochastic MC grid with the COS method, introduced in [29]. Based on the same stochastic grid as, for example, in Section 2.3.3, the COS method is used for the calculation of the continuation values at each path along the time horizon. We call this combined method the *COS Monte Carlo* (CMC) method.

As in [29], we work in the log-domain, denoted by $(X,\varsigma) := (\log(S),\log(v))$. Suppose that the path values (X_m,ς_m) at time t_m are known. We can write the joint density function at t_{m+1}, conditional on values at t_m, as

$$f_{x,\varsigma}(X_{m+1},\varsigma_{m+1}|X_m,\varsigma_m) = f_{x|\varsigma}(X_{m+1}|X_m,\varsigma_{m+1},\varsigma_m)\cdot f_{\varsigma}(\varsigma_{m+1}|\varsigma_m), \tag{2.24}$$

where $f_{x|\varsigma}$ is the density of log-stock X_{m+1} given ς_{m+1} and (X_m,ς_m), and f_{ς} the conditional log-variance density for ς_{m+1} given ς_m. Notice that here we have $f_{\varsigma}(\varsigma_{m+1}|x_m,\varsigma_m) = f_{\varsigma}(\varsigma_{m+1}|\varsigma_m)$.

One can choose a proper integration range $[a,b]\times[a_v,b_v]$ in the log-stock and log-variance domains, so that the integral can accurately be approximated. We refer to [29] for details on the definition of this range based on initial state (x_0,ς_0) and maturity T. The integration of the expectation in (2.5) can now be written as follows:

$$\begin{aligned} c(t_m,e^{X_m},e^{\varsigma_m}) \quad \approx \quad & e^{-r\Delta t}\int_{a_v}^{b_v} f_{\varsigma}(y_2|\varsigma_m)\int_a^b V(t_{m+1},e^{y_1},e^{y_2})\cdot \\ & f_{x|\varsigma}(y_1|X_m,\varsigma_{m+1}=y_2,\varsigma_m)\,dy_1\,dy_2, \end{aligned} \tag{2.25}$$

with $X_m = \log(S_m)$ and $\varsigma_m = \log(v_m)$.

An analytic formula for the log-variance density f_{ς} is available in [29]. The density $f_{x|\varsigma}$ can be recovered from its characteristic function by applying the COS expansion. Here we directly use the results in [29]. On the truncated range $[a,b]$, the density $f_{x|\varsigma}$ of X_{m+1} can be recovered as

$$\begin{aligned} f_{x|\varsigma}(y_1|X_m,\varsigma_{m+1},\varsigma_m) \quad \approx \quad & \frac{2}{b-a}\sum_{j=0}^{N-1}{}'\,\mathrm{Re}\left\{\tilde{\varphi}\left(\frac{j\pi}{b-a};\varsigma_{m+1},\varsigma_m\right)\cdot\right. \\ & \left.\exp\left(ij\pi\frac{X_m-a}{b-a}\right)\right\}\cos\left(j\pi\frac{y_1-a}{b-a}\right), \end{aligned} \tag{2.26}$$

where $\sum'$ indicates that the first term is multiplied by $\frac{1}{2}$; $\mathrm{Re}(\cdot)$ returns the real part of the argument; the characteristic function $\tilde{\varphi}$ is defined by

$$\tilde{\varphi}(u;\varsigma_{m+1},\varsigma_m) = \mathbb{E}^{\mathbb{Q}}\left[\exp(iuX_{m+1})\,\middle|\,X_m=0,\varsigma_{m+1},\varsigma_m\right], \tag{2.27}$$

the analytic formula of which can also be found in [29].

We will show the way of approximating the exposure profile by backward iteration using 2D interpolation. We choose the Gaussian-quadrature rule to set the fixed log-variance grid, denoted by

$$\{a_v = \varsigma_0 < \varsigma_1 < \ldots < \varsigma_{N_2} = b_v\}.$$

Next, we set the grid along the log-stock dimension as

$$\{a = x_0 < x_1 < \ldots < x_Q = b\}.$$

At each early-exercise time $t_m < T$, we compute continuation values at time t_m on the grid $(x_{q_1}, \varsigma_{q_2}), q_1 = 1, \ldots, Q, q_2 = 1, \ldots, N_2$. In this way, we can save the values of $f_\varsigma(\varsigma_{m+1} = \varsigma_k | \varsigma_m = \varsigma_{q_2})$ and $\tilde{\varphi}(\cdot, \varsigma_{m+1} = \varsigma_k, \varsigma_m = \varsigma_{q_2})$ on an $(N_2 \times N_2)$ grid in the initialization and use them for the calculation over time. We simply use a 2D interpolation method (spline method) for approximating the continuation values on all paths.

We wish to compute the continuation value given values of (S_m, v_m) at time t_m. The integral in (2.25) along the log-variance dimension will be approximated by the Gaussian-quadrature rule . Replacing the density in (2.25) by (2.26), the continuation value given $S_m = e^{x_{q_1}}$, $v_m = e^{\varsigma_{q_2}}$ becomes

$$\begin{aligned} c(t_m, e^{x_{q_1}}, e^{\varsigma_{q_2}}) \quad \approx \quad & e^{-r\Delta t} \sum_{k=1}^{N_2} w_k f_\varsigma(\varsigma_k | \varsigma_m = \varsigma_{q_2}) \sum_{j=0}^{N-1}{}' \mathcal{V}_{j,k}(t_{m+1}) \cdot \\ & \mathrm{Re}\left\{ \tilde{\varphi}\left(\frac{j\pi}{b-a}; \varsigma_{m+1} = \varsigma_k, \varsigma_m = \varsigma_{q_2} \right) \exp\left(i j \pi \frac{x_{q_1} - a}{b-a} \right) \right\}, \end{aligned} \tag{2.28}$$

where $\{w_k\}_{k=1}^{N_2}$ are the weights in the Gaussian-quadrature rule, and the coefficients $\mathcal{V}$ with index (j,k) by

$$\mathcal{V}_{j,k}(t_{m+1}) = \frac{2}{b-a} \int_a^b V\left(e^{y_1}, e^{\varsigma_k}, t_{m+1}\right) \cos\left(j\pi \frac{y_1 - a}{b-a} \right) dy_1, \tag{2.29}$$

These coefficients $\mathcal{V}_{j,k}(t_m)$ can be obtained by backward iteration, $m = M-1, \ldots, 1$. At time t_M, the option value is equal to the immediate payoff, i.e.

$$\begin{aligned} \mathcal{V}_{j,k}(t_M) \quad &= \quad \frac{2}{b-a} \int_a^b g\left(e^{y_1}\right) \cos\left(j\pi \frac{y_1 - a}{b-a} \right) dy_1 \\ &= \quad \begin{cases} \frac{2}{b-a} \int_{\log(K)}^{b} \left(e^{y_1} - K\right) \cos\left(j\pi \frac{y_1 - a}{b-a} \right) dy_1, & \text{for a call,} \\ \frac{2}{b-a} \int_{a}^{\log(K)} \left(K - e^{y_1}\right) \cos\left(j\pi \frac{y_1 - a}{b-a} \right) dy_1, & \text{for a put.} \end{cases} \end{aligned} \tag{2.30}$$

where the analytic solution of the integrals can be derived.

At each exposure monitoring date $t_m < T$, we can also have the coefficients $\mathcal{V}_{j,k}(t_m)$:

- For a call option:

$$\mathcal{V}_{j,k}(t_m) = \frac{2}{b-a}\Bigg(\int_a^{x^*_{m,k}} c\left(t_m, e^{y_1}, e^{\varsigma_k}\right) \cos\left(j\pi \frac{y_1-a}{b-a}\right) dy_1 + \int_{x^*_{m,k}}^{b} \left(e^{y_1}-K\right) \cos\left(j\pi \frac{y_1-a}{b-a}\right) dy_1 \Bigg), \tag{2.31}$$

- For a put option:

$$\mathcal{V}_{j,k}(t_m) = \frac{2}{b-a}\Bigg(\int_a^{x^*_{m,k}} \left(K-e^{y_1}\right) \cos\left(j\pi \frac{y_1-a}{b-a}\right) dy_1 + \int_{x^*_{m,k}}^{b} c\left(t_m, e^{y_1}, e^{\varsigma_k}\right) \cos\left(j\pi \frac{y_1-a}{b-a}\right) dy_1 \Bigg), \tag{2.32}$$

where the optimal early-exercise value of log-stock $x^*_{m,k}$ at the log-variance grid ς_k is the solution of the following:

$$g(e^{x^*_{m,k}}) = c\left(t_m, e^{x^*_{m,k}}, e^{\varsigma_k}\right). \tag{2.33}$$

Compared to the COS method for pricing option values, the CMC method is significantly slower when the number of MC paths is high. One reason is that, at each exercise time, calculation of the continuation value is performed, for which interpolation is required for each path.

At the same time, the CMC method maintains the very high accuracy of the COS method. The errors due to the integration ranges, the quadrature and the propagation error have been discussed in [29]. The error of the spline interpolation on the variance grid is small when Q is sufficiently large. Because of the high accuracy, we will use the results of the CMC method as reference values in the discussion of the numerical results.

2.4. NUMERICAL RESULTS

In this section we start with an assessment of the impact of stochastic volatility on exposure profiles by comparing EE and PFE. Next, we consider a detailed analysis of the convergence and accuracy of the methods by means of numerical experiments.

As there are no exact values available for the exposure of Bermudan put options under the Heston stochastic volatility model, we will use the converged results of the COS method as the reference values. The convergence of the COS method has been discussed in [29], and we will set the number of Fourier terms as $N = 2^9$ and the number of the points on the log-variance grid as $N_2 = 2^9$. As mentioned, the COS method is a highly accurate method for pricing Bermudan options. When valuing the exposure, the high accuracy is maintained as long as the integration range is chosen properly (see Section

2.3.4). We reduce the impact of Monte Carlo noise in the comparative analysis by using $H = 10^5$ paths.

To investigate the proposed three methods, three different sets of parameters are tested, see Table 2.2. These test cases were used recently in [29], [41] and [86] and reference values are thus available for individual option prices. Moreover, in these test cases we stress the parameters of the stochastic volatility process by considering different levels for the initial variance, the mean-reversion parameters, vol-of-vol and correlation parameters. These parameters are chosen such that in Tests A and C the well-known Feller condition is satisfied, while in Test B it is not. The purpose of Test B is to test the performance of the algorithms when Feller condition is not satisfied, since it is known that when the Feller condition is not satisfied, the variance process can become zero and numerical methods may suffer from this issue. Apart from the different settings for the model parameters, we consider different maturities, interest rates and moneyness levels.

Table 2.2: Parameter sets for Test A, B and C.

	Test A	Test B	Test C
Spot (S)	10	100	9
Strike (K)	10	100	10
Interest (r)	0.04	0.04	0.10
Exercise Times	50	50	50
Initial Vol ($\sqrt{v_0}$)	0.5745	0.1865	0.2500
Tenor (T)	0.25	0.25	1.00
Mean Reversion (κ)	0.80	1.15	5.00
Mean Var (η)	0.3300	0.0348	0.1600
Vol of Var (σ)	0.700	0.459	0.900
Correlation (ρ)	0.10	-0.64	0.10

2.4.1. IMPACT OF STOCHASTIC VOLATILITY ON EXPOSURE

Here it is shown that stochastic volatility clearly has an impact on exposure profiles. It is most significant for the $\text{PFE}_{97.5\%}$ quantile in the tests considered. We restrict the analysis to Tests A and B because in Test C the mean reversion level is not equal to the initial variance and thus it is not clear which level to use for the variance in the Black-Scholes model. In Figure 2.2, the results are plotted for the parameters from Tests A and B. In general, independent of the underlying dynamics, the plots show that the EE starts at the initial option value, after that, the level drops because of the early exercise possibility. The PFEs also start at the initial option value, because at this stage there is no uncertainty, i.e. the minimum value for which the probability is higher than a specific benchmark equals this initial value. Starting from $t = 0$ $\text{PFE}_{2.5\%}$ drops to zero soon while $\text{PFE}_{97.5\%}$ is always higher than the EE. Due to the early exercise possibility, paths will "terminate" i.e. exercise will take place so that more than 2.5% of the values are equal to zero soon. With the same argument the minimum value for which 97.5% of the prices are lower is much higher and only drops at a later stage as options at more and more paths are being exercised.

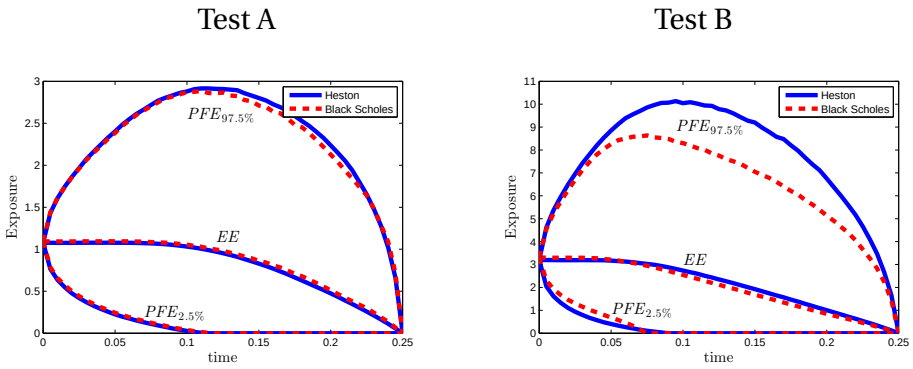

Figure 2.2: EE and PFE profiles under the Black Scholes and Heston model, differences are significant for 97.5% PFE.

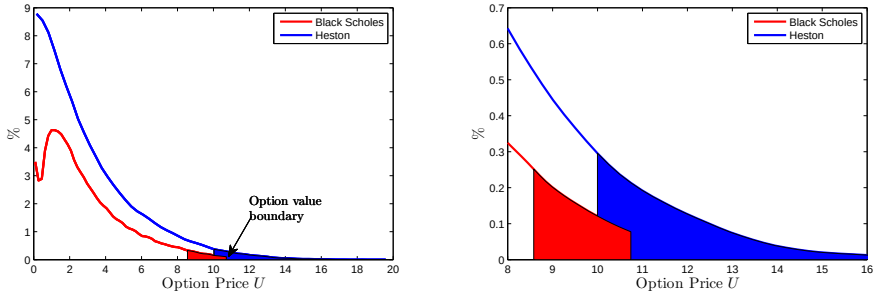

Figure 2.3: Distribution of option values under Heston and Black-Scholes dynamics for Test B at exercise time 17 of 50. The $PFE_{97.5\%}$ is shaded in red (BS) or blue (Heston) respectively, in the right plot the axes are changed to make the boundary more clear.

When the results for the Black-Scholes dynamics are compared to the Heston dynamics, one can conclude that the most significant difference is for $PFE_{97.5\%}$, in both cases. The difference in $PFE_{97.5\%}$ is a factor 10 times larger than the difference for EE and $PFE_{2.5\%}$. Intuitively this makes sense, due to the fact that the mean reversion level is equal to the constant variance level in the Black-Scholes model, the EE is not heavily affected. However, since the volatility is stochastic, extreme cases may occur more frequently (with the parameters chosen), resulting in fatter tails of the distribution that have a significant impact on PFE.

The early exercise value also depends on the volatility so that for any path, there is a different exercise value. From Figure 2.3 it can be seen that the distribution computed under the Black-Scholes dynamics is chopped off at a specific maximum option value, whereas the distribution under the Heston dynamics has a smoothly varying tail. The mass that is originally in the cut of tail in the Black-Scholes case is here located at the left-side boundary.

For the analysis of the accuracy and convergence of the three proposed methods, we

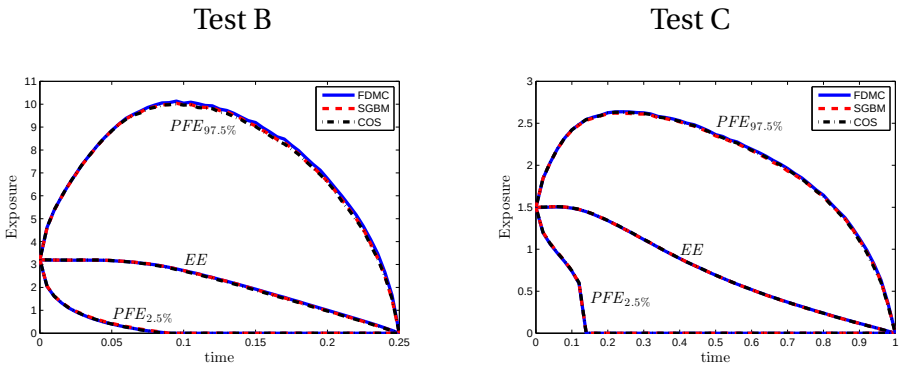

Figure 2.4: EE, $\text{PFE}_{2.5\%}$ and $\text{PFE}_{97.5\%}$, for $H = 10^5$ paths and 50 exercise times.

concentrate on Tests B and C. The results for EE and $\text{PFE}_{97.5\%}$ obtained for the different methods are shown in Figure 2.4 and Table 2.3 (the results for $\text{PFE}_{2.5\%}$ are not shown in the table). The methods are tested on a set of $H = 10^5$ generated Monte Carlo paths. In

Table 2.3: Relative L^2 difference between three methods for 10^5 paths. The error in approximating EE of FD is measured by $\|\text{EE}_{\text{FD}} - \text{EE}_{\text{COS}}\|_{L^2} := \sum_{m=0}^{M} \left(\text{EE}_{\text{FD}}(t_m) - \text{EE}_{\text{SGBM}}(t_m)\right)^2 / \sum_{m=0}^{M} \left(\text{EE}_{\text{COS}}(t_m)\right)^2$, and by replacing EE_{FD} by EE_{SGBM} we define the error in approximating EE of SGBM. The measurement of error for the PFE function for these two algorithms is also defined in this way.

Error	Method	Test B	Test C
EE	FD	5.8864e-03	1.8966e-03
	SGBM	8.0645e-03	1.4943e-03
$\text{PFE}_{97.5\%}$	FD	1.4133e-02	2.7113e-03
	SGBM	4.5856e-03	3.9364e-03

the following subsections, the convergence and error behavior of the FDMC method and SGBM is discussed.

2.4.2. ERROR FDMC

The error for pricing options with the finite difference method for the Heston PDE is extensively studied, see, for example, [33]. The error is mainly introduced near the boundaries, but can be controlled by a combination of a large number of grid points and the use of a non-uniform grid. In all finite difference computations the grids are non-uniform, as discussed in Section 2.3.2. The free parameter λ in (2.12) to determine the region $[\lambda K, K]$ in the spot direction is determined depending on the quantity that is being measured: For PFE a smaller value is desired, whereas for EE the value is larger, in any case $\lambda \in [0.3, 0.7]$. The variance grid is very dense around the $v = 0$ boundary, independent of the measured quantity. The number of grid points in spot (S) and variance (v) directions are denoted by m_1 and m_2, respectively. By experimenting, we know that the numerical error is dominated by the error in spot direction, and therefore the number of grid

points in the S direction is chosen as $m_1 = 2m_2$. With this fixed ratio, the decay in error is measured by decreasing a generic measure Δs. If we decrease Δs by increasing the num-

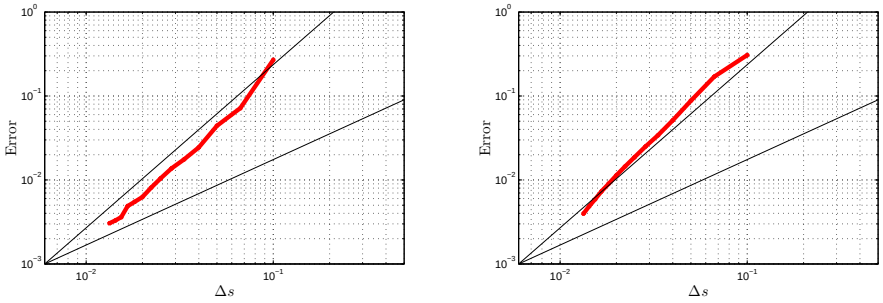

(a) Test B (b) Test C

Figure 2.5: Convergence plots by increasing the number of grid points in space for a single Bermudan option. The relative L^2 norm is used to measure the difference with the reference COS value.

ber of grid points, the numerical convergence is second-order when we price a single Bermudan option in Test C, whereas it is almost second-order for Test B, see Figure 2.5. The grid is chosen to be very dense in the region of the initial market parameters (S_0, v_0), and the price is extracted from the grid by accurate spline interpolation.

When EE and $\text{PFE}_{97.5\%}$ are computed, multiple prices at each exercise time are needed. In this case, interpolation is needed for each path and exercise time which is expected to have an impact on the error. To investigate the scale of this error the same convergence tests are done as in the single option case. In this case the finite difference solution is compared to the semi-analytic CMC method described in Section 2.3.4. The same random scenarios are used for computing the EE for the CMC and the FDMC methods. As

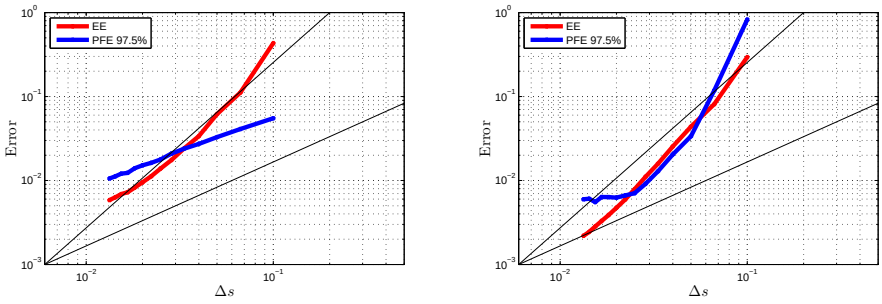

(a) Test B (b) Test C

Figure 2.6: Convergence plots by increasing the number of grid points in space for computing EE and PFE. The relative L^2 norm is used to measure the difference with the reference value obtained by the CMC method.

shown in Figure 2.6, in both Tests B and C the convergence of the error is similar for EE

as it is for pricing a single option. The decrease of the error is of second-order in the number of grid points in Test C and almost second-order in Test B.

For PFE, in Test B the convergence from the start is only first-order. In this test the Feller condition not satisfied. The mesh used in this case has a dense region around the strike, whereas for a PFE computation the strike region is generally not of highest relevance. To enhance the accuracy of the PFE, the non-uniform grid in S direction can be adjusted. Because PFE and EE are mostly computed independently, a conclusion is that measuring PFE or EE would imply using two different grids.

The convergence with respect to Δt is not presented in this research because tests show that the error is dominated by the spatial error.

2.4.3. ERROR SGBM

Here we focus on the convergence of SGBM regarding the option value, the EE and PFE. We use five basis functions (including the constant) for local regression defined in Equation (2.13). In the recursive bifurcation bundling method, an essential property is that the number of bundles must be of the form 4^j, $j = 0,1,2\ldots$, for details we refer to [50]. The bundling scheme is slightly adapted to deal with the two-dimensional Heston dynamics.

In the tests, a large number of paths $H = 10^5$ and bundles J are chosen.

In Section 2.3.3, we have explained two ways of calculating the option value at time t_0. One way is to estimate the coefficient set over all paths at time t_1 and to apply regression at time t_0 (the so-called direct estimator); the other is to store the optimal strategy and take the mean of the discounted cash flow (the so-called path estimator):

- The results calculated directly from the set of Monte Carlo paths are called *direct estimator* results;
- The results calculated by the second set of paths, but with the coefficients from the first set of paths are called the *path estimator* results.

The numerical results for the path estimator should be similar to the results for the direct estimator. Table 2.4 presents the difference between the direct estimator and the path estimator for EE and PFE. Again the error is measured in the relative L^2 norm. We see that the difference between the two results is only of order 10^{-3}.

Table 2.4: The difference between the direct estimator and path estimator for EE and PFE. The number of bundles equals 4^4 and the number of paths is 10^5.

	EE	PFE
Test B	2.8541e-03	6.3035e-03
Test C	1.9462e-03	5.9252e-03

The option value is the maximum value obtained among all possible stopping rules, indicating that the option value calculated by the "optimal" strategy will be less than or equal to the true option value. This provides a criterion for convergence. The result calculated by the optimal strategy will be the lower bound of the Bermudan option value.

We examine the convergence of the Bermudan option value w.r.t the number of bundles for SGBM. The tests are done for ten simulations, and the results are presented in Figure 2.7. We take the regression results of the direct estimator and the results of the optimal strategy of the path estimator for comparison. As we can see, in both Tests B and C, the results of the path and the direct estimators resemble each other better when the number of bundles increases. The two results are very close to the COS reference value for $\beta = 4^4$, see Table 2.5.

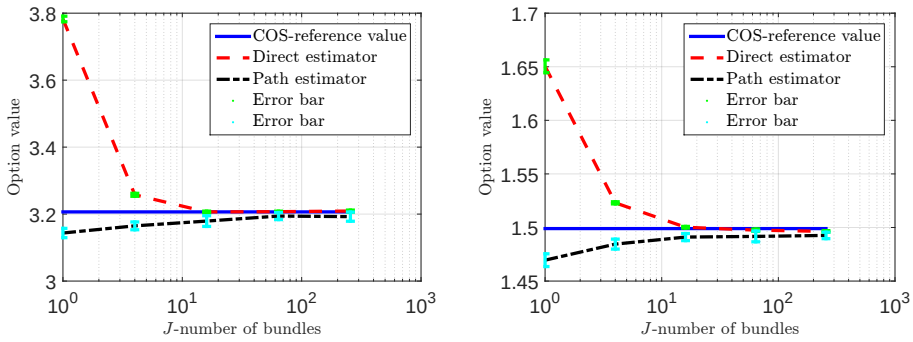

(a) Test B (b) Test C

Figure 2.7: Convergence with respect to the number of bundles $J = \{1, 4, 4^2, 4^3\}$, for the Bermudan option value; the total number of paths $H = 10^5$; the reference value in Test B equals 3.2066 and in Test C 1.4990. The red dashed line is the direct estimator, blue is the COS reference value, and the black dashed line the path estimator.

Table 2.5: The difference between the direct and the path estimator for a Bermudan option value when the number of bundles equals 4^4. The results are computed via ten simulations (s.e. is standard deviation).

	COS(reference)	Direct estimator(s.d.)	Path estimator(s.d.)
Test B	3.2066	3.2091(2.8613e-03)	3.1924(1.3768e-02)
Test C	1.4990	1.4964(7.2086e-04)	1.4926(3.0376e-03)

In addition to the convergence of the Bermudan option value, we examine the convergence of EE and PFE in Figure 2.8. The results of the CMC method are used as the reference values. With the same set of 10^5 generated paths, we increase the number of bundles from 1 to 4^4 for the calculation by the SGBM method. It shows that the error decreases when increasing the number of bundles.

The convergence of the EE and PFE, w.r.t the number of paths, is examined in Figure 2.9. We choose the number of bundles equal to 4^3, and increase the average number of paths in each bundle. The differences of EE and PFE between direct estimator and path estimator are compared. The average number of paths in each bundle is increased from 25 to 2000. It shows that the difference between the path and the direct estimator decreases when the average number of paths in each bundle (i.e. the total number of paths) increases.

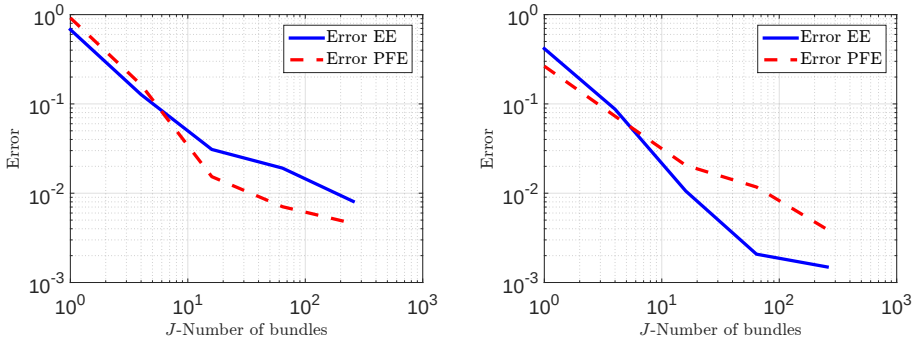

(a) Test B (b) Test C

Figure 2.8: Convergence with respect to the number of bundles $J = \{1, 4, 4^2, 4^3\}$; the total number of paths equals $H = 10^5$.

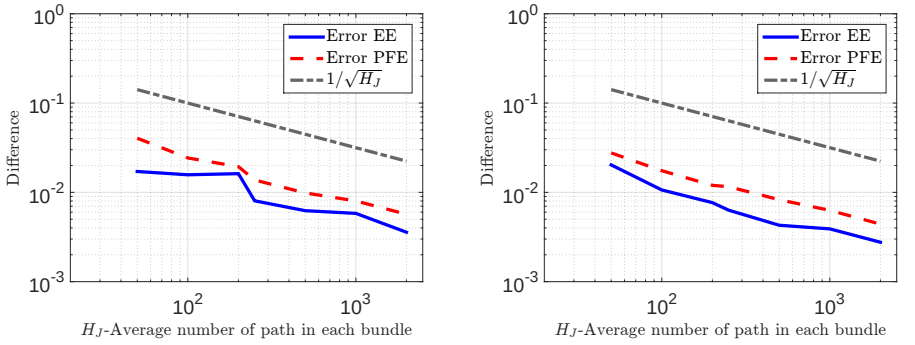

(a) Test B (b) Test C

Figure 2.9: Convergence with respect to the number of paths within each bundle $H_J = H/J$; the number of bundles is fixed $J = 4^3$. We increase the total number of path from $50J$ to $2000J$, i.e. the average number of paths H_J within each bundles is increased from 50 to 2000. The grey line indicates an asymptotic convergence with $1/\sqrt{H_J}$.

These results support the fact that SGBM converges (to the reference values) for Bermudan options, EE and $\text{PFE}_{97.5\%}$.

2.5. CONCLUSIONS

In this chapter, three different approaches for computing exposure profiles within the context of counterparty credit risk are presented. The underlying asset exposure is driven by the Heston stochastic volatility model and Bermudan put options are priced. In all three methods scenarios are generated by a Monte Carlo scheme and exposure values are computed at each path at each exercise time. The pricing procedure is done by either the FDMC method, SGBM or the CMC method.

The CMC method is a combination of the Monte-Carlo method and the COS method which can be used for computing exposures. We adapt the COS method to make it more general and thereby applicable to a wide range of possible states (S_m, v_m), while maintaining its high accuracy. This comes at the cost of computational speed (under the Heston dynamics, particularly when the Feller condition is not satisfied). However, considering its high accuracy, this method is used as a benchmark value to analyze the accuracy and convergence of EE and PFE computed by FDMC and SGBM. By using this benchmark, it is shown that the FDMC, SGBM and CMC methods agree for multiple tests.

As a first result, it is shown that the impact of stochastic volatility on exposure profiles is more significant for its right-tail than for its mean. Whereas the distribution computed under the Black-Scholes dynamics suffers from the tail being chopped off at a certain maximum option value boundary, under the Heston dynamics this feature is not present.

Because any finite difference solution generates option values for an entire grid of underlying values, the FDMC method is promising. The computation time in this method is dominated by the computation of the solution on the grids at each exercise time. When these are stored, the EE computation boils down to a interpolation procedure for all paths at each exercise time. By using the COS method as a benchmark, it is shown that the error introduced by the interpolation is negligible. Compared to the CMC method, the error is within the range of 10^{-3}.

SGBM has been extended to the Heston model for computing exposures. We test the convergence of SGBM w.r.t the number of paths and the number of bundles in several ways. For the considered tests, the computation of EE and PFE shows to be highly accurate with an error compared to CMC in the order of 10^{-3}. SGBM is an efficient Monte Carlo method when valuing exposure distributions along a time horizon.

CHAPTER 3

Pricing CCR of options under Heston Hull-White model

Inclusion of various market factors in the asset dynamics, such as stochastic asset volatility and stochastic interest rates, increases the computational complexity for computing exposure profiles. In this chapter, we will extend the Black-Scholes model by adding the stochastic interest rate and the stochastic volatility. First of all, we explain the backward dynamics framework for assessing the exposure profiles of European, Bermudan and barrier options under the Heston and Heston Hull-White asset dynamics. Then, we demonstrate the potential of SGBM for exposure computation. In addition, the sensitivity of the EE profile can be easily obtained in the SGBM algorithm. Assuming independence between the default event and exposure profiles, we give here examples of calculating exposure, CVA and sensitivities for Bermudan and barrier options.

3.1. INTRODUCTION

In Chapter 2, we have presented SGBM under the Heston's model using monomials of log-stock dynamics. In this chapter, we will further improve the accuracy of SGBM by using multi-variable monomials. We will provide a more general framework for SGBM under multi-dimensional models.

We will show the impact of adding stochastic volatility and stochastic interest rates on the metrics of future losses (i.e. CVA, EE, PFE). A stochastic volatility may explain the implied volatility surface observed in the derivatives market (such as the volatility smile) [43], and uncertainty in the interest rate may give a significant contribution to the price, especially of long-term financial derivatives [62]. The hybrid model chosen to model these stochastic quantities here is the Heston Hull-White model [39].

The flexibility of SGBM is demonstrated by placing the computation of exposure profiles, for different option types under different asset dynamics, in a general unifying framework based on backward recursion. The options considered include European, Bermudan and barrier options.

The reminder of the chapter is structured as follows: Section 3.2 provides affine diffusion models and approximations for the underlying dynamics. Section 3.3 describes the backward dynamics for calculation of the exposure of options, and their exposure sensitivities. In Section 3.4, we present the SGBM algorithm for this purpose. The choice of basis functions and the derivation of the discounted moments is presented there, as well as a simple bundling technique that ensures the accuracy of the local, bundle-wise,

This chapter is based on the article 'Calculation of exposure profiles and sensitivities of options under the Heston and the Heston Hull-White models', published in *Recent Progress and Modern Challenges in Applied Mathematics, Modeling and Computational Science*, Fields Institute Communications series, volume 79, 2017 [32].

regression in SGBM. In Section 3.5, numerical results are presented to show the convergence and efficiency of the method, and the impact of the stochastic interest rate and stochastic volatility on the exposure metrics is studied.

3.2. MODELS

We will present the models with stochastic volatility and stochastic interest rate for the underlying asset in this section.

3.2.1. BLACK-SCHOLES HULL-WHITE MODEL AND HESTON MODEL

The famous Black-Scholes option pricing partial differential equation (PDE) [9] is based on the assumptions that the asset price follows a geometric Brownian motion with constant volatility and constant interest rate. We first relax the assumption of constant interest rate by a stochastic instantaneous short-rate r_t. In practice, interest rates vary over time and by tenor T, as observed in the zero coupon bond curves in the market [13]. The instantaneous forward rate at time t for a maturity $T > t$ is defined by:

$$f^M(t,T) := -\frac{\partial \log P(t,T)}{\partial T}, \tag{3.1}$$

where $P(t,T)$ is the price of the zero-coupon-bond (ZCB).

The characterization of the term structure of interest rates is well-known from Vasicek [85], Cox, Ingersoll, and Ross [22], and Hull and White [44].

In this chapter, we will also employ the *Black-Scholes Hull-White* hybrid (BSHW) model. Under risk-neutral measure $\mathbb{Q}$, the dynamics of the model $\mathbf{X}_t = [X_t, r_t]^T$ are given by the following SDEs [13]:

$$\begin{aligned} dX_t &= \left(r - \frac{1}{2}\sigma^2\right)dt + \sigma dW_t^X, \\ dr_t &= \lambda(\theta(t) - r_t)dt + \eta dW_t^r, \end{aligned} \tag{3.2}$$

where $X_t = \log(S_t)$ represents the log-asset variable; the two correlated Wiener processes (W_t^X, W_t^r) are defined by $W_t^X = \widetilde{W}_t^{(1)}$ and $W_t^r = \rho_{x,r}\widetilde{W}_t^{(1)} + \sqrt{1-\rho_{x,r}^2}\widetilde{W}_t^{(2)}$, where $\widetilde{W}_t^{(1)}$ and $\widetilde{W}_t^{(2)}$ are two independent standard Wiener processes under measure $\mathbb{Q}$ and $|\rho_{x,r}| < 1$ is the instantaneous correlation parameter between the asset price and the short rate process; positive parameters σ and η denote the volatility of equity and interest rate, respectively; the drift term $\theta(t)$ is a deterministic function chosen to fit the term structure observed in the market, which must satisfy:

$$\theta(t) = f^M(0,t) + \frac{1}{\lambda}\frac{\partial}{\partial t}f^M(0,t) + \frac{\eta^2}{2\lambda^2}(1 - \exp(-2\lambda t)). \tag{3.3}$$

Another way of extending the Black-Scholes model is to define the variance as a diffusion process, like in the stochastic volatility model developed by Heston [43]. With state variable $\mathbf{X}_t = [X_t, v_t]^T$, the Heston model is given by:

$$\begin{aligned} dX_t &= \left(r - \frac{1}{2}v_t\right)dt + \sqrt{v_t}dW_t^X, \\ dv_t &= \kappa(\bar{v} - v_t)dt + \gamma\sqrt{v_t}dW_t^v, \end{aligned} \tag{3.4}$$

where r is a constant interest rate; the two correlated Wiener processes (W_t^X, W_t^v) are defined by $W_t^X = \widetilde{W}_t^{(1)}$ and $W_t^v = \rho_{x,v}\widetilde{W}_t^{(1)} + \sqrt{1-\rho_{x,v}^2}\widetilde{W}_t^{(3)}$, where $\widetilde{W}_t^{(1)}$ and $\widetilde{W}_t^{(3)}$ are two independent standard Wiener processes under measure $\mathbb{Q}$ and $|\rho_{x,v}| < 1$ is the instantaneous correlation parameter between the asset price and the variance process; the constant positive parameters κ, $\bar{v}$, γ determine the reverting speed, the reverting level and vol-of-vol parameters, respectively. The associated PDE can be found in [43, p.329].

3.2.2. HESTON HULL-WHITE MODEL AND H1HW MODEL

Consider a state vector including all these stochastic quantities, i.e. $\mathbf{X}_t = [X_t, v_t, r_t]^T$. The corresponding model can be defined by adding a HW interest rate process to the Heston stochastic volatility dynamics, as presented in [39]. The hybrid model of the equity, stochastic Heston asset volatility and stochastic interest rate is represented by the following SDEs:

$$\begin{aligned} dX_t &= \left(r_t - \frac{1}{2}v_t\right)dt + \sqrt{v_t}dW_t^X, \\ dv_t &= \kappa(\bar{v} - v_t)dt + \gamma\sqrt{v_t}dW_t^v, \\ dr_t &= \lambda(\theta(t) - r_t)dt + \eta dW_t^r, \end{aligned} \tag{3.5}$$

where the correlated Wiener processes (W_t^X, W_t^v, W_t^r) are defined by $W_t^X = \widetilde{W}_t^{(1)}$, $W_t^v = \rho_{x,v}\widetilde{W}_t^{(1)} + \sqrt{1-\rho_{x,v}^2}\widetilde{W}_t^{(2)}$, $W_t^r = \rho_{x,r}\widetilde{W}_t^{(1)} - \frac{\rho_{x,v}\rho_{x,r}}{\sqrt{1-\rho_{x,v}^2}}\widetilde{W}_t^{(2)} + \sqrt{\frac{1-\rho_{x,v}^2-\rho_{x,r}^2}{1-\rho_{x,v}^2}}\widetilde{W}_t^{(3)}$, in which $\widetilde{W}_t^{(1)}$, $\widetilde{W}_t^{(2)}$ and $\widetilde{W}_t^{(3)}$ are three independent standard Wiener processes under the risk-neutral measure $\mathbb{Q}$, and $\rho_{x,v}$ and $\rho_{x,r}$ are correlation parameters that satisfy $\rho_{x,v}^2 + \rho_{x,r}^2 < 1$; the parameters $\lambda, \theta(t), \eta$ are as in (3.2), and κ, $\bar{v}$ and γ are as in (3.4); the initial values satisfy $r_0 > 0$ and $v_0 > 0$.

The Heston Hull-White (HHW) SDE system in (3.5) is not affine. Conditional on information at time t, the symmetric covariance matrix at time $s > t$ is given by:

$$\tilde{\sigma}(\mathbf{X}_s)\tilde{\sigma}^T(\mathbf{X}_s) = \begin{pmatrix} v_s & \rho_{x,v}v_s & \sqrt{v_s}\eta\rho_{x,r} \\ * & \gamma^2 v_s & 0 \\ * & * & \eta^2 \end{pmatrix}, \tag{3.6}$$

where the term $\sqrt{v_s}$ is not linear. Grzelak and Oosterlee in [39] approximated the covariance matrix in (3.6) by

$$\tilde{\sigma}(\mathbf{X}_s)\tilde{\sigma}^T(\mathbf{X}_s) \approx \begin{pmatrix} v_s & \rho_{x,v}v_s & \mathbb{E}\left[\sqrt{v_s}\middle|v_t\right]\eta\rho_{x,r} \\ * & \gamma^2 v_s & 0 \\ * & * & \eta^2 \end{pmatrix}, \tag{3.7}$$

where the term $\sqrt{v_s}$ is approximated by its conditional expectation $\mathbb{E}\left[\sqrt{v_s}\middle|v_t\right]$, for which an analytic formula is given by:

$$\mathbb{E}\left[\sqrt{v_s}\middle|v_t\right] = \sqrt{2\bar{c}(s-t)}\exp\left(-\frac{\bar{\lambda}(s-t,v_t)}{2}\right)\sum_{k=0}^{\infty}\frac{1}{k!}\left(\frac{\bar{\lambda}(s-t,v_t)}{2}\right)^k\frac{\Gamma\left(\frac{1}{2}+\frac{2\kappa\bar{v}}{\gamma^2}+k\right)}{\Gamma\left(\frac{2\kappa\bar{v}}{\gamma^2}+k\right)}, \tag{3.8}$$

where Γ is the Gamma function, and the coefficients $\bar{c}$ and $\bar{\lambda}$ are given by

$$\begin{aligned}\bar{c}(s-t) &= \frac{\gamma^2}{4\kappa}(1-\exp(-\kappa(s-t))),\\ \bar{\lambda}(s-t,v_t) &= \frac{4\kappa v_t}{\gamma^2}\cdot\frac{\exp(-\kappa(s-t))}{(1-\exp(-\kappa(s-t))}.\end{aligned} \tag{3.9}$$

This affine approximation of the HHW model with covariance (3.7) is called the H1HW model, and details can be found in [39].

3

3.3. EXPOSURE PROFILE OF OPTIONS

We will study the CVA, EE and PFE of several types of options to show the flexibility of SGBM. We present the backward valuation dynamics framework for European, Bermudan and barrier options in this section. Let the collection of equally-spaced discrete *exposure monitoring dates* be:

$$\mathcal{T} = \{0 = t_0 < t_1 < \cdots < t_M = T, \Delta t = t_{m+1} - t_m\},$$

with T the expiration of the option.

The options will be valued at so-called monitoring dates to determine the exposure profiles over the life of the contract. The payoff of an option contract is the amount received from exercise of the option. In this chapter, we study the stock option, i.e. the underlying asset refers to the shares of some company. The received payoff from immediate exercise of the option at time t_m is given by

$$g(X_m) = \begin{cases}\max\left(\exp(X_m) - K, 0\right), & \text{for a call;}\\ \max\left(K - \exp(X_m), 0\right), & \text{for a put,}\end{cases} \tag{3.10}$$

where K is the strike value and X_m represents the log-asset variable at time t_m.

The *continuation value* of the option at time t_m can be expressed by the conditional expectation of the discounted option value at time t_{m+1}, i.e.

$$c(t_m, \mathbf{X}_m) := \mathbb{E}^{\mathbb{Q}}\left[\frac{B_m}{B_{m+1}} V(t_{m+1}, \mathbf{X}_{m+1}) \middle| \mathbf{X}_m\right], \tag{3.11}$$

where $\mathbf{X}_m$ is the state variable at time t_m, and $V(t_{m+1}, \mathbf{X}_{m+1})$ is the option value at time t_{m+1}.

3.3.1. BERMUDAN OPTIONS

Bermudan options can be exercised at a series of time points before expiry date T. Denote the set of early-exercise dates by

$$\mathcal{T}_B = \{T_1 < T_2 < \ldots < T_N\}.$$

In this chapter, those early exercise dates are included in the collection of the monitoring dates, i.e. $\mathcal{T}_B \subset \mathcal{T}$, and we will further study the value of the option between two early-exercise dates. The exposure of the option between two early exercise dates

does not have any impact on the option value at time zero, but these values can make significant contributions to CVA.

Assume that the option holder is not influenced by the credit quality of the option writer when making the exercise decision. The option value at time $t = 0$ is equal to the expected payoff when exercising the option optimally. The essential idea of pricing Bermudan options by simulation is to determine the optimal exercise strategy. At each exercise date, the option holder compares the received payoff from immediate exercise with the expected payoff from continuation of the option to determine the optimal exercise strategy. The dynamics of pricing Bermudan options in backward induction derived by the Snell envelope [29, 64] can be expressed by:

$$V^{\text{Berm}}(t_m,\mathbf{X}_m) = \begin{cases} g(X_M) & \text{for } t_M = T, \\ \max\big(c(t_m,\mathbf{X}_m), g(X_m)\big), & \text{for } t_m \in \mathcal{T}_B, \\ c(t_m,\mathbf{X}_m), & \text{for } t_m \in \mathcal{T} - \mathcal{T}_B. \end{cases} \tag{3.12}$$

3.3.2. EUROPEAN OPTIONS

Similar to pricing Bermudan options, the exposure profile of a European option can be determined based on simulation. The European option value at time T equals the received payoff $V^{\text{Euro}}(t_M,\mathbf{X}_M) = g(X_M)$; at time points $t_m < T$, the value of the European option is equal to the discounted conditional expected payoff, i.e.,

$$V^{\text{Euro}}(t_m,\mathbf{X}_m) := \mathbb{E}^{\mathbb{Q}}\left[\frac{B_m}{B_M} g(X_M)\Big|\mathbf{X}_m\right], \tag{3.13}$$

where $g(X_M)$ is the received payoff at time $t_M = T$. By the tower property of expectations, it can be calculated in a backward iteration as:

$$\begin{aligned} V^{\text{Euro}}(t_m,\mathbf{X}_m) &= \mathbb{E}^{\mathbb{Q}}\left[\frac{B_m}{B_{m+1}}\mathbb{E}^{\mathbb{Q}}\left[\frac{B_{m+1}}{B_M} g(X_M)\Big|\mathbf{X}_{m+1}\right]\Big|\mathbf{X}_m\right] \\ &= \mathbb{E}^{\mathbb{Q}}\left[\frac{B_m}{B_{m+1}} V^{\text{Euro}}(t_{m+1},\mathbf{X}_{m+1})\Big|\mathbf{X}_m\right] = c(t_m,\mathbf{X}_m), \end{aligned} \tag{3.14}$$

with $m = M-1,\ldots,0$.

3.3.3. BARRIER OPTIONS

Barrier options become active/knocked out when the underlying asset reaches a predetermined level, i.e. the *barrier* level. There are four main types of barrier options: up-and-out, down-and-out, up-and-in, down-and-in options. Here we focus on the *down-and-out* barrier options. A down-and-out barrier option is active initially and gets knocked out (looses its value except for some rebate value) when the underlying hits the barrier; otherwise if the option is not knocked out during its lifetime, the holder will receive the payoff value at the expiry date T. The backward pricing dynamics of the down-and-out barrier options are thus given by [29],

$$V^{\text{barr}}(t_m,\mathbf{X}_m) = \begin{cases} g(S_m)\cdot\mathbb{1}(\{S_m > L_b\}) + r_b\cdot\mathbb{1}(S_m \le L_b), & \text{for } t_M = T, \\ c(t_m,\mathbf{X}_m)\cdot\mathbb{1}(S_m > L_b) + r_b\cdot\mathbb{1}(S_m \le L_b), & \text{for } t_m < T, \end{cases} \tag{3.15}$$

where $\mathbb{1}(\cdot)$ is the indicator function, L_b is the barrier level and r_b is the rebate value.

In short, in order to compute the exposure profiles in these option contracts, we must be able to compute the continuation value at each monitoring date, which is defined via the risk-neutral expectation. We have already presented the SGBM algorithm in Chapter 1, and in the following section, we will present the computation of exposure on the simulated scenarios.

3.3.4. EXPOSURE OF OPTIONS BASED ON MONTE CARLO

Monte Carlo simulation plays a primary role in computing CVA. We present the general procedure of determining the exposure profiles on the simulated paths.

- Generate H independent scenarios under the given risk-neutral dynamics for each monitoring date in $\mathcal{T}$ with the same initial value, and denote the scenarios by $\{\hat{x}_{1,h}, \hat{x}_{2,h}, \ldots, \hat{x}_{M,h}\}_{h=1}^{H}$;
- Valuation of exposure profile, and denote the exposure value on the h-th path at time t_m by $E_{m,h}$, $h = 1, \ldots, H$. The exposure is computed by

$$E_{m,h} = \begin{cases} 0, & \text{if the option is exercised or knocked out,} \\ c(t_m, \hat{x}_{m,h}), & \text{if the option is continued.} \end{cases} \tag{3.16}$$

- Compute the average and the 97.5% quantile of the exposure distribution at each time $t_m \in \mathcal{T}$.

Assuming independence of exposures and defaults, CVA can be computed by the following discrete formula:

$$\text{CVA} \approx \text{LGD} \sum_{m=0}^{M-1} \frac{1}{H} \sum_{h=1}^{H} \left(\exp\left(- \sum_{k=0}^{m-1} r_{k,h} \Delta t \right) E_{m,h} \right) (\text{PD}(t_{m+1}) - \text{PD}(t_m)), \tag{3.17}$$

with $r_{k,h}$ the simulated risk-neutral short rate at time t_k on the h-th scenario.

Similarly, the value at time t_m of the EE and PFE functions can be approximated by:

$$\begin{aligned} \text{EE}^{\mathbb{Q}}(t_m) &\approx \frac{1}{H} \sum_{h=1}^{H} E_{m,h}, \\ \text{PFE}^{\mathbb{Q}}(t_m) &\approx \text{quantile}(E_{m,h}, 97.5\%). \end{aligned} \tag{3.18}$$

The key problem is to calculate the continuation values on each path in the backward algorithm at each monitoring time $t_m < T$, $m = 0, 1, ..., M-1$. SGBM combines regression and bundling techniques to compute these expected values.

3.4. THE STOCHASTIC GRID BUNDLING METHOD

In this section, we extend SGBM for computation to multi-dimensional cases. We present the choice of basis functions based on multi-variables. In addition, since the interest rate may be stochastic in this chapter, discounted moments are required for computing conditional expectations. We present a bundling method that is proper for multi-dimensional models. The convergence of SGBM for this problem is also discussed.

3.4.1. CHOICE OF BASIS FUNCTIONS

In Chapter 2, we chose to use the monomials of the log-asset variables as the basis functions. In this chapter, we will improve the accuracy of the approximation by using monomials of the underlying multi-variables under the given dynamics.

For the polynomial space, it is natural to take *monomials* as the basis, as all monomials with order lower or equal to any degree $d \in \mathbb{N}$ can form a closure. The discounted moments are defined as the discounted expectations of monomials up to order d, expressed by

$$\psi_k(\mathbf{X}_m, t_m, t_{m+1}) = \mathbb{E}^{\mathbb{Q}}\left[\exp\left(-\int_{t_m}^{t_{m+1}} r_s ds\right)(\mathbf{X}_{m+1})^k \Big| \mathbf{X}_m\right], \quad \mathbf{X}_{m+1} \in \mathbb{R}^n, \tag{3.19}$$

with the multi-index notation $k = (k_1, k_2, \ldots, k_n)$, and the sum of components $0 \leq |k| \leq d$.

These discounted moments of affine-diffusion processes of any order can be expressed in closed form, as we have presented in (1.29) of Chapter 1. We let the discount rate in (1.29) be the risk-free short rate, i.e. $q(\mathbf{X}_t) = r_t$. The discounted ChFs of the three models considered are presented in the appendix in this chapter. For the HHW process, we base them on the H1HW approximate model.

Table 3.1 presents the monomial basis set for the hybrid models discussed with degree $d = \{1, 2, 3\}$.

Table 3.1: The monomial basis for the hybrid models.

order d	Heston	BSHW	HHW →H1HW
1	$\{1, X_t, v_t\}$	$\{1, X_t, r_t\}$	$\{1, X_t, v_t, r_t\}$
2	$\{1, X_t, v_t, X_t^2, X_t v_t, v_t^2\}$	$\{1, X_t, r_t, X_t^2, X_t r_t, r_t^2\}$	$\{1, X_t, v_t, r_t, X_t^2, X_t v_t, v_t^2, X_t r_t, r_t^2, v_t r_t\}$
3	$\{1, X_t, v_t, X_t^2, X_t v_t, v_t^2, X_t^3, X_t^2 v_t, X_t v_t^2, v_t^3\}$	$\{1, X_t, r_t, X_t^2, X_t r_t, r_t^2, X_t^3, X_t^2 r_t, X_t r_t^2, r_t^3\}$	

The monomial basis grows rapidly with the dimension of the state variable n and the polynomial order d. In the algorithm of SGBM, bundling will enhance the accuracy and thus a lower degree d can be employed to achieve a certain accuracy level, as we will see in the numerical section 3.5.

3.4.2. A BUNDLING METHOD

We introduce a technique for making bundles in SGBM such that there is an equal number of paths within each bundle. It is called the *equal-number bundling* technique. The same technique of clustering paths is found in [20, 63]. The advantages of this bundling technique are that the number of paths within each bundle will grow in proportion to the number of paths, and that there will be a sufficient number of paths for regression when the total number of paths is large.

We use the Heston model to present the bundling technique, where the 2D state vector is denoted by $\mathbf{X}_t = [X_t, v_t]^T$. First, all paths are sorted w.r.t. their log-asset values, and clustered into J_1 bundles with respect to their ranking, ensuring that within each bundle, the number of paths is equal to $\frac{N}{J_1}$; subsequently, within each bundle we perform

a second sorting stage w.r.t. the variance values and cluster the paths into J_2 bundles. After these two iterations, the total number of bundles will be $J = J_1 \cdot J_2$.

The two steps are visualized in Fig. 3.1, where scatter plots demonstrate the 2D domain for the Heston model, at some time instant t_m. In plot (a), the paths are first clustered into 8 bundles w.r.t. the values of the log-asset, while in plot (b), the paths within each bundle are again clustered into 2 bundles w.r.t. the value of the variance. The total number of bundles is thus 16.

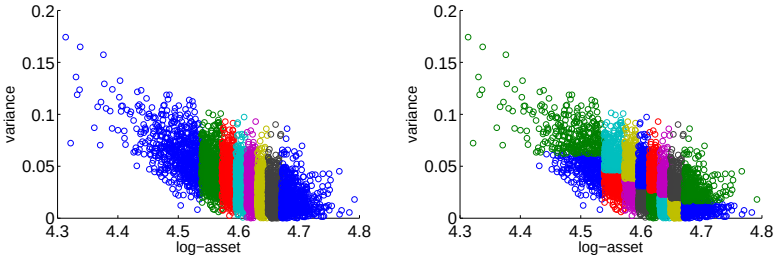

(a) First iteration, J_1 (b) Second iteration, J_2

Figure 3.1: Equal-number bundling. Each colored block represents a disjoint subdomain $\mathbf{I}_{m,j}$.

In a similar way, paths simulated under the HHW model can be clustered by the realized values of the log-asset (X_t), variance (v_t) and interest rate (r_t) values, in this order. We denote the number of bundles in these three dimension by J_1, J_2 and J_3, and the total number of bundles $J = J_1 \cdot J_2 \cdot J_3$.

There are other bundling approaches such as the *recursive-bifurcation-method* and the *k-means clustering method*, used in [50]. For our specific multi-dimensional problems, however, using the recursive-bifurcation-method will give rise to too few paths within some bundles when the correlation parameter ρ is close to 1 or -1, no matter how large the total number of paths is. This problem will not occur if we use the equal-number bundling technique. In addition, it is easy to implement and fast for computation compared to the k-means clustering method.

3.4.3. CALCULATION OF THE CONTINUATION VALUES

At time $t_m < T$, the generated paths are clustered into some non-overlapping bundles using a bundling method. The indices of the paths in the j-th bundle are in a set $\mathscr{B}_m^j$, $j = 1, 2, ..., J$, where J is the number of bundles. The realizations $\hat{x}_{m,h}$ of the state vector $\mathbf{X}_m$ within the j-th bundle form a bounded domain $\mathscr{D}_m^j \subset \mathbb{R}^n$, when $m = 1, 2, \ldots, M-1$, given by

$$\mathscr{D}_m^j = \prod_{l=1}^{n} \left[\max_{h \in \mathscr{B}_m^{j-1}} \left(\hat{x}_{m,h}^{(l)} \right), \max_{h \in \mathscr{B}_m^j} \left(\hat{x}_{m,h}^{(l)} \right) \right], \tag{3.20}$$

where $\hat{x}_{m,h}^{(l)}$ represents the l-th dimension of the realization $\hat{x}_{m,h}$, and $j = 2,3,...,J$. When $j = 1$ we define the domain $\mathscr{D}_m^1 = \prod_{l=1}^{n} \left[\min_{h \in \mathscr{B}_m^1} \left(\hat{x}_{m,h}^{(l)} \right), \max_{h \in \mathscr{B}_m^1} \left(\hat{x}_{m,h}^{(l)} \right) \right]$.

We assume that the option function $V(t_{m+1}, \cdot)$ is an element of the L^2 space, i.e. it is square-integrable with some measure. Suppose that we have the values of this option function on all paths, denoted by $\hat{v}_{m+1,h}$, $n = 1,2,...,N$. With the chosen set of basis functions $\{(\mathbf{X}_{m+1})^k, |k| = 0,1,\ldots,d\}$ in L^2, the option function can be approximated by a linear combination of the basis functions in least squares sense:

$$V(t_{m+1}, \mathbf{X}_{m+1}) \approx \sum_{|k|=0}^{d} \beta_k^{m,j} (\mathbf{X}_{m+1})^k, \tag{3.21}$$

where $\beta_k^{m,j}$ are the coefficients at time t_m for the basis $(\mathbf{X}_{m+1})^k$ within the j-th bundle $\mathscr{B}_m^j$, which is the solution of minimizing the sum of squared residuals, given by

$$\left\{ \beta_k^{m,j}, |k| = 0,1,\ldots,d \right\} = \underset{b_k \in \mathbb{R}}{\arg\min} \sum_{h \in \mathscr{B}_m^j} \left(\hat{v}_{m+1,h} - \sum_{|k|=0}^{d} b_k (\mathbf{X}_{m+1})^k \right)^2. \tag{3.22}$$

Hence the continuation function on the bounded domain $\mathscr{D}_m^j$ can be approximated by a linear combination of the conditional expected discounted basis functions defined by:

$$\begin{aligned} c_2(t_m, \mathbf{X}_m) &:= \mathbb{E}^{\mathbb{Q}} \left[\frac{B_m}{B_{m+1}} \sum_{|k|=0}^{d} \beta_k^{m,j} (\mathbf{X}_{m+1})^k \middle| \mathbf{X}_m \right] \\ &= \sum_{|k|=0}^{d} \beta_k^{m,j} \psi_k(\mathbf{X}_m, t_m, t_{m+1}), \end{aligned} \tag{3.23}$$

where ψ_k is the k-th moment discounted at the interest rate r over the period $[t_m, t_{m+1}]$.

We will approximate the 'true' continuation function $c(t_m, \cdot)$ given in equation (3.11) by the function $c_2(t_m, \cdot)$ defined in equation (3.23) on the bounded domain $\mathscr{D}_m^j$. Since we have analytic formulas of $\{\psi_k\}_{|k|=0}^d$ defined in (3.19), the continuation value on the h-th path within the j-th bundle can be easily computed by:

$$c(t_m, \hat{x}_{m,h}) \approx c_2(t_m, \hat{x}_{m,h}) = \sum_{|k|=0}^{d} \beta_k^{m,j} \psi_k(\hat{x}_{m,h}, t_m, t_{m+1}). \tag{3.24}$$

In addition, we will show that the error of approximation of the continuation function at time t_m is bounded by the error of approximation of the option function at time t_{m+1} in section 3.4.5.

3.4.4. APPROXIMATING THE SENSITIVITIES OF EE

The sensitivities *Delta* (Δ_{EE}) and *Gamma* (Γ_{EE}) of EE w.r.t. the change of the underlying asset price $S_0 = \exp(X_0)$ can be computed in the same backward algorithm for the computation of the exposure profile. At time $t_M = T$, we simply assign value zero to these

derivatives of the EE function. At time $t_m < T$, the sensitivities can be computed by:

$$\begin{aligned}\Delta_{\mathrm{EE}}(t_m) &:= \frac{\partial \mathrm{EE}}{\partial S_0}(t_m) \approx \frac{1}{H}\sum_{h=1}^{H}\frac{\partial E}{\partial x_m}\left(t_m, \hat{x}_{m,h}\right)\cdot\frac{1}{S_0},\\ \Gamma_{\mathrm{EE}}(t_m) &:= \frac{\partial^2 \mathrm{EE}}{\partial S_0^2}(t_m) \approx \frac{1}{H}\sum_{h=1}^{H}\left(\frac{\partial^2 E}{\partial X_m^2}\left(t_m, \hat{x}_{m,h}\right) - \frac{\partial E}{\partial X_m}\left(t_m, \hat{x}_{m,h}\right)\right)\cdot\frac{1}{S_0^2},\end{aligned} \tag{3.25}$$

where $X_m = \log(S_m)$ represents the log-asset value at time t_m. The formulas of the derivatives in (3.25) are detailed here. At time t_m, the first derivative of the EE function can be computed by

$$\frac{\partial \mathrm{EE}}{\partial S_0}(t_m) \approx \frac{1}{H}\sum_{h=1}^{H}\frac{\partial E}{\partial S_0}(t_m, \hat{x}_{m,h}), \tag{3.26}$$

by the chain rule,

$$\frac{\partial E}{\partial S_0}(t_m, \hat{x}_{m,h}) = \frac{\partial E}{\partial X_m}\cdot\frac{\partial X_m}{\partial S_m}\cdot\frac{\partial S_m}{\partial S_0}(t_m, \hat{x}_{m,h}), \tag{3.27}$$

where $X_m := \log(S_m)$, and

$$\frac{\partial X_m}{\partial S_m} = \frac{1}{S_m}, \quad \frac{\partial S_m}{\partial S_0} = \frac{S_m}{S_0}. \tag{3.28}$$

The second equation in (3.28) can be derived as follows. We take as an example, that the asset value $\log(S_t)$ follows an Ito process as follows:

$$d\log S_t = \mu_t dt + \sigma_t dW_t. \tag{3.29}$$

By integrating both sides, we obtain

$$S_t = S_0 \exp\left(\int_0^t \left(\mu_s ds + \sigma_s dW_s\right)\right), \tag{3.30}$$

hence the derivative of S_t w.r.t. S_0 can be expressed by

$$\frac{\partial S_t}{\partial S_0} = \exp\left(\int_0^t \left(\mu_s ds + \sigma_s dW_s\right)\right) = \frac{S_t}{S_0}. \tag{3.31}$$

So, the first derivative of the EE function can be expressed as

$$\frac{\partial \mathrm{EE}}{\partial S_0}(t_m) \approx \frac{1}{H}\sum_{h=1}^{H}\frac{\partial E}{\partial X_m}(t_m, \hat{x}_{m,h})\frac{1}{S_0}. \tag{3.32}$$

From (3.32), the second derivative can be derived by

$$\frac{\partial^2 \mathrm{EE}}{\partial S_0^2}(t_m) \approx \frac{1}{H}\sum_{h=1}^{H}\left(\frac{\partial^2 E}{\partial X_m^2}(t_m, \hat{x}_{m,h}) - \frac{\partial E}{\partial X_m}(t_m, \hat{x}_{m,h})\right)\frac{1}{S_0^2}. \tag{3.33}$$

For those paths on which the option is alive at time t_m, the first and the second derivatives of the exposure function are given by

$$\begin{aligned}\frac{\partial E}{\partial X_m} &:= \frac{\partial c}{\partial X_m} \approx \sum_{|k|=0}^{d}\beta_k^{m,j}\frac{\partial \psi_k}{\partial X_m},\\ \frac{\partial^2 E}{\partial X_m^2} &:= \frac{\partial^2 c}{\partial X_m^2} \approx \sum_{|k|=0}^{d}\beta_k^{m,j}\frac{\partial^2 \psi_k}{\partial X_m^2},\end{aligned} \tag{3.34}$$

with the same coefficient set $\left\{\beta_k^{m,j}\right\}_{|k|=0}^{d}$ as in (3.23), $j \in \mathscr{B}_{m,j}$;

For those paths at which the option has been exercised or knocked out at time t_m, the derivatives of EE are given value zero, as the exposure values on these paths are zero.

3.4.5. CONVERGENCE RESULTS

The so-called *direct estimator* is obtained in the backward algorithm by regression [50]. With convexity of the 'max' function, it can be proven by induction that the direct estimator is often higher than the true value with some bias, and that the direct estimator converges to the option value as the number of bundle and the number of paths within each bundle go to infinity. See Theorem 2 and Theorem 4 in [50].

In addition, an estimator can be made based on the average cash flow of a second set of paths, referred to as the *path estimator*. Using the coefficients obtained by regression based on one set of paths, an approximation of the optimal early exercise strategy of another set of paths can be made by comparing values of continuation and values of immediate exercise. The path estimator is often a lower bound of the option value, converging almost sure as the number of paths goes to infinity [50], since the option value computed by the optimal early exercise strategy is the supremum of the option value at time $t = 0$ by definition. Details of the proof can be found in [50, 64].

For European and barrier options, one can take the discounted average of the MC paths as the reference. For Bermudan options, the direct and path estimators provide a conservative confidence interval for the true option value [50]:

$$\left[V_0^{\text{path}} - 1.96\frac{\hat{s}_{\text{path}}}{\sqrt{N_s - 1}}, V_0^{\text{direct}} + 1.96\frac{\hat{s}_{\text{direct}}}{\sqrt{N_s - 1}}\right], \tag{3.35}$$

where $\hat{s}_{\text{path}}$ and $\hat{s}_{\text{direct}}$ are the sample standard deviations for the path and direct estimator, respectively, and V_0^{path} and V_0^{direct} are the sample means of the path and direct estimators, respectively; these sample means and sample standard deviations are based on N_s independent trials.

The approximation of the option function converges as the number of paths, the number of basis functions and the number of bundles go to infinity, as we have presented in Chapter 1 for a model case. The option function can be approximated well by a piece-wise function, even with a low order $d = 1$. This advantage of the SGBM approach will reduce the computational effort when the dimensionality increases. It ensures the accuracy of the computed continuation values by SGBM on each path, which is important for computing exposure profiles.

3.5. NUMERICAL TESTS

In this section, we will analyze the convergence and accuracy of SGBM for the Heston and the HHW models, respectively w.r.t. the following quantities:

- the value of the option at time $t = 0$;
- the EE and PFE quantities over time $[0, T]$;
- the sensitivities w.r.t. S_0 of the EE function over time $[0, T]$.

The convergence of SGBM for the computation of Bermudan options can be checked by comparing the direct and path estimators. The reference values for European and barrier options can be computed by averaging discounted cash flows for a very large number of paths.

In addition, the COS method can be connected to the MC method [79] for reference values. Under the Heston model, the COS method in [29] can be used to calculate option values and corresponding Greeks at time $t = 0$ for Bermudan and barrier options. By the MC COS method exposure profiles, quantities and sensitivities of the EE function can be computed at monitoring date t_m. We use quantities computed by the COS method as the reference values for EE, PFE and sensitivity functions under the Heston model[1].

The Quadratic Exponential (QE) scheme is employed for accurate simulation of the Heston volatility model [2]. CVA is computed here via formula (3.17) with LGD= 1. The survival probability function is assumed to be independent of exposure with a constant intensity , expressed by $\text{PD}(t) = 1 - \exp(-0.03t)$ over the period $[0, T]$.

3.5.1. THE HESTON MODEL

The parameters for the Heston model in (3.4) are chosen as

Test A: $S_0 = 100$, $r = 0.04$, $K = 100$, $T = 1$; $\kappa = 1.15$, $\gamma = 0.39$, $\bar{v} = 0.0348$, $v_0 = 0.0348$, $\rho_{x,v} = -0.64$, where the Feller condition is not satisfied.

We choose a large number of MC paths, $N = 2 \cdot 10^6$ and a relatively small time step size $\Delta t = 0.05$. The paths will be clustered into $J_1 = 2^j, J_2 = 2^j$, $j = 1,2,3,4$ bundles. The monomial basis in SGBM is of order $d = \{1,2,3\}$. The number of paths is chosen large as we wish to compare the convergence and accuracy using the same set of simulated scenarios for different choices of the number of bundles J and degree p. The number of paths can be greatly reduced in real-life CVA computations because SGBM typically exhibits low variances compared to LSM.

We consider a Bermudan put option under the Heston model with parameter Test A, with 10 equally-spaced exercise dates till $T = 1$.

Figure 3.2(a) shows that the direct and path estimators converge to the option value when increasing the number of bundles (J) and the order of the monomial basis (d), as expected. Monomial basis $d = 3$ enhances the convergence speed compared to $d = 2$ or $d = 1$. Figure 3.2(b) confirms this by showing the difference in the computed EE of the direct and path estimators, where the difference is measured in the relative L^2 norm[2].

In Fig. 3.3, we present the accuracy of SGBM for the exposure quantities, EE, PFE and sensitivities of EE, by comparing to reference values by the MC COS method based on the same set of MC paths. Increasing the number of bundles J and/or the order of the monomial basis d enhances the accuracy of the results, as expected. In particular, a basis of order $d = 2$ achieves the same level of accuracy as order $d = 3$ with twice more

[1] In the MC COS method, we use 400 Fourier terms, and 400 grid points in volatility direction; the COS parameter for the integration domain size is set to $L = 12$ for calculating the reference values.

[2] The relative L^2 norm is defined by:

$$\frac{\|EE_{direct} - EE_{path}\|_{L^2}}{\|EE_{direct}\|_{L^2}} = \frac{\sqrt{\sum_{m=0}^{M} \left(\text{EE}_{direct}(t_m) - \text{EE}_{path}(t_m)\right)^2}}{\sqrt{\sum_{m=0}^{M} \left(\text{EE}_{direct}(t_m)\right)^2}}. \tag{3.36}$$

bundles. By increasing the number of bundles, we can thus employ a monomial basis of lower order, which is an important insight.

Table 3.2 presents option values as well as CVA and sensitivities computed by SGBM plus the corresponding reference values. We see that the direct estimators have smaller variances compared to the path estimators.

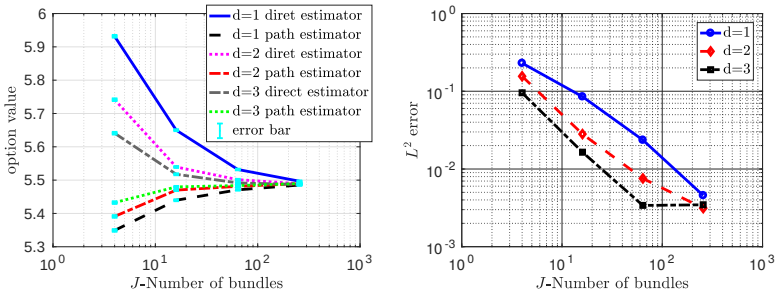

(a) Bermudan option (b) Error in EE

Figure 3.2: Convergence of the Bermudan option value and the EE w.r.t. J - the number of bundles and d - the order of the basis functions, by comparing the direct and path estimators. Strike $K = 100$, expiry date $T = 1$ and exercise times 10. The total number of paths $N = 2 \cdot 10^6$.

Table 3.2: Results of a Bermudan put option under the Heston model. Strike $K = 100$, expiry date $T = 1$ and exercise times 10. The total number of paths $H = 2 \cdot 10^6$, and the order $d = 2$ and the bundle number $J = 2^8$.

Bermudan option under the Heston model			
quantities	direct estimator(std.)	path estimator(std.)	COS
$V(0)$	5.486 (0.000)	5.488 (0.005)	5.486
$\Delta_{\text{EE}}(0)$	-0.329 (0.000)	-	-0.328
$\Gamma_{\text{EE}}(0)$	0.022 (0.000)	-	0.025
CVA	0.093 (0.000)	0.093 (0.000)	0.093 (0.000)

In addition, Fig. 3.4 presents the convergence of SGBM based on basis functions of lower order, $d = 1$, where we increase the number of bundles to 4^6. The conclusion in Chapter 1, that when the size of a bundle approaches zero, the bias caused by approximating a continuous function by a simple linear function goes to zero, is confirmed. This is one advantage of SGBM compared to LSM. We need fewer basis functions by using bundles.

We also consider a down-and-out put barrier option with strike $K = 100$. The option is knocked out when the asset value reaches barrier level $L_b = 0.9K$ before the maturity $T = 1$. After being knocked out, an investor receives a rebate value, $r_b = 10$; otherwise the investor receives the payoff at time $T = 1$. We present these quantities computed by SGBM and the corresponding reference values in Table 3.3.

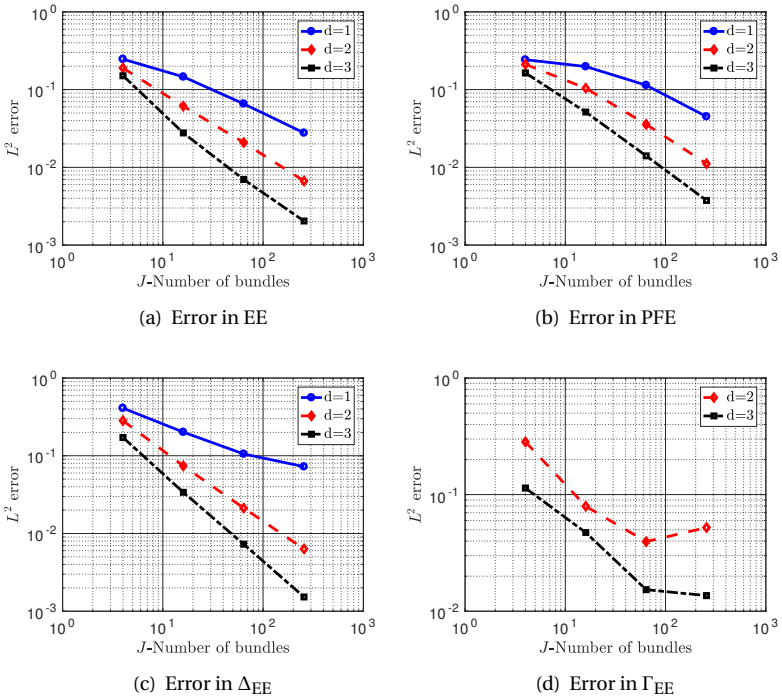

(a) Error in EE

(b) Error in PFE

(c) Error in Δ_{EE}

(d) Error in Γ_{EE}

Figure 3.3: Convergence of the EE, PFE and sensitivities, w.r.t. J - the number of bundles and p - the order of basis functions for a Bermudan put option; the reference is generated by the MC COS method. Strike $K = 100$, expiry date $T = 1$ and exercise times 10. The total number of paths $N = 2 \cdot 10^6$.

Table 3.3: Results of a down-and-out barrier put option under the Heston model. Strike $K = 100$, expiry date $T = 1$, barrier level $L_b = 0.9K$, $r_b = 10$. The total number of paths $H = 2 \cdot 10^6$, and the order $d = 2$ and the bundle number $J = 2^8$.

barrier option under the Heston model			
values $t = 0$	SGBM (std.)	Monte Carlo (std.)	COS
$V(0)$	4.013 (0.000)	4.016 (0.003)	4.015
$\Delta_{EE}(0)$	-0.2631 (0.000)	-	-0.263
$\Gamma_{EE}(0)$	0.0232 (0.000)	-	0.0224
CVA	0.0493 (0.000)	0.0493 (0.000)	0.0493 (0.000)

3.5.2. THE HHW MODEL

SGBM for the Heston Hull-White model is based on forward simulation under the true HHW dynamics while the backward computation employs the discounted moments of the H1HW dynamics.There are basically two issues regarding the SGBM computation of exposure under the HHW model. We will focus on the impact of a long expiry date (say

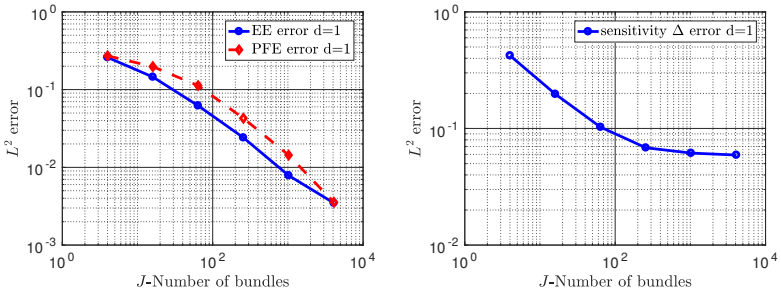

(a) Error in EE and PFE when $d = 1$ (b) Error in Delta when $d = 1$

Figure 3.4: Convergence of the EE, PFE and sensitivity Δ w.r.t. J - the number of bundles for a Bermudan put option when the number of paths within each bundle is 200, the order of the basis functions $d = 1$, and the total number of paths is $200J$; the reference is generated by the MC COS method.

$T = 10$), and we will examine the accuracy of the approximation of the HHW model by the affine H1HW model.

We use the following parameters for the HHW and H1HW models (3.4):

Test B: $S_0 = 100$, $v_0 = 0.05$, $r_0 = 0.02$; $\kappa = 0.3$, $\gamma = 0.6$, $\bar{v} = 0.05$, $\lambda = 0.01$, $\eta = 0.01$, $\theta = 0.02$, $\rho_{x,v} = -0.3$ and $\rho_{x,r} = 0.6$. $T = 10$.

Simulation is done with $N = 10^6$ MC paths and $\Delta t = 0.1$. The details of the SGBM algorithm are as follows: the number of bundles varies as $J_1 = 2^{2+j}$, $J_2 = 2^j$, $J_3 = 2^j$, $j = 1,2,3$ and the orders of the monomial basis are $d = \{1,2\}$.

The accuracy of SGBM is first studied by computing a European put option with $T = 10$. The implied volatility (in %) is used to demonstrate the accuracy of the computed option values, as the implied volatility is typically sensitive to the accuracy of option values [39]. The implied volatility is computed by means of the BS formula for strike values $K = \{40,80,100,120,180\}$. The reference values are computed by the average cash flows on the generated MC paths. The results are presented in Table 3.4. The SGBM results have smaller variances compared to results of a plain Monte Carlo simulation, and maintain a high accuracy when comparing the absolute errors.

Table 3.4: Implied volatility (%) obtained for a European put option with expiry date $T = 10$ under the HHW model, based on 5 simulations.

Implied volatility (%)			
K/S_0	SGBM (std.)	Monte Carlo (std.)	Abs. error (%)
40%	26.481 (0.003)	26.479 (0.03)	0.0014
80%	20.699 (0.003)	20.719 (0.02)	0.0202
100%	19.200 (0.003)	19.242 (0.01)	0.0413
120%	18.369 (0.003)	18.427 (0.01)	0.0585
180%	18.220 (0.003)	18.291 (0.02)	0.0706

We then consider a Bermudan put option with 50 exercise dates equally distributed in the period $[0, T]$. Figure 3.5 shows the SGBM convergence rate by comparing the direct and path estimators. Results of this Bermudan put are presented in Table 3.5. Table 3.6 presents results of SGBM for computing a down-and-out barrier put option. It shows that SGBM converges well also for a non-continuous payoff function.

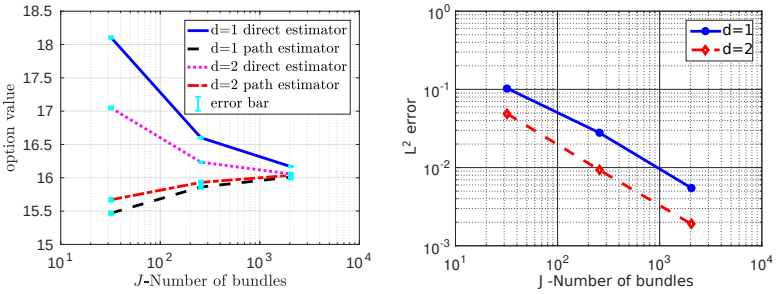

(a) Bermudan option values (b) EE difference

Figure 3.5: Convergence w.r.t. J - the number of bundles and p - the order of the monomial basis by comparing the path and the direct estimator under the HHW model. Strike $K = 100$, $T = 10$ and 50 exercise times. The total number of paths $H = 10^6$.

Table 3.5: Results for a Bermudan put option under the HHW model. Strike $K = 100$, $T = 10$ and 50 exercise times. The total number of paths is $H = 10^6$, and the order $d = 2$ and bundle number $J = 2048$.

Bermudan option under the HHW model			
	values $t = 0$	direct estimator(std.)	path estimator(std.)
$T = 10$	$V(0)$	16.056 (0.002)	16.009 (0.018)
	$\Delta_{EE}(0)$	-0.268 (0.000)	-
	$\Gamma_{EE}(0)$	0.815 (0.001)	-
	CVA	2.968 (0.003)	-

Table 3.6: Results for a down-and-out barrier put option under the HHW model. Strike $K = 100$, $T = 10$, barrier level $L_b = 0.9K$, $r_b = 0$. The total number of paths is $H = 10^6$, and the order $d = 2$ and $J = 2048$ bundles.

Barrier option under the HHW model		
values $t = 0$	direct estimator(std.)	Monte Carlo(std.)
$V(0)$	0.0478 (0.000)	0.0477 (0.001)
$\Delta_{EE}(0)$	0.0017 (0.000)	-
$\Gamma_{EE}(0)$	-0.0001 (0.000)	-
CVA	0.0123 (0.000)	-

3.5.3. SPEED

One benefit of the SGBM algorithm is that one can calculate different financial derivatives on the same underlying in one backward iteration using the same set of simulated paths, as the monomial basis and the discounted moments are the same. Table 3.7 compares the calculation time of a single Bermudan option and of a portfolio, which consists of a Bermudan option, a European option and two barrier options with the same underlying stock. The algorithm is implemented in MATLAB, and runs on an Intel(R) Core(TM) i7-2600 CPU @ 3.40GHz.

Table 3.7: Calculation time in seconds for computing exposure profiles of a Bermudan option and for that of a whole portfolio with expiry date $T = 10$ under the HHW model; SGBM with polynomial order $d = 2$, number of paths $H = 10^6$ and time step size $\Delta t = 0.1$.

Calculation time	direct estimator	path estimator for Bermudan
A single (Bermudan) option	151.5 (sec.)	130.2 (sec.)
Portfolio	306.3(sec.)	131.5 (sec.)

By using parallelization of the SGBM algorithm, the speed can be further enhanced drastically, see a study in [63].

3.5.4. IMPACT OF STOCHASTIC VOLATILITY AND STOCHASTIC INTEREST RATES

We here check the impact of stochastic volatility and stochastic interest rates on exposure profiles and CVA. Next to the already discussed Heston and HHW models, we also consider the Black-Scholes (BS) and the Black-Scholes Hull-White (BSHW) models in this section. The parameter set chosen is the same as in Test B. For comparison, we use the parameters of the other models such that we can ensure that the values of a European put option with a fixed expiry date T has the same price under all models[3].

We define a so-called CVA percentage as $\left(100 \cdot \frac{\text{CVA}}{V(0)}\right)\%$. Table 3.8 presents the percentage CVA for European put options with two maturity times, $T = \{1, 5\}$, for the strike values $K = \{80, 100, 120\}$. It can be seen that the CVA percentage does not change with strike; furthermore, European options with maturity $T = 5$ exhibit a higher CVA percentage than those with maturity $T = 1$. Based on the chosen parameters, we see only a small impact of stochastic volatility and stochastic interest rate on the CVA percentage.

Table 3.9 presents the percentage CVA for Bermudan put options with maturity times $T = \{1, 5\}$ for strike values $K = \{80, 100, 120\}$. We see that the 'in-the-money' options have the smallest CVA percentage. This is understandable as the optimal exercise strategy, in this chapter, does not take into account the risk of a counterparty default. A put option is likely to be exercised before maturity when the strike value is higher than the current stock value, and thus one can expect relatively little exposure.

[3] For example, under the Black-Scholes model, we use the implied interest rate, i.e. $r_T = -\frac{\log(p(0,T))}{T}$, and compute the implied volatility by the analytic BS formula. Under the Heston model, the parameters of the Heston process are the same as those in Test B, and the corresponding interest rate is computed by the bisection algorithm. Under the BSHW model, the parameters of the Hull White process are the same as those in Test B, and the corresponding volatility is determined.

Table 3.8: CVA(%) of European options with $T = 5$ and strike values $K = \{80, 100, 120\}$.

European option, CVA (%)					
	K/S_0	BS	Heston	BSHW	HHW
$T = 1$	80%	2.951 (0.010)	2.959 (0.003)	2.953 (0.005)	2.949 (0.005)
	100%	2.956 (0.011)	2.958 (0.003)	2.952 (0.002)	2.952 (0.002)
	120%	2.955 (0.002)	2.959 (0.001)	2.953 (0.001)	2.952 (0.001)
$T = 5$	80%	13.925 (0.036)	13.941 (0.021)	13.882 (0.016)	13.929 (0.027)
	100%	13.951 (0.039)	13.960 (0.010)	13.901 (0.003)	13.940 (0.018)
	120%	13.919 (0.010)	13.953 (0.007)	13.901 (0.005)	13.936 (0.010)

Table 3.9: CVA(%) of Bermudan options with $T = 5$ and strike values $K = \{80, 100, 120\}$.

Bermudan option, CVA (%)					
	K/S_0	BS	Heston	BSHW	HHW
$T = 1$	80%	2.534 (0.007)	2.460 (0.002)	2.643 (0.003)	2.504 (0.003)
	100%	2.005 (0.003)	1.939 (0.002)	2.165 (0.001)	2.016 (0.001)
	120%	0.906 (0.002)	1.031 (0.001)	0.986 (0.001)	1.068 (0.001)
$T = 5$	80%	10.110 (0.032)	9.876 (0.030)	12.612 (0.014)	10.890 (0.029)
	100%	7.784 (0.011)	8.120 (0.012)	10.965 (0.008)	9.649 (0.019)
	120%	4.453 (0.008)	4.416 (0.020)	6.923 (0.005)	6.259 (0.013)

Figure 3.6 presents the EE and PFE function values w.r.t. time for a Bermudan put option which is at-the-money.

- In Fig. 3.6(b), it can be seen that the PFE values for the HHW model are relatively close to those of the Heston model, and the PFE values for the BSHW model are very similar to those of the BS model. With a short time to maturity ($T = 1$), under our model assumptions and parameters, the stochastic volatility has a more significant contribution to the PFE values compared to the stochastic interest rate. Compared to Figure 3.6(a), we can see that the EE values for the Heston and the BS models are very close. Adding stochastic volatility has more impact on the right-side tails of the exposure profiles than on the EE values.

- In Fig. 3.6(d), in the period $t = [0, 1]$, we see similarities of PFE values between the HHW and the Heston models, and between the BS and the BSHW models; in the period $t = [1, 5]$, the PFE values for the BSHW model tend to be higher than those of the BS model, and the PFE values for the HHW model are also higher than those of the Heston model. Clearly, interest rates have more impact on the exposure profiles in the longer term (say $T = 5$).

- Figures 3.6(a) and (c) show that the stochastic interest rate increases the future EE values of Bermudan options, while the stochastic volatility has the opposite effect.

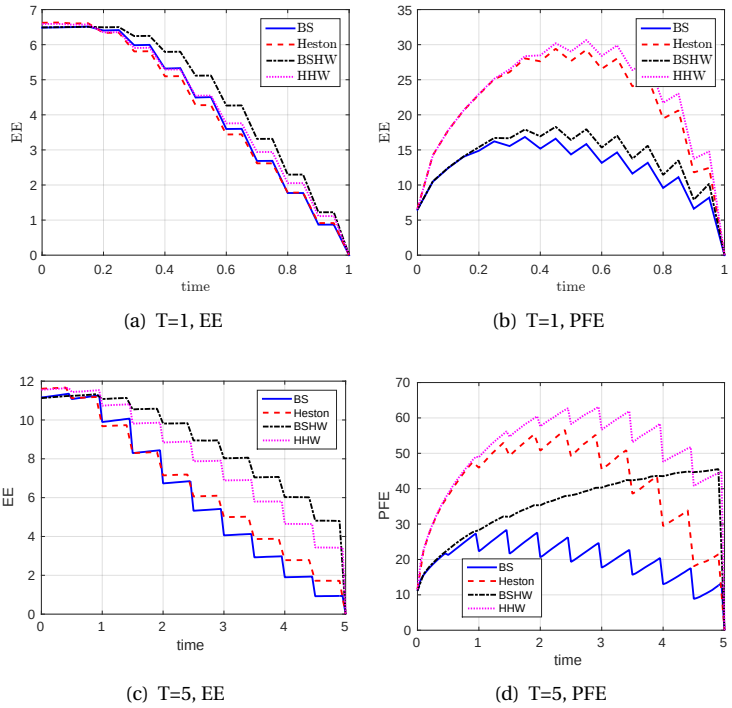

(a) T=1, EE (b) T=1, PFE

(c) T=5, EE (d) T=5, PFE

Figure 3.6: Impact of stochastic volatility and interest rate on EE and PFE with different tenors and different asset dynamics, at the money $K = 100$.

- The PFE curve for the BSHW model in Fig. 3.6(d) looks differently from the other curves because of the positive correlation parameter ($\rho_{x,r} = 0.6$) and the long expiry ($T = 5$). The PFE curve represents events with large option values and for a put option, this means that the associated stock values are low. In the case of a positive correlation parameter $\rho_{x,r}$, the interest rate is low as well. The investor likely holds on to the option. If we set the correlation value to zero in the BSHW model and perform the same computation, the PFE curves under the BSHW model becomes 'spiky' as well.

The stochastic interest rate plays a significant role in the case of a longer maturity derivatives, and results in increasing PFE profiles; stochastic asset volatility appears to have an effect on PFE values at the early stage of a contract. Under the parameters chosen here, at an early stage of the contract (say $t < 1$), the PFE profiles under the HHW model are very similar to those under the Heston model, but at later contract times the PFE profiles under the HHW model increase. It seems that the stochastic volatility has more effect on the right-side tail compared to the expectation of the exposure profile, while adding the stochastic interest rate increases the whole exposure profile, especially in the case of a longer maturity.

3.6. CONCLUSION

In this chapter we generalized the Stochastic Grid Bundling Method (SGBM) towards the computation of exposure profiles and sensitivities for asset dynamics with stochastic asset volatility and stochastic interest rate for European, Bermudan as well as barrier options. The algorithmic structure as well as the essential method components are very similar for CVA as for the computation of early-exercise options, which makes SGBM a flexible CVA valuation framework.

We presented arguments for the choice of the basis functions for the local regression, presented a bundling technique, and showed SGBM convergence of the direct and path estimators with respect to an increasing number of bundles. Numerical experiments demonstrate SGBM's convergence and accuracy.

Using higher-order polynomials as the basis functions is especially important when accurate sensitivities values are needed; otherwise, a polynomial order $d = 1$ is sufficient for option prices and exposure quantities with a sufficiently large number of bundles and paths. The computational efficiency is connected to the number of bundles used in SGBM. A parallel algorithm will be important for a drastic reduction of the computation times, see the studies in [63].

APPENDIX

DISCOUNTED CHF OF THE HESTON MODEL

The joint dChF of the Heston model in Chapter 3 is given by:

$$\begin{aligned}\varphi_{\text{Heston}}(u_1,u_2,t,T;X_t,v_t) &= \mathbb{E}^{\mathbb{Q}}\left[\exp\left(-r(T-t)+iu_1X_t+iu_2v_t\right)\right]\\ &= \exp\left(\widetilde{A}(T-t)+\widetilde{B}_1(T-t)X_t+\widetilde{B}_2(T-t)v_t\right),\end{aligned} \tag{3.37}$$

where the coefficients of the ChF are obtained via the following ODEs:

$$\begin{aligned}\frac{d\widetilde{B}_1}{ds}(s) &= 0,\\ \frac{d\widetilde{B}_2}{ds}(s) &= \frac{1}{2}\widetilde{B}_1(s)(\widetilde{B}_1(s)-1)+\left(\gamma\rho_{x,v}\widetilde{B}_1(s)-\kappa\right)\widetilde{B}_2(s)+\frac{1}{2}\gamma^2\widetilde{B}_2^2(s),\\ \frac{d\widetilde{A}}{ds}(s) &= \kappa\bar{v}\widetilde{B}_2(s)+r(\widetilde{B}_1(s)-1),\end{aligned} \tag{3.38}$$

with initial condition $\bar{B}(0) = iu_1$, $\widetilde{B}_2(0) = iu_2$ and $\widetilde{A}(0) = 0$. The solution is given by:

$$\begin{aligned}\widetilde{B}_1(T-t) &= iu_1,\\ \widetilde{B}_2(T-t) &= \frac{1}{\gamma^2}\left(\kappa-\gamma\rho_{x,v}iu_1+D_1\right)-\frac{2D_1}{\gamma^2\left(1-D_2\exp\left(-D_1(T-t)\right)\right)},\\ \widetilde{A}(T-t) &= r(iu_1-1)(T-t)+\frac{\kappa\bar{v}}{\gamma^2}\left(\kappa-\gamma\rho_{x,v}iu_1-D_1\right)\\ &\quad-\frac{2\kappa\bar{v}}{\gamma^2}\log\left(\frac{1-D_2\exp\left(-D_1(T-t)\right)}{1-D_2}\right),\end{aligned} \tag{3.39}$$

with

$$\begin{aligned} D_1 &= \sqrt{\left(\kappa - \gamma\rho_{x,v} i u_1\right)^2 + \gamma^2 u_1(u_1+i)}, \\ D_2 &= \frac{i u_2 \gamma^2 - \left(\kappa - \gamma\rho_{x,v} i u_1 - D_1\right)}{i u_2 \gamma^2 - \left(\kappa - \gamma\rho_{x,v} i u_1 + D_1\right)}. \end{aligned} \tag{3.40}$$

DISCOUNTED CHF OF THE BLACK-SCHOLES HULL-WHITE MODEL

The joint dChF for the BSHW model is given by:

$$\begin{aligned} \varphi_{\text{BSHW}}(u_1,u_2,t,T;X_t,r_t) &= \mathbb{E}^{\mathbb{Q}}\left[\exp\left(-\int_t^T r_s ds + i u_1 X_t + i u_2 r_t\right)\right] \\ &= \exp\left(\widetilde{A}(t,T) + \widetilde{B}_1(T-t)X_t + \widetilde{B}_2(T-t)r_t\right), \end{aligned} \tag{3.41}$$

where the coefficients of the ChF are obtained via the following ODEs:

$$\begin{aligned} \frac{d\widetilde{B}_1}{ds}(s) &= 0, \\ \frac{d\widetilde{B}_2}{ds}(s) &= -1 + \widetilde{B}_1(s) - \lambda\widetilde{B}_2(s), \\ \frac{d\widetilde{A}}{ds}(s) &= \frac{1}{\sigma^2}\widetilde{B}_1(s)\left(\widetilde{B}_1(s)-1\right) + \lambda\cdot\theta(T-s)\cdot\widetilde{B}_2(s) + \frac{1}{2}\eta^2\widetilde{B}_2(s) \\ &\quad + \rho_{x,r}\sigma\eta\widetilde{B}_1(s)\widetilde{B}_2(s), \end{aligned} \tag{3.42}$$

with initial condition $\widetilde{B}_1(0) = i u_1$, $\widetilde{B}_2(0) = i u_2$, and $\widetilde{A}(0) = 0$. The solution is now given by:

$$\begin{aligned} \widetilde{B}_1(T-t) &= i u_1, \\ \widetilde{B}_2(T-t) &= \frac{i u_1 - 1}{\lambda}\left(1 - \exp\left(-\lambda(T-t)\right)\right) + i u_2 \exp\left(-\lambda(T-t)\right), \\ \widetilde{A}(t,T) &= \frac{1}{2}\sigma^2 i u_1(i u_1 - 1)(T-t) + \int_0^{T-t}\theta(T-s)\cdot\widetilde{B}_2(s)ds \\ &\quad + \frac{\eta^2}{2\lambda^2}\Big(\frac{2}{\lambda}(u_1+i)\left(\exp(-\lambda(T-t))-1\right)(\lambda u_2 - u_1 - i) \\ &\quad + \frac{1}{2\lambda}\left(\exp(-2\lambda(T-t))-1\right)(\lambda u_2 - u_1 - i)^2 - (u_1+i)^2(T-t)\Big) \\ &\quad + \frac{\eta\theta\sigma\rho_{x,r}}{\lambda}\Big(-\frac{i u_1 + u_1^2}{\lambda}\left(\lambda(T-t) + \exp(-\lambda(T-t)) - 1\right) \\ &\quad + u_1 u_2\left(\exp(-\lambda(T-t)) - 1\right)\Big). \end{aligned} \tag{3.43}$$

When $\theta(t) \equiv \bar{\theta}$ is a constant,

$$\int_0^{T-t}\theta(T-s)\widetilde{B}_2(s)ds = \bar{\theta}(i u_1 - 1)(T-t) + \bar{\theta}\left(\frac{(i u_1 - 1)}{\lambda} - i u_2\right)\left(\exp\left(-\lambda(T-t)\right) - 1\right). \tag{3.44}$$

DISCOUNTED CHF OF THE H1HW MODEL

The joint dChF of the H1HW model is given by:

$$\begin{aligned}&\varphi_{\text{H1HW}}(u_1,u_2,u_3,t,T;X_t,v_t,r_t)\\&\quad=\exp\left(\widetilde{A}(t,T)+\widetilde{B}_1(T-t)X_t+\widetilde{B}_2(T-t)v_t+\widetilde{B}_3(T-t)r_t\right),\end{aligned}\tag{3.45}$$

where the coefficients of the ChF are here obtained via the following ODEs:

$$\begin{aligned}\frac{d\widetilde{B}_1}{ds}(s)&=0,\\\frac{d\widetilde{B}_2}{ds}(s)&=\frac{1}{2}\widetilde{B}_1(s)(\widetilde{B}_1(s)-1)+\left(\gamma\rho_{x,v}\widetilde{B}_1(s)-\kappa\right)\widetilde{B}_2(s)+\frac{1}{2}\gamma^2\widetilde{B}_2^2(s),\\\frac{d\widetilde{B}_3}{ds}(s)&=-1+\widetilde{B}_1(s)-\lambda\widetilde{B}_3(s),\\\frac{d\widetilde{A}}{ds}(s)&=\lambda\cdot\theta(T-s)\cdot\widetilde{B}_3(s)+\kappa\bar{v}\widetilde{B}_2(s)+\frac{\eta^2}{2}\widetilde{B}_3^2(s)\\&\quad+\eta\rho_{x,v}\mathbb{E}\left[\sqrt{v_T}\middle|v_t\right]\widetilde{B}_1(s)\widetilde{B}_3(s),\end{aligned}\tag{3.46}$$

with initial conditions $\widetilde{B}_1(0)=iu_1$, $\widetilde{B}_2(0)=iu_2$, $\widetilde{B}_3(0)=iu_3$ and $\widetilde{A}(0)=0$. The solution is given by:

$$\begin{aligned}\widetilde{B}_1(T-t)&=iu_1,\\\widetilde{B}_2(T-t)&=\frac{1}{\gamma^2}\left(\kappa-\gamma\rho_{x,v}iu_1+D_1\right)-\frac{2D_1}{\gamma^2\left(1-D_2\exp(-D_1(T-t))\right)},\\\widetilde{B}_3(T-t)&=\frac{iu_1-1}{\lambda}\left(1-\exp(-\lambda(T-t))\right)+iu_3\exp(-\lambda(T-t)),\\\widetilde{A}(t,T)&=\int_0^{T-t}\theta(T-s)\cdot\widetilde{B}_3(s)ds+(T-t)\frac{\kappa\bar{v}}{\gamma^2}\left(\kappa-\gamma\rho_{x,v}iu_1-D_1\right)\\&\quad-\frac{2\kappa\bar{v}}{\gamma^2}\log\left(\frac{1-D_2\exp\left(-D_1(T-t)\right)}{1-D_2}\right)\\&\quad+\frac{\eta^2}{\lambda^3}(u_1+i)\left(\exp\left(-\lambda(T-t)\right)-1\right)(\lambda u_3-u_1-i)\\&\quad-\frac{\eta^2}{2\gamma^2}(u_1+i)^2(T-t)+\frac{\eta^2}{4\lambda^3}\left(\exp\left(-2\lambda(T-t)\right)-1\right)(\lambda u_3-u_1-i)^2\\&\quad-\frac{\eta\rho_{x,r}}{\lambda}(iu_1+u_1^2)\int_0^{T-t}\mathbb{E}\left[\sqrt{v_{T-s}}\middle|v_t\right]\left(1-\exp\left(-\lambda s\right)\right)ds\\&\quad-\eta\rho_{x,r}u_1u_3\int_0^{T-t}\mathbb{E}\left[\sqrt{v_{T-s}}\middle|v_t\right]\exp\left(-\lambda s\right)ds\end{aligned}\tag{3.47}$$

where expressions D_2, D_1 and $\delta_\pm$ are the same as in (3.40), and when $\theta(t)\equiv\bar{\theta}$ is a constant,

$$\int_0^{T-t}\theta(T-s)\cdot\widetilde{B}_3(s)ds=\bar{\theta}(iu_1-1)(T-t)+\bar{\theta}\left(\frac{(iu_1-1)}{\lambda}-iu_3\right)\left(\exp\left(-\lambda(T-t)\right)-1\right).\tag{3.48}$$

It is computationally expensive to calculate the integrals in I_4, which is a function w.r.t. v_t. We use an approximation where, for a fixed v_t, values of the conditional expectation $\mathbb{E}\left[\sqrt{v_{t+s}}\middle| v_t\right]$ over a short time period can be approximated by a linear function w.r.t. time.

We will use the approximation that

$$\mathbb{E}\left[\sqrt{v_{t+s}}\middle| v_t\right] \approx a(v_t) + b(v_t, \Delta t)s, \quad s \leq \Delta t, \tag{3.49}$$

where $a(v_t) = \sqrt{v_t}$, $b(v_t, \Delta t) = \frac{v_{(t+\Delta t)} - v_t}{\Delta t}$, $\Delta t = 0.05$. Various experiments have shown that this approximation is sufficiently accurate in the present context.

CHAPTER 4

Wrong way risk modeling and credit valuation adjustment

In previous chapters, we computed CVA by the expression in (1.11). In this practical formula, the unilateral CVA is given by an integration of the product of the discounted expected exposure, the counterparty's default probability and the percentage of loss given default (LGD) [38]. The calculation is based on the assumption that the probability of the counterparty's default is *independent* of the exposure to this counterparty.

However, there may be dependency between this default probability and the market risk factors that determine the value of a financial derivative, and this may impact the CVA value. So-called wrong way risk (WWR) occurs when the credit quality of the counterparty and the exposure to this counterparty are adversely correlated. Banks are required to monitor and manage WWR by stress testing and scenario analysis [5].

This chapter studies the impact of WWR on credit valuation adjustment (CVA) for European and Bermudan options, based on an intensity model. We model WWR by a dependency between the underlying asset and the intensity of the counterparty's default. We consider three different models.

In addition, we take the difference between the default-free and the default-adjusted exposure values for the purpose of the CVA calculations. Two numerical algorithms, the COS method and the Stochastic Grid Bundling Method (SGBM) are generalized and employed for the computations. We will perform a CVA stress test for European options, show differences in the optimal exercise boundaries and in corresponding Bermudan option values. CVA VaR and CVA Expected Shortfall (ES) are two important risk measures of CVA risk. We will also compute these quantities in Appendix 3 of this chapter, where we already make use of the computational techniques for historical measure simulated paths and risk neutral computations, without using sub-simulation, as proposed in Chapter 5 of this thesis.

4.1. INTRODUCTION

We consider the impact of WWR on CVA for European and American put options. Basel III classifies two types of WWR: so called general and specific WWR [5]. The former appears due to positive correlations of exposure and market factors, while the latter is due to a wrong structure of an investment when a connection exists between the counterparty and the underlying. In this chapter, we consider specific WWR. We will employ an intensity model for the default of the counterparty under the risk-neutral probability measure. WWR can be included by correlation between the default probability and

This chapter is based on the article 'Wrong Way Risk Modeling and Computation in Credit Valuation Adjustment for European and Bermudan Options', submitted for publication, 2016 [31].

the market risk factors of the portfolio. Intensity models have been used for defaultable corporate bonds, for example, by Jarrow and Turnbull (1995) [52] or Madan and Unal (1998) [66]. Based on affine models for defaultable bonds, Duffie and Singleton (1999) [27] presented a valuation framework for derivatives (where the underlying can be a defaultable corporate bond). The default-adjusted value of some contingent claim was modeled by discounting at a *default-adjusted* short rate. Bielecki and Rutkowski (2002) [8] explained the use of an enlarged filtration for valuation when dealing with both default and market information.

Ruiz [74, 75], using market data, presented a relation between the underlying and the (one-year) intensity of the associated counterparties by scatter-plots of historical data. Research on modeling WWR by a dependency structure between the intensity and underlying market factors has also been performed, for example, by Hull and White (2012) [46]. They connect the underlying to an intensity model by a deterministic relation. Based on this model, Shen (2014) discussed the impact of WWR on CVA and exposure profiles for Bermudan options under the GBM asset dynamics [77]. Brigo et.al. (2014) [12] modeled the intensity by a CIR jump diffusion model, where the diffusion term is correlated with the short rate, and presented case studies for portfolios of swaps. A similar model was presented by Duffie and Singleton (1999) [27] for credit spread options.

An early paper on the pricing of European and American options under default risk is Johnson and Stulz (1987) [53]. Optimal exercise decisions for American options can be impacted by CCR. Hull and White (1995) [45] showed that the impact of CCR for American options is significantly lower than for European options as the exercise policy can be adjusted (see also Klein and Yang (2010) [57]). The impact of different early-exercise policies is related to the way banks split their handling of credit and market risk. The system may not to be optimal in the case of Bermudan options, where early-exercise decisions and corresponding hedges should not only take the product's market price, but also the release of CVA into account. This is important for options bought by a bank. We will analyze the difference in optimal exercise boundaries for Bermudan options with and without WWR model.

The dependency between the underlying stock and the intensity rate is modeled here in three ways, i.e., the intensity is either a deterministic function of the log-stock value, or by a model with correlation in the diffusion of the stochastic intensity and the log-asset processes, or by means of jumps with correlated jump sizes in the processes. The stochastic models are based on the class of affine jump-diffusion processes, see Duffie et.al. (2000) [26].

The reminder of this chapter is as follows. Section 4.2 presents CVA, WWR, the intensity model and the pricing dynamics for default-free and default-adjusted options. Section 4.3 discusses the three models to describe the dependency structure between the underlying and the intensity, in the affine jump diffusion (AJD) class. The algorithms that we employ for the computations of option values with default risk are the COS method, based on Fourier-cosine expansions and the FFT, by Fang and Oosterlee (2009) [28], extended to higher dimensions by Ruijter and Oosterlee (2012) [72], and the Stochastic Grid Bundling Method (SGBM), developed by Jain and Oosterlee (2015) [50]. We present these two algorithms in section 4.4. Numerical results in Section 4.5 are used

to study the effect of WWR, the impact of the dependency structure on CVA and on CVA Shortfall.

4.2. VALUATION FRAMEWORK

In this section, we will present the intensity model, and show that CVA values for options can be computed as the difference of the default-free and the default-adjusted option values.

4.2.1. INTENSITY MODEL

Intensity models have been studied for several years. We start with the general setting, assuming that a probability space $(\Omega, \mathscr{F}, \mathbb{Q})$ is given over the time horizon $[0, T]$. The sample space Ω is the set of all possible outcomes w, the sigma algebra $\mathscr{F}$ is the collection of all events, and probability measure $\mathbb{Q}$ is a function $\mathbb{Q} : \mathscr{F} \to [0, 1]$. In this chapter we consider derivatives valuation, and it is thus convenient to choose $\mathbb{Q}$ as a risk-neutral measure. Under this risk-neutral measure, all securities can be priced as discounted values. We assume the risk-free short rate r constant, and denote the risk-free savings account by $B_t = \exp(r\,t)$.

Let a Markov-process $\{\mathbf{X}_t, t \in [0, T]\}$ on some n-dimensional space $\mathscr{D} \subset \mathbb{R}^n$ represent all information of the underlying market factors, such as the underlying equity, interest rate, credit spread of the counterparty, and so on. The filtration is generated by $\mathbf{X}_t$ and is denoted by $\mathscr{F}_t = \sigma(\mathbf{X}_s, s \in [0, t])$.

Nonnegative function $\widetilde{h} : \mathbb{R}^n \to \mathbb{R}$ is the $\mathscr{F}_t$-measurable intensity of a jump process N_t. We take the first jump-to-default time τ of the process N_t as the default time of the counterparty, $\tau := \inf\{t : \int_0^t \widetilde{h}(\mathbf{X}_s)\,ds \geq E_1\}$, where E_1 is an exponential random variable with mean 1, independent of $\mathscr{F}_t$. Define the jump process as $N_t = \mathbb{1}(\tau \leq t)$. $\widetilde{h}(\mathbf{X})$ is the state-dependent (pre-default) intensity of the jump time τ.

G denotes the survival probability w.r.t. the filtration $\mathscr{F}$, given by

$$G_t = \mathbb{E}^{\mathbb{Q}}\left[\mathbb{1}(\tau > t)\middle|\mathscr{F}_t\right] = \exp\left(-\int_0^t \widetilde{h}(\mathbf{X}_s)\,ds\right), \tag{4.1}$$

where $\widetilde{h}(\mathbf{X}_t)$ depends on the state variables.

We construct an *enlarged filtration* $\mathscr{G}_t = \mathscr{F}_t \vee \mathscr{H}_t$, where $\mathscr{H}_t = \sigma(N_s, s \in [0, t])$. The enlarged filtration $\mathscr{G}_t$ contains information of market factors and default events [60]. A useful result in [8] can be used to switch filtrations: Given a $\mathscr{G}_T$-measurable random variable W, one can show that [8][pp 145, Corollary 5.1.1]:

$$\mathbb{E}^{\mathbb{Q}}\left[\mathbb{1}(\tau > T)W\middle|\mathscr{G}_t\right] = \mathbb{1}(\tau > t)\,\frac{\mathbb{E}^{\mathbb{Q}}\left[W\mathbb{1}(\tau > T)\middle|\mathscr{F}_t\right]}{\mathbb{E}^{\mathbb{Q}}\left[\mathbb{1}(\tau > t)\middle|\mathscr{F}_t\right]} = \mathbb{1}(\tau > t)\mathbb{E}^{\mathbb{Q}}\left[\frac{G_T}{G_t}W\middle|\mathscr{F}_t\right]. \tag{4.2}$$

With W in (4.2) the discounted cash flow if default did not happen prior to time T, one can show that the price of the defaultable claim is the risk-neutral expectation of the payoff discounted at the *default-adjusted rate*, $R(\mathbf{X}_s) := r + \widetilde{h}(\mathbf{X}_s)$.

For a European option, with $g(\mathbf{X}_T)$ the promised payment at time T, discounted by the short rate at time t, i.e.,

$$\begin{aligned}\mathbb{E}^{\mathbb{Q}}\left[\frac{B_t}{B_T}g(\mathbf{X}_T)\mathbb{1}(\tau>T)\middle|\mathscr{G}_t\right] &= \mathbb{1}(\tau>t)\mathbb{E}^{\mathbb{Q}}\left[\frac{G_T}{G_t}\frac{B_t}{B_T}g(\mathbf{X}_T)\middle|\mathscr{F}_t\right]\\ &= \mathbb{1}(\tau>t)\mathbb{E}^{\mathbb{Q}}\left[\frac{D_t}{D_T}g(\mathbf{X}_T)\middle|\mathscr{F}_t\right].\end{aligned} \tag{4.3}$$

Here, we defined,

$$D_t := \exp\left(\int_0^t R(\mathbf{X}_s)ds\right) = \frac{B_t}{G_t}, \tag{4.4}$$

which includes the counterparty credit quality.

Assume that for the issued T-period defaultable bonds, the counterparty pays 1 at expiration time T in the event of no default, otherwise zero. We can read the price of the defaultable bonds directly from the market. It is well-known that corporate bonds offer a higher yield because of the extra risk (default risk). The difference between the yield on a corporate bond and a government bond is called the *credit spread*. The $t=0$ value of a T-period defaultable zero-coupon-bond (ZCB) is given by

$$\widetilde{P}(0,T) = \mathbb{E}^{\mathbb{Q}}\left[\frac{1}{D_T}\right], \tag{4.5}$$

where the intensity can be considered as the credit spread associated to the counterparty.

Suppose that the market credit spread is flat over different tenors, denoted by $\overline{h}$, then the market price of this defaultable ZCB is given by

$$\widetilde{P}_{\text{market}}(0,T) = \exp\left(-(r+\overline{h})T\right), \tag{4.6}$$

which gives market information of the credit quality of the counterparty.

One can hence retrieve information of the counterparty credit quality directly from defaultable bonds issued by the counterparty, or from the credit-default-swap (CDS) market. The calibration of a default model can be done by comparing Formula (4.5) to the market price of the defaultable bonds (4.6) .

4.2.2. CVA FOR DEFAULTABLE EUROPEAN-STYLE CLAIMS

We first focus on European-style claims, where an investor receives the payoff at expiration time $t=T$ in the case of no default, and there is zero recovery when a default event happens prior to expiration.

With log-stock $X_t = \log(S_t)$ one of the market factors, the promised payoff at $t=T$ in the event of no default is $g(X_T)$, given by

$$g(X_T) = \begin{cases}\max\left(\exp(X_T)-K,0\right), & \text{for a call,}\\ \max\left(K-\exp(X_T),0\right), & \text{for a put,}\end{cases} \tag{4.7}$$

where K is the strike price.

The *default-free* price of the claim at time $t \in [0, T]$ is given by:

$$V(t,\mathbf{X}_t) = \mathbb{E}^{\mathbb{Q}}\left[\frac{B_t}{B_T} g(X_T)\Big|\mathbf{X}_t\right], \tag{4.8}$$

where V is an L^2 bounded function.

We define the *default-adjusted* value prior to a default event, i.e. the market value of a European option taking account the price of CCR at time t as the expected payoff discounted at the intensity-adjusted rate:

$$U(t,\mathbf{X}_t) = \mathbb{E}^{\mathbb{Q}}\left[\frac{D_t}{D_T} g(X_T)\Big|\mathbf{X}_t\right], \tag{4.9}$$

where U is an L^2 bounded function, the expression of which is derived by (4.2). Duffie and Singleton (1999) [27] have given a general formula for pricing the default-adjusted value.

In this chapter, we avoid the discussion about recovery by setting the recovery equal to zero. There are at least two ways of defining recovery, see [27].

At a future time t, with the counterparty default time $\tau < t$, there is no need for discussion under the zero recovery assumption; otherwise, the time-t price of the corresponding CVA to the option writer, conditional on $\tau > t$, is given by

$$\text{CVA}(t,\mathbf{X}_t) = \mathbb{E}^{\mathbb{Q}}\left[\mathbb{1}(t<\tau<T)\frac{B_t}{B_\tau}E_\tau\Big|\tau>t,\mathbf{X}_t\right] = \frac{B_t}{G_t}\mathbb{E}^{\mathbb{Q}}\left[\int_t^T \frac{E_s}{B_s} d(-G_s)\Big|\mathbf{X}_t\right], \tag{4.10}$$

where $E_t = \max(0, V(t,\mathbf{X}_t))$ is the exposure to the counterparty when default occurs at time $\tau = t$ before expiration T. The second part of the equation is found by Proposition 5.1.1 in [8][pp 147].

When exposure and default probability in Equation (4.10) are independent, we obtain the well-known CVA formula from [38][pp 197, Appendix 7B], which is often used in practice. This formula requires the computation of the exposure profile over the time horizon. Here, however, we use a different formulation for the computation of CVA. CVA is, by definition, the difference between the default-free and the market contract value, in which the latter has accounted for counterparty default. The computation of CVA can thus be performed by taking the difference between the default-free and default-adjusted contract values.

When $\tau > t$, the formula for CVA is thus by definition:

$$\text{CVA}(t,\mathbf{X}_t) = V(t,\mathbf{X}_t) - U(t,\mathbf{X}_t). \tag{4.11}$$

Equations (4.10) and (4.11) are equivalent when the exposure is defined as the *replacement costs* of the European options, since the default-free option value $V(t,\mathbf{X}_t)$, depending on the state variable and time t, is non-negative. Hence for options, we can write the exposure as

$$E_t = V(t,\mathbf{X}_t), \tag{4.12}$$

With the definition of exposure in (4.12), one can use the tower property to show that

$$\begin{aligned} V(t,\mathbf{X}_t) - U(t,\mathbf{X}_t) &= \frac{B_t}{G_t}\mathbb{E}^{\mathbb{Q}}\left[(G_t - G_T)\frac{g(X_T)}{B_T}\Big|\mathbf{X}_t\right] \\ &= \frac{B_t}{G_t}\mathbb{E}^{\mathbb{Q}}\left[\int_t^T \frac{1}{B_s}\cdot \underbrace{B_s\mathbb{E}^{\mathbb{Q}}\left[\frac{g(X_T)}{B_T}\Big|\mathbf{X}_s\right]}_{V(s,\mathbf{X}_s)} d(-G_s)\Big|\mathbf{X}_t\right] \\ &= \frac{B_t}{G_t}\mathbb{E}^{\mathbb{Q}}\left[\int_t^T \frac{E_s}{B_s} d(-G_s)\Big|\mathbf{X}_t\right] = \mathrm{CVA}(t,\mathbf{X}_t). \end{aligned} \tag{4.13}$$

Comment: Computation of CVA using (4.10) is typically done by generating a large number of Monte Carlo scenarios over a set of discrete future dates and by computation of the exposure for each scenario at each discrete time. Expression (4.11) requires the default-free and default-adjusted values, respectively. The use of (4.11) instead of (4.10) may enhance the computational efficiency for CVA calculations, particularly for computing the *CVA shortfall* over a time horizon. However, (4.10) forms a general methodology for computing CVA, when netting and collateral agreements are considered.

4.2.3. VALUATION OF DEFAULTABLE BERMUDAN OPTIONS

We also consider the impact of CCR and WWR on CVA for Bermudan options. A Bermudan option can be exercised at a set of dates $\mathcal{T} = \{t_1, \ldots, t_M\}$, where $t_1 > 0$ is the first and t_M the last exercise date. The payoff of immediate exercise t is given by $g(X_t)$, with g as in (4.7) and X_t represents for the log-asset variable. Of course, $g(X_t) \geq 0$ for all $X_t \in \mathbb{R}$.

When the claim is defaultable and CCR is present, a specific exercise strategy can be applied. For example, it is may be optimal to exercise the Bermudan option earlier when a default is likely in the near future compared to the default-free case. An exercise policy is to optimize the default-adjusted value, taking explicitly into account the change in credit quality of a counterparty. When the probability of counterparty default is low, it may be fine to exercise the option by optimizing the default-free value.

Policy I: Optimize the default-free value. We look for a stopping time $\xi^{\mathrm{I}} = \xi^{\mathrm{I}}(\mathbf{X}_0, w) \in \mathcal{T}$, with $w \in \Omega$, such that

$$\mathbb{E}^{\mathbb{Q}}\left[\frac{g(X_{\xi^{\mathrm{I}}})}{B_{\xi^{\mathrm{I}}}}\Big|\mathbf{X}_0\right] = \sup_{\xi\in\mathcal{T}}\mathbb{E}^{\mathbb{Q}}\left[\frac{g(X_\xi)}{B_\xi}\Big|\mathbf{X}_0\right], \tag{4.14}$$

and the corresponding optimal *default-free* expected value obtained with ξ^{I} reads,

$$V^{\mathrm{I}}(\mathbf{X}_0, 0) = \mathbb{E}^{\mathbb{Q}}\left[\frac{g(X_{\xi^{\mathrm{I}}})}{B_{\xi^{\mathrm{I}}}}\Big|\mathbf{X}_0\right]. \tag{4.15}$$

The corresponding *default-adjusted* expected value at initial time $t = 0$, with stopping time ξ^{I}, is then given by:

$$U^{\mathrm{I}}(\mathbf{X}_0, 0) = \mathbb{E}^{\mathbb{Q}}\left[\frac{g(X_{\xi^{\mathrm{I}}})}{D_{\xi^{\mathrm{I}}}}\Big|\mathbf{X}_0\right]. \tag{4.16}$$

Policy II: Optimize the default-adjusted value. We look for the stopping time $\xi^{\text{II}} = \xi^{\text{II}}(\mathbf{X}_0, w) \in \mathcal{T}$, with $w \in \Omega$, such that

$$\mathbb{E}^{\mathbb{Q}}\left[\frac{g(X_{\xi^{\text{II}}})}{D_{\xi^{\text{II}}}}\middle|\mathbf{X}_0\right] = \sup_{\xi\in\mathcal{T}}\mathbb{E}^{\mathbb{Q}}\left[\frac{g(X_\xi)}{D_\xi}\middle|\mathbf{X}_0\right]. \tag{4.17}$$

We define the corresponding optimal *default-adjusted* expected value by

$$U^{\text{II}}(0,\mathbf{X}_0) = \mathbb{E}^{\mathbb{Q}}\left[\frac{g(X_{\xi^{\text{II}}})}{D_{\xi^{\text{II}}}}\middle|\mathbf{X}_0\right]. \tag{4.18}$$

Using the same strategy, the corresponding *default-free* expected value is given by

$$V^{\text{II}}(0,\mathbf{X}_0) = \mathbb{E}^{\mathbb{Q}}\left[\frac{g(X_{\xi^{\text{II}}})}{B_{\xi^{\text{II}}}}\middle|\mathbf{X}_0\right]. \tag{4.19}$$

The $t = 0$ CVA values for the Bermudan option using Policy j, where $j \in \{I, II\}$, are defined by:

$$\text{CVA}^j(0,\mathbf{X}_0) = V^j(0,\mathbf{X}_0) - U^j(0,\mathbf{X}_0). \tag{4.20}$$

Equation (4.20) is equivalent to the CVA formula in (4.10), when the exposure to the counterparty at a future time t prior to the default event on $w \in \Omega$ is defined as the replacement costs, given by

$$E_t^j(w) = \begin{cases} V^j(t,\mathbf{X}_t(w)), & t < \xi^j(w), \\ 0, & t \geq \xi^j(w), \end{cases}$$

where $E^j(w,t)$ is the exposure under Policy j at time t on path w; the optimal stopping time $\xi^j(w)$ is determined by (4.14) or (4.17), and V^j is the expected value of continuing the option at time t using Policy j, i.e.,

$$V^j(t,\mathbf{X}_t(w)) = \mathbb{E}^{\mathbb{Q}}\left[\frac{B_t}{B_{\xi^j}}g(X_{\xi^j})\middle|\mathbf{X}_t(w)\right]. \tag{4.21}$$

For Bermudan options, Equation (4.10) is equivalent to Equation (4.11) for computing CVA:

$$\begin{aligned} V^j(0,\mathbf{X}_0) - U^j(0,\mathbf{X}_0) &= \mathbb{E}^{\mathbb{Q}}\left[\frac{g(X_{\xi^j})}{B_{\xi^j}}\left(1 - G(\xi^j)\right)\middle|\mathbf{X}_0\right] \\ &= \mathbb{E}^{\mathbb{Q}}\left[\int_0^{\xi^j}\frac{1}{B_s}\cdot\underbrace{B_s\mathbb{E}^{\mathbb{Q}}\left[\frac{g(X_{\xi^j})}{B_{\xi^j}}\middle|\mathbf{X}_s\right]}_{V^j(t,\mathbf{X}_t)}d(-G_s)\middle|\mathbf{X}_0\right] \\ &= \mathbb{E}^{\mathbb{Q}}\left[\int_0^T\frac{E_s^j}{B_s}d(-G_s)\middle|\mathbf{X}_0\right] = \text{CVA}^j(0,\mathbf{X}_0). \end{aligned} \tag{4.22}$$

4.2.4. RECURSION FOR BERMUDAN OPTIONS

The optimal stopping problem for the default-free value in (4.14) is well-known. As in [3], one can define the Snell envelope for the discounted (at the short rate) exercise values, and the corresponding Hamilton-Jacobi-Bellman equation can be solved by backward recursion. In our setting, we also need to compute the expectation defined in (4.16) under the same exercise policy, which is easy when we know the exercise and continuation regions.

In a similar way, the optimal stopping problem for the default-adjusted value in (4.17) can be solved by constructing sequences of random variables to define the Snell envelope for the exercise values discounted at the intensity-adjusted rate. The difference in the backward recursion procedures for these two problems results in different exercise and continuation regions.

Let $j \in \{\text{Policy I, II}\}$ be the index of the chosen policy. To reduce notation, from now on we write state variable $\mathbf{X}_{t_m} = \mathbf{X}_m$, with t_m the m-th exercise opportunity.

First of all, the default-free and default-adjusted values at expiration date $t_M = T$ are given by the payoff function, i.e.

$$U^j(t_M, \mathbf{X}_M) = V^j(t_M, \mathbf{X}_M) = g(X_M), \tag{4.23}$$

where X_M is the corresponding log-asset value in the state vector $\mathbf{X}_M$.

At an exercise date $t_m < T$, *assuming* $\tau > t_m$, the expected default-free and default-adjusted payoff of continuing, i.e., holding the option at time t_m, are given respectively by

$$\begin{aligned} c_r^j(t_m, \mathbf{X}_m) &= \mathbb{E}^{\mathbb{Q}}\left[\frac{B_m}{B_{m+1}} V^j(t_{m+1}, \mathbf{X}_{m+1}) \middle| \mathbf{X}_m\right], \\ c_R^j(t_m, \mathbf{X}_m) &= \mathbb{E}^{\mathbb{Q}}\left[\frac{D_m}{D_{m+1}} U^j(t_{m+1}, \mathbf{X}_{m+1}) \middle| \mathbf{X}_m\right], \end{aligned} \tag{4.24}$$

where c_r^j represents the default-free and c_R^j the default-adjusted continuation function under the policy j, and both are L^2 bounded.

The optimal exercise boundary $\mathbf{x}_m^j$ using Policy j at t_m is determined by solving the equation:

$$\begin{aligned} &\text{Policy I:} \quad g(x_m^{\mathrm{I}}) - c_r^{\mathrm{I}}(t_m, \mathbf{x}_m^{\mathrm{I}}) = 0, \\ &\text{Policy II:} \quad g(x_m^{\mathrm{I}}) - c_R^{\mathrm{II}}(t_m, \mathbf{x}_m^{\mathrm{II}}) = 0, \end{aligned} \tag{4.25}$$

where the log-asset value x_m^j is the log-asset value in the vector $\mathbf{x}_m^j$.

The optimal exercise boundary determines the continuation region $\mathscr{C}^j$ and the exercise region $\mathscr{G}^j$, by policy j, at t_m:

$$\begin{aligned} \mathscr{C}^j(t_m) &= \begin{cases} \{\mathbf{x} | g(x) < c_r^j(t_m, \mathbf{x})\}, & j = \text{Policy I}, \\ \{\mathbf{x} | g(x) < c_R^j(t_m, \mathbf{x})\}, & j = \text{Policy II}, \end{cases} \\ \mathscr{G}^j(t_m) &= \begin{cases} \{\mathbf{x} | g(x) \geq c_r^j(t_m, \mathbf{x})\}, & j = \text{Policy I}, \\ \{\mathbf{x} | g(x) \geq c_R^j(t_m, \mathbf{x})\}, & j = \text{Policy II}, \end{cases} \end{aligned} \tag{4.26}$$

with x is the log-asset value in $\mathbf{x}$.

By Policy II, the continuation value accounts for the default risk, being discounted at the default-adjusted value, and one compares this default-adjusted continuation value with the immediate exercise value.

Based on this, the values of the option at time t_m, conditional on $\mathbf{X}_m$, using Policy I are given by:

$$\begin{aligned} V^{\mathrm{I}}(t_m,\mathbf{X}_m) &= \max\left(g(X_m), c_r^{\mathrm{I}}(t_m,\mathbf{X}_m)\right), \\ U^{\mathrm{I}}(t_m,\mathbf{X}_m) &= \begin{cases} g(X_m), & \mathbf{X}_m \in \mathscr{G}^{\mathrm{I}}(t_m), \\ c_R^{\mathrm{I}}(t_m,\mathbf{X}_m), & \mathbf{X}_m \in \mathscr{C}^{\mathrm{I}}(t_m). \end{cases} \end{aligned}$$

In a similar way, the values of the option at time t_m conditional on $\mathbf{X}_m$ using Policy II are given by:

$$\begin{aligned} U^{\mathrm{II}}(t_m,\mathbf{X}_m) &= \max\left(g(X_m), c_R^{\mathrm{II}}(t_m,\mathbf{X}_m)\right), \\ V^{\mathrm{II}}(t_m,\mathbf{X}_m) &= \begin{cases} g(X_m), & \mathbf{X}_m \in \mathscr{G}^{\mathrm{II}}(t_m), \\ c_r^{\mathrm{II}}(t_m,\mathbf{X}_m), & \mathbf{X}_m \in \mathscr{C}^{\mathrm{II}}(t_m). \end{cases} \end{aligned}$$

We employ Bellman's principle by backward recursion computation until time zero, where the option value is equal to the corresponding continuation value.

4.3. MODELING WWR BY AJD MODELS

We use the affine-jump-diffusion (AJD) class to describe the dependency structure between the underlying asset and the intensity. Affine dynamics can describe the dependency structure between the intensity and the underlying market factors. The AJD class is defined by the following SDE system [26]:

$$d\mathbf{X}_t = \tilde{\mu}(\mathbf{X}_t)\,dt + \tilde{\sigma}(\mathbf{X}_t)\,d\mathbf{W}_t + d\mathbf{J}_t, \tag{4.27}$$

where $\mathbf{W}_t$ is a standard Brownian motion in $\mathbb{R}^n$; $\tilde{\mu}:\mathscr{D}\to\mathbb{R}^n$, $\tilde{\sigma}:\mathscr{D}\to\mathbb{R}^{d\times d}$ and $\mathbf{J}_t\in\mathbb{R}^n$ is a pure jump process independent of $\mathbf{W}_t$, whose jump sizes are governed by a probability distribution ν on $\mathbb{R}^n$. More specifically, the jump times of $\mathbf{J}_t$ are the jump times of a Poisson process with jump-arrival rate $\tilde{\lambda}$, and the $\mathbf{J}_t$ jump sizes are governed by probability ν. For complex-valued numbers $\mathbf{c}\in\mathbb{C}^d$, we define $\Theta(\mathbf{c}) = \int_{\mathbb{R}^n}\exp(\mathbf{c}\cdot\mathbf{z})\,d\nu(\mathbf{z})$, where the integral should be well-defined. This *jump transform function* Θ determines the jump-size distribution [26]. We can choose jump distribution ν so that the corresponding jump transform Θ is known explicitly.

Given a fixed affine discount rate $q:\mathscr{D}\to\mathbb{R}$, the affinity property is satisfied when the coefficients are defined by:

$$\begin{aligned} \tilde{\mu}(\mathbf{X}_t) &= K_0 + K_1\mathbf{X}_t, \quad K_0\in\mathbb{R}^n, K_1\in\mathbb{R}^{d\times d}, \\ (\tilde{\sigma}(\mathbf{X}_t)\tilde{\sigma}^T(\mathbf{X}_t))_{i,j} &= (H_0)+(H_1)_{i,j}\mathbf{X}_t, \quad H_0\in\mathbb{R}^{d\times d}, H_1\in\mathbb{R}^{d\times d\times d}, \\ q(\mathbf{X}_t) &= q_0 + q_1\mathbf{X}_t, \quad r_0\in\mathbb{R}, r_1\in\mathbb{R}^n. \end{aligned} \tag{4.28}$$

The discounted (at rate q) characteristic function (ChF) is then defined by:

$$\varphi_q(\mathbf{u},t,T;\mathbf{X}_t) = \mathbb{E}^{\mathbb{Q}}\left[\exp\left(-\int_t^T q(\mathbf{X}_s)ds\right)\exp\left(i\mathbf{u}\mathbf{X}_T\right)\Big|\mathbf{X}_t\right]. \tag{4.29}$$

With the short rate, i.e. $q(\mathbf{x}) = r$, we denote the discounted ChF by φ_r; when discounted at the intensity-adjusted rate, $q(\mathbf{x}) = R(\mathbf{x})$, we denote the intensity-adjusted discounted ChF by φ_R. Duffie and Singleton [26] showed that the discounted ChF for process $\mathbf{X}_t$ is given by the following formula:

$$\varphi_q(\mathbf{u}, t, T; \mathbf{X}_t) = \exp\left(\widetilde{A}(T-t) + \mathbf{X}_t \widetilde{\mathbf{B}}(T-t)\right), \tag{4.30}$$

where the coefficients $\widetilde{A}$ and $\widetilde{\mathbf{B}}$ satisfy the following ODEs:

$$\begin{aligned} \frac{d\widetilde{\mathbf{B}}}{ds}(s) &= -q_1 + K_1^T \widetilde{\mathbf{B}}(s) + \frac{1}{2}\widetilde{\mathbf{B}}^T(s) H_1 \widetilde{\mathbf{B}}(s), \\ \frac{dA}{ds}(s) &= -q_0 + K_0 \widetilde{\mathbf{B}}(s) + \frac{1}{2}\widetilde{\mathbf{B}}^T(s) H_0 \widetilde{\mathbf{B}}(s) + \bar{\lambda}\left[\Theta(\widetilde{\mathbf{B}}(s)) - 1\right], \end{aligned} \tag{4.31}$$

with initial conditions $\widetilde{\mathbf{B}}(0) = i\mathbf{u}$ and $\widetilde{A}(0) = 0$.

The discounted ChF will be used in the COS method and SGBM in Section 4.4.

We will compare three ways to describe the dependency structure of the log-asset price and the intensity. It is not trivial to ensure that the intensity is non-negative under the affine structure. However, we use specific parameter settings to keep the intensity positive at a high probability over a certain time horizon.

4.3.1. A DETERMINISTIC FUNCTION

The point of departure in our study here are asset dynamics based on geometric Brownian motion (GBM) and jump diffusion, which we correlate with an intensity process[1]. These are some chosen reference models, not necessarily used in practice, with the purpose of analyzing the impact of WWR under different model assumptions.

With $X_t = \log(S_t)$ the one-dimensional log-asset process, as a first attempt, we model the dynamics of the underlying and the intensity before a default event by:

$$\begin{aligned} dX_t &= (r - \frac{1}{2}\sigma_x^2)dt + \sigma_x dW_t, \\ \widetilde{h}(X_t) &= a(t) + bX_t, \end{aligned} \tag{4.32}$$

with $\sigma_x > 0$ the volatility of the log-asset process, W_t a standard Brownian motion, coefficient $b \in \mathbb{R}$ is constant, and $a(t)$ is a deterministic function that satisfies $a(0) = \overline{h} - bX_0$, where $\overline{h}$ is the credit spread as in (4.6). We call this model *the DF model*. Coefficient b denotes the strength of the dependence between the log-asset and the intensity. When holding put options, WWR occurs when b is negative, otherwise we deal with right way risk (RWR).

Comparing to the market price of the ZCB in (4.6), with coefficient b fixed, the formula for $a(t)$ is given by:

$$a(t) = \overline{h} - bX_0 - \left(r - \frac{1}{2}\sigma_x^2\right)bt + \frac{1}{2}b^2\sigma_x^2 t^2. \tag{4.33}$$

[1] Stochastic asset volatility is not considered here.

The log-asset and the intensity processes can be represented by the following formulas:

$$\begin{aligned} X_t &= X_0 + \left(r - \frac{1}{2}\sigma_x^2\right)t + \sigma_x W_t, \\ \widetilde{h}_t &= \overline{h} + \frac{1}{2}\sigma_x^2 t^2 b^2 + b\sigma_x W_t. \end{aligned} \tag{4.34}$$

From (4.34) it follows that coefficient b does not affect X_t. The variance of the intensity is given by $b^2\sigma_x^2 t$. The expectation of the intensity at time t is given by $\overline{h} + \frac{1}{2}\sigma_x^2 t^2 b^2$.

The intensity is governed by the process that also controls the log-asset price. It is positive over the time horizon $[0, T]$ with probability $(1 - 2\zeta)$, when the value of coefficient b lies in the interval,

$$\left(\Delta^+(\Phi^{-1}(1-\zeta), T), \Delta^-(\Phi^{-1}(\zeta), T)\right), \tag{4.35}$$

where Φ is the cumulative distribution function (CDF) of the standard normal distribution, and $\Delta^\pm$ is given by:

$$\Delta^\pm(Z, t) = \sigma_x t^{-\frac{3}{2}}\left(-Z \pm \sqrt{Z^2 - 2t\overline{h}}\right), \tag{4.36}$$

The derivation of the boundaries (4.35) for the coefficient b is presented in Appendix 1 in this chapter. With this result, we can set limits for coefficient b with certain tolerance regarding negative values of the intensity.

Comment: Compared to the model given by Hull and White [46], and the models proposed by Ruiz [74], the DF model has the drawback that the intensity may become negative. The affine structure of the DF model has, of course, advantages for computation, like the availability of an analytic formula of the defaultable ZCB price. The deterministic function $a(t)$ enables fitting the term-structure of bonds with different tenors. The financial meaning of the coefficients seems clear. The stock value of the company impacts the credit spread.

4.3.2. CIR MODEL WITH JUMPS

As a second model, we use the CIR model with upward jumps to ensure that the intensity stays non-negative, which we call *the CIR-jump (CIRJ) model*. Assume that (X_t, Y_t) is governed by

$$\begin{aligned} dX_t &= \left(r - \frac{1}{2}\sigma_x^2 - \bar{\lambda}\bar{\mu}\right)dt + \sigma_x dW_t^1 + dJ_t^1, \\ dY_t &= \gamma(\theta - Y_t)dt + \sigma_y\sqrt{Y_t}dW_t^2 + dJ_t^2, \\ \widetilde{h}(Y_t) &= \zeta^{\text{CIR}}(t) + Y_t, \end{aligned} \tag{4.37}$$

where γ, θ and σ_y are positive constants, representing the speed of mean reversion, the reverting level and the intensity volatility, respectively. Here, the diffusion terms are not correlated but we assume that J_t^1 and J_t^2 jump simultaneously, and their intensities [2] are correlated. The resulting model is an affine model.

[2] Notice that $\bar{\lambda}$ is the intensity of jumps in the process (X_t, Y_t), not related to the default time τ.

The marginal distribution of the jumps in Y_t is exponential with mean μ_y^J; conditional on a realization of the jump size in Y_t, say z_y, the jump size in X_t is normally distributed with mean $\mu_x^J + \rho_J z_y$ and variance σ_x^J. The jump transform function Θ is given by [26]:

$$\Theta(c_1, c_2) = \frac{\exp\left(\mu_x^J c_1 + \frac{1}{2}\left(\sigma_x^J\right)^2 c_1^2\right)}{1 - \mu_y^J c_2 - \rho_J \mu_y^J c_1}, \tag{4.38}$$

with the risk-neutral jump size $\bar{\mu} = \Theta(1,0)$, see (4.37); the initial values of the process are (X_0, Y_0), and the function satisfies $\widetilde{h}(0) = \overline{h}$.

CIR process Y_t is non-negative, and hence the intensity is non-negative as long as ζ^{CIR} is positive along the time horizon. Function ζ^{CIR} is given by

$$\zeta^{\text{CIR}}(t) = \overline{h} - \frac{2\bar{\lambda}\mu_y^J(e^{d_1 t} - 1)}{\bar{g} + 2\mu_y^J(e^{d_1 t} - 1)} - \frac{2\gamma\theta}{\bar{g}}(e^{d_1 t} - 1) - \frac{4Y_0 d_1^2}{\bar{g}^2} e^{d_1 t}, \tag{4.39}$$

where

$$d_1 = \sqrt{\gamma^2 + 2\sigma_y^2}, \quad \bar{g} = \gamma e^{d_1 t} - \gamma + d_1 + d_1 e^{d_1 t}. \tag{4.40}$$

Jumps thus occur at the same time in these two processes. The financial meaning is that due to unexpected events, the stock and the credit quality are simultaneously affected. By this model, we assume that the stock increases/decreases sharply, while the credit of the option writer improves/deteriorates at the same time. With a put option, WWR incurs to option holders when ρ_J is negative, as the exposure to the counterparty increases.

The mean and variance of the log-asset model are given by

$$\begin{aligned}
\text{mean}(X_t) &= X_0 + \left(r - \frac{1}{2}\sigma_x^2\right)t + \bar{\lambda}t(\mu_x^J - \bar{\mu} + \rho_J \mu_y^J), \\
\text{var}(X_t) &= t\sigma_x + t\bar{\lambda}\left\{(\sigma_x^J)^2 + (\mu_x^J)^2 + 2(\mu_y^J \rho_J)^2 - 2\mu_y^J \mu_x^J \rho_J\right\}, \\
\underset{t\to\infty}{\text{var}}(Y_t) &= \frac{\sigma_y^2 \theta}{2\gamma} + \frac{\bar{\lambda}(\mu_y^J)^2}{\gamma},
\end{aligned} \tag{4.41}$$

where the variances can be obtained by the first and second moments using the non-discounted ChF, and the long-term variance of Y_t can be obtained by taking the limit.

From (4.41), we see that the parameters μ_y and $\bar{\lambda}$ control the default risk, and also have an impact on the stock value. Jump size correlation ρ_J is the key correlation between these two processes, and it influences the impact of the jump term in the stock process. By varying three parameters $(\mu_y, \bar{\lambda}, \rho_J)$ in the jump terms the default-adjusted and default-free values are influenced, since the underlying process will change.

Comment: We have not seen previous WWR studies based on simultaneous jumps in the intensity process and the underlying asset process. The use of a jump-diffusion process for the intensity can be found in [12, 25]. The CIRJ model considers the correlation between the two factors when there is some sudden change in the market. Even when the jump size correlation coefficient $\rho_J = 0$, there may still be correlation between

variables X_t and Y_t, as the jumps in these two processes happen simultaneously with intensity $\bar{\lambda}$. One can show that when $\rho_J = 0$,

$$\mathbb{E}[X_t Y_t] - \mathbb{E}[X]\mathbb{E}[Y] = \frac{\bar{\lambda}\mu_y^J \mu_x^J}{\gamma}(1 - e^{-\gamma t}), \tag{4.42}$$

which implies that X_t and Y_t are independent, when at least one of the parameters $(\bar{\lambda}, \mu_y^J, \mu_x^J)$ equals zero.

4.3.3. HULL-WHITE MODEL WITH JUMPS

We also model the default intensity by a Hull-White model with jumps, and the joint behavior of the intensity and the underlying asset by correlated Brownian motions and simultaneous jumps. We refer to this model as *the Hull-White-Jump (HWJ) model*. The underlying asset and the intensity process follow the SDE system, given by:

$$\begin{aligned} dX_t &= (r - \frac{1}{2}\sigma_x^2 - \bar{\lambda}\bar{\mu})dt + \sigma_x dW_t^1 + dJ_t^1, \\ dY_t &= \gamma(\theta - Y_t)dt + \sigma_y(\bar{\rho}dW_t^1 + \sqrt{1-\bar{\rho}^2}dW_t^2) + dJ_t^2, \\ \widetilde{h}(Y_t) &= \zeta^{\mathrm{HW}}(t) + Y_t, \end{aligned} \tag{4.43}$$

with initial values (X_0, Y_0). We use the same notation, $\sigma_x, \gamma, \theta, \sigma_y$ as in the CIRJ model, as the parameters have the same meaning; the jump terms (J_1, J_2) are defined in the same way as in (4.37) with parameters $(\mu_x, \sigma_x^J, \mu_y^J, \bar{\lambda}, \rho_J)$, as is the risk-neutral jump size $\bar{\mu} = \Theta(1,0)$; correlation $\bar{\rho}$ in the diffusion terms defines an additional dependency; deterministic function ζ^{HW} is used to fit the term-structure of defaultable zero-coupon bonds and satisfies $\zeta^{\mathrm{HW}}(0) = \overline{h} - Y_0$.

With these coefficients, function ζ^{HW} can be determined by calibration to the market prices of defaultable ZCBs, given by (4.6):

$$\zeta^{\mathrm{HW}}(t) = = \overline{h} - \bar{\lambda} - \theta + (\theta + Y_0)e^{-\gamma t} + \frac{\sigma_y^2}{2\gamma^2}\left(1 - e^{-\gamma t}\right)^2 + \frac{\gamma\bar{\lambda}}{\gamma + \mu_y^J(1 - e^{-\gamma t})}.$$

Processes X_t and Y_t are correlated via the diffusion terms and the simultaneous jumps with correlated jump sizes. The jumps in the Y_t process are all positive, to reduce the possibility of a negative intensity (although the intensity may still go negative). As we have discussed, we accept negative values of the intensity with a very small probability.

The diffusion correlation coefficient $\bar{\rho}$ and the jump size correlation ρ_J play a prominent role in the dependency structure. As the dependency in the jump terms (J_1, J_2) is as defined in the CIRJ model, we will focus on the impact of the diffusion correlation $\bar{\rho}$ in the numerical experiments to follow.

The ChFs discounted at the short rate r and at the default-adjusted rate R under the proposed three models are presented in Appendix 2 in this chapter. The derivation is based on the result in (4.30).

4.4. NUMERICAL ALGORITHMS

We will employ the COS method and the SGBM algorithm for approximating the default-free and default-adjusted values in this section.

4.4.1. THE COS METHOD

The discounted density is the Fourier transform of the discounted ChF. Hence it can be recovered by a Fourier cosine expansion on a specific interval as in [28, 72]. We denote the density of $\mathbf{X}_{m+1}$ discounted at the rate q and conditional on $\mathbf{X}_m$ by $\hat{f}^q_{\mathbf{X}_{m+1}|\mathbf{X}_m}$. According to [72], in a two-dimensional setting, the discounted density can be written by a Fourier cosine expansion as follows

$$\hat{f}^q_{\mathbf{X}_{m+1}|\mathbf{X}_m}(\mathbf{y};\mathbf{x}) \approx \frac{2}{b_1-a_1}\frac{2}{b_2-a_2}\sum_{k_1=0}^{N_1-1}{}'\sum_{k_2=0}^{N_2-1}{}'\mathscr{P}^q_{k_1,k_2}(\mathbf{x})\cos\left(k_1\pi\frac{y_1-a_1}{b_1-a_1}\right)\cos\left(k_2\pi\frac{y_2-a_2}{b_2-a_2}\right), \quad (4.44)$$

where the symbol $\sum'$ indicates that the first term of the summation is weighted by $\frac{1}{2}$; $\mathbf{y}=[y_1,y_2]^T$, $\mathbf{x}=[x_1,x_2]^T$, and the coefficients $\mathscr{P}^q_{k_1,k_2}$ are given by

$$\begin{aligned}\mathscr{P}^q_{k_1,k_2}(\mathbf{x}) = {}& \frac{1}{2}\mathrm{Re}\left\{\varphi_q\left(\frac{k_1\pi}{b_1-a_1},\frac{k_2\pi}{b_2-a_2};t_m,t_{m+1},\mathbf{x}\right)\exp\left(-\frac{ik_1a_1\pi}{b_1-a_1}-\frac{ik_2a_2\pi}{b_2-a_2}\right)\right\}\\ &+\frac{1}{2}\mathrm{Re}\left\{\varphi_q\left(\frac{k_1\pi}{b_1-a_1},-\frac{k_2\pi}{b_2-a_2};t_m,t_{m+1},\mathbf{x}\right)\exp\left(-\frac{ik_1a_1\pi}{b_1-a_1}+\frac{ik_2a_2\pi}{b_2-a_2}\right)\right\}, \quad (4.45)\end{aligned}$$

where $k_1=0,\ldots,N_1-1$, $k_2=0,\ldots,N_2-1$, and Re represents the real part of the argument; the truncated interval $[a_1,b_1]\times[a_2,b_2]$ is given by

$$\begin{aligned}a_1 &= \mathbb{E}^{\mathbb{Q}}[X_T]-L_1\sqrt{\mathrm{var}(X_T)}, \quad b_1=\mathbb{E}^{\mathbb{Q}}[X_T]+L_1\sqrt{\mathrm{var}(X_T)},\\ a_2 &= \mathbb{E}^{\mathbb{Q}}[Y_T]-L_2\sqrt{\mathrm{var}(Y_T)}, \quad b_2=\mathbb{E}^{\mathbb{Q}}[Y_T]+L_2\sqrt{\mathrm{var}(Y_T)}, \quad (4.46)\end{aligned}$$

where L_1 and L_2 are constants that define the length of the interval.

Notice that we require two discounted ChFs, one discounted by the short rate, another by the intensity-adjusted rate. We use the notation $\mathscr{P}^r_{k_1,k_2}$ for the coefficients of the PDF discounted at the short rate and $\mathscr{P}^R_{k_1,k_2}$ when discounting at the intensity-adjusted rate.

We present the backward recursion steps when pricing default-adjusted and default-free Bermudan puts, by either using Policy I or II. The difference is in the way optimal exercise boundaries are determined. We use index $j=\{\text{Policy I, II}\}$ to refer to the corresponding values under these two policies.

At an exercise time $t_m<T$, the expected default-adjusted value of continuing the option is given, respectively, by

$$\begin{aligned}c^j_r(t_m,\mathbf{x}) &\approx \sum_{k_1=0}^{N_1-1}{}'\sum_{k_2=0}^{N_2-1}{}'\mathscr{P}^r_{k_1,k_2}(\mathbf{x})\mathscr{V}^j_{k_1,k_2}(t_{m+1}),\\ c^j_R(t_m,\mathbf{x}) &\approx \sum_{k_1=0}^{N_1-1}{}'\sum_{k_2=0}^{N_2-1}{}'\mathscr{P}^R_{k_1,k_2}(\mathbf{x})\mathscr{U}^j_{k_1,k_2}(t_{m+1}), \quad (4.47)\end{aligned}$$

where the coefficients read

$$\mathcal{V}^j_{k_1,k_2}(t_{m+1}) \approx \int_{a_1}^{b_1}\int_{a_2}^{b_2} V^j(\mathbf{y},t_{m+1})\cos\left(k_1\pi\frac{y_1-a_1}{b_1-a_1}\right)\cos\left(k_2\pi\frac{y_2-a_2}{b_2-a_2}\right)dy_2dy_1,$$

$$\mathcal{U}^j_{k_1,k_2}(t_{m+1}) \approx \int_{a_1}^{b_1}\int_{a_2}^{b_2} U^j(\mathbf{y},t_{m+1})\cos\left(k_1\pi\frac{y_1-a_1}{b_1-a_1}\right)\cos\left(k_2\pi\frac{y_2-a_2}{b_2-a_2}\right)dy_2dy_1 \quad (4.48)$$

At time $t_M = T$, $V^j = U^j = g(\cdot)$; for a put option, the immediate exercise payoff is larger than zero when the stock price at time T is lower than strike K. We have

$$\begin{aligned}\mathcal{V}^j_{k_1,k_2}(t_M) &= \mathcal{U}^j_{k_1,k_2}(t_M)\\ &= \int_{a_1}^{\log(K)} g(y_1)\cos\left(k_1\pi\frac{y_1-a_1}{b_1-a_1}\right)dy_1\int_{a_2}^{b_2}\cos\left(k_2\pi\frac{y_2-a_2}{b_2-a_2}\right)dy_2. \quad (4.49)\end{aligned}$$

The optimal exercise boundary at each exercise date is represented by a two-dimensional surface. We define a grid along the intensity direction, denoted by $\{a_2 = w_0 < w_2 < \ldots < w_Q = b_2\}$, with Q grid points. On each interval $[w_{l-1}, w_l]$, $l = 1,\ldots,Q$, we approximate the optimal exercise log-stock values by a constant $x^j_{m,l}$, using the following expression:

$$\begin{aligned}&\text{Policy I:} \quad g(x^{\mathrm{I}}_{m,l}) - c^{\mathrm{I}}_r\left(t_m,[x^{\mathrm{I}}_{m,l},\bar{w}_l]^T\right) = 0,\\ &\text{Policy II:} \quad g(x^{\mathrm{II}}_{m,l}) - c^{\mathrm{II}}_R\left(t_m,[x^{\mathrm{II}}_{m,l},\bar{w}_l]^T\right) = 0, \quad (4.50)\end{aligned}$$

where $\bar{w}_l = \frac{1}{2}(w_{l-1}+w_l)$.

For a put, the exercise region $[a_1, x^j_{m,l}]\times[w_{l-1},w_l]$, and the continuation region $[x^j_{m,l}, b_1]\times[w_{l-1},w_l]$, for each $l = 1,\ldots,Q$. Hence the coefficients at time t_m are given by

$$\begin{aligned}\mathcal{V}^j_{k_1,k_2}(t_m) &= \sum_{l=1}^{Q}\left(\int_{w_{l-1}}^{w_l}\int_{x^j_{m,l}}^{b_1} c^j_r(\mathbf{y},t_m)\cos\left(k_1\pi\frac{y_1-a_1}{b_1-a_1}\right)\cos\left(k_2\pi\frac{y_2-a_2}{b_2-a_2}\right)dy_1dy_2\right.\\ &\quad\left.+\int_{a_1}^{x^j_{m,l}} g(y_1)\cos\left(k_1\pi\frac{y_1-a_1}{b_1-a_1}\right)dy_1\int_{w_{l-1}}^{w_l}\cos\left(k_2\pi\frac{y_2-a_2}{b_2-a_2}\right)dy_2\right),\\ \mathcal{U}^j_{k_1,k_2}(t_m) &= \sum_{l=1}^{Q}\left(\int_{w_{l-1}}^{w_l}\int_{x^j_{m,l}}^{b_1} c^j_R(\mathbf{y},t_m)\cos\left(k_1\pi\frac{y_1-a_1}{b_1-a_1}\right)\cos\left(k_2\pi\frac{y_2-a_2}{b_2-a_2}\right)dy_1dy_2\right.\\ &\quad\left.+\int_{a_1}^{x^j_{m,l}} g(y_1)\cos\left(k_1\pi\frac{y_1-a_1}{b_1-a_1}\right)dy_1\int_{w_{l-1}}^{w_l}\cos\left(k_2\pi\frac{y_2-a_2}{b_2-a_2}\right)dy_2\right), \quad (4.51)\end{aligned}$$

where c_r^j and c_R^j is given by (4.47).

The computation of summation in (4.51) can be enhanced by using Fast-Fourier-Transform (FFT) techniques, see [28, 72].

The COS method can also be employed when the ChF function can be approximated. Borovykh et. al. [10] provides a pricing method for Bermudan options based on an analytic approximation of the ChF using the COS method under local Lévy models with default.

4.4.2. STOCHASTIC GRID BUNDLING METHOD

SGBM can be generalized to pricing default-adjusted Bermudan options in a straightforward way. We give details of SGBM in the 2D case, for the CIRJ and the HWJ models.

The default-free option values are dependent only on the underlying log-stock $X = \log(S)$ and the path-dependent early-exercise policy, whereas the default-adjusted values are also impacted by the intensity factor Y. Within the regression step of SGBM, we choose different basis functions for computing default-free and default-adjusted values. For example, we use the polynomial basis $\{1, X, X^2\}$ for the default-free case, and the polynomial basis $\{1, X, Y, X^2, XY, Y^2\}$ for the default-adjusted case.

Let $\left(\begin{bmatrix}\hat{X}_{1,h}\\ \hat{Y}_{1,h}\end{bmatrix}, \ldots, \begin{bmatrix}\hat{X}_{M,h}\\ \hat{Y}_{M,h}\end{bmatrix}\right)_{h=1}^{H}$ be H generated scenarios, where the underlying evolves with the chosen risk-neutral models. We will perform the valuation by backward in time recursion, from time $t_M = T$ to $t_0 = 0$. For notational convenience, we do not specify the policy $j = \{I, II\}$ of the values.

At the final exercise opportunity, t_M, the option is either expiring or exercised, and the probability of default happening exactly at time $t_M = T$ is zero. At time t_M the default-free and default-adjusted option values are equal, i.e. $\hat{v}_{M,h} = g(\hat{X}_{M,h})$ and $\hat{u}_{M,h} = g(\hat{X}_{M,h})$.

At an exercise time $t_m < T$, prior to expiry, we define J bundles for bundling the Monte Carlo paths, which we denote by $\{\mathscr{B}_{m,j}\}_{j=1}^{J}$. We subdivide the paths into bundles based on cross-sectional samples of the state variable. For $j = 1, \ldots, J$, on each Monte Carlo path within the bundle $\mathscr{B}_{m,j}$, we approximate the default-free function V and default-adjusted function U at time t_{m+1}, respectively, by a linear combination of the basis functions:

$$\begin{aligned}
\hat{v}_{m+1,h} &= V(t_{m+1}, [\hat{X}_{m+1,h}, \hat{Y}_{m+1,h}]^T) \approx \sum_{k=0}^{d} \beta_k^{m,j} \left(\hat{X}_{m+1,h}\right)^k, \\
\hat{u}_{m+1,h} &= U\left(t_{m+1}, [\hat{X}_{m+1,h}, \hat{Y}_{m+1,h}]^T\right) \approx \sum_{|k|=0}^{d} \eta_{k_1,k_2}^{m,j} \left(\hat{X}_{m+1,h}\right)^{k_1} \left(\hat{Y}_{m+1,h}\right)^{k_2}, \quad (4.52)
\end{aligned}$$

where d is the degree of the monomials, $|k| = k_1 + k_2$, $\hat{v}_{m+1,h}$ and $\hat{u}_{m+1,h}$ are the realized default-free and default-adjusted values, respectively, on the l-th path at time t_m, where $l \in \mathscr{B}_{m,j}$, and the coefficients η_k^r and η_k^R are obtained by minimizing least-squares errors.

With the obtained coefficients, the default-free or default-adjusted continuation values defined in Equation (4.24) for paths within the bundle $\mathscr{B}_{m,j}$ at time t_m can be ap-

proximated by:

$$\begin{aligned}\hat{c}^{r}_{m,h} &\approx \sum_{k=0}^{d} \beta^{m,j}_{k} \psi^{r}_{k}\left([\hat{X}_{m,h}, \hat{Y}_{m,h}]^{T}, t_m, t_{m+1}\right),\\ \hat{c}^{R}_{m,h} &\approx \sum_{|k|=0}^{d} \eta^{m,j}_{k_1,k_2} \psi^{R}_{k_1,k_2}\left([\hat{X}_{m,h}, \hat{Y}_{m,h}]^{T}, t_m, t_{m+1}\right),\end{aligned} \tag{4.53}$$

where the functions ψ^r and ψ^R are defined by

$$\begin{aligned}\psi^{r}_{k}(\mathbf{X}_m, t_m, t_{m+1}) &= \exp\left(-r(t_{m+1}-t_m)\right)\mathbb{E}^{\mathbb{Q}}\left[X^{k}_{m+1}\middle|\mathbf{X}_m\right],\\ \psi^{R}_{k_1,k_2}(\mathbf{X}_m, t_m, t_{m+1}) &= \mathbb{E}^{\mathbb{Q}}\left[\exp\left(-\int_{t_m}^{t_{m+1}} R_s ds\right) X^{k_1}_{m+1} Y^{k_2}_{m+1}\middle|\mathbf{X}_m\right],\end{aligned} \tag{4.54}$$

which represent the conditional expectations discounted at the corresponding rate, conditional on $\mathbf{X}_m$.

We refer to ψ^r and ψ^R as the *discounted moments*. It is straightforward to derive an analytic formula for the discounted moments from the corresponding discounted ChF. By regressing over each bundle $\mathscr{B}_{m,j}$, the expected default-free and default-adjusted values of continuing the option on each path are approximated.

The early-exercise decision at each path is determined by:

- Policy I:

$$\begin{aligned}\hat{v}_{m,h} &= \max(g(\hat{X}_{m,h}), \hat{c}^{r}_{m,h}),\\ \hat{u}_{m,h} &= \begin{cases} g(\hat{X}_{m,h}), & g(\hat{X}_{m,h}) > \hat{c}^{r}_{m,h},\\ \hat{c}^{R}_{m,h}, & g(\hat{X}_{m,h}) \le \hat{c}^{r}_{m,h}.\end{cases}\end{aligned} \tag{4.55}$$

- Policy II:

$$\begin{aligned}\hat{u}_{m,h} &= \max(g(\hat{X}_{m,h}), \hat{c}^{R}_{m,h}),\\ \hat{v}_{m,h} &= \begin{cases} g(\hat{X}_{m,h}), & g(\hat{X}_{m,h}) > \hat{c}^{R}_{m,h},\\ \hat{c}^{r}_{m,h}, & g(\hat{X}_{m,h}) \le \hat{c}^{R}_{m,h}.\end{cases}\end{aligned} \tag{4.56}$$

We proceed by moving one step backward in time, to t_{m-1}, where the paths are again subdivided into new bundles (based on the samples at time t_{m-1}) and perform the required SGBM computations. The algorithm iterates back to time t_0, where we do not need bundles, and we can perform the regression over all paths.

The option value obtained is the *SGBM direct estimator*. By computing option values based on another set of MC paths using the obtained coefficients gives the *SGBM path estimator*. These values should be close.

In this chapter, we only present results obtained via the SGBM direct estimator. The SGBM path estimator has been computed and it confirmed the convergence of the algorithm.

4.5. NUMERICAL RESULTS

We will study the effect of WWR on CVA for European and Bermudan options in this section. We will use the three models for the dependency structure of the underlying asset and the intensity.

The effect of WWR on European options can be analyzed by a CVA stress test, for example, by varying the dependency coefficients. For Bermudan options, we will compare the optimal exercise boundaries over the time horizon and the corresponding CVA values. The impact of the two exercise policies discussed is studied as well.

As mentioned, CVA is governed by three components: the credit quality, the underlying asset, and their dependency structure, i.e. by WWR or RWR. In order to isolate the impact of WWR (RWR) from the other components, we define a *WWR ratio:* $\frac{\text{CVA}_\text{W}}{\text{CVA}_\text{I}}$, where only the correlation/dependency coefficients (such as the coefficients b, ρ_J or $\bar{\rho}$) are varied, while keeping other parameter fixed. CVA_W is the maximum CVA value when the intensity and the underlying asset are 'wrongly' correlated in the worst case, and CVA_I is the CVA value when the underlying asset and intensity are independent.

The optimal exercise boundary for the Bermudan options is obtained by the COS method, and SGBM is used to find reference values for the corresponding initial option values. We use the Euler SDE discretization for generating the scenarios under the three models, as in [34]. Within the SGBM, the number of Monte Carlo scenarios generated is 10^5 and the number of discrete monitoring dates is 20. To ensure the SGBM accuracy, we use 100 bundles at each discrete date.

4.5.1. WWR: THE DF MODEL

The DF model may be a basic model for the intensity, but it provides useful insight in the connection between the underlying stock and the intensity.

We compute the CVA of a European and a Bermudan put, respectively, and vary coefficient b and volatility σ_x in the numerical experiments. We set the other parameters as: $S_0 = 100$, $K = 100$, $r = 0.004$, $\overline{h} = 0.1$, $T = 0.5$.

Figure 4.1 presents a CVA stress test for a European put, varying coefficient b and volatility $\sigma_x = \{0.1, 0.2, 0.4\}$. We choose a 90% nonnegativity intensity interval for coefficient b, which varies as σ_x changes. The interval is larger when the volatility is smaller. We present the WWR ratio in plot (a) and the CVA value in plot (b) of Figure 4.1. CVA increases as the value of coefficient b gets smaller, as expected.

Figure 4.1(a) shows that, given a fixed value of the coefficient b, the impact of WWR on the CVA value of the associated option is larger for higher log-asset volatilities σ_x. From Equation (4.34) it is clear that the volatility of the intensity is related to $|b|\sigma_x$. The intensity model's volatility thus plays an important role in the WWR. Figure 4.1(b) shows that the log-asset volatility is the determining factor for the CVA value. In the DF model, the volatility of the asset does not only impact the absolute value of CVA, but the strength of WWR as well.

Figure 4.2 presents the optimal exercise boundaries for a Bermudan option. Under Policy I variations in b do not have an impact on the optimal exercise boundary, and under Policy II we vary $b = \{0, -0.2, 0.6\}$. When taking CCR into account, the optimal exercise boundaries of a put option increase. By comparing the optimal exercise boundary for $b = -0.2$ with that for $b = -0.6$, we see that, due to WWR, the optimal exercise

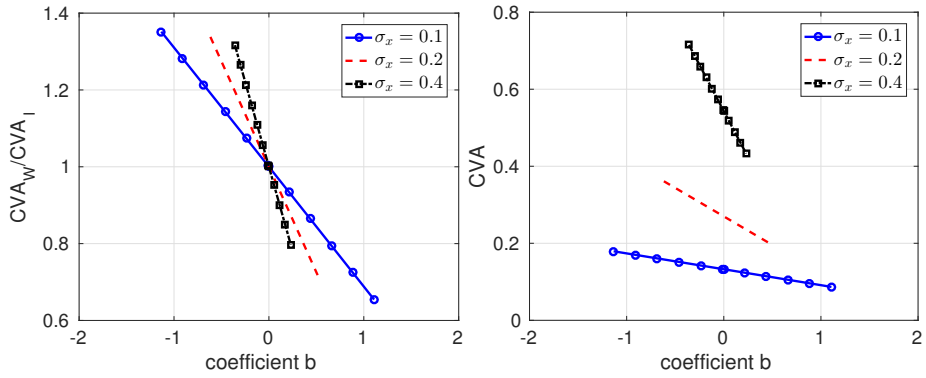

(a) WWR ratio (b) CVA

Figure 4.1: The DF model: CVA test for a European put varying coefficient, $b \in [-1.134, 1.108]$ when $\sigma_X = 0.1$, $b \in [-0.617, 0.514]$ when $\sigma_X = 0.2$, $b \in [-0.358, 0.231]$ when $\sigma_X = 0.4$. The blue line represents $\sigma_X = 0.1$, the red-dashed line $\sigma_X = 0.2$ and the black-block-line $\sigma_X = 0.4$. Results are obtained by the COS method, the number of Fourier terms is 500 and the coefficient of the integration range $L = 8$.

boundaries increase.

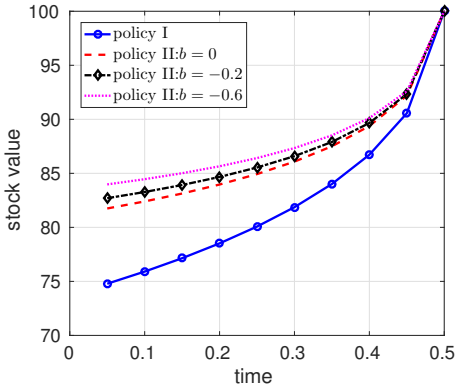

Figure 4.2: The DF model: optimal exercise boundaries for a Bermudan put using the two exercise policies with $b = \{0, -0.2, -0.6\}$. The number of exercise opportunities $M = 10$. The log-asset volatility $\sigma_X = 0.2$.

Table 4.1 compares the default-free, default-adjusted and CVA values using the two policies. We see that by using Policy I, the default-free value is not impacted by variation in b, but the default-adjusted value gets smaller as b decreases. Hence the value of CVA increases under Policy I when WWR increases: By varying b, from zero to -0.2 and -0.6, CVA increased by 0.02 and 0.07, respectively. Policy II reduces the CVA value, and the impact of WWR on CVA using Policy II is smaller: By varying b from zero to -0.2 and -0.6, CVA values using Policy II increase by 0.01 and 0.04, respectively.

Under the dependency structure described by the DF model, the CVA value is higher when WWR increases, for European and Bermudan options under either policy.

		Policy I			Policy II		
b	method	V^{I}	U^{I}	$\mathrm{CVA}^{\mathrm{I}}$	V^{II}	U^{II}	$\mathrm{CVA}^{\mathrm{II}}$
0	COS	5.541	5.317	0.224	5.531	5.330	0.201
	SGBM	5.540	5.317	0.223	5.530	5.330	0.201
	std	0.002	0.001	0.001	0.002	0.001	0.000
−0.2	COS	5.541	5.292	0.248	5.527	5.313	0.214
	SGBM	5.540	5.291	0.249	5.526	5.312	0.214
	std	0.001	0.001	0.000	0.001	0.001	0.000
−0.6	COS	5.541	5.243	0.298	5.518	5.281	0.237
	SGBM	5.541	5.243	0.298	5.518	5.281	0.237
	std	0.001	0.001	0.001	0.001	0.001	0.000

Table 4.1: The DF model: Default-free and default-adjusted values and CVA for a Bermudan put exercised by two policies with $b = \{0, -0.2, -0.6\}$, respectively. Volatility $\sigma_x = 0.2$. The basis functions in SGBM are $\{1, X, X^2\}$ for the default-free and default-adjusted values, as the DF model is a 1D model and X_t is the only factor.

4.5.2. WWR: THE CIRJ MODEL

The dependency in the CIRJ model is in the jump term with different correlation ρ_J for the jump intensities. Here, the intensity process directly influences the underlying asset process in the CIRJ model. Changing parameters $\{\bar{\lambda}, \mu_y^J, \rho_J\}$ will affect the underlying log-asset process.

To compare results, we fix the volatility "σ_x^{BS}" and compute the log-asset volatility σ_x by the default-free value of an at-the-money European put (with all other parameters fixed), i.e., σ_x, is the solution of the following formula:

$$\mathrm{BS}(S_0, r, T, K, \sigma_x^{\mathrm{BS}}) = \text{default-free}(S_0, r, T, K, \sigma_x, \sigma_y, (\bar{\lambda}, \mu_y^J, \rho_J)), \tag{4.57}$$

where $K = S_0$.

We then vary the values of $\{\sigma_x^{\mathrm{BS}}, \bar{\lambda}, \mu_y^J, \rho_J\}$ to see the impact of these parameters on WWR and on CVA. The other parameters are chosen as: $S_0 = K = 100$, $T = 0.5$, $r = 0.004$, $\overline{h} = 0.1$, $Y_0 = 0.02$, $\gamma = 5$ see Eq.(4.37), $\theta = 0.02$, $\sigma_y = 0.1$, $\mu_x^J = 0$, $\sigma_x^J = 0.05$.

Figure 4.3 presents the WWR and CVA values for a European put by varying the parameters. When $\rho_J = 0$, variations in the other parameters do not have any impact on the WWR or CVA values; in Figure 4.3(a) it is shown that with $\rho_J \neq 0$, the WWR increases when the jump parameters μ_y^J and $\bar{\lambda}_J$ increase and σ_x^{BS} decreases. It appears to be the contribution of the correlated jump terms to the total variance of the log-asset process that determines the WWR. Figure 4.3 shows that σ_x^{BS}, which represents the level of the total variance in the log-asset process, is an important factor for the CVA values.

Now, we consider a Bermudan option that can be exercised $M = 10$ times prior to and upon expiration T. After fixing $\sigma_x^{\mathrm{BS}} = 0.2$, $\bar{\lambda} = 5$, $\mu_y^J = 0.04$, we compare the optimal exercise boundaries when varying the jump size correlation $\rho_J = \{0, -0.9\}$ in Figure 4.4.

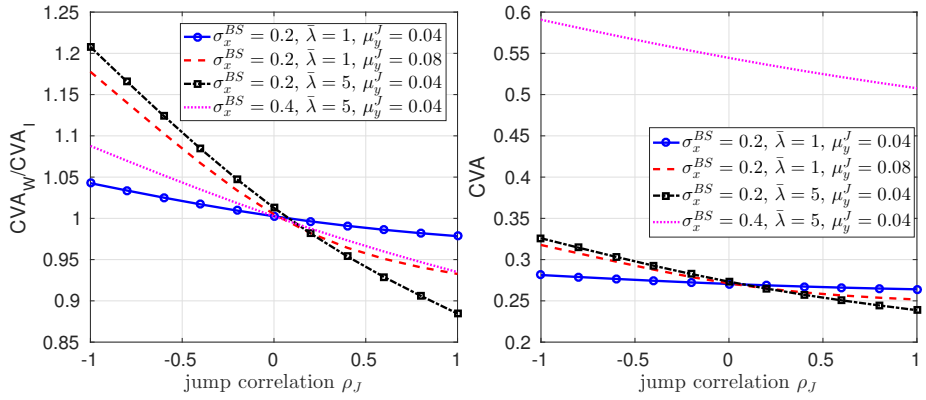

(a) WWR ratio (b) CVA

Figure 4.3: The CIRJ model: CVA test for a European put varying $\{\sigma_x^{\text{BS}}, \bar{\lambda}, \mu_y^J, \rho_J\}$. Results are obtained by the COS method, the number of Fourier terms $N_1 = 60$, $N_2 = 60$. integration range $L_1 = 8$, $L_2 = 6$.

In this 2D setting, the optimal exercise boundary at each exercise date is a surface, and we choose to plot the stock value along the time horizon of this optimal exercise surface at a fixed point of the Y-grid. As discussed, varying ρ_J has an immediate effect on the log-asset process, and the optimal exercise boundaries for $\rho_J = \{0, -0.9\}$ using Policy I are different. The exercise region (the area below the curve) always increases when ρ_J gets negative, for each policy. In the CIRJ model, when the jump in the intensity process is upward, the jump in the log-asset process tends to be downward when ρ_J is negative (notice that we choose $\mu_x^J = 0$).

Results in Table 4.2 show that the impact of ρ_J on the CVA values of a Bermudan put is much smaller than on the CVA values of the European put. The CVA values even become smaller when ρ_J is negative. Under this model, the CVA of a Bermudan put in the presence of WWR need not be higher than CVA without WWR.

4.5.3. WWR: THE HWJ MODEL

There are two correlation coefficients in the HWJ model, the jump size correlation ρ_J is defined as in the CIRJ model. Correlation ρ_J defines the same dependency as in the CIRJ model, studied in Section 4.5.2. An extreme case is $\bar{\lambda} = 0$, i.e. there is no jump in (X_t, Y_t), and hence we can focus on the diffusion correlation $\bar{\rho}$.

Different from ρ_J, correlation $\bar{\rho}$ does not influence the underlying asset process X_t. We will vary the value of the coefficients σ_x and σ_y to study the effect of the volatility on WWR and CVA. The other parameters are chosen as: $r = 0.004$, $S_0 = 100$, $K = 100$, $\overline{h} = 0.1$, $Y_0 = 0.02$, $\gamma = 5$, $\theta = 0.02$.

We first perform a CVA stress test for a European put, by varying $\bar{\rho}$ from -1 to 1, in Figure 4.5 with $\sigma_x = \{0.1, 0.2\}$ and $\sigma_y = \{0.1, 0.2\}$. Figure 4.5(a) shows that the WWR ratio curves with the same value of σ_x are very close. It implies that, given a fixed value of $\bar{\rho}$, an important factor for WWR is the intensity volatility σ_y, and σ_x only has a minor impact on the WWR. Correlation $\bar{\rho}$ is the factor of the contribution of the correlated diffusion

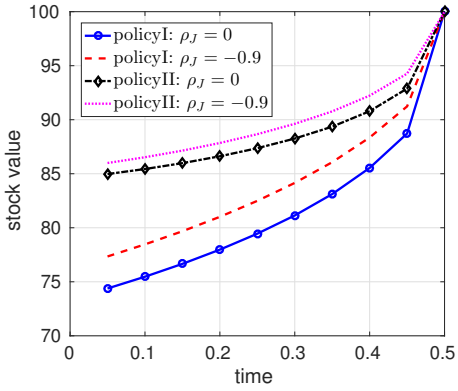

Figure 4.4: The CIRJ model: Optimal exercise boundary along the time horizon for a Bermudan put, $M = 10$. The results are obtained by the COS method. The stock value along the time horizon, fixing the value on the Y-grid, $\bar{w}_l = 0.0979$. Parameters $\bar{\lambda} = 5$, $\mu_y^J = 0.04$, $\sigma_x^{\text{BS}} = 0.2$.

$\bar{\lambda} = 5$		Policy I			Policy II		
ρ_J	method	V^{I}	U^{I}	CVA^{I}	V^{II}	U^{II}	CVA^{II}
0	COS	5.539	5.308	0.230	5.526	5.327	0.199
	SGBM	5.541	5.312	0.229	5.526	5.335	0.191
	std	0.002	0.002	0.001	0.002	0.002	0.001
−0.9	COS	5.544	5.322	0.222	5.530	5.346	0.184
	SGBM	5.551	5.335	0.217	5.537	5.361	0.177
	std	0.001	0.002	0.001	0.001	0.002	0.002

Table 4.2: The CIRJ model: Initial values of a Bermudan put, $M = 10$. The SGBM basis functions for the default-free computation are $\{1, X, X^2\}$, and for the default-adjusted value $\{1, X, Y, X^2, Y^2, XY\}$. The volatility in the BS formula is $\sigma_x^{\text{BS}} = 0.2$; $\mu_y^J = 0.04$ and $\bar{\lambda} = 5$.

terms to the total variance of the log-asset process. Figure 4.5(b) shows again that the log-asset volatility is the important factor for the CVA values.

Next, we also study Bermudan options by comparing the optimal exercise boundaries in Figure 4.6. The optimal boundaries using Policy I do not change when varying ρ_J (see the blue line). We study the cases $T = 0.5$ and $T = 5$ (the option can be exercised $M = 10$ times). Plot (a) shows that the effect of the diffusion correlation is very small (almost identical curves). With longer time intervals between two exercise dates in plot (b), the optimal exercise boundary with $\bar{\rho}_J = -0.9$ is slightly higher than for $\rho_J = 0$.

Table 4.3 compares results using the COS and SGBM methods. We compare the results when $T = 0.5$. Using Policy I, when the correlation $\bar{\rho}$ gets negative (up to -0.9), the default-free values stay the same, whereas the default-adjusted values become smaller. When we increase the value of the intensity volatility σ_y, from 0.1 to 0.2, the differences in the default-adjusted values increase. It shows that σ_y only impacts the default-

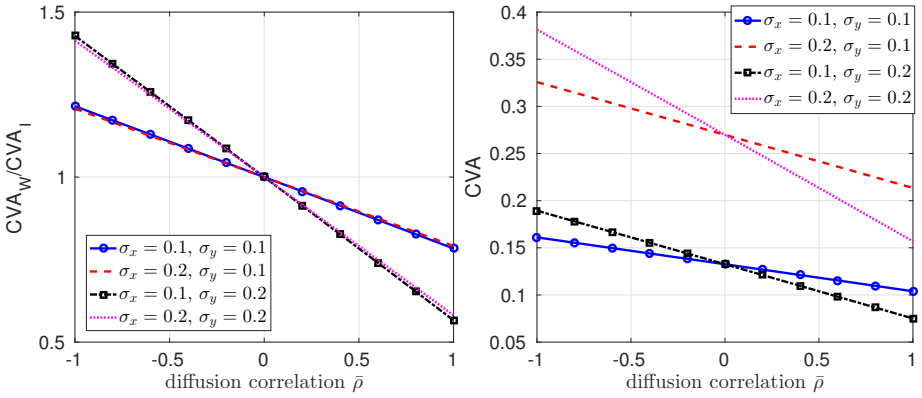

(a) WWR ratio (b) CVA $\bar{\rho}$

Figure 4.5: The HWJ model: CVA test varying $\bar{\rho}$ from -1 to 1 with $\bar{\lambda} = 0$. Results are obtained via the COS method, $N_1 = 60$, $N_2 = 60$, $L_1 = 8$, $L_2 = 6$.

adjusted value and the WWR. The use of Policy II cannot eliminate the increase in CVA values in the presence of WWR, but it can reduce the differences in the CVA values.

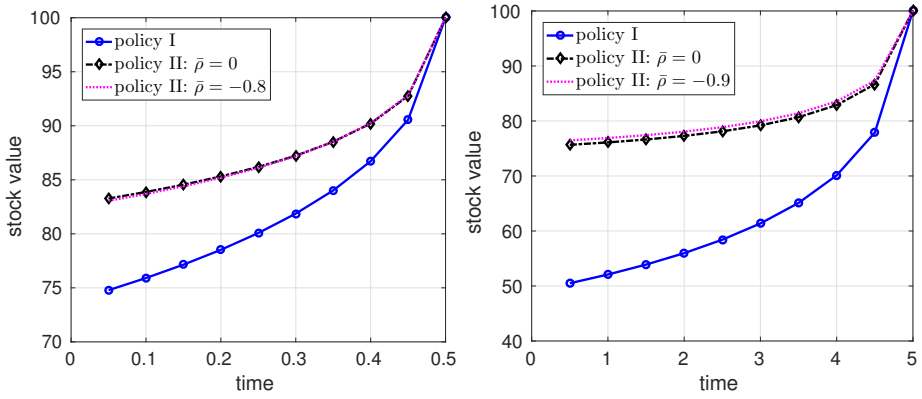

(a) $T = 0.5$ (b) $T = 5$

Figure 4.6: The HWJ model: Optimal exercise boundaries along the time horizon, with $\sigma_y = 0.2$, $\sigma_x = 0.2$, jump intensity $\bar{\lambda} = 0$. Plot (a): Optimal exercise stock values on the Y-grid $\bar{w}_l = 0.1027$, when $T = 0.5$; Plot (b): Optimal exercise stock value on the Y-grid $\bar{w}_l = 0.1030$, when $T = 5$.

COMPARISON OF THE MODELS

When comparing the results in Tables 4.1, 4.2 and 4.3, we see that in the case of independence of the two processes, the values of the default-free and default-adjusted Bermudan put corresponding to the two policies are very close when using the same values for σ_x^{BS} and $\overline{h}$. For the DF model and the HWJ model, the CVA values of the Bermudan

$\bar{\lambda}=0$			Policy I			Policy II		
σ_y	$\bar{\rho}$	method	V^{I}	U^{I}	$\mathrm{CVA}^{\mathrm{I}}$	V^{II}	U^{II}	$\mathrm{CVA}^{\mathrm{II}}$
0.1	0	COS	5.541	5.317	0.224	5.531	5.331	0.200
		SGBM	5.541	5.316	0.224	5.530	5.332	0.198
		std	0.002	0.002	0.001	0.001	0.002	0.001
0.1	−0.9	COS	5.541	5.284	0.257	5.526	5.305	0.221
		SGBM	5.541	5.284	0.258	5.527	5.306	0.221
		std	0.000	0.001	0.001	0.001	0.001	0.001
0.2	0	COS	5.541	5.317	0.224	5.530	5.332	0.198
		SGBM	5.542	5.318	0.224	5.530	5.335	0.195
		std	0.001	0.001	0.001	0.001	0.001	0.001
0.2	−0.9	COS	5.541	5.250	0.290	5.521	5.280	0.240
		SGBM	5.541	5.251	0.291	5.521	5.281	0.240
		std	0.002	0.002	0.001	0.002	0.002	0.001

Table 4.3: The HWJ model: Initial values for a Bermudan put, when $\bar{\lambda}=0$ and $T=0.5$; $M=10$. The SGBM basis functions for the default-free value are $\{1, X, X^2\}$, and for the default-adjusted values $\{1, X, Y, X^2, Y^2, XY\}$.

put always increase w.r.t. the WWR, but for the CIRJ model it does not. The intensity processes in the DF and the HWJ models do not change the properties of the underlying asset process, but in the CIRJ model the existence of WWR also changes the jump term in the log-asset process, which may explain the different results.

When comparing Figures 4.2 and 4.6, we see that WWR has more impact on the optimal exercise boundary in the DF model compared to the HWJ model (when $\rho_J = 0$). The main difference in the dependency structure defined by coefficient b and coefficient $\bar{\rho}$ is that the intensity value in the DF model is determined by the drift and the diffusion terms of the stock process, whereas in the HWJ model, coefficient $\bar{\rho}$ only impacts the diffusion terms.

For these three models, we present one Monte Carlo path in Figure 4.7, where we see that for the paths for the CIRJ and the HWJ models, high values of intensity do not necessarily imply lower stock values. The dependency structure defined by these three models is different. The impact of WWR on European and Bermudan options may thus also be different.

4.6. CONCLUSION

We studied the effect of WWR on European and Bermudan options by means of three types of dependency structure. The results show that the effects of WWR for European and Bermudan options differs. Different exercise policies can be followed when CCR is present, which may impact the corresponding CVA values of Bermudan options. The

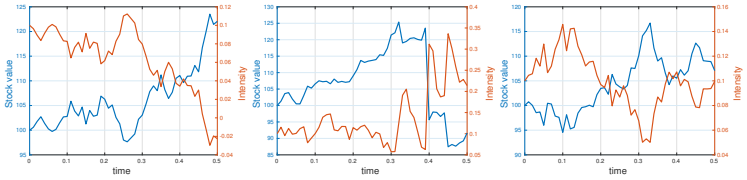

(a) DF (b) CIRJ (c) HWJ

Figure 4.7: One path under the risk-neutral measure: The blue lines represent the stock values and the red dashed lines the value of the Y process. Plot (a) is by the DF model with $b=-0.6$, $\sigma_x=0.2$; plot (b) by the CIRJ model $\sigma_x^{\text{BS}}=0.2$, $\bar{\lambda}=5$, $\rho_J=-0.9$, $\mu_y^J=0.04$; plot (c) by the HWJ model with $\sigma_x=0.2$, $\bar{\lambda}=0$ and $\bar{\rho}=-0.9$.

way to define the dependency structure also plays a role regarding the WWR. The three types of dependency structure we considered, gave different results for the optimal exercise boundaries of the Bermudan options and the corresponding option values. Increasing WWR always increased CVA in the case of European options, but for some dependency structure, the CVA of a Bermudan option may decrease when WWR incurs. In addition to the correlation coefficients, the volatility of the intensity plays an important role regarding the WWR. When computing the CVA as the difference between the default-free and default-adjusted values, the CVA VaR and CVA ES can be computed without subsimulations by means of the developed algorithms.

APPENDIX 1: BOUNDARIES OF THE COEFFICIENT b

The intensity h_t can be regarded as a function of coefficient b, given by

$$h_t=\left(\frac{1}{2}\sigma_x^2t^2\right)b^2+\left(\sigma_x\sqrt{t}Z\right)b+\overline{h}, \tag{4.58}$$

where $Z\sim\mathcal{N}(0,1)$ and $t\in[0,T]$.

The value of random variable Z is between $\Phi^{-1}(\zeta)$ and $\Phi^{-1}(1-\zeta)$ at a probability $(1-2\zeta)$, where $\zeta<0.5$. With $z_0:=\Phi^{-1}(1-\zeta)>0$, interval $[-z_0,z_0]$ is the confidence interval of Z at level $((1-2\zeta))$.

By fixing Z and t, the expression in (4.58) becomes a quadratic function in b, and its roots are given by the solution to the function,

$$\Delta^{\pm}(Z,t) \quad = \quad \sigma_x^{-1}t^{-\frac{3}{2}}(-Z^2\pm\sqrt{Z^2-2t\overline{h}}). \tag{4.59}$$

The two roots are determined by Z and t; when fixing t, we find:

- When $Z^2<2t\overline{h}$, i.e. when $Z\in(-\sqrt{2t\overline{h}},\sqrt{2t\overline{h}})$, the expression in (4.58) has two complex-valued roots and intensity h is thus always positive;
- When $Z^2\geq 2t\overline{h}$, the expression in (4.58) has two real-valued roots; It is positive when $b<\Delta^-(Z,t)$ or $b>\Delta^+(Z,t)$.

We look for values of b so that h_t is non-negative for $Z \in [-z_0, z_0]$, where $z_0 > \sqrt{2t\bar{h}} > 0$. The derivatives of the two roots,

$$\frac{\partial \Delta^{\pm}(Z,t)}{\partial Z} = \sigma_x^{-1} t^{-\frac{3}{2}} \left(-1 \pm \frac{Z}{\sqrt{Z^2 - 2t\bar{h}}} \right), \tag{4.60}$$

where $\left| \frac{Z}{\sqrt{Z^2-2t\bar{h}}} \right| < 1$, and hence we have:

- When $Z \in [-z_0, -\sqrt{2t\bar{h}}]$,

$$\frac{\partial \Delta^{-}(Z,t)}{\partial Z} > 0, \quad \frac{\partial \Delta^{+}(Z,t)}{\partial Z} < 0, \tag{4.61}$$

from which we see that, on the interval $Z \in [-z_0, -\sqrt{2t\bar{h}}]$, the root Δ^- is monotonically increasing and the root Δ^+ is monotonically decreasing, and $h_t > 0$ for $Z \in [-z_0, -\sqrt{2t\bar{h}}]$ when the value of the coefficient b satisfies:

$$b \in \left(-\infty, \Delta^{-}\left(-z_0, t \right) \right) \cup \left(\Delta^{+}\left(-\sqrt{2t\bar{h}}, t \right), +\infty \right); \tag{4.62}$$

- When $Z \in [\sqrt{2t\bar{h}}, z_0]$, we have:

$$\frac{\partial \Delta^{-}(Z,t)}{\partial Z} < 0, \quad \frac{\partial \Delta^{+}(Z,t)}{\partial Z} > 0, \tag{4.63}$$

so, on the interval $Z \in [\sqrt{2t\bar{h}}, z_0]$, Δ^- is monotonically decreasing and Δ^+ is monotonically increasing.

Then, $h_t > 0$ for $Z \in [\sqrt{2t\bar{h}}, z_0]$ when the value of b satisfies:

$$b \in \left(-\infty, \Delta^{-}\left(\sqrt{2t\bar{h}}, t \right) \right] \cup \left(\Delta^{+}\left(z_0, t \right), +\infty \right); \tag{4.64}$$

The intersection of Set (4.62) and Set (4.64), gives us the set of b-values for which $h_t > 0$ for $Z \in [-z_0, z_0]$, given by

$$b \in \left(\Delta^{+}\left(z_0, t \right), \Delta^{-}(-z_0, t) \right). \tag{4.65}$$

Next we will show that the set of the b-value that satisfies $h_t > 0$, for $Z \in [-z_0, z_0]$ over the time horizon $t \in [0, T]$, is given by

$$b \in \left(\Delta^{+}\left(z_0, T \right), \Delta^{-}(-z_0, T) \right), \tag{4.66}$$

when $z_0 > \frac{8}{3} t\bar{h}$.

Fixing Z, and taking the derivative of the two roots w.r.t. the time t, gives

$$\frac{\partial \Delta^{\pm}(Z,t)}{\partial t} = \frac{\sigma_x^{-1} t^{-\frac{5}{2}}}{2\sqrt{Z^2 - 2t\bar{h}}} \left(Z \pm \sqrt{Z^2 - 2t\bar{h}} \right) \left(Z \pm 2\sqrt{Z^2 - 2t\bar{h}} \right). \tag{4.67}$$

From (4.67), $\frac{\partial\Delta^-(-z_0,t)}{\partial t} < 0$ and $\frac{\partial\Delta^+(z_0,t)}{\partial t} > 0$ when $z_0 > \sqrt{\frac{8}{3}t\overline{h}}$. We can choose $\zeta \leq \Phi(-\frac{8}{3}t\overline{h})$ to satisfy this condition. Then, $\Delta^+(z_0,t)$ is increasing monotonically w.r.t. time t, and $\Delta^-(-z_0,t)$ is decreasing monotonically w.r.t. time t. Hence, the bounded interval for the coefficient b, given by (4.65), satisfies $h_t > 0$ for the time period $[0,T]$ at a probability $(1-2\zeta)$.

APPENDIX 2: DISCOUNTED CHFS

DF MODEL

The default-adjusted discounted ChF of the DF model is given by

$$\varphi_R^{\mathrm{DF}}(\mathbf{u},t,T;X_t) = \exp\left[-\int_t^T R_s ds + iu_1 X_T \middle| X_t\right], \tag{4.68}$$

the expression of which is as follows

$$\varphi_R^{\mathrm{DF}}(u,t,T;X_t) = \exp\left(-\int_t^T a(s)ds + \widetilde{A}^R(T-t) + \widetilde{B}^R(T-t)X_t\right), \tag{4.69}$$

with the coefficients

$$\begin{aligned}
\widetilde{A}^R(T-t) &= \left[-r + iu\left(r - \frac{1}{2}\sigma_x^2\right) - \frac{1}{2}\sigma_x^2 u^2\right](T-t) \\
&\quad \frac{b}{2}\left[iu\sigma_x^2 - \left(r - \frac{1}{2}\sigma_x^2\right)\right](T-t)^2 + \frac{1}{6}\sigma_x^2(T-t)^3, \\
\widetilde{B}^R(T-t) &= iu - b(T-t).
\end{aligned} \tag{4.70}$$

The corresponding short rate discounted ChF of the DF model is given by

$$\varphi_r^{\mathrm{DF}}(X_t,t,T) = \exp\left[-r(T-t) + iu_1 X_T \middle| X_t\right], \tag{4.71}$$

the expression of which is as follows

$$\varphi_r^{\mathrm{DF}}(X_t,t,T) = \exp\left(\widetilde{A}^r(T-t) + \widetilde{B}^r(T-t)X_t\right), \tag{4.72}$$

where the coefficients are given by

$$\begin{aligned}
\widetilde{A}^r(s) &= \left[-r + iu\left(r - \frac{1}{2}\sigma_x^2\right) - \frac{1}{2}\sigma_x^2 u^2\right](T-t), \\
\widetilde{B}^r(s) &= iu.
\end{aligned} \tag{4.73}$$

CIRJ MODEL

The default-adjusted discounted ChF of the CIRJ model is given by

$$\varphi_R^{\mathrm{CIRJ}}(\mathbf{u},t,T;(X_t,Y_t)) = \exp\left[-\int_t^T R_s ds + iu_1 X_T + iu_2 Y_T \middle| (X_t,Y_t)\right], \tag{4.74}$$

the expression of which is as follows

$$\varphi_R^{\text{CIRJ}}\left(\begin{bmatrix}u_1\\u_2\end{bmatrix},t,T,\begin{bmatrix}X_t\\Y_t\end{bmatrix}\right)=\exp\left(-\int_t^T\zeta^{\text{CIR}}(s)ds+\widetilde{A}^R(T-t)+\widetilde{B}_1^R(T-t)X_t+\widetilde{B}_2^R(T-t)Y_t\right) \tag{4.75}$$

with the coefficients

$$\begin{aligned}\widetilde{B}_1^R(T-t) &= iu_1,\quad \widetilde{B}_2^R(T-t)=\frac{\gamma}{\sigma_y^2}+\frac{d_1}{\sigma_y^2}\frac{1+d_2e^{d_1(T-t)}}{1-d_2e^{d_1(T-t)}},\\ \widetilde{A}^R(T-t) &= \left[-r-\bar{\lambda}+iu_1\left(r-\frac{1}{2}\sigma_x^2-\bar{\lambda}\bar{\mu}\right)-\frac{1}{2}\sigma_x^2u_1^2\right](T-t)\\ &\quad+\frac{\gamma\theta}{\sigma_y^2}\left[(\gamma+d_1)(T-t)-2\log\left(\frac{d_2e^{d_1(T-t)}-1}{d_2-1}\right)\right]\\ &\quad+\bar{\lambda}\bar{G}\left[\frac{2\sigma_y^2\mu_y^J}{g_1g_2}\log\left(\frac{g_1+d_2g_2e^{d_1(T-t)}}{g_1+d_2g_2}\right)-\frac{\sigma_y^2(T-t)}{g_1}\right],\end{aligned} \tag{4.76}$$

and

$$d_1=\sqrt{\gamma^2+2\sigma_y^2},\quad d_2=\frac{iu_2\sigma_y^2-\gamma-d_1}{iu_2\sigma_y^2-\gamma+d_1},\quad \bar{G}=\exp\left(iu_1\mu_x^J-\frac{1}{2}\left(u_1\sigma_x^J\right)^2\right),$$
$$g_1=-(1-iu_1\rho_J\mu_y^J)\sigma_y^2+(d_1+\gamma)\mu_y^J,\ g_2=(1-iu_1\rho_J\mu_y^J)\sigma_y^2+(d_1-\gamma)\mu_y^J. \tag{4.77}$$

The short rate discounted ChF of the CIRJ model is given by

$$\varphi_r^{\text{CIRJ}}(\mathbf{u},t,T;(X_t,Y_t))=\exp\left[-r(T-t)+iu_1X_T+iu_2Y_T\middle|(X_t,Y_t)\right], \tag{4.78}$$

the expression of which is as follows

$$\varphi_r^{\text{CIRJ}}\left(\begin{bmatrix}u_1\\u_2\end{bmatrix},t,T;\begin{bmatrix}X_t\\Y_t\end{bmatrix}\right)=\exp\left(A^r(T-t)+\widetilde{B}_1^r(T-t)X_t+\widetilde{B}_2^r(T-t)Y_t\right), \tag{4.79}$$

where the coefficients

$$\begin{aligned}\widetilde{B}_1^r(T-t) &= iu_1,\ \widetilde{B}_2^r(T-t)=\frac{2iu_2\gamma}{iu_2\sigma_y^2+e^{\gamma(T-t)}\left(-iu_2\sigma_y^2+2\gamma\right)},\\ \widetilde{A}^r(T-t) &= \left[-r-\bar{\lambda}+iu_1\left(r-\frac{1}{2}\sigma_x^2-\bar{\lambda}\bar{\mu}\right)-\frac{1}{2}\sigma_x^2u_1^2\right](T-t)\\ &\quad+\bar{\lambda}\bar{G}\left[\frac{\sigma_y^2(T-t)}{\tilde{c}_1}+\log\left(\frac{iu_2\tilde{c}_1-\tilde{c}_0\tilde{c}_2e^{\gamma(T-t)}}{iu_2\tilde{c}_1-\tilde{c}_0\tilde{c}_2}\right)\cdot\frac{(\tilde{c}_1-\tilde{c}_2)\sigma_y^2}{\gamma\tilde{c}_1\tilde{c}_2}\right]\\ &\quad+\frac{2\gamma\theta}{\sigma_y^2}\left[\gamma(T-t)-\log\left(\frac{\tilde{c}_0e^{\gamma(T-t)}-iu_2\sigma_y^2}{\tilde{c}_0-iu_2\sigma_y^2}\right)\right]\end{aligned} \tag{4.80}$$

where

$$\tilde{c}_1=1-iu_1\rho_J\mu_y^J-2\gamma\mu_y^J,\quad \tilde{c}_2=1-iu_1\rho_J\mu_y^J,\quad \tilde{c}_0=iu_2\sigma_y^2-2\gamma. \tag{4.81}$$

HWJ MODEL

The default-adjusted discounted ChF of the HWJ model is given by

$$\varphi_R^{\text{HWJ}}(\mathbf{u},t,T;(X_t,Y_t)) = \exp\left[-\int_t^T R_s ds + iu_1X_T + iu_2Y_T\middle|(X_t,Y_t)\right], \tag{4.82}$$

the expression of which is given by

$$\begin{aligned}&\varphi_R^{\text{HWJ}}(\mathbf{u},t,T;(X_t,Y_t))\\ &\quad= \exp\left(-\int_t^T \zeta^{\text{HW}}(s)ds + \widetilde{A}^R(T-t) + \widetilde{B}_1^R(T-t)X_t + \widetilde{B}_2^R(T-t)Y_t\right),\end{aligned} \tag{4.83}$$

with the coefficients

$$\begin{aligned}&\widetilde{B}_1^R(T-t) = iu_1,\ \widetilde{B}_2^R(T-t) = \exp\left(-\gamma(T-t)\right)\left(iu_2-\frac{1}{\gamma}\right)+\frac{1}{\gamma},\\ &\widetilde{A}^R(T-t) = \left[-r-\bar{\lambda}+\left(r-\frac{1}{2}\sigma^2-\bar{\lambda}\bar{\mu}\right)iu_1-\frac{1}{2}\sigma^2u_1^2\right](T-t)+\frac{\sigma_y^2}{2\gamma^2}(T-t)\\ &\quad+\frac{1}{\gamma}(\gamma\theta+iu_1\bar{\rho}\sigma_x\sigma_y)\left[\left(1-e^{-\gamma(T-t)}\right)\left(iu_2+\frac{1}{\gamma}\right)-(T-t)\right]\\ &\quad+\frac{\sigma_y^2}{2\gamma^2}\left[\left(e^{-\gamma(T-t)}-1\right)\left(2iu_2+\frac{2}{\gamma}\right)-\left(e^{-2\gamma(T-t)}-1\right)\left(iu_2-\frac{1}{2}\gamma u_2^2+\frac{1}{2\gamma}\right)\right]\\ &\quad+\frac{\bar{\lambda}\bar{G}}{\gamma g+\mu_y^J}\log\left(\frac{\mu_y^J\left(e^{-\gamma(T-t)}-1\right)+\gamma\left(iu_2\mu_y^Je^{-\gamma(T-t)}-g\right)}{\gamma(iu_2\mu_y^J-g)}\right)\\ &\quad+\frac{\bar{\lambda}\bar{G}\gamma}{\gamma g+\mu_y^J}(T-t),\end{aligned} \tag{4.84}$$

where $g = 1-iu_1\rho_J\mu_y^J$, $\bar{G} = \exp\left(iu_1\mu_x^J-\frac{1}{2}\left(u_1\sigma_x^J\right)^2\right)$.

The short rate discounted ChF of the HWJ model is given by

$$\varphi_r^{\text{HWJ}}(\mathbf{u},t,T;(X_t,Y_t)) = \exp\left[-r(T-t)+iu_1X_T+iu_2Y_T\middle|(X_t,Y_t)\right], \tag{4.85}$$

the expression of which is as follows

$$\varphi_r^{\text{HWJ}}\left(\begin{bmatrix}u_1\\u_2\end{bmatrix},t,T,\begin{bmatrix}X_t\\Y_t\end{bmatrix}\right) = \exp\left(\widetilde{A}^r(T-t)+\widetilde{B}_1^r(T-t)X_t+\widetilde{B}_2^r(T-t)Y_t\right), \tag{4.86}$$

with the coefficients

$$\begin{aligned}\widetilde{B}_1^r(T-t) &= iu_1,\ \widetilde{B}_2^r(T-t) = iu_2e^{-\gamma(T-t)}.\\ \widetilde{A}^r(T-t) &= \left[-r-\bar{\lambda}+\left(r-\frac{1}{2}\sigma^2-\bar{\lambda}\bar{\mu}\right)iu_1-\frac{1}{2}\sigma^2u_1^2\right](T-t)\\ &\quad+\frac{iu_2}{\gamma}\left(\theta\gamma+iu_1\bar{\rho}\sigma_x\sigma_y\right)\left(1-e^{-\gamma(T-t)}\right)-\frac{\sigma_y^2u_2^2}{4\gamma}\left(1-e^{-2\gamma(T-t)}\right)\\ &\quad+\frac{\bar{\lambda}}{g\gamma}\bar{G}\left[\log\left(\frac{iu_2\mu_y^Je^{-\gamma(T-t)}-g}{iu_2\mu_y^J-g}\right)+\gamma(T-t)\right],\end{aligned} \tag{4.87}$$

4

APPENDIX 3: CVA VAR AND CVA ES

According to the Basel Committee on Banking Supervision: '...CVA risk is defined as the risk of losses arising from changing CVA values in response to changes in counterparty credit spread and market risk factors that drive market prices of derivative transactions...' [6][Annex1]. The CVA Expected Shortfall (ES) is an important measure of CVA risk. Employing the developed algorithms, we can directly compute the CVA VaR and CVA ES without sub-simulations. As an example, we demonstrate the results of CVA VaR with different values of the coefficient b under the DF model.

The calculation of the CVA ES can be summarized as in [14]. We first generate scenarios under the real-world probability measure (denoted by $\mathbb{P}$) up to the risk horizon. Then, for each real-world scenario, the CVA values are calculated until expiration, based on the risk-neutral measure. Subsequently, one determines the empirical real-world ($\mathbb{P}$) CVA distribution, selects a quantile at a confidence level (say 97.5%) and computes the CVA VaR. The CVA $\text{VaR}_{97.5\%}$ is the 97.5% quantile of the CVA loss $(\text{CVA}_t - \text{CVA}_0)$. The corresponding CVA ES reflects the expected value of the losses in the worst 2.5% of the scenarios under $\mathbb{P}$. The formula for the CVA ES at time t is as follows:

$$\text{CVA-ES}(t) = \mathbb{E}^{\mathbb{P}}\left[L_t \middle| L_t > \text{VaR}_{L_t}(97.5\%)\right], \tag{4.88}$$

where the CVA loss $L_t := \text{CVA}_t - \text{CVA}_0$; $\text{VaR}_{L_t}(97.5\%)$ is the 97.5% quantile of the loss distribution L_t; CVA_t represents the CVA value at time t, under the risk-neutral probability measure.

Calculation of the CVA VaR and the CVA ES requires a change of probability measure (between $\mathbb{P}$ and $\mathbb{Q}$). More details about the change of probability measure can be found in Chapter 5. It may require sub-simulation (i.e., nested simulation) or even "sub-sub simulation", which requires a huge computational effort. However, in our setting of CVA calculation and with the algorithms under consideration, there is no need for sub-simulation for the computation of CVA VaR or CVA ES. We take the difference between the default-free and the default-adjusted values for computing CVA instead of computing the expectation as the integral over the time horizon, and by this we avoid one layer of sub-simulation. Secondly, we can compute risk-neutral expectations on any simulated real-world scenario by the algorithms (COS and SGBM). The COS and SGBM algorithms for efficient CVA computation on risk-neutral scenarios can be found in [32, 78], and those algorithms for efficient computation on both real-world and risk-neutral scenarios, without sub- simulation, can be found in [30].

As an example, we compute the CVA ES for a Bermudan put under the DF model. Figure 4.8 shows the CVA ES from time zero until the option's expiration by the COS method. We compare the CVA ES values for $b = \{-0.2, -0.6\}$ using the two policies. It shows that WWR has a more significant impact on the CVA ES values, compared to the time-zero CVA values. By Policy II the CVA ES values decrease significantly.

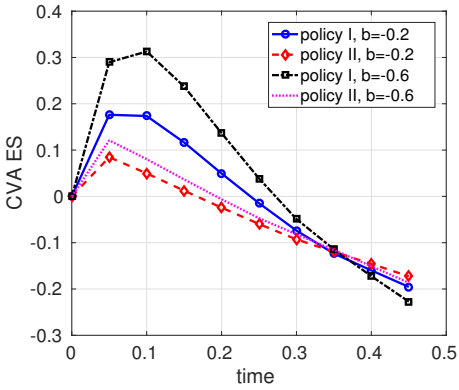

Figure 4.8: The CVA ES for a Bermudan put under the DF model; $S_0 = 100$, $K = 100$, $r = 0.004$, $\sigma_x^{\mathbb{Q}} = 0.2$, real-world log-return $\mu^{\mathbb{P}} = 0.006$, real-world volatility $\sigma_x^{\mathbb{P}} = 0.2$, $\overline{h} = 0.1$, $T = 0.5$, and coefficient $b = \{-0.2, -0.6\}$.

CHAPTER 5

Efficient computation of exposure profiles on real-world scenarios

This chapter presents a computationally efficient technique for the computation of exposure distributions at any future time under the risk-neutral and some observed real-world probability measures, needed for computation of credit valuation adjustment (CVA) and potential future exposure (PFE). In particular, we present a valuation framework for Bermudan swaptions. The essential idea is to approximate the required value function via a set of risk-neutral scenarios and use this approximated value function on the set of observed real-world scenarios. This technique significantly improves the computational efficiency by avoiding nested Monte Carlo simulation and by using only basic methods such as regression. We demonstrate the benefits of this technique by computing exposure distributions for Bermudan swaptions under the Hull-White and the G2++ models.

5.1. INTRODUCTION

The aim of the regulatory capital base, in the Basel framework, is to improve a bank's resilience against future losses due to defaults of counterparties [5]. Credit exposure to counterparties occurs due to financial transactions or investments via OTC (over the counter) derivatives products. It is defined as the market value of the *replacement costs* of transactions if a counterparty defaults, assuming no recovery. Banks are required to hold regulatory capital to back exposure in the future to all their counterparties.

The Basel Committee gives specific definitions for the credit exposure metrics and adjustments regarding the future credit risk, to banks/firms [4]. EE and PFE are important indicators for the safety of a bank's portfolio to market movements and are therefore used as metrics for capital requirements by regulators in Basel II and III [38]. PFE is used for trading limits for portfolios with counterparties as it may indicate at any future date the maximum amount of exposure with a predefined confidence. For example, the 99% PFE is the level of potential exposure that can be exceeded with a probability of 1%. CVA is a charge which has a direct impact on the balance sheet and the income statement of a firm as it is an adjustment to the value of financial derivatives.

There are three basic steps in calculating future distributions of exposure [38]:

- generation of scenarios using the models that represent the evolution of the underlying market factors;
- valuation of the portfolio for each scenario at each exposure monitoring date;

This chapter is based on the article 'Efficient computation of exposure profiles on real-world and risk-neutral scenarios for Bermudan swaptions', published in *Journal of Computational Finance*, 20(1):139–172, 2016. [30].

- determination of exposure values at each date for each scenario.

There is no doubt that CVA must be computed under the risk-neutral measure, as it is the market price of counterparty default risk. It is the cost of setting up a hedge portfolio to mitigate the credit risk that arises from exposure against a counterparty. In the setting of a CVA computation, scenarios are generated under the risk-neutral measure to compute 'risk-neutral exposure distributions'.

In contrast, for risk analysis it is argued that expectations (EE) and quantiles (PFE) of future exposure values must be obtained via scenarios that can reflect the 'real-world' in a realistic way. We know that the risk-neutral probability measure used in the pricing process does not reflect the 'real-world' probability of future outcomes, as it has been adjusted based on the assumption that market participants are risk-neutral.

The Girsanov theorem states that the risk-neutral volatility should be equal to the real-world volatility, when an equivalent measure exists [3]. However, it is well-known that in practice the risk-neutral market implied volatility differs from the observed real-world volatility [48, 80]. The observed historical dynamics and the calibrated risk-neutral dynamics may exhibit a different behavior, which is a challenge for risk management as the computational cost becomes high.

In practice, calculation of exposure values on each 'real-world' scenario at each monitoring date needs to be performed under a risk-neutral measure. For certain products, like Bermudan swaptions, the valuation is based on Monte Carlo simulations, that can be computationally intensive, especially since pricing then requires another, 'nested set' of Monte Carlo paths. The computational cost increases drastically due to the number of real-world scenarios, risk-neutral paths and the number of monitoring dates.

Employing a simplification, i.e. assuming that the observed real-world scenarios are 'close' to the risk-neutral scenarios and that calculation just takes place under one measure, may lead to serious problems, as there are significant differences between the resulting distributions. Stein [81] showed that exposures computed under the risk-neutral measure depend on the choice of numéraire, and can be manipulated by choosing a different numéraire. As a conclusion, it is crucial that calculations of EE and PFE must be done under the real-world instead of the risk-neutral measure.

The computational problem poses a great challenge to practitioners to enhance the computational efficiency. Available solutions include reduction of the number of monitoring dates, the number of Monte Carlo paths, application of variance reduction techniques, using interpolation and enhanced computational platforms such as GPUs. Even with all these efforts, calculations cost a lot of time [81].

For Bermudan swaptions, Joshi and Kwon [54] provided an efficient approach for approximating CVA, which relies only on an indicator of future exercise time along scenarios, the decision of which is based on the regressed functions. The expected exposure at a monitoring date is then obtained from the corresponding deflated path-wise cash flows. This approximation method however cannot, in a straightforward fashion, be used for PFE on the real-world scenarios. For PFE computations, Stein [80] proposed to avoid nested MC simulations by combining the real-world and the risk-neutral probability measures. The computed results lie 'between' the computed PFE values under the real-world and the risk-neutral probability measures.

In this chapter we will focus on accurate computation of these risk measures for a

heavily-traded OTC derivative, the Bermudan swaption. There are well-developed methods that can be used to compute the time-zero value of Bermudan swaptions, like regression and simulation-based Monte Carlo methods, such as the Least Squares Method (LSM) [1, 64] or the Stochastic Grid Bundling Method (SGBM) [49, 50, 55], the finite difference (FD) PDE method or the Fourier expansion-based COS method [28].

This chapter presents an efficient method to significantly enhance the computational efficiency of exposure values computation without the nested simulation. The key is to approximate the value function by a linear combination of basis functions obtained by risk-neutral scenarios, and to compute the expected payoff using the approximated value function to determine the optimal early-exercise strategy on the paths representing the observed real-world scenarios. Only two sets of scenarios, one under the risk-neutral and one under the observed historical dynamics, are needed to compute the exposure distributions at any future time under the two measures. We apply this numerical scheme within the context of the LSM and SGBM approaches.

The chapter is organized as follows. Section 5.2 presents background, mathematical formulation of EE, PFE and CVA, and the dynamic programming framework for pricing Bermudan swaptions. The interest rate models used are presented in Section 5.3. We explain the essential insight for computation under two measures, based on the risk-neutral scenarios, and describe the algorithms for computing the exposure profiles for SGBM in Section 5.4 and LSM in Section 5.5. We provide reference values for exposure, based on Fourier-cosine expansions in Section 5.6. Section 5.7 presents numerical results with the algorithms developed for the one-factor Hull-White and two-factor G2++ models.

5.2. CVA, EE AND PFE AS RISK MEASURES

In this section, we present the general framework for computing the exposure measurements. It is important to choose suitable probability measures to compute CVA, EE and PFE. We will discuss the practical background and the choice of probability measures.

5.2.1. CALIBRATION AND BACK-TESTING

It is well-known that there are differences between the calibrated historical dynamics and the dynamics implied by market prices. The reason is that models calibrated to historical data tend to reflect future values based on historical observations and models calibrated to market prices reflect market participants' expectations about the future. Some research on building a joint framework in the real and risk-neutral worlds is done by Hull et al. [48]. They propose a joint measure model for the short rate, in which both historical data and market prices can be used for calibration and the calibrated risk-neutral and real-world measures are equivalent.

The practical setting regarding calibrating model parameters is however involved. Back-testing of counterparty risk models is required by the Basel Committee for those banks with an Internal Model Method approval, for which PFE is an important indicator for setting limits. Back-testing refers to comparison of the outcomes of a bank's model against realized values in the past. The bank's model must be consistent with regulatory constraints, in other words, be able to pass the back-testing of PFE. A bank has to strike

a balance between managing its risk and meeting the expectations of the shareholders. An over-conservative estimate of market factors for exposure computation would lead to high regulatory capital reservings.

In short, a model used by a bank for generating scenarios should be able to reflect the real world, to meet requirements of back-testing limits by regulators and the return rate by investors. Based on these, Kenyon et al. [56] proposed a *Risk-Appetite measure*, which would fit in with these requirements. When a calibrated model under this *Risk-Appetite measure* cannot pass the back-testing, the bank needs to reconsider preferences. From back-testing, one may find a so-called 'PFE-limit implied volatility' of a model, by which, combined with a given budget, a bank's risk preference can be computed.

In [73], Ruiz called the model that describes the evolution of the underlying market factors the *Risk-Factor-Evolution* (RFE) model, on which the back-testing is done periodically. The related probability measure is called the *RFE measure* there. In that work, the model used to describe the real world is introduced first, and the relevant probability measure is defined based on the model. In some sense, there are 'different' probability measures induced by the back-testing setting that describe the outcome, assuming the underlying factors evolve according to the calibrated model.

5.2.2. MATHEMATICAL FORMULATION

Consider an economy within a finite time horizon $[0, T]$. The probability space $(\Omega, \mathscr{F}, \mathbb{P})$ describes the uncertainty and information with Ω the sample space consisting of outcome elements w, $\mathscr{F}$ a σ-algebra on Ω, and $\mathbb{P} : \mathscr{F} \to [0,1]$ the probability measure that specifies the probability of events happening on the measure space $(\Omega, \mathscr{F})$. Information up to time t is included in the filtration $\{\mathscr{F}_t, t \in [0, T]\}$.

Assume further a complete market without arbitrage opportunities. There exists an equivalent martingale measure such that a price associated to any attainable claim is computed as an expectation under this probability measure w.r.t. the associated numéraire. We choose to use a risk-neutral probability measure, denoted by $\mathbb{Q} : \mathscr{F} \to [0,1]$ with numéraire $B_t = \exp\left(\int_0^t r_s ds\right)$, where $\{r_s, s \in [0,t]\}$ is the risk-neutral short rate. The numéraire B_t represents a savings account with $B_0 = 1$.

Inspired by Kenyon et al. [56] and Ruiz [73], we define a probability measure of observed history that can pass the back-testing. We use the notation $\mathbb{A} : \Omega' \to [0,1]$ to present the *observed historical* probability measure on some measure space $(\Omega', \mathscr{F}')$ that we choose to reflect the probability of events in the real world. The probability measure $\mathbb{A}(\Omega') = 1$. The observed historical measure $\mathbb{A}$ may not be equivalent to the chosen risk-neutral measure $\mathbb{Q}$. As a probability space that includes realized outcomes in the past, the observed measure space should satisfy $\Omega' \subset \Omega$ and the associated filtration $\mathscr{F}'_t \subset \mathscr{F}_t$.

Let the stochastic process $\{\mathbf{X}_t \in \mathbb{R}^n, t \in [0, T]\}$ on $(\Omega, \mathscr{F})$ represent all influential market factors. We further define the market factor $\{\mathbf{X}_t\}_0^T$ on the space $(\Omega', \mathscr{F}')$ as the same mapping as the one on $(\Omega, \mathscr{F})$, i.e. for an outcome w that may happen in both Ω and Ω' with different probability, one will have the same realized values for the market factors. Fixing an outcome $w \in \Omega' \subset \Omega$ the stochastic process is a function of time t, i.e. $\mathbf{X}_t(w) : [0, T] \to \mathbb{R}^n$, which is a path of $\mathbf{X}_t$.

5.2.3. EE,PFE,EPE AND MPFE

We are going to define the profiles of EE and PFE under the observed historical probability measure $\mathbb{A}$, since simulations generated by the corresponding calibrated dynamics are used to reflect the real evolution of the underlying market factors.

The curve PFE(t) is a function of future time t until the expiry of the transactions T, and its peak value indicates the maximum potential exposure of a portfolio over the horizon $[0,T]$. We define the PFE curve at time $t \in [0,T]$ as the 99% quantile of the exposure distribution, measured by the observed probability measure $\mathbb{A}$, given by

$$\text{PFE}(t) = \inf\left\{ y \middle| \mathbb{A}\left(\{w : E_t(w) < y\}\right) \geq 99\% \right\}, \tag{5.1}$$

where $w \in \Omega'$ and $\mathbf{X}_0(w) = x$.

The maximum PFE (MPFE) is used to measure the peak value at the PFE curve over the time horizon $[0,T]$, given by

$$\text{MPFE} = \max_{t\in[0,T]} \text{PFE}(t). \tag{5.2}$$

In a similar way, another measure of credit risk of a portfolio is the expected exposure (EE), which is the average exposure at any future date, denoted by EE(t). The value of the EE curve at a monitoring date t under the observed measure $\mathbb{A}$ is given by

$$\text{EE}(t) = \mathbb{E}^{\mathbb{A}}[E_t] = \int_{\Omega'} E_t(w) d\mathbb{A}(w), \tag{5.3}$$

where $w \in \Omega'$ and $\mathbf{X}_0(w) = x$. The real-world EPE over a time period $[0,T]$ is given by

$$\text{EPE}(0,T) = \frac{1}{T}\int_0^T \text{EE}(t) ds. \tag{5.4}$$

In particular, we are interested in Bermudan swaptions, the pricing dynamics of which is presented in the following section

5.2.4. PRICING OF BERMUDAN SWAPTIONS

A Bermudan swaption is an option where the owner has the right to enter into an underlying swap either on the swaption's expiry or at a number of other predefined exercise dates before the expiry date. As soon as the swaption is exercised, the underlying swap starts. We assume here that the expiry date of the swap is predefined, so the duration of the swap is calculated from the swaption exercise date until a fixed end date. The underlying dynamics for the short rate governing the Bermudan swaption are either the one-factor Hull-White model or the two-factor G2++ model. Details of these well-known governing dynamics are presented in Chapter 5.3.

We assume that the exercise dates coincide with the payment dates of the underlying swaps, and consider an increasing maturity structure, $0 < T_1 < \cdots < T_N < T_{N+1}$, with T_{N+1} the fixed end date of the underlying swap, T_1, T_N the first and last opportunities to enter, respectively, and we define $T_0 = 0$. We assume that when an investor enters a swap at time T_n, $n = 1,2,...,N$, the payments of the underlying swap will occur at $T_{n+1}, T_{n+2}, \cdots, T_{N+1}$ with time fraction $\tau_n = T_{n+1} - T_n$. Let N_0 represent the notional

amount and K be the fixed strike. We use indicator $\delta = 1$ for a payer Bermudan swaption and $\delta = -1$ for a receiver Bermudan swaption.

The payoff for entering the underlying swap at time T_n associated with payment times $\mathcal{T}_n = \{T_{n+1}, \ldots, T_{N+1}\}$, conditional on $\mathbf{X}_{T_n} = \mathbf{x}$, is given by [13]:

$$g_n(\mathbf{x}) \quad = \quad N_0 \left(\sum_{k=n}^{N} P(T_n, T_{k+1}, \mathbf{x}) \tau_k \right) \max\Big(\delta\big(S(T_n, \mathcal{T}_n, \mathbf{x}) - K\big), 0\Big), \tag{5.5}$$

where the forward swap rate $S(t, \mathcal{T}_n, \mathbf{x})$ at time $t \leq T_n$, associated with time $T_n, \ldots, T_{N+1}$, is defined by:

$$S(T_n, \mathcal{T}_n, \mathbf{x}) = \frac{1 - P(T_n, T_{N+1}, \mathbf{x})}{\sum_{k=n}^{N} P(T_n, T_{k+1}, \mathbf{x}) \tau_k}, \tag{5.6}$$

and $P(T_n, T_k, \mathbf{x})$ is the price of a Zero-Coupon Bond (ZCB), conditional on $\mathbf{X}_{T_n} = \mathbf{x}$, associated with times T_n and T_k. The analytic formula of the ZCB is related to the risk-neutral model for the underlying variable.

5

We refer to a function g_n, a bounded Borel function, as the *payoff function* at time T_n, which represents the value of the future payments of exercising the option at time T_n. For completeness, we define $g_0 \equiv 0$. We choose for the stochastic process $\{\mathbf{X}_t, t \in [0, T_N]\}$ an *Itô diffusion*. In that case, $g_n(\mathbf{X}_{T_n})$ is a continuous variable, as $\mathbf{X}_{T_n}$ is a continuous random variable. The value of *not* exercising the option at $t \in [0, T_N)$ is the value of continuing the option at time t.

Let time $t \in [T_n, T_{n+1})$, where the exercise opportunities are restricted to dates later than T_n, i.e. $\{T_{n+1}, \ldots, T_N\}$. The value of the Bermudan claim is the risk-neutral expectation of the (discounted) future payoff when exercising optimally [68]. With the strong Markov property of the Itô diffusions [68], the value of this Bermudan claim at time t, conditional on $\mathbf{X}_t = \mathbf{x}$, is the value that is obtained by maximizing the following object function [34]:

$$c(t, \mathbf{x}) = \max_{j \in \{n+1, \ldots, N\}} \mathbb{E}^{\mathbb{Q}} \left[\frac{B_t}{B_{T_j}} g_j(\mathbf{X}_{T_j}) \Big| \mathbf{X}_t = \mathbf{x} \right], \tag{5.7}$$

where $n = 0, \ldots, N-1$. We refer to value function $c(t, \cdot)$ as the *continuation* function at time t.

We wish to determine the exposure at a set of discrete exposure monitoring dates, $\{0 = t_0 < t_1 < \cdots < t_M = T_N\}$, with time step $\Delta t_k = t_{k+1} - t_k$, $k = 0, \ldots, M-1$. These exposure monitoring dates include the swaption exercise dates $\{T_1, T_2, \ldots, T_N\}$ and t_M is equal to T_N. There are some exposure monitoring dates between each two exercise dates, as we are also interested in the exposure at those intermediate dates.

Figure 5.1 presents the time lines of the exercise dates of a Bermudan swaption and the monitoring dates used for exposure computation for convenience. This Bermudan swaption can be exercised 7 times between year 4 and year 10, i.e. year 4 is the first exercise date and year 10 is the expiry (the last exercise date). The exposure monitoring dates are each 1/5 year from time zero until year 10. The monitoring date $t_{20} = 4$ coincides with the first exercise date, and monitoring date $t_{50} = 10$ is equal the last exercise opportunity.

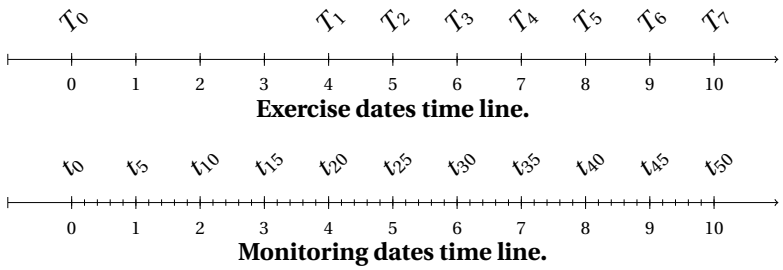

Figure 5.1: Time lines.

We compute the exposure of a Bermudan claim at monitoring dates $\{t_m\}_{m=0}^{M}$. Value function V then satisfies [34]:

$$V(t_m,\mathbf{x}) = \begin{cases} g_N(\mathbf{x})) & t_M = T_N \\ \max(c(t_m,\mathbf{x}), g_n(\mathbf{x})), & t_m = T_n,\ n < N \\ c(t_m,\mathbf{x}), & T_n < t_m < T_{n+1},\ n < N \end{cases} \tag{5.8}$$

where the continuation function c is computed as the conditional expectation of the future option value, given by

$$c(t_m,\mathbf{x}) = \mathbb{E}^{\mathbb{Q}}\left[\frac{B_m}{B_{m+1}} V(t_{m+1},\mathbf{X}_{m+1})\middle|\mathbf{X}_m = \mathbf{x}\right], \tag{5.9}$$

which can be proved to be equivalent to (5.7) by induction.

The optimal exercise strategy is now as follows: At state $\mathbf{X}_{T_n} = \mathbf{x}$, exercise takes place when $g_n(\mathbf{x}) > c(T_n,\mathbf{x})$, and the option is kept at all non-exercise monitoring dates t_m. Value function V and continuation function c are defined over the time period $[0, T_N]$ and space $\mathscr{D} \in \mathbb{R}^n$.

The pricing dynamics in (5.8) are most conveniently handled by means of a backward recursive iteration. From known value g_N at time $t_M = T_N$, we compute $V(t_{M-1},\cdot)$, and subsequently function $V(t_{M-2},\cdot)$, and so on, until time zero. The essential problem hence becomes to determine value function V and continuation function c at all monitoring dates $\{t_m\}_{m=1}^{M}$.

Remark: Given a fixed path $w' \in \Omega'$ or $w \in \Omega$, we compute the option values for the scenario as $V(t_m,\mathbf{X}_m(w))$ at any monitoring date t_m by (5.8). Once the option for scenario w is exercised at a specific date, the option terminates and the exposure values regarding this option along the scenario from the exercise date to T become zero.

When a sufficiently large number of scenarios for the risk-neutral model are generated, the option value can be determined at all monitoring dates for any scenario and we obtain a matrix of exposure values called *the exposure profile*.

The exposure profile computed from observed real-world scenarios that are calibrated based on historical dates is an empirical real-world exposure density, from which we can estimate the real-world EE and PFE at each exposure monitoring date. However, with risk-neutral short rate processes, the exposure profiles on risk-neutral scenarios are needed to compute the discounted EE.

We see that the key of computing exposure profiles on the generated scenarios is the value function V and the continuation function c at all monitoring dates $\{t_m\}_{m=1}^{M}$.

Nested Monte Carlo simulation is often used when a simulation-based algorithm is employed for the valuation, which is expensive as simulations of risk-neutral paths are needed for each (real-world) scenario at each monitoring date. Suppose that accurate pricing requires K_I risk-neutral paths at M monitoring dates, then the computational time would be $O(M^2 K_I K_a)$ for K_a real-world scenarios for computing EE and PFE profiles.

5.3. INTEREST RATE MODELS

In this section, we will present two interest rate models for describing the evolution of the short interest rate.

5.3.1. ONE-FACTOR HULL-WHITE MODEL

When the *risk-neutral short rate* follows the well-known Hull-White model, the dynamics are given by:

$$r_t = \theta(t) + x_t, \tag{5.10}$$
$$dx_t = -\lambda x_t + \sigma dW_t^{\mathbb{Q}}, \tag{5.11}$$

where $x_0 = 0$, the positive constants λ and σ are the speed of mean reversion and the volatility, respectively, $W_t^{\mathbb{Q}}$ is a standard Wiener process under measure $\mathbb{Q}$, and the deterministic reversion level $\theta(t)$ fitting the yield curve is given by

$$\theta(t) = f^M(0,t) + \frac{\sigma^2}{2\lambda^2}\left(1 - e^{-\lambda t}\right)^2, \tag{5.12}$$

where $f^M(0,T)$ represents the market instantaneous forward curve at time 0 for the maturity T given by

$$f^M(0,T) = -\frac{\partial \log P^M(0,T)}{\partial T}, \tag{5.13}$$

where $P^M(0,T)$ is the market value of the discount factor for maturity T.

The formulas of a ZCB and the analytic formulas of the discounted ChF under the HW model are given in Appendix 1 in this chapter.

We also give the dynamics for generating the *observed real world scenario*, given by the following:

$$r_t = \mu(t) + x_t, \tag{5.14}$$
$$dx_t = -\kappa x_t + \eta dW_t^{\mathbb{A}}, \tag{5.15}$$

where $x_0 = 0$. The positive constants κ and η are the speed of mean reversion and the volatility, respectively, $W_t^{\mathbb{A}}$ is a standard Wiener process under measure $\mathbb{A}$, and the deterministic reversion level $\mu(t)$ is given by

$$\mu(t) = f^M(0,t) + \frac{\eta^2}{2\kappa^2}\left(1 - e^{-\kappa t}\right)^2. \tag{5.16}$$

where parameters κ, η have been calibrated by empirical time series of the short rate.

We take this form for the dynamics that reflect the real-world evolution of the short rate. There may be other choices for the definition of the observed real-world dynamics in combination with risk-neutral dynamics, such as proposed by Hull et al. [48].

5.3.2. G2++ MODEL

When the risk-neutral short rate $\{r_t\}_0^T$ under the risk-neutral measure $\mathbb{Q}$ follows the G2++ model, the stochastic process $\mathbf{X}_t = [x_t^{(1)}, x_t^{(2)}]^T$ follows the dynamics:

$$
\begin{aligned}
r_t &= x_t^{(1)} + x_t^{(2)} + \gamma(t), && (5.17)\\
dx_t^{(1)} &= -\lambda_1 x_t^{(1)} dt + \sigma_1 dW_t^{\mathbb{Q},1}, && (5.18)\\
dx_t^{(2)} &= -\lambda_2 x_t^{(2)} dt + \sigma_2 \left(\rho dW_t^{\mathbb{Q},1} + \sqrt{1-\rho^2} dW_t^{\mathbb{Q},2} \right), && (5.19)
\end{aligned}
$$

where $x_0^{(1)} = 0$, $y_0^{(2)} = 0$, parameters $\lambda_1, \lambda_2, \sigma_1, \sigma_2$ are positive constants, and $(W_t^{\mathbb{Q},1}, W_t^{\mathbb{Q},2})$ is a standard two-dimensional Brownian motion with correlation $|\rho| < 1$. The deterministic function $\gamma(t)$ is given by:

$$
\begin{aligned}
\gamma(t) &= f^M(0,t) + \frac{\sigma_1^2}{2\lambda_1}\left(1 - e^{-\lambda_1 t}\right)^2 + \frac{\sigma_2^2}{2\lambda_2}\left(1 - e^{-\lambda_2 t}\right)^2 \\
&\quad + \rho \frac{\sigma_1 \sigma_2}{\lambda_1 \lambda_2}\left(1 - e^{-\lambda_1 t}\right)\left(1 - e^{-\lambda_2 t}\right). && (5.20)
\end{aligned}
$$

The formulas of a ZCB and the analytic formulas of the discounted ChF under the G2++ model are given in Appendix 2 in this chapter.

Here we also present the dynamics representing the real-world evolution of the underlying factors, by

$$
r_t = x_t^{(1)} + x_t^{(2)} + \nu(t), \tag{5.21}
$$

with $r_0 = f^M(0,0)$ and the process $\mathbf{x}_t = [x_t^{(1)}, x_t^{(2)}]^T$ satisfies

$$
\begin{aligned}
dx_t^{(1)} &= -\kappa_1 x_t^{(1)} dt + \eta_1 dW_t^{\mathbb{A},1}, \\
dx_t^{(2)} &= -\kappa_2 x_t^{(2)} dt + \eta_2 \left(\hat{\rho} dW_t^{\mathbb{A},1} + \sqrt{1-\hat{\rho}^2} dW_t^{\mathbb{A},2} \right), && (5.22)
\end{aligned}
$$

where $x_0^{(1)} = 0$, $y_0^{(2)} = 0$, and $(W_t^{\mathbb{A},1}, W_t^{\mathbb{A},2})$ is a two-dimensional Brownian motion with correlation $|\hat{\rho}| < 1$, and $\nu(t)$ given by

$$
\begin{aligned}
\nu(t) &= f^M(0,t) + \frac{\eta_1^2}{2\kappa_1}\left(1 - e^{-\kappa_1 t}\right)^2 + \frac{\eta_2^2}{2\kappa_2}\left(1 - e^{-\kappa_2 t}\right)^2 \\
&\quad + \hat{\rho} \frac{\eta_1 \eta_2}{\kappa_1 \kappa_2}\left(1 - e^{-\kappa_1 t}\right)\left(1 - e^{-\kappa_2 t}\right). && (5.23)
\end{aligned}
$$

The positive constants κ_1, κ_2, η_1, η_2 and the correlation $\hat{\rho}$ are calibrated by historical data.

5.4. STOCHASTIC GRID BUNDLING METHOD, SGBM

The computation of the conditional risk-neutral expectation is the most expensive part in the algorithm for dynamics (5.8). We propose an algorithm based on SGBM, that can *approximate* the continuation function in (5.9) by basic polynomial functions on the risk-neutral scenarios. Based on these approximated continuation functions, we can perform risk-neutral valuation on the real-world scenarios without nested simulations. To compute CVA and PFE, one only needs one set of H_q risk-neutral scenarios and one set of H_a real-world scenarios

Pricing in the context of the SGBM approach is based on risk-neural scenarios; Computation of discounted expected option values is performed locally in so-called bundles by means of local regression. We will store the bundle-wise approximated continuation functions, and use them to compute exposure profiles for the observed real-world scenarios for a Bermudan swaption.

5.4.1. RISK-NEUTRAL SCENARIOS

Let $\{X^q_{1,h},\dots,X^q_{M,h}\}_{h=1}^{H_q}$ be H_q scenarios where the underlying factor evolves with the risk-neutral model. Pricing is done by a backward-in-time iteration as in (5.8), from time t_M to time $t_0 = 0$.

To initialize the computation, the option value at expiry $t_M = T_N$ is computed as the immediate payoff g_N, i.e. the option value realized on the h-th scenario at time t_M, $\hat{v}^q_{M,h} = g_N(X^q_{M,h})$. As the option either expires or is exercised at time t_M, the exposure equals zero for all paths at time t_M, $\{\hat{E}^q_{M,h} = 0\}_{h=1}^{H_q}$.

At monitoring dates t_m, $m = M-1,\dots,1$, J bundles $\{\mathscr{B}_{m,j}\}_{j=1}^{J}$ are defined, consisting of Monte Carlo path values at t_m, that have very similar realized values based on the cross-sectional risk-neutral samples $\{X^q_{m,h}\}_{h=1}^{H_q}$. The realized values of the risk-neutral paths form a bounded domain, and these bundles divide the domain into disjoint sub-domains $\{\mathscr{D}_{m,j}\}_{j=1}^{J}$.

Figure 5.2 shows the Monte Carlo paths in four bundles and the associated disjoint sub-domains at an exposure monitoring date in the case of a one-dimensional model, i.e. the Hull-White model. The bundles are based on the values of the realized short rate at time $t = 0.5$. The continuation function $c(t_m,\cdot)$ is approximated 'in a bundle-wise fashion' by approximating the value function at time t_{m+1} for the paths in a bundle.

For $j = 1,\dots,J$, on the MC paths in bundle $\mathscr{B}_{m,j}$, value function $V(t_{m+1},\cdot)$ is approximated by a linear combination of monomials up to order d, i.e.

$$V(t_{m+1},\mathbf{X}_{m+1}) \approx \sum_{|k|=0}^{d} \beta_k^{m,j} (\mathbf{X}_{m+1})^k, \tag{5.24}$$

where k represents a multi-index notation in the case of the G2++ model, and an integer in the case of the Hull-White model, the coefficients $\beta_k^{m,j}$ of the k-th basis function minimize the sum of squared residuals over the paths in bundle $\mathscr{B}_{m,j}$, i.e.,

$$\sum_{h\in\mathscr{B}_{mj}} \left(\hat{v}^q_{m+1,h} - \sum_{|k|=0}^{d} \beta_k^{m,j} \left(X^q_{m+1,h}\right)^k \right)^2, \tag{5.25}$$

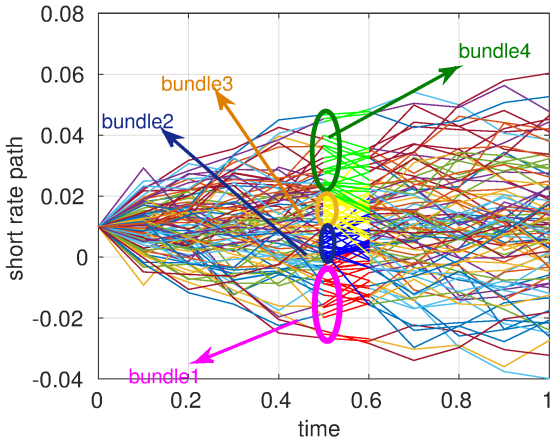

Figure 5.2: An example of bundles and the disjoint sub-domains at time $t = 0.5$.

with $\{\hat{v}^q_{m+1,h}\}_{h=1}^{H_q}$ the option values at time t_{m+1} on the cross-sectional sample $\{X^q_{m+1,h}\}_{h=1}^{H_q}$.

Using the approximated value function in (5.24) instead of the 'true value' in (5.9), the continuation function on $\mathscr{D}_{m,j}$ can be approximated by:

$$c(t_m, \mathbf{x}) \approx \sum_{|k|=0}^{d} \beta_k^{m,j} \psi_k(\mathbf{x}, t_m, t_{m+1}), \tag{5.26}$$

where $\mathbf{x} \in \mathscr{D}_{m,j}$ and function ψ_k is the conditional risk-neutral discounted expectation of basis function ϕ_k, defined by

$$\psi_k(\mathbf{x}, t_m, t_{m+1}) := \mathbb{E}^{\mathbb{Q}}\left[\frac{B_m}{B_{m+1}}(\mathbf{X}_{m+1})^k \middle| \mathbf{X}_m = \mathbf{x}\right]. \tag{5.27}$$

The analytic formulas for $\{\psi_k\}_{k=0}^d$ can be obtained easily, and often analytically, when polynomial terms are chosen as the basis functions, see Section 5.4.4.

The expected values on the paths of the bundle $\mathscr{B}_{m,j}$ can then be approximated by

$$\hat{c}^q_{m,h} \approx \sum_{|k|=0}^{d} \beta_k^{m,j} \psi_k(X^q_{m,h}, t_m, t_{m+1}), \tag{5.28}$$

where $h \in \mathscr{B}_{m,j}$.

After computation of the continuation values for all paths $\{\hat{c}^q_{m,h}\}_{h=1}^{H_q}$ at time t_m, we determine the option value at time t_m by:

$$\hat{v}^q_{m,h} = \begin{cases} \max\left(g_n(X^q_{m,h}), \hat{c}^q_{m,h}\right), & t_m = T_n, \\ \hat{c}^q_{m,h}, & t_m \in (T_n, T_{n+1}), \end{cases} \tag{5.29}$$

where g_n is the exercise function.

The exposure value on the h-th path from time t_m to expiry t_M is updated by the following scheme:

1. when exercised at exercise time $t_m = T_n$, value zero is assigned to the exposures along the path from time t_m to expiry, i.e. $\hat{E}^q_{k,h} = 0, \quad k = m, \ldots, M$;

2. when the option is 'alive' at an exercise date, or when t_m is a monitoring date between to exercise dates, the exposure at the path is equal to the approximated continuation value: $\hat{E}^q_{m,h} = \hat{c}^q_{m,h}$, and exposure values at later times remain unchanged.

The algorithm proceeds by moving one time step backward to time t_{m-1}, where the paths are again divided into new bundles based on the realized values $\{X^q_{m-1,h}\}_{h=1}^{H_q}$, and the continuation function is approximated in a bundle-wise fashion. Option values are evaluated and the exposure profile is updated. The algorithm proceeds, recursively, back to $t_0 = 0$. At time t_0 regression takes place for all paths to get the coefficients $\{\beta^0_k\}_{k=0}^d$, i.e. the option value at time zero is approximated by

$$\hat{v}^q_0 \approx \sum_{|k|=0}^{d} \beta^0_k \psi_k(x_0, t_0, t_1). \tag{5.30}$$

During the backward recursive iteration, information about the boundaries of the disjoint sub-domains, $\mathscr{D}_{m,j}$, is stored along with the associated coefficients $\{\beta^{m,j}_k\}_{k=0}^d$ for each index, $j = 1, \ldots, J$, at each monitoring date, t_m, $m = 0, \ldots, M-1$. Based on this information, we can retrieve the piece-wise approximated continuation function for each time t_m.

With the risk-neutral exposure profiles, $\{\hat{E}^q_{1,h}, \ldots, \hat{E}^q_{M,h},\}_{h=1}^{H_q}$, the discounted EE of a Bermudan swaption can be approximated by:

$$\mathrm{EE}^*(t_m) \approx \frac{1}{H_q} \sum_{h=1}^{H_q} \exp\left(- \sum_{k=0}^{m+1} \frac{1}{2} \left(\hat{r}^q_{k,h} + \hat{r}^q_{k+1,h} \right) \Delta t_k \right) \hat{E}^q_{m,h}, \tag{5.31}$$

where $\left\{ \hat{r}^q_{1j}, \ldots, \hat{r}^q_{Mj} \right\}_{j=1}^{H_q}$ represent simulated risk-neutral short rate values.

5.4.2. REAL-WORLD SCENARIOS

During the computations on the risk-neutral scenarios, we have stored the bundle-wise coefficients $\{\beta^{m,j}_k\}_{k=0}^d$ and the associated sub-domains $\{\mathscr{D}_{m,j}\}_{j=1}^J$, by which we can perform valuation and exposure computation for any scenario without nested simulation.

We present the steps to compute exposure profiles on a set of H_a observed real-world scenarios $\{X^a_{1,h}, \ldots, X^a_{M,h}\}$. These profiles are also determined by a backward iteration from time t_M till time t_0.

At expiry date t_M, the exposure equals zero, $\{\hat{E}^a_{M,h} = 0\}_{h=1}^{H_a}$;

At a monitoring dates $t_m < t_M$, for each index $j = 1, \ldots, J$, we determine those paths for which $X^a_{m,h} \in \mathscr{D}_{m,h}$, and compute the continuation values for these paths by

$$\hat{c}^a_{m,h} \approx \sum_{|k|=0}^{d} \beta^{m,j}_k \psi_k(X^a_{m,h}, t_m, t_{m+1}), \tag{5.32}$$

where $X^a_{m,h} \in \mathscr{D}_{m,j}$.

Based on these continuation values, we update the exposure profile on this set of real-world scenarios.

At an exercise time $t_m = T_n$, we compare the approximated continuation value $\hat{c}^a_{m,h}$ with the immediate exercise values $g_n(X^a_{m,h})$ for each path; when the immediate exercise value is largest, the option is exercised at this path at time t_m, and exposure values at this path from time t_m to expiry are set to zero, i.e. $\hat{E}^a_{k,h} = 0, \quad k = m, \ldots, M$.

Otherwise, $\hat{E}^a_{m,h} = \hat{c}^a_{m,h}$ and the later exposure values remain unchanged.

When t_m is an intermediate exposure monitoring date, the exposure values are equal to the continuation values in (5.32).

Notice that the time-zero option value is the same for the risk-neutral and the real-world scenarios, i.e. $\hat{v}^q_0 = \hat{v}^a_0$. Values of the observed real-world PFE and EE curves at monitoring dates t_m can be approximated by:

$$\begin{aligned} \text{PFE}(t_m) &= \text{quantile}(\hat{E}^a_{m,h}, 99\%), \\ \text{EE}(t_m) &= \frac{1}{H_a} \sum_{h=1}^{H_a} \hat{E}^a_{m,h}. \end{aligned} \tag{5.33}$$

5.4.3. SGBM BUNDLING TECHNIQUE

An essential technique within SGBM is the bundling of asset path values at each monitoring date, based on the cross-sectional risk-neutral samples. Numerical experiments have shown that the algorithm converges w.r.t. the number of bundles [32, 50].

Various bundling techniques have been presented in the literature, such as the recursive-bifurcation method, k-means clustering [50] and the equal-number bundling method [32]. Here, we use the *equal-number bundling* technique, as explained in Chapter 3. In the equal-number bundling, at each time step t_m, we rank the paths by their realized values, $\{X^q_{m,h}\}_{h=1}^{H_q}$, and place the paths with indices between $(j-1)H_q/J+1$ and jH_q/J into the j-th bundle, $\mathscr{B}_{m,j}$, $j = 1, \ldots, J-1$. The remaining paths are placed in the J-th bundle, $\mathscr{B}_{m,J}$. Asset paths do not overlap among bundles at time t_m and each path is placed in a bundle.

The advantage of the equal-number bundling technique is that the number of paths within each bundle is proportional to the total number of asset paths. An appropriate number of paths in each bundle is important for accuracy during the local regression. As mentioned, the bundling technique is also used to determine the disjoint sub-domains on which the value function is approximated in a piece-wise fashion.

For high-dimensional problems, one can either use the equal-number bundling technique along each dimension, as employed in [32]; or one can project the high-dimensional vector onto a one-dimensional vector and then apply the equal-number bundling technique, see [50, 63]. In this chapter, for SGBM computation under the G2++ model, we project the 2D variable $(x^{(1)}_t, x^{(2)}_t)$ onto $(x^{(1)}_t + x^{(2)}_t)$ for using the one-dimensional equal-number bundling technique.

5.4.4. FORMULAS FOR THE DISCOUNTED MOMENTS IN SGBM

When we choose *monomials* as the basis functions within the bundles in SGBM, the conditional expectation of the discounted basis functions is equal to the *discounted moments*. There is a direct link between the discounted moments and the discounted characteristic function (dChF), which we can also use to derive analytic formulas for the discounted moments.

In the one-dimensional case, i.e. the Hull-White model, let the basis functions be $(r_t)^k$, $k = 0, \ldots, d$. The discounted moments ψ_k, conditional on r_m over the period (t_m, t_{m+1}), are given by:

$$\psi_k^{\mathrm{HW}}(r_m, t_m, t_{m+1}) := \mathbb{E}^{\mathbb{Q}}\left[\exp\left(-\int_{t_m}^{t_{m+1}} r_s ds\right)(r_{m+1})^k \Big| r_m\right]. \tag{5.34}$$

In the two-dimensional case, i.e. the G2++ model, let the basis function be $\left(x_t^{(1)}\right)^{k_1}\left(x_t^{(2)}\right)^{k_2}$, $k = (k_1, k_2)$ and $|k| = 0, \ldots, d$. The k-th discounted moments over the period (t_m, t_{m+1}) conditional on $\mathbf{X}_m$, are given by

$$\psi_k^{\mathrm{G2}}(\mathbf{X}_m, t_m, t_{m+1}) := \mathbb{E}^{\mathbb{Q}}\left[\exp\left(-\int_{t_m}^{t_{m+1}} r_s ds\right)\left(x_{m+1}^{(1)}\right)^{k_1}\left(x_{m+1}^{(2)}\right)^{k_2} \Big| \mathbf{X}_m\right]. \tag{5.35}$$

Further the corresponding discounted moments can be obtained via the relations between dChF and moments presented in (1.29).

5.5. LEAST SQUARES METHOD, LSM

In this section, we will build an algorithm based on the Least Squares Method (LSM) via the same technique as presented in Section 5.4.

LSM is a regression-based Monte Carlo method, which is very popular among practitioners. The objective of the LSM algorithm is to find for each path the optimal stopping policy at each exercise time T_n, and the option value is computed as the average value of the generated discounted cash flows. The optimal early-exercise policy for the 'in-the-money' paths is determined by comparing the immediate exercise value and the approximated continuation value, which is approximated by a linear combination of (global) basis functions $\{\phi_k\}_{k=0}^d$.

One can always combine the (expensive) nested Monte Carlo simulation with LSM for the computation of EE and PFE on observed real-world scenarios. We will however adapt the original LSM algorithm to obtain a more efficient method for computing risk-neutral and real-world exposures. The technique is similar to the one described for SGBM: valuation on the risk-neutral scenarios, approximation of the continuation function, and computation of risk-neutral and real-world exposure quantities.

The involved part in LSM is that discounted cash flows, realized on a path, are not representative for the 'true' continuation values. In the LSM algorithm, the approximated continuation values are only used to determine the exercise policy, and therefore one cannot use them to determine the maximum of the immediate exercise value and discounted cash flows to approximate the option value [32], as is done in SGBM.

The challenge is thus to approximate exposure values by means of the realized discounted cash flows over all paths.

In [54], Joshi presents a way to employ realized discounted cash flows and the sign of the regressed values for an efficient computation of CVA on risk-neutral scenarios. However, since the average of the discounted cash flows is not the value of a contract under the observed real-world measure, it cannot be used to compute real-world EE or PFE quantities.

Here, we propose two LSM-based algorithms for approximation of continuation values with realized cash flows. They can be seen as alternative algorithms compared to SGBM for computation of exposure values, when we do not have expressions for the discounted moments (or when LSM is the method of choice for many other tasks). We will test the accuracy of the algorithms compared to SGBM and to reference values generated by the COS method in the numerical section.

5.5.1. RISK-NEUTRAL SCENARIOS

First of all, we briefly explain the original LSM algorithm with the risk-neutral scenarios. At the final exercise date, $t_M = T_N$, the option holder can either exercise an option or not, and the generated cash flows are given by $q_{M,h} = g_N(X^q_{M,h}), \quad h = 1,\dots,K^q$.

At exposure monitoring dates $t_m \in (T_{n-1}, T_n)$ at which the option cannot be exercised, the realized discounted cash flows are updated by:

$$q_{m,h} = q_{m+1,h} \exp\Big(-\frac{1}{2}(\hat{r}^q_{m,h} + \hat{r}^q_{m+1,h})\Delta t\Big). \tag{5.36}$$

At an exercise date $t_m = T_n$ prior to the last exercise opportunity, the exercise decision is based on the comparison of the immediate payoff by exercising and the continuation value when holding the option on the 'in-the-money' paths; the continuation values at those 'in-the-money' paths are approximated by projecting the (discounted) cash flows of these paths onto some global basis functions $\{\phi_1,\dots,\phi_B\}$;

The option is exercised at an in-the-money path, when the payoff is larger than the continuation value. After determining the exercise strategy at each path, the discounted cash flows read:

$$q_{m,h} = \begin{cases} g_n\left(X^q_{m,h}\right), & \text{exercised,} \\ q_{m+1,h} \exp\Big(-\frac{1}{2}(\hat{r}^q_{m,h} + \hat{r}^q_{m+1,h})\Delta t\Big), & \text{to be continued.} \end{cases} \tag{5.37}$$

Again computation of the discounted cash flows at any monitoring date takes place recursively, backward in time. At time $t_0 = 0$, the option value is approximated by $\hat{v}^q_{0,h} \approx \frac{1}{H_q}\sum_{h=1}^{H_q} q_{0,h}$.

During the backward recursion, the discounted cash flows realized on all paths at each monitoring date t_m are computed.

For the computation of the real-world EE and PFE quantities, valuation needs to be done *on the whole domain* of realized asset values, as we need the continuation values at each monitoring date for all paths. We therefore propose to use the realized discounted cash flows determined by (5.37) or (5.36) on the risk-neutral scenarios.

One possible algorithm in the LSM context is that we also employ two disjoint sub-domains, similar as in SGBM. At each monitoring date $t_m \in (T_{n-1}, T_n]$, MC paths are divided into two *bundles* based on the realized values of the underlying variable, so that the approximation can take place in two disjoint sub-domains, given by

$$\mathscr{U}_{n,1} = \{\mathbf{x} \big| g_n(\mathbf{x}) \leq 0\}, \quad \mathscr{U}_{n,2} = \{\mathbf{x} \big| g_n(\mathbf{x}) > 0\}. \tag{5.38}$$

The continuation function is approximated on these two sub-domains as

$$c(t_m, \mathbf{x}) \approx \sum_{|k|=0}^{d} \zeta_k^{m,j} \mathbf{x}^k, \tag{5.39}$$

where $\mathbf{x} \in \mathscr{U}_{n,j}$, the coefficients $\zeta_k(t_m, j)$ are obtained by minimizing the sum of squared residuals over the two bundles, respectively, given by:

$$\sum_{X_{m,h}^q \in \mathscr{U}_{n,j}} \left(q_{m+1,h} \exp\left(-\frac{1}{2}(\hat{r}_{m,h}^q + \hat{r}_{m+1,h}^q)\Delta t \right) - \sum_{k=1}^{B} \zeta_k(t_m, j) \left(X_{m,h}^q \right)^k \right)^2. \tag{5.40}$$

We refer to this technique as the *LSM-bundle* technique.

The other possible algorithm is to perform the regression over all MC paths, and to compute the approximated continuation function on each path. The regression is as in (5.40) using basis functions and discounted cash flows, but for all paths. We call this the *LSM-all* algorithm. Notice that the exercise decision is still based on the 'in-the-money' paths with approximated payoff using (5.39) at exercise dates $T_n < T_N$, $n = 1, \ldots, N-1$.

We compute the risk-neutral exposure profiles with the approximated value functions in (5.39) by means of the same backward recursion procedure as in Section 5.4.1.

5.5.2. REAL-WORLD SCENARIOS

The LSM-bundle algorithm can directly be used for computing exposure on the observed real-world scenarios. It is based on the same backward iteration as in Section 5.4.2, however, the continuation values are computed by the function in (5.39), i.e.

$$\hat{c}_{m,h}^a \approx \sum_{|k|=0}^{d} \zeta_k^{m,j} \left(X_{m,h}^a \right)^k. \tag{5.41}$$

At an early-exercise date $t_m = T_n < T_N$, the early-exercise policy is determined for 'in-the-money' paths by comparing $\hat{c}_{m,h}^a$ and the immediate exercise value $g_n(X_{m,h}^a)$. Exposure values along the path from time t_m to expiry are set to zero if the option at a path is exercised.

By the LSM-all algorithm, we use the continuation function approximated in (5.39) for determining the optimal early-exercise time on each real-world path, and the regressed function is based on all paths to compute exposure values. We will compare the LSM-bundle and LSM-all algorithms in the numerical section part.

5.5.3. DIFFERENCES BETWEEN SGBM AND LSM ALGORITHMS

SGBM differs from LSM w.r.t. the bundling and the local regression based on the discounted moments. By these components, SGBM approximates the continuation function in a more accurate way than LSM, but at a (small) additional computational cost. Here, we give some insights in these differences.

The use of SGBM bundles may improve the local approximation on the disjoint subdomains, and we can reduce the number of basis functions.

Another important feature of SGBM is that 'option values' are obtained from regression, to obtain the coefficients for the continuation function.

Loosely speaking, the continuation function is approximated locally on the bounded sub-domains $\{\mathscr{D}_{m,j}\}_{j=1}^{J}$ by projection on the functions $\{\psi_k\}_{k=0}^{d}$.

Compared to SGBM, LSM is based on the discounted cash flows for regression to approximate the expected payoff, however, discounted cash flows do not represent the 'realized expected payoff' on all MC paths. In LSM the expected payoff is only used to determine the optimal early-exercise time and not the option value. One cannot compute the option value by using the maximum of the expected payoff and the exercise value, as it will lead to an upward bias for the time-zero option value [64].

SGBM does not suffer from this and the maximum of the exercise value and the regressed continuation values gives us the *direct estimator*. It is recommended to also compute the *path estimator* for convergence of the SGBM algorithm. Upon convergence, the direct and the path estimators should be very close [50].

The LSM approach is a very efficient and adaptive algorithm for computing option values at time zero. The LSM-based algorithms for computing exposure can be regarded as alternative ways of computing the future exposure distributions based on simulation. We will analyze the accuracy of all variants in the numerical sections.

5.6. THE COS METHOD

In this section we explain the computation of the continuation function of Bermudan swaptions under the one-factor Hull-White model by the COS method. The COS method is an efficient and accurate method based on Fourier-cosine expansions. It can be used to determine reference values for the exposure. For Lévy processes and early-exercise options, the computational speed of the COS method can be enhanced by incorporating the Fast Fourier Transform (FFT) into the computations. We cannot employ the FFT, because resulting matrices with the Hull-White model do not have a special form (Toeplitz and Hankel matrices, see [28]) to employ the FFT.

In addition, we use the 2D cosine-expansions developed in [72] here to recover the density under the G2++ model.

5.6.1. HULL-WHITE MODEL

First of all, we write out the payoff function under the Hull-White model using (5.63) and (5.5). The payoff function g_n at time T_n, $n = 1,2\ldots,N$, under the Hull-White model is given by

$$g_n(x) = N_0\delta\left(1 - \sum_{j=n}^{N} \hat{c}_j \overline{A}(T_n, T_{j+1}) \exp\left(\overline{B}(T_n, T_{j+1})x\right)\right), \tag{5.42}$$

where $\hat{c}_j = \tau_j K$, $j = n, \ldots, N-1$, $\hat{c}_N = 1 + \tau_N K$, $\overline{A}$ and $\overline{B}$ are coefficients associated to the ZCB price, given in (5.63), $\delta = 1$ for a payer swaption and $\delta = -1$ for a receiver swaption.

In a one-dimensional model, we write $\mathbf{X}_t = x_t$. We will approximate the density function on an integration range $[a, b]$, which should be chosen such that the integral of the discounted density function over the region $[a, b]$ resembles very well the value of a ZCB between time t and T given $X_t = x$. In this chapter, we choose the integration range over a period $[0, T]$ by

$$a = \theta(T) - \sqrt{\frac{\sigma^2}{2\lambda}\left[1 - e^{-2\lambda T}\right]}L, \quad b = \theta(T) + \sqrt{\frac{\sigma^2}{2\lambda}\left[1 - e^{-2\lambda T}\right]}L, \tag{5.43}$$

where L is the parameter chosen to control the length of the integration range. In the numerical section, we choose $L = 8$.

The discounted density can be recovered by a linear combination of cosine terms expressed by[28]

$$\hat{f}_{x_{m+1}|x_m}(y; x) \approx \frac{2}{b-a}\sum_{k=0}^{Q-1}{}' \mathscr{P}_k(x, t_m, t_{m+1}) \cos\left(k\pi \frac{y-a}{b-a}\right), \tag{5.44}$$

where the symbol $\sum'$ in (5.44) implies that the first term of the summation is multiplied by $\frac{1}{2}$, and the Fourier-coefficients $\mathscr{P}_k$ are given by:

$$\mathscr{P}_k(x, t_m, t_{m+1}) := \mathrm{Re}\left\{\varphi^{\mathrm{HW}}\left(\frac{k\pi}{b-a}; t_m, t_{m+1}, x\right) \cdot \exp\left(-\frac{iak\pi}{b-a}\right)\right\}, \tag{5.45}$$

where φ^{HW} is the discounted ChF under the Hull-White model, given in (5.64) in Appendix 1.

With equation (5.9), the continuation function, conditional on $X_{t_m} = x$, at any monitoring date $t_m \in [0, T_N)$ can be computed as an integral over $[a, b]$:

$$\begin{aligned} c(t_m, x) &\approx \int_a^b V(t_{m+1}, y) \hat{f}_{x_{m+1}|x_m}(y; t_m, t_{m+1}, x)\, dy, \\ &\approx \frac{2}{b-a}\sum_{k=0}^{Q-1}{}' \mathscr{P}_k(x, t_m, t_{m+1}) \mathscr{V}_k(t_{m+1}), \end{aligned} \tag{5.46}$$

where the coefficients $\mathscr{V}_k(t_{m+1})$ are defined by

$$\mathscr{V}_k(t_{m+1}) := \int_a^b V(t_{m+1}, y) \cos\left(k\pi \frac{y-a}{b-a}\right) dy. \tag{5.47}$$

The coefficients $\{\mathscr{V}_k\}_{k=0}^{Q-1}$ can be computed at exposure monitoring dates $\{t_m\}_{m=1}^{M}$, by the backward recursion as in (5.8). Analytic formulas, in the case of the Hull-White model, for the coefficients $\{\mathscr{V}_k\}_{k=0}^{Q-1}$ can be computed by backward recursion.

At the expiry date, $t_M = T_N$, the option value equals the payoff of the underlying swap, i.e. $V(t_M,\cdot) = g_N(\cdot)$. We are only interested in the 'in-the-money' region regarding the function g_n, for which we need to solve $g_N(x^*(T_N)) = 0$.

Function g_N is positive on the range $(a, x^*(T_N))$ for a receiver Bermudan swaption, and on the range $(x^*(T_N), b)$ for a payer Bermudan swaption. We compute the integral on the range where $g_N > 0$ for the coefficients $\mathcal{V}_k(t_M)$. The formulas for the integral are given by:

$$\begin{aligned}\mathcal{V}_k(t_M) &= \int_a^b g_N(y)\cos\left(k\pi\frac{y-a}{b-a}\right)dy \\ &= \begin{cases}\mathcal{G}_k\left(a, x^*(T_N), T_N\right), & \text{for a receiver swaption,}\\ \mathcal{G}_k\left(x^*(T_N), b, T_N\right), & \text{for a payer swaption,}\end{cases}\end{aligned} \tag{5.48}$$

where the coefficient $\mathcal{G}_k$ is presented in Appendix 3.

In the COS method, computation also takes place in backward fashion. We distinguish an early-exercise date from an intermediate date between two exercise times. At an intermediate date, $t_m \in (T_{n-1}, T_n)$, $V(t_m,\cdot) = c(t_m,\cdot)$, thus the coefficients $\mathcal{V}_k$ at time t_m are given by

$$\mathcal{V}_k(t_m) = \int_a^b c(t_m, y)\cos\left(k\pi\frac{y-a}{b-a}\right)dy = \mathcal{C}_k(a, b, t_m), \tag{5.49}$$

where the coefficient $\mathcal{C}_k$ is presented in Appendix 3.

At an early-exercise date $t_m = T_n$, $n = N-1,\ldots,1$, the option value is the maximum of the continuation value and the immediate exercise value, hence we solve the following equation

$$c\left(T_n, x^*(T_n)\right) - g_n\left(x^*(T_n)\right) = 0.$$

Solution $x^*(T_n)$ represents the optimal early-exercise boundary at time T_n. The equation can be solved by some root-finding algorithm, such as the Newton-Raphson method.

The coefficients $\{\mathcal{V}_k(t_m)\}_{k=0}^{Q-1}$ at time $t_m = T_n$ with the optimal exercise value $x^*(T_n)$ are given by:

$$\begin{aligned}\mathcal{V}_k(T_n) &= \int_a^b \max\left(c(T_n, y), g_n(y)\right)\cos\left(k\pi\frac{y-a}{b-a}\right)dy \\ &= \begin{cases}\mathcal{G}_k\left(x^*(T_n), b, T_n\right) + \mathcal{C}_k\left(a, x^*(T_n), T_n\right), & \text{payer}\\ \mathcal{G}_k\left(a, x^*(T_n), T_n\right) + \mathcal{C}_k\left(x^*(T_n), b, T_n\right), & \text{receiver}\end{cases}\end{aligned} \tag{5.50}$$

The computation of the coefficients $\{\mathcal{V}_k\}_{k=0}^{Q-1}$ depends on the early-exercise boundary value at each exercise date T_n. The continuation function from the Fourier-cosine expansions in (5.46) converges with respect to the number of Fourier terms Q when the integration interval is chosen properly.

At each t_m, the continuation values for all scenarios can be computed by (5.46). Risk-neutral and real-world exposure profiles are obtained by backward iteration as in Sections 5.4.1 and 5.4.2. One can employ interpolation to enhance the computational speed for the computation of the continuation values.

5.6.2. G2++ MODEL

This section presents computation of the Bermudan swaptions under the G2++ model applying the 2D-cosine-expansion techniques [72]. First, we write out the the payoff function g_n under the G2++ model at time T_n,

$$g_n(\mathbf{x}) = N_0\delta\left(1-\sum_{j=n}^{N}\hat{c}_j\overline{C}(T_n,T_{j+1})\exp\left(\overline{D}_1(T_n,T_{j+1})x^{(1)}+\overline{D}_2(T_n,T_{j+1})x^{(2)}\right)\right), \tag{5.51}$$

where $\hat{c}_j=\tau_j K$, $j=n,\ldots,N-1$, $\hat{c}_N=1+\tau_N K$, $\overline{C}$, $\overline{D}_1$ and $\overline{D_2}$ are coefficients associated to the ZCB price, given in (5.68), $\delta=1$ for a payer swaption and $\delta=-1$ for a receiver swaption.

On an integration range $[a_1,b_1]\times[a_2,b_2]$, we approximate the discounted density by its Fourier-cosine expansions [72]

$$\begin{aligned}\hat{f}_{\mathbf{X}_{m+1}|\mathbf{X}_m}(\mathbf{y};\mathbf{x}) \;\approx\; & \frac{2}{b_1-a_1}\frac{2}{b_2-a_2}\sum_{k_1=0}^{Q_1-1}{}'\sum_{k_2=0}^{Q_2-1}{}'\mathscr{P}_{k_1,k_2}(\mathbf{x},t_m,t_{m+1})\cdot\\ & \cos\left(k_1\pi\frac{y_1-a_1}{b_1-a_1}\right)\cos\left(k_2\pi\frac{y_2-a_2}{b_2-a_2}\right),\end{aligned} \tag{5.52}$$

where the symbol $\sum'$ in (5.44) implies that the first term of the summation is multiplied by $\frac{1}{2}$, Q_1 and Q_2 represent the number of cosine terms, and the Fourier-coefficients $\mathscr{P}_k$ are given by:

$$\begin{aligned}&\mathscr{P}_{k_1,k_2}(\mathbf{x},t_m,t_{m+1})\\ &=\frac{1}{2}\left[\mathrm{Re}\left\{\varphi_{\mathrm{G2}}\left(\frac{k_1\pi}{b_1-a_1},\frac{k_2\pi}{b_2-a_2};t_m,t_{m+1},\mathbf{x}\right)\exp\left(-\frac{ik_1\pi a_1}{b_1-a_1}-\frac{ik_2\pi a_2}{b_2-a_2}\right)\right\}\right.\\ &\quad\left.+\mathrm{Re}\left\{\varphi_{\mathrm{G2}}\left(\frac{k_1\pi}{b_1-a_1},\frac{k_2\pi}{b_2-a_2};t_m,t_{m+1},\mathbf{x}\right)\exp\left(-\frac{ik_1\pi a_1}{b_1-a_1}+\frac{ik_2\pi a_2}{b_2-a_2}\right)\right\}\right],\end{aligned} \tag{5.53}$$

where φ_{G2} is the discounted ChF presented as (5.71) in Appendix 2.

The continuation function, conditional on $\mathbf{X}_{t_m}=\mathbf{x}$, at any exposure monitoring date $t_m\in[0,T_N)$ can be computed as an integral over $[a,b]$:

$$\begin{aligned}c(t_m,\mathbf{x}) \;&\approx\; \int_{a_1}^{b_1}\int_{a_2}^{b_2}V(t_{m+1},\mathbf{y})\hat{f}_{\mathbf{X}_{m+1}|\mathbf{X}_m}(\mathbf{y};\mathbf{x})d\mathbf{y},\\ &\approx\; \frac{2}{b_1-a_1}\frac{2}{b_2-a_2}\sum_{k_1=0}^{Q_1-1}{}'\sum_{k_2=0}^{Q_2-1}{}'\mathscr{P}_{k_1,k_2}(\mathbf{x},t_m,t_{m+1})\mathscr{V}_{k_1,k_2}(t_{m+1}),\end{aligned} \tag{5.54}$$

where the coefficients $\mathcal{V}_k(t_{m+1})$ are defined by

$$\mathcal{V}_{k_1,k_2}(t_{m+1}) := \int_{a_1}^{b_1}\int_{a_2}^{b_2} V(t_{m+1},\mathbf{y})\cos\left(k_1\pi\frac{y_1-a_1}{b_1-a_1}\right)\cos\left(k_2\pi\frac{y_2-a_2}{b_2-a_2}\right)dy_1\,dy_2, \tag{5.55}$$

with $k_1 = 0,\ldots,Q_1-1$, $k_2 = 0,\ldots,Q_2-1$.

The coefficients $\{\mathcal{V}_{k_1,k_2}\}$ can be computed at monitoring dates $\{t_m\}_{m=1}^M$, by the backward recursion as in (5.8) in a similar way as under the Hull-White model.

Now we need to deal with a 2D integral. At expiration, we need to find out the exercise region, and at those early-exercise dates T_n prior to the expiration T_N, we need to determine the continuation region and early-exercise region. For this purpose, we divide the domain of the first dimension, $[a_1,b_1]$, into Q_3 subintervals:

$$[a_1,b_1] = [w_1,w_2]\cup[w_2,w_3]\ldots\cup[w_l,w_{l+1}]\ldots\cup[w_{Q_3},w_{Q_3+1}], \tag{5.56}$$

and the center of the subinterval is given by $\bar{w}_l = \frac{1}{2}(w_l + w_{l+1})$.

For each subinterval, we determine the value $x^*_{l,m}$ at expiration and other early-exercise dates, i.e. when $t_m = T_n$, $n = N, N-1,\ldots,1$, for the computation of the integral.

- At time $t_M = T_N$, $x^*_{l,M}$ is the zero solution of the payoff function g_N over each small interval $[w_l,w_{l+1}]$

$$g_N\left([\bar{w}_l,x^*_{l,M}]^T\right) = 0. \tag{5.57}$$

  The region of positive payoff at time t_M is given by

$$[w_l,w_{l+1}]\times[x^*_{l,M},b_2],\ \text{payer};\quad [w_l,w_{l+1}]\times[a_2,x^*_{l,M}],\ \text{receiver}, \tag{5.58}$$

  with $l = 1,2\ldots,Q_3$.

- At time $t_m = T_n$, $n = N-1,\ldots,1$, $x^*_{l,m}$ determines the early-exercise boundary over each small interval $[w_l,w_{l+1}]$

$$g_N\left([\bar{w}_l,x^*_{l,M}]^T\right) = c\left(t_m,[\bar{w}_l,x^*_{l,M}]^T\right). \tag{5.59}$$

  The early-exercise region is given by

$$[w_l,w_{l+1}]\times[x^*_{l,m},b_2],\ \text{payer};\quad [w_l,w_{l+1}]\times[a_2,x^*_{l,m}],\ \text{receiver}, \tag{5.60}$$

  with $l = 1,2\ldots,Q_3$.

In this way, we compute the integration in (5.55) by the summation of integrals over Q_3 sub-domains at those early-exercise dates. For instance, for a payer option, the coefficients $\mathcal{V}_{k_1,k_2}$ at $t_m = T_n$ are approximated as

$$\mathcal{V}_{k_1,k_2}(t_m) \approx \sum_{l=1}^{Q_3}\left(\int_{w_l}^{w_{l+1}}\int_{x^*_{l,M}}^{b_2} g_n(\mathbf{y})d\mathbf{y} + \int_{w_l}^{w_{l+1}}\int_{a_2}^{x^*_{l,M}} c(t_m,\mathbf{y})d\mathbf{y}\right). \tag{5.61}$$

This technique of decomposing the integration domain has been demonstrated for computing Bermudan geometric basket put options by Ruijter and Oosterlee [72]. On those non-exercise dates, the integration is done over the whole region $[a_1,b_1]\times[a_2,b_2]$.

5.7. NUMERICAL EXPERIMENTS

We test the developed algorithms for different test cases under the one-factor Hull-White model and the two-factor G2++ model, respectively.

The notional amount of the underlying swap is set equal to 100. We define a $T_1 \times T_N$ Bermudan swaption as a Bermudan option written on the underlying swap that can be exercised between T_1 and T_N, the first and last early-exercise opportunities. The option can be exercised annually after T_1, and the payment of the underlying swap is made by the end of each year until fixed end date $T_{N+1} = T_N + 1$, i.e. the time fraction $\tau_n = 1$.

We take a fixed strike K to be $40\%S$, $100\%S$ and $160\%S$, where S is the swap rate associated with date T_1 and payment dates $\mathcal{T}_1 = \{T_2, \ldots, T_{N+1}\}$ given by equation (5.6). It is the ATM strike of the European swaption which expires at date T_1 associated with payment dates $\mathcal{T}_1$.

5.7.1. EXPERIMENTS WITH THE HULL-WHITE MODEL

We generate risk-neutral and real-world scenarios using the Hull-White model presented in Section 5.3 with risk-neutral parameters λ and η obtained by market prices, and real-world parameters κ and η by historical data.

Table 5.1 reports the time-zero option values, CVA and the real-world EPE and MPFE of 1Y×5Y and 4Y×10Y receiver Bermudan swaptions by the COS method, SGBM, and the LSM-bundle and LSM-all algorithms.

For the computation of future exposure distributions, one needs to combine the COS method computations with Monte Carlo scenario generation, so there are standard errors as well for the corresponding CVA, EPE and MPFE values. We present $100 \times$ CVA values instead of CVA to enlarge the differences and standard errors in Table 5.1.

The reference results by the COS method are obtained with $Q = 100$ cosine terms. In the SGBM algorithm, we use as basis functions $\{1, r, r^2\}$ for the approximation of the continuation values and 10 bundles containing an equal number of paths. In LSM, we choose a cubic function based on $\{1, r, r^2, r^3\}$ for the approximation. It is observed that SGBM and LSM converge with respect to the number of basis functions, and from our experiments we also find that for longer maturities, to main the accuracy, one needs either a larger number of basis functions or a larger number of bundles.

As shown in Table 5.1, the differences in the computed time-zero option values between all algorithms are very small. The LSM-bundle and LSM-all algorithms return the same time-zero option value as they are based on the same technique to determine the early-exercise policy. Compared to LSM, SGBM has improved accuracy with smaller variances. The absolute differences in V_0-values between SGBM and COS are as small as 10^{-3}, and the standard errors are less than 1%. The largest difference in V_0 between LSM and COS is $6 \cdot 10^{-3}$ with a standard error between $1-2\%$ in the table.

SGBM is particularly accurate for computing the MPFE values. Results in Table 5.1 show that the absolute differences for MPFE computed by SGBM and by COS are less than 0.01. The LSM-all algorithm does not result in satisfactory results for the exposure values. MPFE is over-estimated, while EPE is under-estimated. The LSM-bundle algorithm however shows significant improvements with smaller errors.

For the computation of EPE and MPFE, the results obtained via these algorithms have a similar standard error. It shows that the dominating factor in the EPE and MPFE

variances is connected to the number of generated scenarios.

1Y×5Y					
K/S	value	COS	SGBM	LSM-bundle	LSM-all
40%	V_0	4.126	4.127(0.00)	4.126(0.01)	4.126(0.01)
	MPFE	9.125(0.06)	9.118(0.06)	9.039(0.05)	8.8(0.05)
	EPE	1.704(0.00)	1.705(0.00)	1.708(0.01)	1.806(0.01)
	100CVA	15.87(0.01)	15.74(0.01)	15.75(0.08)	15.87(0.08)
100%	V_0	5.463	5.464(0.00)	5.461(0.01)	5.461(0.01)
	MPFE	11.07(0.05)	11.07(0.05)	11.06(0.05)	10.9(0.04)
	EPE	2.094(0.00)	2.096(0.00)	2.098(0.00)	2.215(0.00)
	100CVA	18.56(0.02)	18.33(0.02)	18.35(0.04)	18.44(0.04)
160%	V_0	7.11	7.11(0.00)	7.113(0.01)	7.113(0.01)
	MPFE	14.43(0.04)	14.42(0.04)	14.26(0.04)	13.92(0.04)
	EPE	2.368(0.00)	2.369(0.00)	2.372(0.01)	2.483(0.01)
	100CVA	21.28(0.02)	20.95(0.02)	20.98(0.05)	21.01(0.05)
4Y×10Y					
K/S	value	COS	SGBM	LSM-bundle	LSM-all
40%	V_0	4.235	4.236(0.00)	4.237(0.01)	4.237(0.01)
	MPFE	14.12(0.12)	14.13(0.12)	13.86(0.11)	13.16(0.09)
	EPE	1.827(0.00)	1.829(0.00)	1.834(0.01)	1.91(0.01)
	100CVA	38.22(0.02)	37.98(0.02)	38.04(0.13)	38.34(0.13)
100%	V_0	6.199	6.199(0.00)	6.201(0.02)	6.201(0.02)
	MPFE	19.29(0.11)	19.29(0.11)	19.08(0.12)	18.08(0.10)
	EPE	2.606(0.00)	2.607(0.00)	2.616(0.01)	2.719(0.01)
	100CVA	53.35(0.05)	52.92(0.05)	53.03(0.14)	53.26(0.14)
160%	V_0	8.691	8.691(0.00)	8.687(0.02)	8.687(0.02)
	MPFE	24.33(0.09)	24.34(0.09)	24.28(0.09)	23.42(0.09)
	EPE	3.526(0.00)	3.527(0.00)	3.539(0.01)	3.628(0.01)
	100CVA	71.94(0.06)	71.35(0.06)	71.47(0.09)	71.5(0.10)

Table 5.1: Bermudan receiver swaption under the Hull-White model. (a) 1Y×5Y $S \approx 0.0109$; risk-neutral $\sigma = 0.020$; $\lambda = 0.020$; real-world $\eta = 0.010$; $\kappa = 0.015$. (b) $S \approx 0.0113$; risk-neutral $\sigma = 0.010, \lambda = 0.012$; real-world $\eta = 0.006$ $\kappa = 0.008$. Risk-neutral and real-world scenarios are generated; the forward rate is flat, $f^M(0,t) = 0.01$; the default probability function $\mathrm{PS}(t) = 1 - \exp(-0.02t)$ and LGD = 1; option values and CVA are based on $H_q = 100 \cdot 10^3$ risk-neutral scenarios; MPFE and EPE are based on $H_a = 100 \cdot 10^3$ real-world scenarios; the number of monitoring dates $M = T_N/\Delta t$ with $\Delta t = 0.05$; standard errors are in parentheses, based on 10 independent runs.

Figure 5.3 compares the statistics of the risk-neutral and real-world exposure distributions: the mean in Fig.5.3(a) and the 99% quantile in Fig.5.3(b), for a 4Y/10Y receiver Bermudan swaption along time horizon $[0,10]$. The significant difference between the

curves shows that one cannot use quantiles computed by risk-neutral exposure distributions to represent the real-world PFE. There are downward jumps in the EE and PFE curves at each early-exercise date $\{4Y, 5Y, \ldots\}$, as the swaption on some of the paths is exercised.

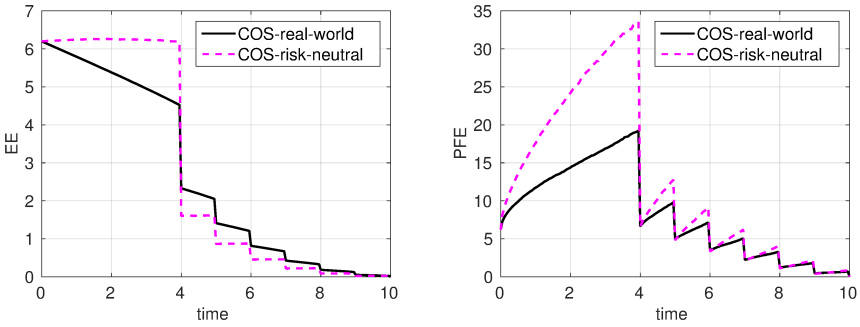

(a) exposure average (b) exposure quantile 99%

Figure 5.3: Comparison of the mean and 99% quantile of the exposure distributions, computed by the COS method, based on risk-neutral and real-world scenarios, for the 4Y/10Y Bermudan receiver swaption, as specified in Table 5.1 when $K/S = 1$.

The mean and the 99% percentile of the real-world exposure are the required EE and PFE values. Figure 5.4 compares the EE and PFE curves obtained by the different algorithms for the period 2Y to 4Y and the period 6Y to 8Y. LSM tends to over-estimate the PFE prior to the first early-exercise opportunity and to under-estimate it afterwards. The SGBM results are as accurate as the reference values.

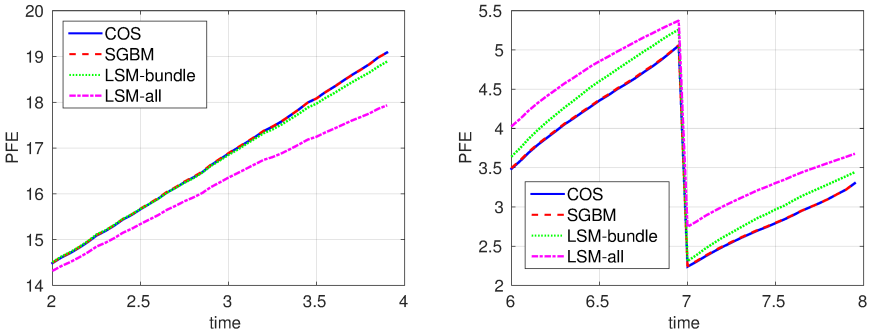

(a) PFE, 2Y to 4Y (b) PFE, 6Y to 8Y

Figure 5.4: Comparison of PFE curves obtained by COS, SGBM and LSM for years $[2,4]$ to years $[6,8]$, for the 4Y/10Y Bermudan receiver swaption specified in Table 5.1, when $K/S = 1$.

The main reason for SGBM's excellent fit in the tails of the distributions is that, at

each date, the algorithm provides an accurate local approximation of the continuation function for the whole realized domain of the underlying factor.

Figure 5.5(a) compares the reference continuation functions (by COS) to the approximated continuation functions (by SGBM and LSM) on the bounded realized risk-neutral region at time 6.5Y for the 4Y/10Y receiver swaption. The approximation by LSM-all is not accurate at the upper and lower regions, which explains its performance in Table 5.1. We observe an accuracy improvement in the results by the LSM-bundle algorithm. From the plot we observe that SGBM's approximated function resembles the reference value well on the whole domain. Fig.5.5(b) presents the empirical density of the risk-neutral short rate and the observed real-world short rate, where we see that the realized domain under the risk-neutral measure is wider spread.

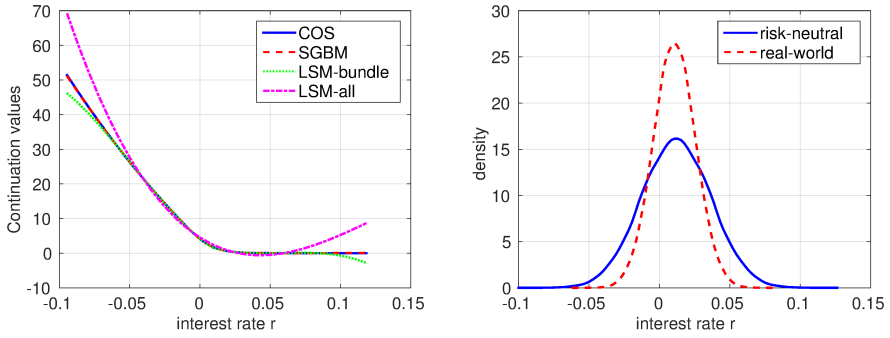

(a) continuation function (b) short rate density

Figure 5.5: Comparison of continuation functions via all algorithms at 6.5 Y, for the 4Y/10Y Bermudan receiver swaption, specified in Table 5.1, when $K/S = 1$.

Table 5.2 gives the computational times for these algorithms. SGBM is significantly faster than the reference COS algorithm; LSM is less accurate but faster than SGBM. The experiments are performed on a computer with CPU Intel Core i7-2600 3.40GHz×8 and RAM memory 15.6 Gigabytes. The computational cost increases proportionally w.r.t. parameter M.

T_N	M	COS	SGBM	LSM-bundle	LSM-all
5Y	100	60.9s	4.48s	3.32s	1.67s
10Y	200	122.7s	9.02s	7.09s	3.26s

Table 5.2: Computational costs (seconds) for computation of risk-neutral and real-world exposures distributions.

5.7.2. EXPERIMENTS WITH THE G2++ MODEL

The dynamics of the risk-neutral and real-world G2++ models are given in Section 5.3, where the associated parameters, i.e. the reversion speed κ_1, κ_2, the volatility η_1, η_2, and the correlation $\hat{\rho}$ are based on historical data, and risk-neutral parameters $\lambda_1, \lambda_2, \sigma_1, \sigma_2$ and ρ are based on market prices.

In this two-dimensional model, we use the following monomials as the basis functions in the LSM algorithm:

$$\left\{1, x_t^{(1)}, x_t^{(2)}, \left(x_t^{(1)}\right)^2, x_t^{(1)} x_t^{(2)}, \left(x_t^{(2)}\right)^2, \left(x_t^{(1)}\right)^3, \left(x_t^{(1)}\right)^2 x_t^{(2)}, x_t^{(1)} \left(x_t^{(2)}\right)^2, \left(x_t^{(2)}\right)^3\right\},$$

and the basis functions in the SGBM algorithm are given by:

$$\left\{1, x_t^{(1)}, x_t^{(2)}, \left(x_t^{(1)}\right)^2, x_t^{(1)} x_t^{(2)}, \left(x_t^{(2)}\right)^2\right\},$$

from which we observe that the number of basis functions increases rapidly w.r.t. the dimension of the underlying variable.

The associated discounted moments, required in SGBM, can easily be derived from the analytic formula of the discounted ChF of the G2++ model, and, as for Hull-White model, we use $J = 10$ bundles in SGBM. In SGBM, we can either use the two-dimensional equal-number bundling method, introduced in [32], or the one-dimensional version based on projecting the high-dimensional variable onto a one-dimensional variable. Here, we create the bundles based on the realized values of $(x_t^{(1)} + x_t^{(2)})$ on each path at time t_m.

Table 5.3 reports the time-zero option value results for SGBM and LSM as well as the exposure measures for receiver Bermudan swaptions, where we can analyze the difference between the results by these algorithms.

Figure 5.6 presents the PFE curves computed on the real-world scenarios and the mean and the 99% quantiles of the risk-neutral exposure distributions at each monitoring date. As expected, there is clear difference between the statistics of the risk-neutral and the real-world exposure distributions.

Table 5.4 presents the computational cost of the algorithms for this two-dimensional model. The cost increases w.r.t. the dimension of the variable.

5.8. CONCLUSION

This chapter presents computationally efficient techniques for the simultaneous computation of exposure distributions under the risk-neutral and the observed real-world probability measures. They are based on only two sets of scenarios, one generated under the risk-neutral dynamics and another under the observed real-world dynamics, and on basic techniques such as regression. Compared to nested Monte-Carlo simulation, the techniques presented significantly reduce the computational cost and maintain high accuracy, which we demonstrated by numerical results for Bermudan swaptions, comparing to references results generated by the Fourier-based COS method. We illustrate the easy implementation for both the one-factor Hull-White and the two-factor G2++ models.

(a) 1Y×5Y				
K/S	value	COS	SGBM	LSM-bundle
40%	V_0	1.740	1.742(0.00)	1.748(0.00)
	MPFE	5.059(0.05)	5.057(0.05)	5.049(0.09)
	EPE	0.770(0.00)	0.771(0.00)	0.776(0.01)
	100CVA	7.475(0.00)	7.486(0.01)	7.514(0.03)
100%	V_0	2.895	2.897(0.00)	2.903(0.01)
	MPFE	6.518(0.02)	6.521(0.02)	6.442(0.15)
	EPE	1.111(0.00)	1.113(0.00)	1.112(0.00)
	100CVA	10.04(0.01)	10.05(0.01)	10.07(0.02)
160%	V_0	4.561	4.560(0.00)	4.566(0.00)
	MPFE	9.624(0.04)	9.627(0.04)	9.677(0.11)
	EPE	1.327(0.00)	1.328(0.00)	1.330(0.00)
	100CVA	12.66(0.01)	12.66(0.01)	12.69(0.02)
(b) 3Y×10Y				
K/S	value	COS	SGBM	LSM-bundle
40%	V_0	0.858	0.861(0.00)	0.863(0.00)
	MPFE	2.652(0.02)	2.785(0.02)	2.709(0.05)
	EPE	0.444(0.00)	0.447(0.00)	0.446(0.00)
	100CVA	8.649(0.01)	8.683(0.01)	8.688(0.03)
100%	V_0	2.466	2.466(0.00)	2.474(0.00)
	MPFE	7.159(0.02)	7.157(0.02)	7.099(0.03)
	EPE	1.058(0.00)	1.06(0.00)	1.064(0.00)
	100CVA	19.52(0.02)	19.53(0.02)	19.62(0.03)
160%	V_0	5.418	5.42(0.00)	5.428(0.01)
	MPFE	12.06(0.02)	12.06(0.02)	12.18(0.02)
	EPE	1.836(0.00)	1.838(0.00)	1.843(0.00)
	100CVA	35.48(0.02)	35.49(0.02)	35.59(0.06)

Table 5.3: Receiver Bermudan swaption under the G2++ model. (a) $S \approx 0.0104$; risk-neutral $\sigma_1 = 0.015$, $\sigma_2 = 0.008$, $\lambda_1 = 0.07$, $\lambda_2 = 0.08$, $\rho = -0.6$; real-world $\eta_1 = 0.005$, $\eta_2 = 0.01$, $\kappa_1 = 0.54$, $\kappa_2 = 0.07$, $\hat{\rho} = -0.8$. (b) $S \approx 0.0102$; risk-neutral $\sigma_1 = 0.005$, $\sigma_2 = 0.008$, $\lambda_1 = 0.09$, $\lambda_2 = 0.15$, $\rho = -0.6$; real-world $\eta_1 = 0.002$, $\eta_2 = 0.006$, $\kappa_1 = 0.04$, $\kappa_2 = 0.07$, $\hat{\rho} = -0.8$. Risk-neutral and real-world scenarios are generated; forward rate $f^M(0,t) = 0.01$; the default probability function $\mathrm{PS}(t) = 1 - \exp(-0.02t)$ and LGD = 1; option values and CVA are based on $H_q = 100 \cdot 10^3$ risk-neutral scenarios; MPFE and EPE are based on $H_a = 100 \cdot 10^3$ real-world scenarios; the number of monitoring dates $M = T_N/\Delta t$ with $\Delta t = 0.05$.

We recommend SGBM because of its accuracy and efficiency in the computation of continuation values. A highly satisfactory alternative is to use the LSM-bundle approach. The reference COS method is highly efficient for computing time-zero values of the Bermudan swaption, but for the computation of exposure, there is room for im-

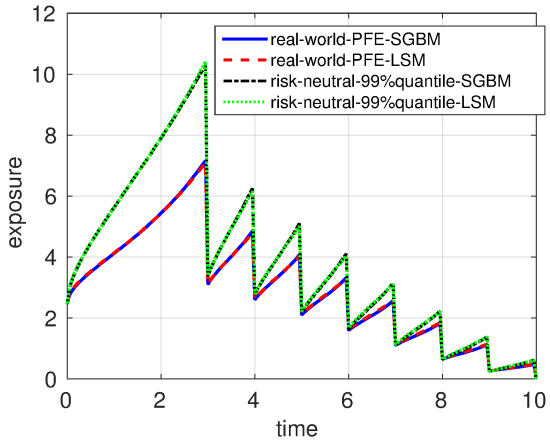

Figure 5.6: PFE and the 99% quantile of the exposure distributions of a receiver Bermudan swaption, as specified in Table 5.3 when $K/S = 1$.

T_N	M	LSM-bundle	SGBM	COS
5Y	100	6.28s	8.10s	868.14s
10Y	200	12.96	15.07s	1840.72s

Table 5.4: Computational costs (seconds) for the computation of risk-neutral and real-world exposures distributions under the G2++ model.

provement in terms of computational speed.

The results for the parameter values chosen show that there are clear differences in exposure distributions on the risk-neutral and the real-world scenarios. The proposed algorithms are based on the requirement that the sample space induced by the observed historical model is a subspace of the sample space under the risk-neutral measure.

The valuation framework presented is flexible and may be used efficiently for any type of Bermudan-style claim, such as Bermudan options and swaptions. For a Bermudan option, one can compute the sensitivities of CVA by SGBM at the same time, which is an additional benefit. The algorithms developed can be extended easily to the situation in which model parameters are piecewise constant over the time horizon.

APPENDIX 1: ZCB AND DISCOUNTED CHF UNDER THE HULL-WHITE MODEL

The value of a ZCB under the HW model between times $[t, T]$, conditional on $r_t = x$, under the risk neutral measure $\mathbb{Q}$ is given by

$$P^{\mathrm{HW}}(t, T, x) = \overline{A}(t, T) e^{\overline{B}(t,T)x}, \tag{5.62}$$

where coefficients $\overline{A}$ and $\overline{B}$ are given by

$$\begin{aligned}\overline{B}(t,T) &= \frac{1}{\lambda}\left[1-e^{-\lambda(T-t)}\right],\\ \overline{A}(t,T) &= \frac{P^M(0,T)}{P^M(0,t)}\exp\left\{\overline{B}(t,T)f^M(0,t)-\frac{\sigma^2}{4\lambda}(1-e^{-2\lambda t})\overline{B}(t,T)^2\right\}.\end{aligned} \tag{5.63}$$

The dChF for the underlying variable r_t can be expressed by the following formula:

$$\begin{aligned}&\varphi^{\mathrm{HW}}(u;t,T,r_t)=\mathbb{E}^{\mathbb{Q}}\left[\exp\left(-\int_t^T r_s ds+iur_T\right)\middle|r_t\right]\\ =\;&\exp\left(-\int_t^T\theta(s)ds+iu\theta(T)\right)\mathbb{E}^{\mathbb{Q}}\left[\exp\left(-\int_t^T g_s ds+iug_T\right)\middle|x_t=r_t-\theta(t)\right]\\ =\;&\exp\left(-\int_t^T\theta(s)ds+iu\theta(T)+\tilde{A}(T-t)+\tilde{B}(T-t)x_t\right)\end{aligned} \tag{5.64}$$

where the analytic formula of the integral for function θ over time $[t,T]$ is given by

$$\int_t^T\theta(s)ds=\int_t^T f^M(s)ds+\frac{\sigma^2}{4\lambda^3}\left(\lambda(T-t)+4\left(e^{-\lambda T}-e^{-\lambda t}\right)-\left(e^{-2\lambda T}-e^{-2\lambda t}\right)\right), \tag{5.65}$$

and the coefficients are the solutions of the ODEs, given by

$$\begin{aligned}\frac{d\widetilde{B}}{ds}(s)&=-1-\lambda\widetilde{B}(s),\\ \frac{d\widetilde{A}}{ds}(s)&=\frac{1}{2}\sigma^2\left(\widetilde{B}(s)\right)^2,\end{aligned} \tag{5.66}$$

with $\widetilde{B}(0)=iu$ and $\widetilde{A}(0)=0$.

The analytic solution of the ODEs is given by

$$\begin{aligned}\widetilde{B}(T-t) &= iue^{-\lambda(T-t)}-\frac{1}{\lambda}\left(1-e^{-\lambda(T-t)}\right),\\ \widetilde{A}(T-t) &= \frac{\lambda^2}{2\sigma^3}\left(\sigma(T-t)-2\left(1-e^{-\lambda(T-t)}\right)+\frac{1}{2}(1-e^{-2\lambda(T-t)})\right)\\ &\quad-\frac{iu\lambda^2}{2\sigma^2}\left(1-e^{-\lambda(T-t)}\right)^2-\frac{u^2\lambda^2}{4\sigma}\left(1-e^{-2\lambda(T-t)}\right).\end{aligned} \tag{5.67}$$

APPENDIX 2: ZCB AND DISCOUNTED CHF UNDER THE G2++ MODEL

The value of a ZCB between times t and T under the G2++ model is given by

$$P^{\mathrm{G2}}(t,T,x_t^{(1)},x_t^{(2)})=\overline{D}(t,T)\exp\left(-\overline{C}_1(t,T)x_t^{(1)}-\overline{C}_2(t,T)x_t^{(2)}\right), \tag{5.68}$$

where the coefficients are given by:

$$\begin{aligned}\overline{D}(t,T) &= \frac{P^M(0,T)}{P^M(0,t)}\exp\left\{\frac{1}{2}\left(\mathscr{H}(t,T)-\mathscr{H}(0,T)+\mathscr{H}(0,t)\right)\right\},\\ \overline{C}_1(t,T) &= \frac{1}{\lambda_1}\left(1-e^{-\lambda_1(T-t)}\right),\quad \overline{C}_2(t,T)=\frac{1}{\lambda_2}\left(1-e^{-\lambda_2(T-t)}\right),\end{aligned} \tag{5.69}$$

with the function $\mathscr{H}(t,T)$

$$\mathscr{H}(t,T) = \sigma_1^2\int_t^T \overline{C}_1(s)^2 ds + \sigma_2^2\int_t^T \overline{C}_2(s)^2 ds + 2\rho\sigma_1\sigma_2\int_t^T \overline{C}_1(s)\overline{C}_2(s) ds. \quad (5.70)$$

The 2D discounted ChF of the G2++ model for variable $\mathbf{X}_t = [x_t^{(1)}, x_t^{(2)}]$ is given as follows:

$$\begin{aligned}\varphi^{G2}(u_1,u_2;t,T,x_t^{(1)},x_t^{(2)}) &= \mathbb{E}^{\mathbb{Q}}\left[\exp\left(-\int_t^T r_s ds\right) + iu_1 x_T^{(1)} + iu_2 x_t^{(2)}\middle| x_t^{(1)}, x_t^{(2)}\right] \\ &= \exp\left(-\int_t^T \gamma(s)ds + \widetilde{A}^{G2}(T-t) + \widetilde{B}_1(T-t)x_t^{(1)} + \widetilde{B}_2(T-t)x_t^{(2)}\right), \quad (5.71)\end{aligned}$$

where the analytic formula of the integral for the function γ over time $[t,T]$ is given by,

$$\begin{aligned}\int_t^T \gamma(s)ds &= \int_0^T f^M(0,s)ds + \frac{\sigma_1^2}{4\lambda_1^3}\left(4(e^{-\lambda_1 T} - e^{-\lambda_1 t}) - 2(e^{-2\lambda_1 T} - e^{-2\lambda_1 t}) + 2(T-t)\lambda_1\right) \\ &\quad + \frac{\sigma_2^2}{4\lambda_2^3}\left(4(e^{-\lambda_2 T} - e^{-\lambda_2 t}) - 2(e^{-2\lambda_2 T} - e^{-2\lambda_2 t}) + 2(T-t)\lambda_2\right) \\ &\quad + \frac{\rho\sigma_1\sigma_2}{\lambda_1\lambda_2}\left[\frac{1}{\lambda_1}\left(e^{-\lambda_1 T} - e^{-\lambda_1 t}\right) + \frac{1}{\lambda_2}\left(e^{-\lambda_2 T} - e^{-\lambda_2 t}\right) + T - t\right] \\ &\quad - \frac{\rho\sigma_1\sigma_2}{\lambda_1\lambda_2(\lambda_1+\lambda_2)}\left(e^{-(\lambda_1+\lambda_2)T} - e^{(\lambda_1+\lambda_2)t}\right). \quad (5.72)\end{aligned}$$

and the coefficients $\widetilde{B}_1$, $\widetilde{B}_2$ and $\widetilde{A}^{G2}$ are determined by the following ODEs:

$$\begin{aligned}&\frac{d\widetilde{B}_1}{ds}(s) = -1 - \lambda_1\widetilde{B}_1(s), \quad \frac{d\widetilde{B}_2}{ds}(s) = -1 - \lambda_2\widetilde{B}_2(s), \\ &\frac{d\widetilde{A}^{G2}}{ds}(s) = \frac{1}{2}\sigma_1^2\widetilde{B}_1^2(s) + \rho\sigma_1\sigma_2\widetilde{B}_1(s)\widetilde{B}_2(s) + \frac{1}{2}\sigma_2^2\widetilde{B}_2^2(s), \quad (5.73)\end{aligned}$$

with initial conditions $\widetilde{B}_1(0) = iu_1$, $\widetilde{B}_2(0) = iu_2$ and $\widetilde{A}^{G2}(0) = 0$.

Their solution is given by:

$$\begin{aligned}\widetilde{B}_1(T-t) &= iu_1 e^{-\lambda_1(T-t)} - \frac{1}{\lambda_1}\left(1 - e^{-\lambda_1(T-t)}\right), \\ \widetilde{B}_2(T-t) &= iu_2 e^{-\lambda_2(T-t)} - \frac{1}{\lambda_2}\left(1 - e^{-\lambda_2(T-t)}\right), \\ \widetilde{A}^{G2}(T-t) &= \frac{\sigma_1^2}{2}\int_t^T \widetilde{B}_1(s)ds + \rho\sigma_1\sigma_2\int_t^T \widetilde{B}_1(s)\widetilde{B}_2(s)ds + \frac{\sigma_2^2}{2}\int_t^T \widetilde{B}_2^2(s)ds, \quad (5.74)\end{aligned}$$

where the integral can be computed analytically.

APPENDIX 3: COEFFICIENTS $\mathscr{G}_k$ AND $\mathscr{C}_k$

The coefficients $\mathscr{G}_k$ at time T_n over $[x_c, x_d]$ are computed by

$$\begin{aligned}\mathscr{G}_k\Big(x_c, x_d, T_n\Big) &= N_0 \int_{x_c}^{x_d} \cos\Big(k\pi \frac{y-a}{b-a}\Big) g_N(y)\, dy \\ &= N_0 \delta\Big(\mathscr{A}_k^1(x_c, x_d) - \mathscr{A}_k^2(x_c, x_d, T_n)\Big), \end{aligned} \tag{5.75}$$

where the coefficients are given by

$$\begin{aligned}\mathscr{A}_k^1(x_c, x_d) &= \begin{cases} x_d - x_c, & k = 0, \\ \frac{b-a}{k\pi}\left[\sin\left(k\pi \frac{x_d-a}{b-a}\right) - \sin\left(k\pi \frac{x_c-a}{b-a}\right)\right], & k \neq 0, \end{cases} \\ \mathscr{A}_k^2(x_c, x_d, T_n) &= \sum_{j=n}^{N} \frac{\hat{c}_j \overline{A}_{n,j+1}}{\left(\frac{k\pi}{b-a}\right)^2 + \overline{B}_{n,j+1}^2} \Bigg[\frac{k\pi}{b-a} \sin\Big(k\pi \frac{x_d-a}{b-a}\Big) e^{-\overline{B}_{n,j+1} x_d} - \\ &\quad \overline{B}_{n,j+1} \cos\Big(k\pi \frac{x_d-a}{b-a}\Big) e^{-\overline{B}_{n,j+1} x_d} - \frac{k\pi}{b-a} \sin\Big(k\pi \frac{x_c-a}{b-a}\Big) e^{-\overline{B}_{n,j+1} x_c} + \\ &\quad \overline{B}_{n,j+1} \cos\Big(k\pi \frac{x_c-a}{b-a}\Big) e^{-\overline{B}_{n,j+1} x_c} \Bigg], \end{aligned} \tag{5.76}$$

where $\overline{A}_{n,j+1} := \overline{A}(T_n, T_{j+1})$ and $\overline{B}_{n,j+1} := \overline{B}(T_n, T_{j+1})$. $\overline{A}$ and $\overline{B}$ are given by (5.63) in Appendix 1.

The coefficients $\mathscr{C}_k$ at time t_m over $[x_c, x_d]$ are computed via an integral

$$\begin{aligned}\mathscr{C}_k(x_c, x_d, t_m) &:= \int_{x_c}^{x_d} c(t_m, y) \cos\Big(k\pi \frac{y-a}{b-a}\Big)\, dy \\ &\approx \frac{2}{b-a} \sum_{l=0}^{Q-1}{}' \Big(\int_{x_c}^{x_d} \mathscr{P}_l(y, t_m, t_{m+1}) \cos\Big(k\pi \frac{y-a}{b-a}\Big)\, dy \Big) \mathscr{V}_l(t_{m+1}) \\ &= \frac{2}{b-a} \sum_{l=0}^{Q-1}{}' \mathrm{Re}\Big\{ \mathscr{W}_l(t_m, t_{m+1}) \mathscr{X}_{k,l}(x_c, x_d) \Big\} \mathscr{V}_l(t_{m+1}), \end{aligned} \tag{5.77}$$

in which coefficients $\{\mathscr{V}_l(t_{m+1})\}_{l=0}^{Q-1}$ have been computed at time t_{m+1}, and coefficients

$\mathscr{W}$ and $\mathscr{X}$ are given by

$$\mathscr{W}_l(t_m, t_{m+1}) = \exp\left\{ -\int_{t_m}^{t_{m+1}} \theta(s)ds + \frac{il\pi}{b-a}\theta(t_{m+1}) - \widetilde{B}_l\theta(t_m) \right\} \exp\left\{ -\frac{ial\pi}{b-a} + \widetilde{A}_l \right\},$$

$$\begin{aligned}\mathscr{X}_{k,l}(x_c, x_d) &= \int_{x_c}^{x_d} \cos\left(k\pi\frac{y-a}{b-a}\right) e^{\widetilde{B}_l y} dy \\ &= \frac{1}{\left(\frac{k\pi}{b-a}\right)^2 + \widetilde{B}_l^2} \left[\frac{k\pi}{b-a} \sin\left(k\pi\frac{x_d-a}{b-a}\right) e^{\widetilde{B}_l x_d} + \widetilde{B}_l \cos\left(k\pi\frac{x_d-a}{b-a}\right) e^{\widetilde{B}_l x_d} \right. \\ &\quad \left. - \frac{k\pi}{b-a} \sin\left(k\pi\frac{x_c-a}{b-a}\right) e^{\widetilde{B}_l x_c} - \widetilde{B}_l \cos\left(k\pi\frac{x_c-a}{b-a}\right) e^{\widetilde{B}_l x_c} \right], \end{aligned} \tag{5.78}$$

with $\widetilde{B}_l = \widetilde{B}(\Delta t)$ and $\widetilde{A}_l = \widetilde{A}(\Delta t)$ when $u = \frac{l\pi}{b-a}$, $l = 0, 1, \ldots, Q$. Analytic formulas of $\widetilde{B}$ and $\widetilde{A}$ are presented by (5.67) in Appendix 1.

5

CHAPTER 6

Conclusions and Outlook

6.1. CONCLUSIONS

In this thesis, we have presented an efficient algorithm, SGBM, for computing future exposure profiles, under the risk-neutral probability measure for the purpose of CVA calculation, and under the real-world probability measure for the purpose of quantifying credit risk.

We demonstrated that SGBM converges w.r.t. the number of paths, the number of bundles and the polynomial order. The algorithm is highly adaptive for various models and financial contracts. It is an adequate scheme for computing exposure profiles because of its accuracy over all paths. The derivation of analytic formulas of discounted moments was presented using the relation between the discounted ChF and the discounted moments.

We investigated the impact of stochastic volatility and stochastic interest rate in asset models on the exposure distribution of option contracts over the risk horizon. In SGBM, we derived the analytic formulas of the discounted ChF for the hybrid models used in this thesis. For the options with early-exercise features, we proposed an algorithm for computing exposure profiles without sub-simulation. We propose a bundling technique under 2D and 3D models that balances the requirements for the number of paths and the number of bundles.

For the purpose of having a benchmark, we also developed the COS method for computation of exposure profiles for Bermudan options. The COS method is further developed for the valuation of Bermudan options and their exposure under the Hull-White and the G2++ models.

We proposed three models for the stochastic intensity to deal with wrong way risk (WWR). In these models, we defined the dependency structure of the intensity and the other market factors in three ways: a deterministic function, the correlation between diffusion terms, or/and the correlation in the jump terms. Based on the proposed models, CVA stress testing for European options is performed and we see that the WWR risk caused higher CVA values for European option contracts.

As an extension, we showed the changes in the exercise region of a Bermudan option in the presence of CCR and WWR, by studying the early-exercise regions, in the case of no default risk, a constant intensity and a stochastic intensity. We find that a Bermudan put option is more likely to be exercised when there exists CCR. The impact of WWR on CVA of Bermudan options, however, is model-dependent.

We presented the computation of CVA VaR and CVA ES for option contracts without any sub-simulation based on the algorithms developed by us in this thesis.

The algorithms developed in this thesis may provide a solution for the computational

demand in practice. The study of WWR can be interesting for the impact on the exercise-behavior.

6.2. OUTLOOK

The algorithms and models proposed need to be tested with real market data. A next topic following the results in this thesis, can be to use real market data to test the efficiency and accuracy of the algorithm.

Additional factors that need to be considered are to include volatility in LGD, the impact of netting and collateral agreements. We know that in the financial world, LGD is not a constant as assumed in this thesis. Instead, LGD varies w.r.t. the market movements as well. The volatility in LGD may make significant contribution to CVA.

Another important issue for future research is to study the debit valuation risk (DVA). In this thesis, we have studied the unilateral CVA. In practice, however, CCR is bilateral to both parties in a contract. The CVA from the perspective of the counterparty, is DVA. It arises due to one's own default risk.

Netting and collateral agreements are commonly used in practice and banks should consider the corresponding risk. Other risks that banks need to manage include KVA (capital valuation adjustment), FVA (funding valuation adjustment), costs of margin, collateral and transaction [38]. In recent years, banks have started to set up a so-called 'XVA desk' to support the pricing, and the risk and collateral management. Effective and adequate ways for computation and modeling for these risks are highly in demand [14].

There are many challenges in the field of CCR. Research on these topics is appreciated to help building a resilient financial market.

References

[1] L. B. G. Andersen. A simple approach to the pricing of Bermudan swaptions in the multifactor LIBOR market model. *Journal of Computational Finance*, 3(2):5–32, 1999-2000.

[2] L. B. G. Andersen. Simple and efficient simulation of the Heston stochastic volatility model. *Journal of Computational Finance*, 11(3):1–42, 2008.

[3] L. B. G. Andersen and V. V. Piterbarg. *Interest Rate Modeling*. Atlantic Financial Press, London, 2010.

[4] Basel Committee on Banking Supervision. Annex 4 to "International convergence of capital measurement and capital standards - a revised framework". 2005. Available at http://www.bis.org/publ/bcbs107.htm.

[5] Basel Committee on Banking Supervision. Basel III: A global regulatory framework for more resilient banks and banking systems - revised version June 2011. *Basel Committee on Banking Supervision*, June 2011. Available at https://www.bis.org/publ/bcbs189.htm.

[6] Basel Committee on Banking Supervision. Consultative document: Review of the credit valuation adjustment risk framework. *Basel Committee on Banking Supervision*, July 2015. Available at http://www.bis.org/bcbs/publ/d325.pdf.

[7] Basel Committee on Banking Supervision. Review of the credit valuation adjustment (CVA) risk framework - consultative document. 2015.

[8] T. R. Bielecki and M. Rutkowski. *Credit Risk: Modeling, Valuation and Hedging*. Springer Science & Business Media, Berlin, 2002.

[9] F. Black and M. Scholes. The pricing of options and corporate liabilities. *Journal of Political Economy*, pages 637–654, 1973.

[10] A. Borovykh, A. Pascucci, and C. W. Oosterlee. Pricing Bermudan options under local Lévy models with default. *Available at SSRN 2771632*, 2016.

[11] M. Brennan and E. Schwartz. The valuation of American put options. *Journal of Finance*, 32(2):449–462, 1977.

[12] D. Brigo, A. Capponi, and A. Pallavicini. Arbitrage-free bilateral counterparty risk valuation under collateralization and application to credit default swaps. *Mathematical Finance*, 24(1):125–146, 2014.

[13] D. Brigo and F. Mercurio. *Interest Rate Models-Theory and Practice: with Smile, Inflation and Credit*. Springer Science & Business Media, 2007.

[14] D. Brigo, M. Morini, and A. Pallavicini. *Counterparty Credit Risk, Collateral and Funding: With Pricing Cases for All Asset Classes*. The Wiley Finance Series. John Wiley & Sons, Chichester, West Sussex, 2013.

[15] M. Broadie and M. Cao. Improved lower and upper bound algorithms for pricing American options by simulation. *Quantitative Finance*, 8(8):845–861, 2008.

[16] M. Broadie and P. Glasserman. A stochastic mesh method for pricing high-dimensional American options. *Journal of Computational Finance*, 7:35–72, 2004.

[17] M. Broadie, P. Glasserman, and Z. Ha. Pricing American options by simulation using a stochastic mesh with optimized weights. In *Probabilistic Constrained Optimization*, pages 26–44. Springer, 2000.

[18] J. F. Carriere. Valuation of the early-exercise price for options using simulations and nonparametric regression. *Insurance: mathematics and Economics*, 19(1):19–30, 1996.

[19] E. Clément, D. Lamberton, and P. Protter. An analysis of a least squares regression method for American option pricing. *Finance and Stochastics*, 6(4):449–471, 2002.

[20] F. Cong and C. W. Oosterlee. Pricing Bermudan options under Merton jump-diffusion asset dynamics. *International Journal of Computer Mathematics*, 92(12):2406–2432, 2015.

[21] F. Cong and C. W. Oosterlee. Multi-period mean–variance portfolio optimization based on Monte-Carlo simulation. *Journal of Economic Dynamics and Control*, 64:23–38, 2016.

[22] J. C. Cox, J. E, Ingersoll, and S. A. Ross. A theory of the term structure of interest rates. *Econometrica*, 53(2):385–407, 1985.

[23] C. de Graaf. Efficient PDE based numerical estimation of credit and liquidity risk measures for realistic derivative portfolios. 2016.

[24] C. S. de Graaf, Q. Feng, D. Kandhai, and C. W. Oosterlee. Efficient computation of exposure profiles for counterparty credit risk. *International Journal of Theoretical and Applied Finance*, 17(04):1450024, 2014.

[25] D. Duffie and N. Garleanu. Risk and valuation of collateralized debt obligations. *Financial Analysts Journal*, 57(1):41–59, 2001.

[26] D. Duffie, J. Pan, and K. J. Singleton. Transform analysis and asset pricing for affine jump-diffusions. *Econometrica*, 68(6):1343–1376, 2000.

[27] D. Duffie and K. J. Singleton. Modeling term structures of defaultable bonds. *Review of Financial Studies*, 12(4):687–720, 1999.

[28] F. Fang and C. W. Oosterlee. Pricing early-exercise and discrete barrier options by Fourier-cosine series expansions. *Numerische Mathematik*, 114(1):27–62, 2009.

[29] F. Fang and C. W. Oosterlee. A Fourier-based valuation method for Bermudan and barrier options under Heston's model. *SIAM Journal on Financial Mathematics*, 2(1):439–463, Jan. 2011.

[30] Q. Feng, S. Jain, P. Karlsson, D. Kandhai, and C. W. Oosterlee. Efficient computation of exposure profiles on real-world and risk-neutral scenarios for Bermudan swaptions. *Journal of Computational Finance*, 20(1):139–172, 2016.

[31] Q. Feng and C. W. Oosterlee. Wrong way risk modeling and computation in credit valuation adjustment for European and Bermudan options. *Available at SSRN*, 2016.

[32] Q. Feng and C. W. Oosterlee. Calculation of exposure profiles and sensitivities of options under the Heston and the Heston Hull-White models. 79, 2017.

[33] S. Foulon and K. in 't Hout. ADI finite difference schemes for option pricing. *International Journal of Numerical Analysis and Modeling*, 7(2):303–320, 2010.

[34] P. Glasserman. *Monte Carlo Methods in Financial Engineering*. Springer Science & Business Media, New York, 2003.

[35] P. Glasserman and B. Yu. Simulation for American options: regression now or regression later? In *Monte Carlo and Quasi-Monte Carlo Methods 2002*, pages 213–226. Springer, 2004.

[36] P. Glasserman, B. Yu, et al. Number of paths versus number of basis functions in American option pricing. *The Annals of Applied Probability*, 14(4):2090–2119, 2004.

[37] A. S. Goldberger. *Econometric Theory*. New York: John Wiley & Sons., 1964.

[38] J. Gregory. *Counterparty Credit Risk: the New Challenge for Global Financial Markets*. John Wiley & Sons, Chichester, West Sussex, 2010.

[39] L. A. Grzelak and C. W. Oosterlee. On the Heston model with stochastic interest rates. *SIAM Journal on Financial Mathematics*, 2(1):255–286, 2011.

[40] T. Haentjens and K. in 't Hout. ADI finite difference schemes for the Heston–Hull–White PDE. *Journal of Computational Finance*, 16(1):83–110, 2012.

[41] T. Haentjens and K. J. in 't Hout. ADI schemes for pricing American options under the Heston model. *arXiv preprint arXiv:1309.0110*, pages 1–26, 2013.

[42] B. E. Hansen. *Econometrics*. Manuscript(2016), 2016.

[43] S. Heston. A closed-form solution for options with stochastic volatility with applications to bond and currency options. *Review of Financial Studies*, 6(2):327–343, Apr. 1993.

[44] J. Hull and A. White. Pricing interest-rate-derivative securities. *Review of Financial Studies*, 3(4):573–592, 1990.

[45] J. Hull and A. White. The impact of default risk on the prices of options and other derivative securities. *Journal of Banking & Finance*, 19(2):299–322, 1995.

[46] J. Hull and A. White. CVA and wrong-way risk. *Financial Analysts Journal*, 68(5):58–69, 2012.

[47] J. C. Hull. *Options, Futures, and Other Derivatives*. Pearson Education India, 2006.

[48] J. C. Hull, A. Sokol, and A. White. Modeling the short rate: the real and risk-neutral worlds. *Rotman School of Management Working Paper*, (2403067), 2014.

[49] S. Jain and C. W. Oosterlee. Pricing high-dimensional Bermudan options using the stochastic grid method. *International Journal of Computer Mathematics*, 89(9):1186–1211, 2012.

[50] S. Jain and C. W. Oosterlee. The Stochastic Grid Bundling Method: Efficient pricing of Bermudan options and their greeks. *Applied Mathematics and Computation*, 269:412 – 431, 2015.

[51] S. Jain, F. Roelofs, and C. W. Oosterlee. Valuing modular nuclear power plants in finite time decision horizon. *Energy Economics*, 36:625–636, 2013.

[52] R. A. Jarrow and S. M. Turnbull. Pricing derivatives on financial securities subject to credit risk. *Journal of Finance*, 50:53–53, 1995.

[53] H. Johnson and R. Stulz. The pricing of options with default risk. *Journal of Finance*, 42(2):267–280, 1987.

[54] M. S. Joshi and O. K. Kwon. Least squares Monte Carlo credit value adjustment with small and unidirectional bias. *Available at SSRN 2717250*, 2016.

[55] P. Karlsson, S. Jain, and C. W. Oosterlee. Counterparty credit exposures for interest rate derivatives using the Stochastic Grid Bundling Method. *Applied Mathematical Finance*, 23(3):175–196, 2016.

[56] C. Kenyon, A. Green, and M. Berrahoui. Which measure for PFE? The risk appetite measure A. *ArXiv preprint arXiv:1512.06247*, 2015.

[57] P. Klein and J. Yang. Counterparty credit risk and American options. *Journal of Derivatives*, 20(4):7–21, 2013.

[58] L. Koralov and Y. G. Sinai. *Theory of Probability and Random Processes*. Springer Science & Business Media, 2007.

[59] D. Lando. On Cox processes and credit risky securities. *Review of Derivatives Research*, 2(2-3):99–120, 1998.

[60] D. Lando. *Credit Risk Modeling: Theory and Applications*. Princeton University Press, 2009.

[61] M. G. Larson and F. Bengzon. *The Finite Element Method: Theory, Implementation, and Applications*, volume 10. Springer Science & Business Media, 2013.

[62] B. Lauterbach and P. Schultz. Pricing warrants: An empirical study of the Black-Scholes model and its alternatives. *Journal of Finance*, 45(4):1181–1209, 1990.

[63] Á. Leitao and C. W. Oosterlee. GPU acceleration of the Stochastic Grid Bundling Method for early-exercise options. *International Journal of Computer Mathematics*, 92(12):2433–2454, 2015.

[64] F. A. Longstaff and E. S. Schwartz. Valuing American options by simulation: a simple least-squares approach. *Review of Financial Studies*, 14(1):113–147, 2001.

[65] D. G. Luenberger. *Optimization by Vector Space Methods*. John Wiley & Sons, 1969.

[66] D. B. Madan and H. Unal. Pricing the risks of default. *Review of Derivatives Research*, 2(2-3):121–160, 1998.

[67] R. C. Merton. On the pricing of corporate debt: The risk structure of interest rates. *Journal of Finance*, 29(2):449–470, 1974.

[68] B. Øksendal. *Stochastic Differential Equations*. Springer, New York, 2003.

[69] F. W. Olver. *NIST Handbook of Mathematical Functions*. Cambridge University Press, 2010.

[70] A. Papoulis and S. U. Pillai. *Probability, Random Variables, and Stochastic processes*. Tata McGraw-Hill Education, 2002.

[71] D. Pollard. *Convergence of Stochastic Processes*. Springer Science & Business Media, 2012.

[72] M. J. Ruijter and C. W. Oosterlee. Two-dimensional Fourier cosine series expansion method for pricing financial options. *SIAM Journal on Scientific Computing*, 34(5):B642–B671, 2012.

[73] I. Ruiz. Backtesting counterparty risk: How good is your model? Technical report, Working Paper, iRuiz Consulting, 2012.

[74] I. Ruiz. Technical note : on wrong way risk. *The Capco Institute Journal of Financial Transformation*, 39(4):69–71, 2014.

[75] I. Ruiz, P. Del Boca, and R. Pachón. Optimal right-and wrong-way risk from a practitioner standpoint. *Financial Analysts Journal*, 71(2):47–60, 2015.

[76] R. Seydel. *Tools for Computational Finance*. Springer, 2006.

[77] Y. Shen. *Credit Value Adjustment for Multi-Asset Options*. PhD thesis, Delft University of Technology, Delft, 2014.

[78] Y. Shen, J. Anderluh, and J. Van Der Weide. Algorithmic counterparty credit exposure for multi-asset Bermudan options. *International Journal of Theoretical and Applied Finance*, 18(01):1550001, 2015.

[79] Y. Shen, J. Weide, and J. Anderluh. A benchmark approach of counterparty credit exposure of Bermudan option under Lévy process: The Monte Carlo-COS method. *Procedia Computer Science*, 00, 2013.

[80] H. J. Stein. Joining risks and rewards. *Available at SSRN 2368905*, 2013.

[81] H. J. Stein. Fixing underexposed snapshots–proper computation of credit exposures under the real world and risk neutral measures. *Available at SSRN 2365540*, 2014.

[82] L. Stentoft. Value function approximation or stopping time approximation: A comparison of two recent numerical methods for American option pricing using simulation and regression. *Journal of Computational Finance*, 18:1–56, 2010.

[83] D. Tavella and C. Randall. *Pricing Financial Instruments: The Finite Difference Method*. Wiley, New York, 2000.

[84] J. N. Tsitsiklis and B. Van Roy. Regression methods for pricing complex American-style options. *Trans. Neur. Netw.*, 12(4):694–703, July 2001.

[85] O. Vasicek. An equilibrium characterization of the term structure. *Journal of Financial Economics*, 5(2):177–188, 1977.

[86] M. Vellekoop and H. Nieuwenhuis. A tree-based method to price American options in the Heston model. *Journal of Computational Finance*, 13(1):1–21, 2009.

[87] S. H. Zhu and M. Pykhtin. A guide to modeling counterparty credit risk. *GARP Risk Review, July/August*, 2007.

Curriculum Vitæ

Qian FENG

04-01-1986	Born in Qiqihar, China.

EDUCATION

2005–2009	Bachelor in Mathematics and Applied Mathematics Beijing Normal University, Beijing, China.
2010–2012	Master in Applied Mathematics Delft University of Technology, Delft, the Netherlands.
2012–2016	PhD Researcher Centrum Wiskunde & Informatica, Amsterdam, the Netherlands.
2017	PhD. Mathematics Delft University of Technology, Delft, the Netherlands *Thesis:* Advanced Estimation of Credit Valuation Adjustment *Promotor:* Prof. dr. C. W. Oosterlee.

List of Publications

5. **Q. Feng**, **R. Feng**, and **C. W. Oosterlee**. Efficient calculation of Solvency capital requirement for guaranteed minimum withdrawal benefits. Working paper, 2017.

4. **Q. Feng**, and **C. W. Oosterlee**. Wrong way risk modeling and computation in credit valuation adjustment for European and Bermudan options. Working paper, submitted for publication, 2016.

3. **Q. Feng** , **S. Jain**, **P. Karlsson**, **B. D. Kandhai** and **C. W. Oosterlee**. Efficient computation of exposure profiles on real-world and risk-neutral scenarios for Bermudan swaptions. *Journal of Computational Finance*, 20(1):139–172, 2016.

2. **Q. Feng**, and **C. W. Oosterlee**. Monte Carlo calculation of exposure profiles and greeks for Bermudan and barrier options under the Heston Hull-White Model. *Recent Progress and Modern Challenges in Applied Mathematics, Modeling and Computational Science*, Fields Institute Communications series, volume 79, 2017.

1. **C. S. L. de Graaf**, **Q. Feng**, **B. D. Kandhai** and **C. W. Oosterlee**. Efficient computation of exposure profiles for counterparty credit risk . *International Journal of Theoretical and Applied Finance*, 17(04):1450024, 2014.

List of Attended Conferences

Presentations:

5. The 19th European Conference on Mathematics for Industry (ECMI 2016), Santiago de Compostela, Spain, June 2016.

4. Workshop Student Computational Finance Day 2016, Delft, the Netherlands, May 2016.

3. Mini-Workshop in Stochastic Computing and Optimization, Würzburg, Germany, October 2014.

2. SIAM Conference Financial Mathematics and Engineering (FM14), Chicago, USA, November 2014.

1. The 8th World Congress of the Bachelier Finance Society, Brussels, Belgium, June 2014.

Posters:

2. Actuarial and Financial Mathematics Conference, Brussels, Belgium, February 2015.

1. Actuarial and Financial Mathematics Conference, Brussels, Belgium, February 2014.